TECHNICAL REPORT SL-92-28

US Army Corps of Engineers

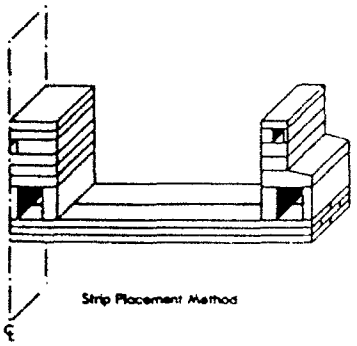

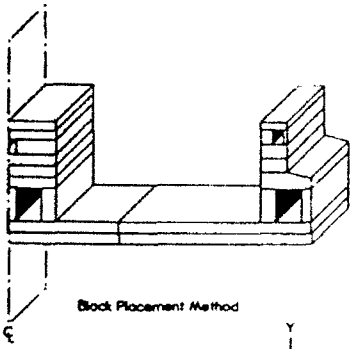

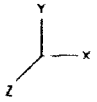

STRUCTURES LABORATORY

NONLINEAR, INCREMENTAL STRUCTURAL ANALYSIS OF OLMSTED LOCKS AND DAMS

Volume I
MAIN TEXT

by

Sharon Garner, Anthony A. Bombich, C. Dean Norman

Structures Laboratory

and

Chris Merrill, Barry Fehl, H. Wayne Jones

Information Technology Laboratory

DEPARTMENT OF THE ARMY
Waterways Experiment Station, Corps of Engineers
3909 Halls Ferry Road, Vicksburg, Mississippi 39180-6199

December 1992
Final Report

Prepared for US Army Engineer District, Louisville
Louisville, Kentucky 40201-0059

Destroy this report when no longer needed. Do not return it to the originator.

The findings in this report are not to be construed as an official Department of the Army position unless so designated by other authorized documents.

The contents of this report are not to be used for advertising, publication, or promotional purposes. Citation of trade names does not constitute an official endorsement or approval of the use of such commercial products.

REPORT DOCUMENTATION PAGE

Form Approved
OMB No 0704-0188

1. AGENCY USE ONLY (Leave blank)	2. REPORT DATE	3. REPORT TYPE AND DATES COVERED
	December 1992	Final Report

4. TITLE AND SUBTITLE

Nonlinear, Incremental Structural Analysis of Olmsted Locks and Dams; Volume 1: Main Text

5. FUNDING NUMBERS

MIPR No. RM-B-90-375

6. AUTHOR(S)

Sharon Garner, Anthony A. Bombich, C. Dean Norman, Chris Merrill, Barry Fehl, H. Wayne Jones

7. PERFORMING ORGANIZATION NAME(S) AND ADDRESS(ES)

U.S. Army Engineer Waterways Experiment Station
Structures and Information Technology Laboratories
3909 Halls Ferry Road
Vicksburg, MS 39180-6199

8. PERFORMING ORGANIZATION REPORT NUMBER

Technical Report SL-92-28

9. SPONSORING/MONITORING AGENCY NAME(S) AND ADDRESS(ES)

U.S. Army Engineer District, Louisville
Louisville, KY 40201-0059

10. SPONSORING/MONITORING AGENCY REPORT NUMBER

11. SUPPLEMENTARY NOTES

Available from National Technical Information Service, 5285 Port Royal Road, Springfield, VA 22161. This report is in two volumes.

12a. DISTRIBUTION/AVAILABILITY STATEMENT

Approved for public release; distribution is unlimited.

12b. DISTRIBUTION CODE

13. ABSTRACT *(Maximum 200 words)*

The Olmsted Locks and Dam will be located on the Ohio River and the locks will be a W-frame type of structure, which is currently unprecedented within the Corps of Engineers. Because of this fact and due to the high fly ash concrete mixture planned for the project, an extensive nonlinear, incremental structural analysis (NISA) was performed. Parameters evaluated included two different placing schemes, plane stress and plane strain analyses, two different concrete mixtures, creep, and shrinkage.

The report contains two phases. In the first phase, parameters such as plane stress and plane strain, block and strip placement schemes, and mixtures 6 and 11 were evaluated. The second phase included performance of several analyses based on the load case combinations contained in ETL 1110-2-324, "Special Design Provisions for Massive Concrete Structures," and included evaluation of the effects of creep and shrinkage. The second phase results were also used to validate the analyses performed in the first phase.

14. SUBJECT TERMS

Finite element
Incremental construction
Massive concrete structures
Nonlinear
Thermal stress

15. NUMBER OF PAGES

247

16. PRICE CODE

17. SECURITY CLASSIFICATION OF REPORT	18. SECURITY CLASSIFICATION OF THIS PAGE	19. SECURITY CLASSIFICATION OF ABSTRACT	20. LIMITATION OF ABSTRACT
UNCLASSIFIED	UNCLASSIFIED		

PREFACE

The work described in this report was conducted for the US Army Engineer District, Louisville, by the Structural Mechanics Division (SMD), Structures Laboratory (SL), and the Computer-Aided Engineering Division (CAED), Information Technology Laboratory (ITL), US Army Engineer Waterways Experiment Station (WES). The investigation was authorized by DD form 448, MIPR No. RM-B-90-375, dated 5 January 1990. The technical report resulting from this investigation is published in two volumes.

The investigation was accomplished under the general supervision of Messrs. Bryant Mather, Director, SL; James T. Ballard, Assistant Director, SL; Dr. Jimmy P. Balsara, Chief, SMD; and Dr. N. Radhakrishnan, Director, ITL, and under the direct supervision of Dr. C. Dean Norman, SMD, and Mr. H. Wayne Jones, CAED. This report was prepared by Mr. Anthony A. Bombich, Concrete Technology Division (CTD), SL, Ms. Sharon Garner, SMD, Dr. Norman, Mr. Chris Merrill, CAED, Mr. Barry Fehl, CAED, and Mr. Jones. The authors acknowledge Mr. Michael Hammons, CTD, for his assistance during this investigation and Mr. Byron McClellan, CEORL-ED-A, for his support and encouragement in performing the work described in this report.

At the time of publication of this report, Director of WES was Dr. Robert W. Whalin. Commander was COL Leonard G. Hassell, EN.

CONTENTS

VOLUME I

VOLUME II

CONVERSION FACTORS, NON-SI TO SI (METRIC)
UNITS OF MEASUREMENT

Non-Si units of measurement used in this report can be converted to SI (metric) as follows:

Multiply	By	To Obtain
Btu (International Table) per pound (mass) . degree Fahrenheit	4,186.8	joules per kilogram kelvin
Btu (International Table) inch per hour . square inch . degree Fahrenheit	20.7688176	watts per metre kelvin
Calories per gram	4.184	kilojoules per kilogram
Fahrenheit degrees	5/9	Celsius degrees or kelvins*
feet	0.3048	metres
inches	25.4	millimetres
kips (force) per inch	1.213659	kilonewtons per metre
miles per hour (U.S. statute)	1.609347	kilometres per hour
pounds (force) per square inch	0.006894757	megapascals
pounds (mass) per cubic inch	27,679.899	kilograms per cubic metre
pounds (mass) per cubic foot	16.01846	kilograms per cubic metre

* To obtain Celsius (C) temperature reading from Fahrenheit (F) readings, use the following formula: $C = (5/9)(F-32)$. To obtain Kelvin (K) readings, use $K = (5/9)(F-32) + 273.15$.

Nonlinear, Incremental Structural Analysis of Olmsted Locks and Dam

PART I: INTRODUCTION

Background

1. In September 1989, the U.S. Army Engineer Waterways Experiment Station (WES) was asked by the US Army Engineer District (USAED), Louisville, to conduct a nonlinear, incremental structural analysis (NISA) for the Olmsted Locks project. The Olmsted project was authorized for construction by the Water Resources Development Act of 1988 and is to be constructed at mile 964.4* of the Ohio River (rignt bank). The lock is designed as a W-frame structure, founded on piles, with two parallel lock chambers of approximately 110-ft width and 1,200-ft length. Since the Corps of Engineers has had no experience in constructing mass concrete structures of this type (i.e. W-frame), the USAED, Louisville, emphasized that the NISA should focus on defining and evaluating potential construction problems that might be encountered. Guidance in the form of Engineering Technical Letter (ETL) 1110-2-324, "Special Design Provisions for Massive Concrete Structures" (Headquarters, Department of the Army, 1990), is provided to assist in this determination. ETL 1110-2-324 provides a rational, conservative, systematic NISA approach that will ensure safe, cost-effective, and durable structures are designed for construction.

2. Contents of this report include an introduction provided in Part I, a presentation of material parameters in Part II, a Phase I NISA study in Part III, and a Phase II NISA study in Part IV.

Objectives

3. The objectives of this study are to utilize ETL 1110-2-324 guidance to ensure a conservative NISA that will address the following:

a. Define and evaluate potential construction problems that might be encountered in constructing the pile-founded, W-shaped lock.

---

* A table of factors for converting non-SI units of measurement to SI (metric) units can be found on page 3.

b. Define and evaluate materials and construction procedures which will lead to a cost-effective, durable, and safe structure.

c. Identify areas that may potentially, if further studied, result in construction cost savings.

d. Determine initial states of stress for earthquake analyses.

Scope

4. To meet the objectives of this study in a timely manner, it was necessary to develop, using sound engineering judgement, a rational approach to reduce the number of analyses required for this NISA study. Consequently, a two-phased approach was conceived to fulfill this requirement and to perform the NISA study. The Phase I NISA used concrete material properties determined by standard methods for the two selected mixtures for two-dimensional (2-D) analyses to evaluate the two proposed placement methods. Limited three dimensional (3-D) and 2-D out-of-plane analyses was also performed to verify results of these 2-D analyses. A final set of NISA's, using guidance from ETL 1110-2-324 (Headquarters, Department of the Army, 1990), were then performed with placement parameters identified in Phase I. In addition to load cases specified in ETL 1110-2-324, a load case consisting of assumed maximum bounds for creep, minimum bounds for shrinkage, and average aging modulus and adiabatic temperature curves, along with gravity and service loads, were performed using both concrete mixtures. Results of the Phase II NISA were then used to verify that the Phase I results were bracketed. This step validated the use of the Phase I analyses to reduce the number of parameters unique to this study and still provide conservative results in the Phase II NISA.

PART II: MATERIAL PARAMETERS

General

5. To effectively model the response of the concrete during the construction process, several material parameters must be provided by the user in the heat transfer and stress analyses. These parameters are of two types: (a) constants, which are included in the input files for the analyses, and (b) time-dependent functions, which are supplied as algebraic functions of time or as data arrays in ABAQUS user subroutines (Hibbitt, Karlsson, and Sorenson 1988). The time-dependent properties that are required by the DFLUX and UMAT subroutines are briefly discussed. For a more in-depth discussion see Garner and Hammons (1991).

Concrete Mixtures

6. The design and selection of the concrete mixtures used in the incremental construction analyses is described by Hammons and et al. (1991). A matrix of 12 mixtures was developed to cover the range of expected combinations of water-cement (W/C) ratio and fly ash (F/C) replacements for field use and to make use of both Class F and Class C fly ashes. Of these 12 mixtures, mixtures 6 and 11 were determined to be the most likely mixtures used in construction and, therefore, were chosen for use in the analysis.

7. F/C replacement and W/C ratios for the two mixtures are given in Table 1. Mixture proportions are given in Table 2. Mixture proportions listed are for the mass concrete mixtures planned for use in the majority of the structures. In very narrow sections, such as culvert walls, maximum coarse aggregate size will be limited to 1-1/2 in. The effects of this limitation on concrete properties will be discussed in Part III of this report.

8. The cement used was a Type II, moderate, heat of hydration (<70 cal/gm), low alkali American Society for Testing and Material (ASTM) C 150 (ASTM 1990) portland cement. Mixture 11 used a Class C fly ash and mixture 6 used a Class F fly ash per ASTM C 618 (ASTM 1990). Fine aggregate was a natural river sand with a small amount of filler sand added to make up for a deficiency in fines. All coarse aggregates were limestones.

Table 1

Concrete Mixtures

Mixture	W/C ratio (by mass)	F/C ratio (by volume)
6	0.40	0.40
11	0.45	0.50

Table 2

Mixture Proportions

Material	Weights per One Cubic Yard Batch, lb	
	Mixture 6	Mixture 11
Type II portland cement	215.9	159.0
Class C fly ash	0.0	133.7
Class F fly ash	107.4	0.0
Fine aggregate	998.3	1,025.3
Coarse aggregate (3/4-in. maximum)	1,231.8	1,235.5
Coarse aggregate (1-1/2-in. maximum)	546.1	547.9
Coarse aggregate (3-in. maximum)	695.0	697.4
Filler	76.0	78.1
Air-entraining admixture, oz	13.6	8.5
Water	144.0	143.0

Thermal Properties

9. The heat transfer capability of ABAQUS uses the finite element method to numerically solve the governing differential equation

$$\nabla^T k \nabla \theta + Q = \rho c_p \frac{\partial \theta}{\partial t} \tag{1}$$

where

$\theta(x,y,z,t)$ = the temperature at a point described by the coordinates (x,y,z) at time t

k = thermal conductivity

$Q(t)$ = applied heat flux

ρ = density

c_p = specific heat

The necessary material parameters, therefore, are the density, thermal conductivity, and specific heat of each material, and a mathematical description of the applied heat flux generated by the concrete.

Concrete thermal properties

10. Thermal properties for the concrete mixtures simulated in this study were based upon the results of tests to yield specific heat, thermal conductivity, density, and coefficient of linear thermal expansion which were conducted at WES for Olmsted mixtures 6 and 11 (Hammons et al. 1991). The different concrete mixture tests were conducted at a single test age of 28 days on the assumption that the necessary thermal properties for a given mass concrete mixture did not vary with age. This assumption was verified during an earlier study (Hammons, Smith, Neeley 1990) where the results of tests conducted at ages of 3 and 28 days showed negligible differences. The results used as input to ABAQUS are shown in Table 3.

Table 3

Concrete Thermal Properties Used in ABAQUS

Properties	Mixture 6 and Mixture 11
Density, lb/in.^{3}	0.08449
Specific heat, Btu/lb - °F	0.22
Thermal conductivity, Btu-in./day-in^2 - °F	2.24
Coefficient of thermal expansion, millionths/°F	4.0

Adiabatic temperature rise

11. The applied heat flux supplied by the heat of hydration of cementitious materials in the concrete mixture is given by the adiabatic temperature rise of the mixture. The adiabatic temperature rise for each concrete mixture is described by a curve that represents temperature rise of a concrete specimen as a function of time where no heat loss or gain is permitted. Adiabatic temperature rise tests were performed at WES for concrete mixtures 6 and 11 (Hammons et al. 1991). These adiabatic curves were input into ABAQUS through the subroutine DFLUX as a set of temperature-time datum arrays. The adiabatic curves used in the heat transfer analyses in the DFLUX subroutine are shown in Figures 1 and 2.

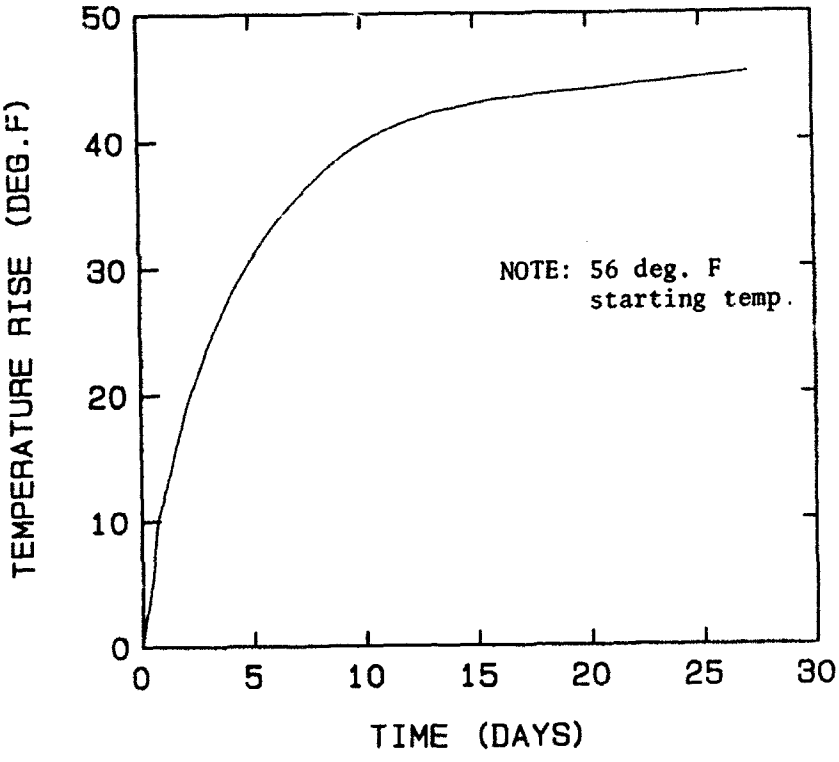

Figure 1. Mixture 11 adiabatic temperature rise

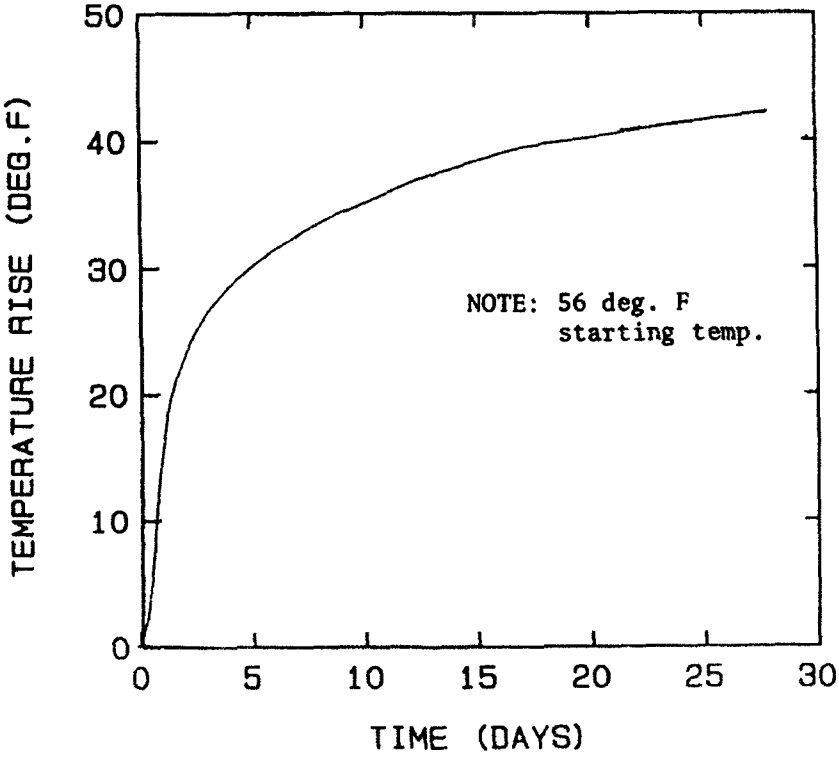

Figure 2. Mixture 6 adiabatic temperature rise

Foundation thermal properties

12. The initial foundation information provided by the USAED, Louisville, specified that the top 5 ft of soil underlying the structure is to be removed and backfilled with a selected foundation material. The soil underlying the backfill was specified as McNairy zone 1 clay. Three potential foundation materials were considered for the backfill including no. 57 limestone, compacted river sand, and quarry-run limestone. Specific selection of the backfill material to be used for construction was not made during this investigation. Since thermal properties of the candidate foundation materials were not available, it was necessary to estimate these properties. The backfill material which thermally represented the worst case was to be used. USAED, Louisville, provided physical properties of these materials which included dry density, moist density, moisture content, void ratio, and percent saturation in a moist condition to assist in determination of the thermal properties. These data are shown in Table 4.

13. The initial temperature distribution in the foundation is based upon the results of a heat transfer analysis of a 20-ft typical soil column. The scenario for preparation of the foundation and its configuration is described as follows. Prior to concrete placement, the soil is to be dewatered to a depth of 6 ft. The top 5 ft of soil is to be excavated and backfilled with the selected foundation material. Dewatering could either be terminated after the first lift in the structure is placed, at which time all the soil would become saturated, or it could be continued throughout the construction period.

14. The procedure for selecting the backfill material to use involved first estimating the thermal properties of the candidate materials. Then through a series of thermal simulations of placement of the lock floor, the material producing the worst case thermally was determined. The first step in estimating the thermal properties of the foundation materials was to check the physical properties provided for consistency against the equations for three-phase composition of soils. Since inconsistencies existed, corrections and modifications were made with the concurrence of USAED, Louisville. Table 5 shows the physical properties assumed in this investigation.

15. Thermal properties for the foundation materials were calculated from the corrected physical properties using equations developed by Kersten (1949). Kersten's equations allow the computation of thermal conductivity and specific heat as functions of soil texture and physical properties.

Table 4

Physical Properties Provided for Foundation Materials

	No. 57 Limestone 0'-5'	Compacted River Sand 0'-5'	Quarry-run Limestone 0'-5'	McNairy Zone 1 (clay) 5'-20'
Wet density, pcf	110.0	130.0	120.0	117.0
Dry density, pcf	105.0	115.0	109.0	90.6
Void ratio	0.30	0.43	0.35	0.80
Moisture content, moist (percent)	5.0	15.0	10.0	28.0
Percent saturation, moist (percent)	5.0	95.0	25.0	95.0
Range of particle sizes	1/4"-1"	dust to #4	dust to 6"	fine

16. The insitu specific heat, (c_{wet}) was computed using the equation

$$c_{wet} = \frac{100\,c_{dry} + Moisture\ Content}{100 + Moisture\ Content} \qquad (2)$$

for each foundation material. Values of dry specific heat (c_{dry}) for each material were obtained from Kersten (1949), and moisture contents for each material were taken from Table 5.

17. Thermal conductivity for the foundations materials were computed from two equations by Kersten. The equation used for No. 57 limestone, compacted river sand, and quarry-run limestone was calculated using Kersten's equations for sandy soil with less than 50 percent silt or clay content. This equation is

$$k_{wet} = [0.7\log(Moisture\ Content) + 0.4]10^{0.01\rho_{dry}} \qquad (3)$$

The equation used for computing the thermal conductivity of McNairy zone 1 clay is

$$k_{wet} = [0.9\log(Moisture\ Content) + 0.2]10^{0.01\rho_{dry}} \qquad (4)$$

where thermal conductivity corrected for moisture content, k_{wet}, is in Btu-in/hr-in^2-°F and the dry density, ρ_{dry}, is in lb/ft^3.

Table 5

Physical Properties Used for Foundation Materials

	No. 57 Limestone 0 - 5 ft	Compacted River Sand 0 - 5 ft	Quarry-run Limestone 0 - 5 ft	McNairy Zone 1 (clay) 5 - 20 ft
Dry density (pcf)	105.0	115.0	109.0	90.6
Solid density (pcf)	(166.0)*	164.4	(166.0)*	162.4
Wet density (pcf)	110.0	132.8*	120.0	117.0
Saturated density (pcf)	127.9*	133.8*	130.5*	118.0*
Void ratio	0.581*	0.43	0.523*	0.80
Porosity	0.367*	0.30*	0.343*	0.444*
Percent saturation, moist condition (percent)	22.9*	95.0	51.0*	95.0*
Moisture content, moist condition (percent)	5.0	15.4*	10.0	28.0
Moisture content, saturated condition (percent)	22.8	16.2	19.6	30.6
Range of particle sizes	1/4 to 1"	dust to #4	dust to 6'	fine

* Computed or corrected at WES
** Test results from Olmsted limestone coarse aggregate at WES

18. Table 6 shows the computed thermal properties for the three candidate backfill foundation materials and McNairy zone 1 clay at natural moisture and saturated states. Also shown are physical properties to describe the condition and all input values used for computing the thermal properties. All thermal properties listed are shown in units consistent with their use in ABAQUS.

Table 6

Computed Thermal Properties of Foundation Materials in Units Consistent with Input to ABAQUS (Physical Properties Included)

	No. 57 Limestone	Compacted River Sand	Quarry-run Limestone	McNairy Zone 1 (clay)
Dry condition:				
Density, ρ_{dry}, lb/in.^{3} (lb/ft^3)*	0.06076 (105.0)	0.06651 (115.0)	0.06308 (109.0)	0.05243 (90.6)
Specific Heat**, c_{dry}, Btu/lb - °F	0.226	0.18	0.226	0.21
Moist (wet) condition:				
Moisture content, percent	5.0	15.4	10.0	28.0
Saturation, percent	22.9	95.0	51.0	95.0
Density, ρ_{wet}, lb/in.^{3} (lb/ft^3)	0.06366 (110.0)	0.07685 (132.8)	0.06944 (120.0)	0.06771 (117.0)
Specific heat, c_{wet}, Btu/lb - °F	0.263	0.289	0.296	0.383
Thermal conductivity, k_{wet}, Btu-in/day-in^2-°F	1.663	2.878	2.250	1.480
Saturated condition:				
Moisture content, percent	22.8	16.2	19.6	30.6
Saturation, percent	100.0	100.0	100.0	100.0
Density, lb/in.^{3} (lb/ft^3)	0.07402 (127.9)	0.07743 (133.8)	0.07552 (130.5)	0.06829 (118.0)
Specific heat, c_{sat}, Btu/lb - °F	0.37	0.294	0.353	0.395
Thermal conductivity, k_{sat}, Btu-in/day-in.^{2}-°F	2.525	2.930	2.673	1.525

* - Values in customary units are shown in parentheses.
** - From Kersten (1949).

19. To determine the worst case backfill foundation material, a parametric study was conducted to evaluate the potential effect of the candidate materials on concrete temperatures in the floor slab. A total of nine incremental construction finite element thermal analysis runs were made. The study used a 2-D finite element model of the chamber monolith which included 20 ft of foundation material. The chamber monolith walls were not included in this study. A complete description of the finite element model, construction parameters, and the thermal boundary conditions used are found in Part III. For convenience, a brief description of the construction and thermal parameters affecting computer runs in this parameter study are presented in the following paragraphs.

20. Evaluation of the backfill materials was performed by observing the effects of vertical, one-dimensional (1-D) heat flow on vertical temperature distributions during and following simulated construction of the 12-ft-thick concrete floor as thermal properties of the backfill material were varied. Figure 3 shows a horizontal section from the finite element model representing the vertical layout of soil layers and concrete lifts. The concrete consisted of three 4-ft lifts placed at intervals of 10 days. Exposed horizontal concrete surfaces were assigned surface heat transfer coefficients based upon the wind velocity and the time of year. Exposed surfaces were subjected to expected air daily temperatures for Paducah, KY, and the placement date of lift 1 corresponded to 20 June. Placement temperature of all concrete was 60 °F. All runs were continued for a total elapsed time of 234 days which extended computation of concrete temperatures until February 20 which is a month past the dates of coldest air temperatures. Concrete thermal properties and adiabatic temperature rise for mixture 11 were used.

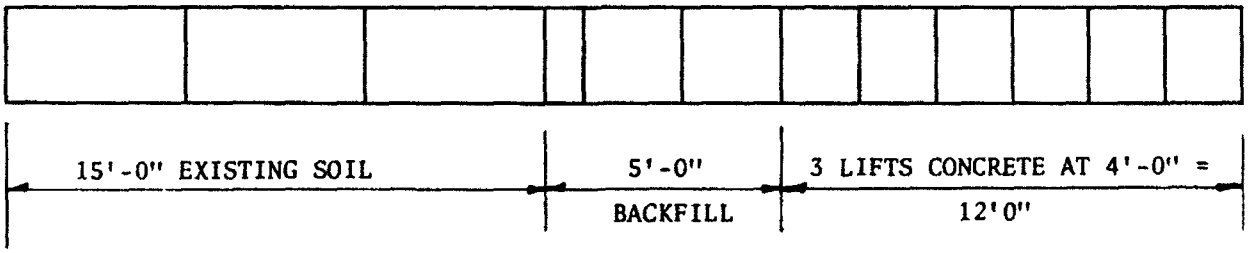

Figure 3. Typical section for backfill evaluation

21. In all computer runs, the foundation material modeled for depths between 5 and 20 ft was clay. The clay layer between depths of 5 and 20 ft

was saturated in all analyses except the first. Changing the soil properties in ABAQUS after lift 1 is placed is not easily achieved; therefore, the saturation state of the backfill in all runs was assumed to be the case from placement of lift 1 onward. Thermal properties of the candidate backfill materials were varied in the top 5-ft layer of the foundation column to be representative of the backfill in both saturated and moist (dewatered) states.

22. Analysis of the values of computed thermal properties for the backfill materials shown in Table 6 indicated that those of compacted river sand and/or no. 57 limestone represented the extremes of the values for density, specific heat (heat capacity), and thermal conductivity (conductance) in both moist and saturated states. The properties for quarry-run limestone were not used. This was fortuitous since the wide range of particle distribution (dust to 6 in.) resulted in greater variation in the computed thermal properties for any given volume of this material. Table 7 provides a summary of the properties used in the foundation for these runs again expressed in units consistent with input to ABAQUS (Hibbitt, Karlsson, and Serenson 1988). Notice that each property of the backfill material on the last six runs is identified with an L or H. These designations indicated that the associated value represents the lowest or highest value, respectively, of that property for the given saturation (moist or saturated). From these runs, the effects of all the combinations for lowest or highest values possible for density, specific heat, and thermal conductivity were evaluated. As noted in Table 7, the materials used in runs 3, 4B, 6, and 7 are composites of the high or low values needed to fill out the matrix.

23. As expected, the largest differences in concrete temperatures were observed in lift 1 nearest the foundation-concrete interface. Differences were reduced at higher elevations in the concrete. Maximum differences in concrete temperature at the bottom of lift 1 were 2.5, 3.3, and 2.84 °F at 5, 10, and 15 days, respectively, after concrete placement. The difference in concrete temperature was still 2.6 °F at 40 days and 1.1 °F at 90 days. Maximum differences in concrete temperature at midheight of lift 1 were 0.87, 1.60, and 1.80 °F at 5, 10, and 15 days, respectively, after placement. The difference in concrete temperature was still 2.2 °F at 40 days and 1.1 °F at 90 days. In all cases the highest concrete temperatures were produced in run 5 in which wet no. 57 limestone was the backfill material. Its thermal properties were characterized as being the lowest of all materials simulated. Although concrete temperatures did not vary by more than 1 °F at any location

Table 7

Summary of Soil Thermal Properties Used in Foundation Backfill Evaluation Study

Depth of Layer	Run Number	1	2	3	3B	4	4B	5	6	7
6 to 20 ft	Foundation Material	Saturated Clay	Saturated Clay	Saturated Clay	Saturated Clay	Saturated Clay	Saturated Clay	Saturated Clay	Saturated Clay	Saturated Clay
	Density, lb/in.^{3}	0.06887	0.06887	0.06829	0.06829	0.06829	0.06829	0.06829	0.06829	0.06829
	Specific heat, Btu/lb-°F	0.395	0.395	0.395	0.395	0.395	0.395	0.395	0.395	0.395
	Thermal Conductivity, Btu-in/hr-in.^{2}-°F	1.525	1.525	1.525	1.525	1.525	1.525	1.525	1.525	1.525
5 to 6 ft	Foundation Material	Wet Clay	Saturated Clay	Saturated Clay	Saturated Clay	Saturated Clay	Saturated Clay	Saturated Clay	Saturated Clay	Saturated Clay
	Density, lb/in.^{3}	0.0677	0.06887	0.06829	0.06829	0.06829	0.06829	0.06829	0.06829	0.06829
	Specific heat, Btu/lb-°F	0.383	0.395	0.395	0.395	0.395	0.395	0.395	0.395	0.395
	Thermal Conductivity, Btu-in/hr-in.^{2}-°F	1.48	1.525	1.525	1.525	1.525	1.525	1.525	1.525	1.525
0 to 5 ft	Backfill Material	Wet Sand	Wet Sand	Saturated Sand	Saturated Sand	Sat. #57 Limestone	Sat. #57 Limestone	Wet #57 Limestone	Sat. Min. Values	Sat. Max. Values
	Density, lb/in.^{3}	0.07685	0.07685	0.07743 (H)	0.07743 (H)	0.07402 (L)	0.07402 (L)	0.06366 (L)	0.07402 (L)	0.07743 (H)
	Specific heat, Btu/lb-°F	0.289	0.289	0.289 (L)	0.294 (L)	0.37 (H)	0.37 (H)	0.263 (L)	0.294 (L)	0.37 (H)
	Thermal Conductivity, Btu-in/hr-in.^{2}-°F	2.88	2.88	2.88 (L)	2.93 (H)	2.525 (L)	2.93 (H)	1.663 (L)	2.525 (L)	2.93 (H)
Comments		Initial Values Assumed for Sand	Same as 1, but saturated clay at 5-6 ft	Sat. sand w/wet sp. ht. and therm. cond.	Final values for saturated sand	Saturated limestone	Saturated limestone w/ th. cond. of sand	Wet limestone w/minimum values overall	Saturated soil/ minimum values	Saturated soil/ maximum values

KEY:
L - Lowest value for particular property and saturation of soils considered.
H - Highest value for particular property and saturation of soils considered.
sp. ht. - Specific heat

in all of the remaining runs, the lowest temperatures were found in Runs 3B, 4B, and 7 in which the highest value for thermal conductivity was used.

24. The results of the study also showed that for all except run 5 with wet no. 57 limestone as the backfill material, concrete temperatures at the center of lift 2 varied by less than 0.3 °F and did not differ at all at the top of lift 2 or in lift 3. Temperatures for wet limestone were 1 °F higher than the other runs at the center of lift 2 and 0.5 °F higher at the top of lift 2. Using the backfill material yielding the highest temperatures in the bottom of the concrete as the worst case, the properties of wet no. 57 limestone were used for the backfill material on all incremental construction simulations in this investigation. The results using any combination of the full range of thermal properties characterizing saturated backfill candidate soils were very similar. The selection criteria for a saturated backfill material, if necessary, to be used in the thermal analyses for this investigation, would be based upon the material in which confidence in its calculated properties is greatest. This material would be saturated compacted river sand.

Mechanical Properties

25. Mechanical properties are supplied to the time-dependent creep model (UMAT) used in the analyses in two ways: (a) constants such as 3-day modulus of elasticity and 3-day compressive strength are given in the input file, and (b) creep, shrinkage, and modulus are incorporated into the model as functions of age. The process of modifying the equations in UMAT for a particular concrete is known as the model calibration. The calibration and verification of the model for each of the two mixtures has been described in detail in a previous report (Hammons et al. 1991). For reference, the creep, shrinkage, and modulus functions used for each mixture are discussed in the following paragraphs.

Shrinkage

26. American Concrete Institute ACI 209-R82 (ACI 1989) defines shrinkage as the decrease with time of concrete volume. This decrease is due to changes in the moisture content of the concrete and to the physicochemical changes in concrete. Shrinkage due to moisture loss, or drying shrinkage, occurs only at the surface of mass concrete structures and is generally considered less significant than autogenous shrinkage for these types of structures. Therefore, it is not simulated in the material model. Additional

volumetric changes not directly attributable to temperature fluctuations or moisture loss occur during hydration of the cementitious materials. The "shrinkage" curve included in UMAT describes these volumetric changes.

27. The mixture 6 shrinkage curve was based on test data. However, mixture 11 exhibited very little shrinkage. Analysis of the mixture revealed that several shrinkage-compensating compounds were produced during hydration of the cement. This phenomenon is not likely to be reproduced in the field, so in order to include some shrinkage in the analyses, an equation based on previous data for mass concrete mixtures (Hammons, Smith, and Neely 1990) was modified to yield a final total shrinkage of 20 microstrains. The curves used for mixtures 6 and 11 are given by the following equations.

For mixture 6

$$\epsilon_{shrinkage} = 58.69 \times 10^{-6} (1-e^{-0.02649t}) + 9.46 \times 10^{-6} (1-e^{-0.5298t}) \quad (5)$$

For mixture 11

$$\epsilon_{shrinkage} = 13.11 \times 10^{-6} (1-e^{-0.15t}) + 9.29 \times 10^{-6} (1-e^{-0.02263t}) \quad (6)$$

where t is time since placement of the concrete in days.

Creep and modulus

28. Creep is defined by ACI Committee 209 (198) as the time-dependent increase of strain in hardened concrete subject to sustained stress. It is the total measured strain in a loaded specimen minus the sum of the initial instantaneous (or elastic) strain due to the applied stress and the shrinkage and thermal strains in an identical load-free specimen subjected to the same history of relative humidity and temperature.

29. This definition assumes that elastic strain does not change with time. However, in a mass concrete structure stresses and modulii are constantly changing throughout the structure and the construction period, and initial elastic strain has little meaning. Therefore, the stress-strain relationship of the concrete must be based on age-related modulus and creep functions.

30. In the material model, creep is given by a 3-day creep compliance curve. This curve represents the difference between total specific strain (strain per unit stress) obtained from a 3-day creep test and the elastic specific strain obtained from modulus tests at various ages. The relationship between total specific strain (J(t)), creep compliance (C(t)) and elastic specific strain (1/E(t)) is shown in Figure 4. The 3-day creep compliance can be translated to obtain the creep strain for a load applied at time t by a modulus-related aging factor. The creep compliance, modulus, and aging factor

functions in UMAT were determined based on test data reported by Hammons et al. (1991).

31. The equations for mixture 6 follow:

$$C(t) = 1 \times 10^{-6} [0.3216(1-e^{-0.0353(t-to)}) + 0.1633(1-e^{-0.4415(t-to)}) + 0.0927(1-e^{-1.325(t-to)})] \quad (7)$$

$$E(t) = 1 \times 10^{6} [2.06998(1-e^{-0.0595(t-1)}) + 1.1327(1-e^{-0.4076(t-1)}) + 0.2776(1-e^{-2.6492(t-1)}) + 1.35] \quad (8)$$

$$AF(t) = [E(3)/E(t)]^2 \quad (9)$$

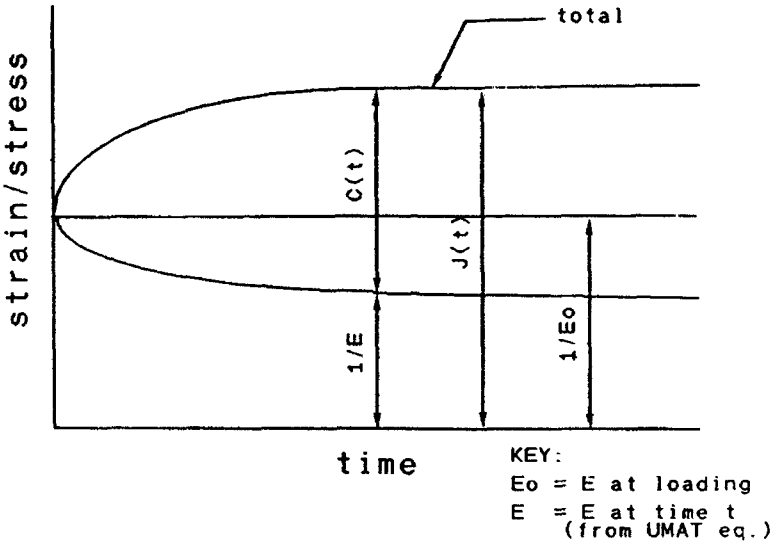

Figure 4. Relationship between creep compliance, elastic strain, and total specific strain

where

t = age of the concrete in days

t_0 = age at time of loading

C(t) = specific creep, in./in. per psi

E(t) = modulus of elasticity at time t, psi

E(3) = the modulus at 3 days

AF(t) = the aging factor

The equations for mixture 11 are given below.

$$C(t) = 1 \times 10^{-6} [0.3949(1-e^{-0.05298(t-to)}) + 0.2263(1-e^{-0.6623(t-to)}) + 0.126(1-e^{-2.649(t-to)})] \quad (10)$$

$$E(t) = 1 \times 10^{6} [2.86(1-e^{-0.0595(t-1)}) + 2.63(1-e^{-0.8831(t-1)}) - 0.9776(1-e^{-2.649(t-1)}) + 0.57] \quad (11)$$

$$AF(t) = [E(3)/E(t)]^2 \quad (12)$$

Other mechanical properties

32. Material properties input as constants to the UMAT subroutine are given in Table 8.

Table 8

Material Properties for UMAT

Material Property	Mixture 6	Mixture 11
3-day modulus (psi)	2.49×10^6	2.1×10^6
Poisson's Ratio	0.15	0.15
3-day compressive Strength (psi)	820.0	675.0
Tensile strain capacity (in/in)	0.0001	0.0001
Coefficient of thermal expansion (in/in per °F)	4.0×10^{-6}	4.0×10^{-6}

PART III: PHASE I STUDY

General

33. Phase I consists of heat transfer and stress analyses with plane stress and plane strain assumptions using both concrete mixtures identified in Part II for the strip and block construction methods. A limited 3-D analysis was performed using only one concrete mixture and one placement method for verification of the 2-D analysis results. All Phase I analyses used average material properties for aging modulus, creep, shrinkage, and adiabatic temperature rise.

34. A primary focus of Phase I is to reduce the parameters for the in-depth study to be conducted in Phase II. Expected findings are the preferred construction method and the most appropriate type of stress analysis (plane stress or plane strain) for use in Phase II.

35. It should be noted that when results are presented and discussed, stresses refer to concrete only (unless otherwise noted), time is absolute with reference to the start of construction, and distributions are with respect to an entire section.

Selection of Sections for Analysis

36. The unusual design and massive dimensions of the W-frame lock chamber monoliths presented construction problems that have not previously been encountered in Corps-designed lock structures. Each W-frame monolith was approximately 320 ft wide and 80 ft long, with a 12-ft-thick floor section. Because of the volume of concrete required in each floor lift (roughly 4,000 cu yd), floor lifts could not be placed without vertical joints. Tensile stresses due to thermal and shrinkage effects can be expected to occur during the placement of a thick concrete floor, and a knowledge of the location and magnitude of these stresses was necessary to determine a concrete placement sequence that would best allow the floor to act as a continuous monolithic structure. Two possible placement schemes for the chamber monolith floors were proposed by the USAED, Louisville. These placement schemes are shown in Figure 5 and are referred to in this report as the strip placement method and the block placement method.

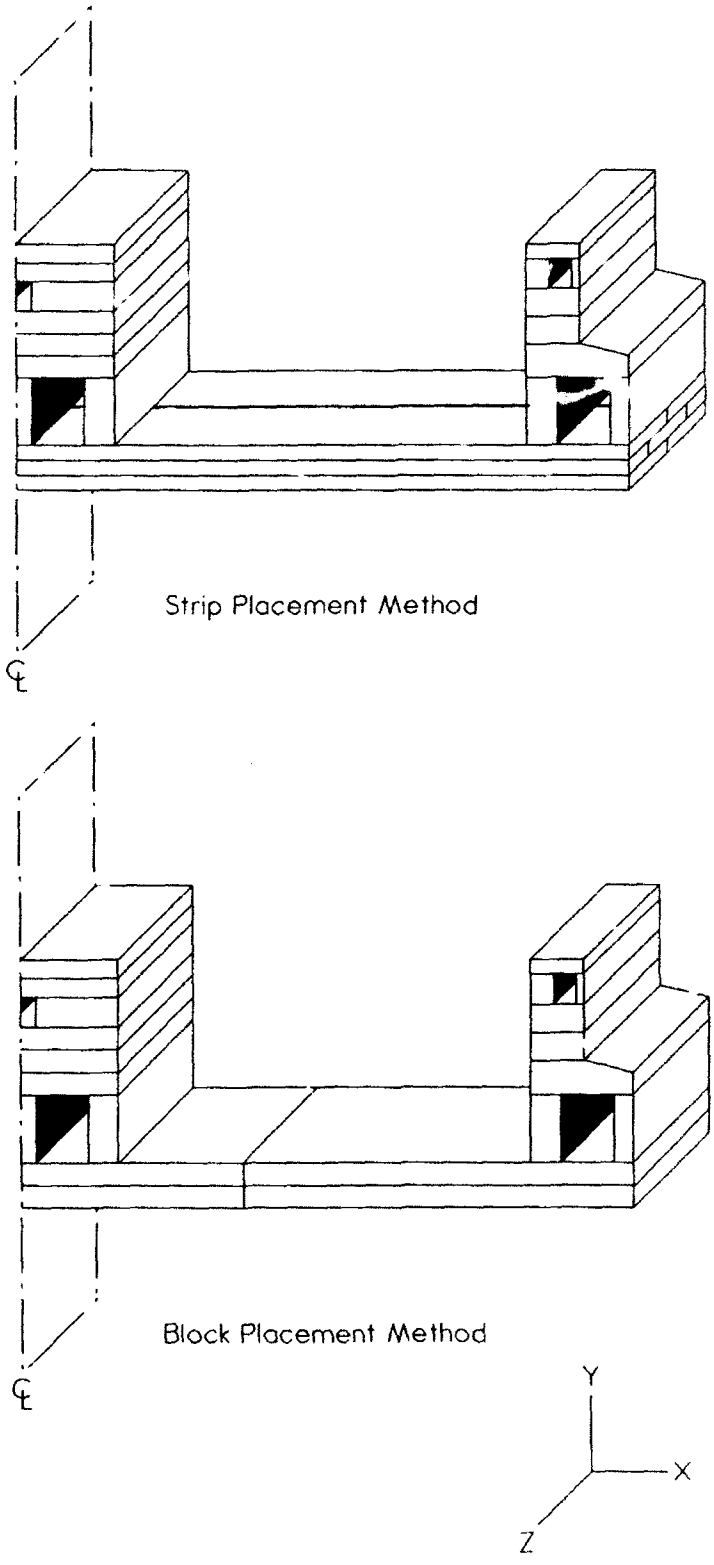

Figure 5. Monolith placement schemes

37. Lock chamber walls are usually relatively thin when compared to floor sections. They tend to cool quickly, reach near ambient temperatures soon after placement and experience relatively low tensile stresses. However, the 52-ft-thick center wall was an area of concern. Also, the method proposed for placing culvert walls was unusual for a mass concrete structure. Each wall was to be placed as a single continuous lift for the entire 18-ft height of the culvert.

38. In the strip placement method, all vertical joints were transverse to the direction of flow. In the block placement method, all vertical joints were parallel to the direction of flow. Two sections were selected for the initial 2-D analyses: (a) a typical W-frame section transverse to the axis of flow, and (b) a typical floor section parallel to the axis of flow. Lock monoliths were assumed symmetric relative to the axis of flow, and the W-frame section represented one-half of the transverse cross section.

39. A quarter section of the W-frame monolith was chosen for the 3-D analysis. To simplify the analysis, this section included only the floor and the center wall.

Finite Element Grid Generation

2-D grid development

40. Eight-node heat transfer, plane stress, and plane strain elements were used in the 2-D grids. These elements provide nonlinear fields for temperatures and displacements. Standard 3 x 3 integration (with nine calculation points per element) was used for all heat transfer analyses, and reduced integration (with four calculation points per element) was used in the stress analyses.

41. Element size for the finite element grids was based upon two constraints. Because of the type of integration procedure used in the ABAQUS transient heat transfer algorithm, a relationship exists between the minimum usable time-step and the distance between nodes (Hibbitt, Karlsson, and Sorenson 1988). A maximum time-step of 0.25-day is desirable to accurately reproduce temperature changes that occur during the first 2 days after placement of the concrete. The maximum distance between nodes corresponding to this time-step is 14 in. This yields an element length of 28 in. for an eight-node element. However, studies of Melvin Price Locks and Dam (Truman, Petruska, and Fehri in preparation) and the Red River Waterway Thermal Studies (Hammons

et al. 1991) have shown that this limit is critical only in the direction of heat flow. This means that in a lock monolith floor section, where heat loss occurs in the vertical direction except near the outer edges, longer elements can be used. Even in the direction of heat flow, increasing the element length to 30 in. does not interfere with convergence and produces errors in temperature of less than 1 °F. The second constraint on element size is based on lift dimensions: a minimum of two elements is required to define the stress distribution across a section. This means that 2-ft-high elements must be used in 4-ft lifts. Due to these restrictions, floor elements were 24 in. high. With a few exceptions, wall element size was restricted to a maximum of 30 by 30 in.

42. To accurately model incremental construction, newly placed lifts must be added in a stress-free state. Otherwise, fictitious stresses are induced which may cause excessive cracking and numerical instabilities if the displacements are large or the tensile capacity of the new concrete is low. ABAQUS normally adds newly placed elements based on their total displacement from an initial condition, which is the undeformed shape on the entire structure. This concept places an initial strain on newly placed elements which results in stresses that do not accurately model the stress conditions of the physical structure. Once the new elements are placed, strains continue to be based on the displacement from the initial condition instead of upon the relative displacement of the newly placed elements. To avoid an initial strain condition and to base strains on relative displacements, two modeling methods are recommended: (a) according to the "ABAQUS 4.8 Users Manual," a shared node can be replaced by a node at each surface and an intermediate node that can be shifted when the new lift is initialized to give a new, stress-free starting point for the new concrete, or (b) the AMP=STEP parameter can be used in the input deck in the initialization step for each lift to allow the initial displacement to take place without stress.

43. The first method requires the use of heat transfer interface elements to provide temperatures at the additional nodes for input to the stress analysis. This also ensures a more accurate temperature distribution at lift interfaces and was the method used initially in the analyses of the strip placement method. Due to ease of modeling, the second method was used in the analyses of the block placement method, including the 3-D analysis.

44. Two-dimensional stress analyses were made using both plane strain and plane stress elements. A plane strain analysis, in which the out-of-plane

strain is zero, is more appropriate for very long structures. In a plane strain analysis the UMAT model calculates incremental strains in the out-of-plane direction and stresses due to those strains. Because of the condition imposed by the plane strain elements, i.e. zero strain in the out-of-plane direction, these out-of-plane strains are totally restrained. Within each increment, the Poisson effect of out-of-plane tensile stresses is added to in-plane tensile stresses, giving a maximum in-plane tensile stress. However, total restraint is not a realistic condition, and predicted out-of-plane tensile stresses can be excessive. Since the UMAT model uses an interactive stress/strain cracking criteria with a maximum allowable stress of $2f'_t$ under a zero strain condition (Norman, Campbell, and Garner 1988), cracking due to these out-of-plane stresses can occur. This cracking is not based on realistic out-of-plane stresses and can result in nonconvergence as cracks continue to open. A plane stress analysis, with no out-of-plane stresses should yield lower-bound in-plane tensile stresses for the structure.

45. Grids used in the 2-D analyses are shown in Figures 6 and 7.

3-D grid development

46. Due to the large amounts of disk space and computer time needed for a 3-D analysis, the land wall was not included in the model and a coarser grid was required for the 3-D model. The maximum dimension in the direction of heat flow was extended to 36 in., and element dimensions along the axis of flow were limited only by pile spacing except at joints and at the end face of the monolith. Since the primary purpose of the 3-D analyses was to verify the 2-D results, slight errors in predicted temperatures due to the required use of larger elements will produce acceptable results.

47. The 3-D analyses were made using 20-node brick heat transfer and stress elements. Full $3 \times 3 \times 3$ integration was used in the heat transfer analysis and reduced integration ($2 \times 2 \times 2$) was used in the stress analysis. The 3-D grid of the structure is shown in Figure 8.

Construction Parameters and Boundary Conditions

48. Lift heights and vertical floor joint locations were selected by USAED, Louisville, based on practical concrete placement rates. Floor lift height was 4 ft in the strip placement method and 6 ft in the block placement method. Culvert walls were to be placed in single lifts. Lift locations for the two placement methods are shown in Figures 9 and 10.

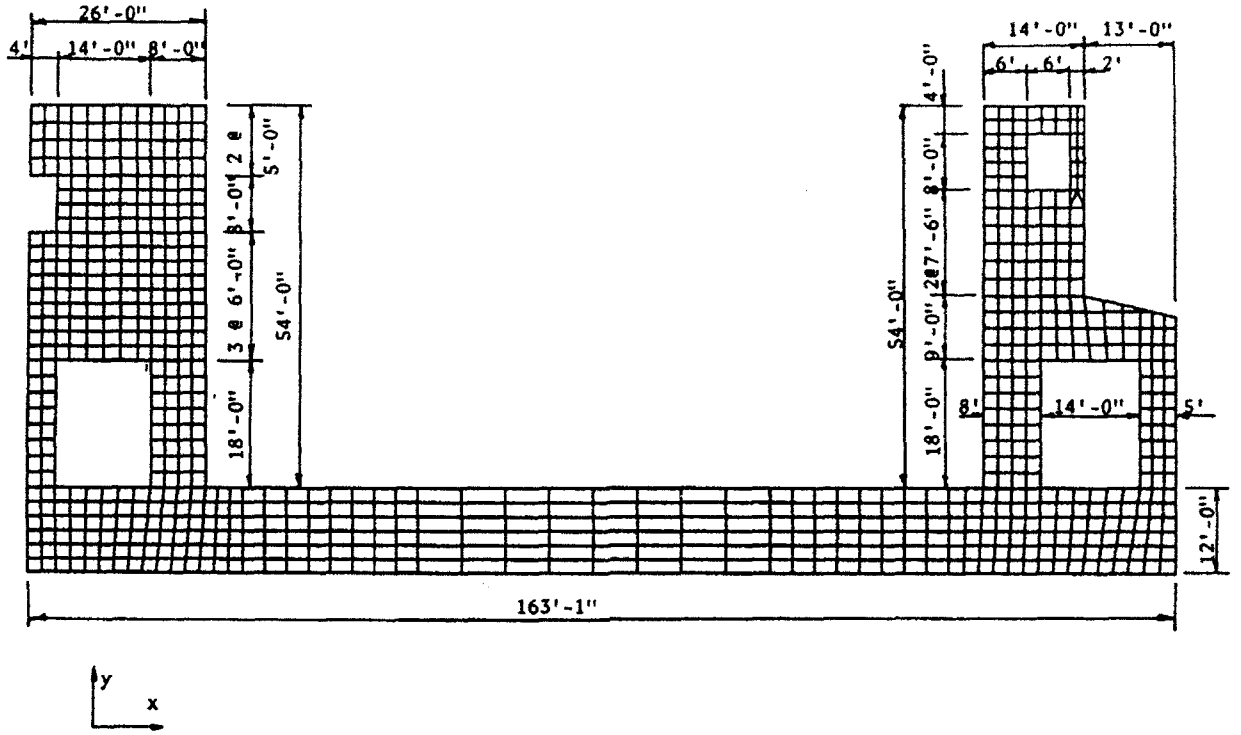

Figure 6. 2-D grid for lock section

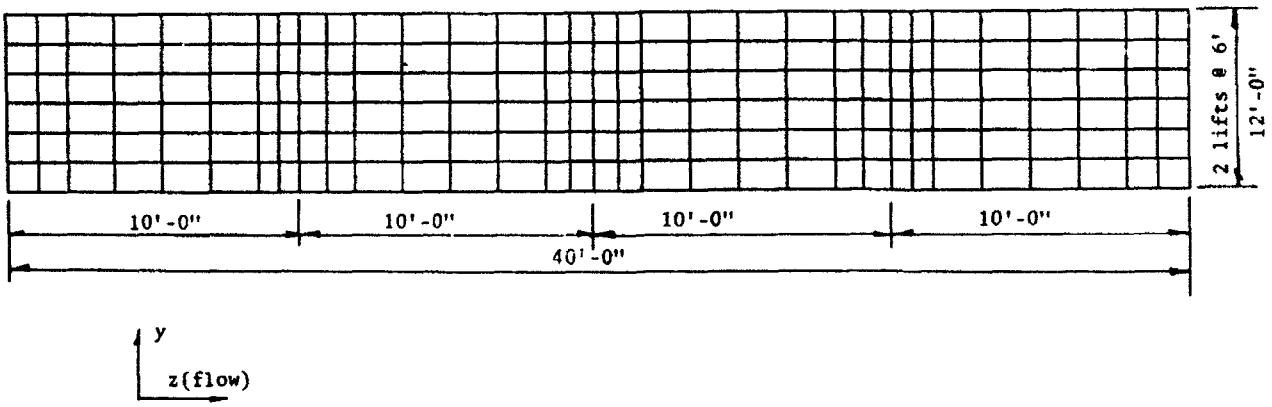

Figure 7. 2-D out-of-plane grid, floor only

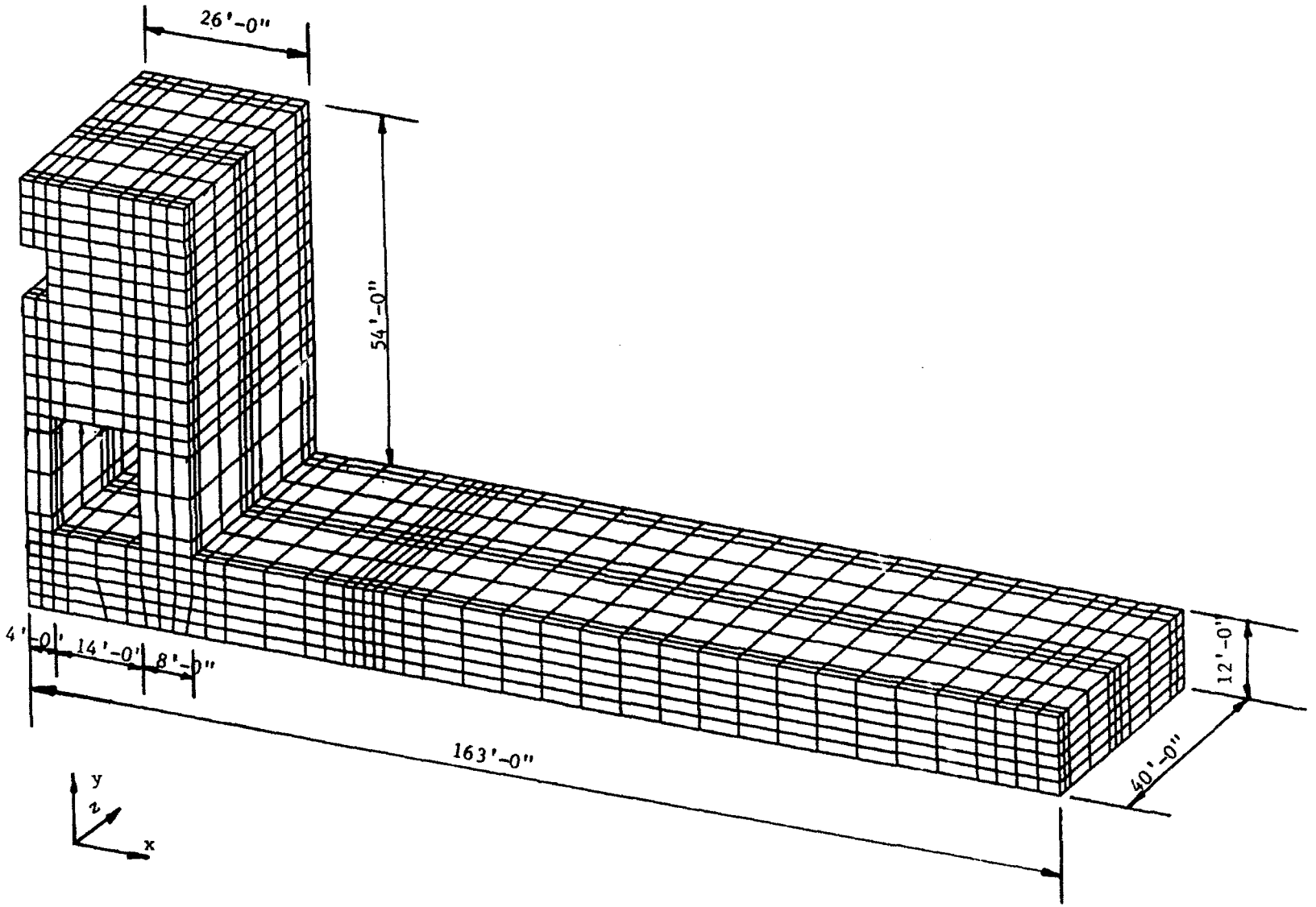

Figure 8. 3-D grid

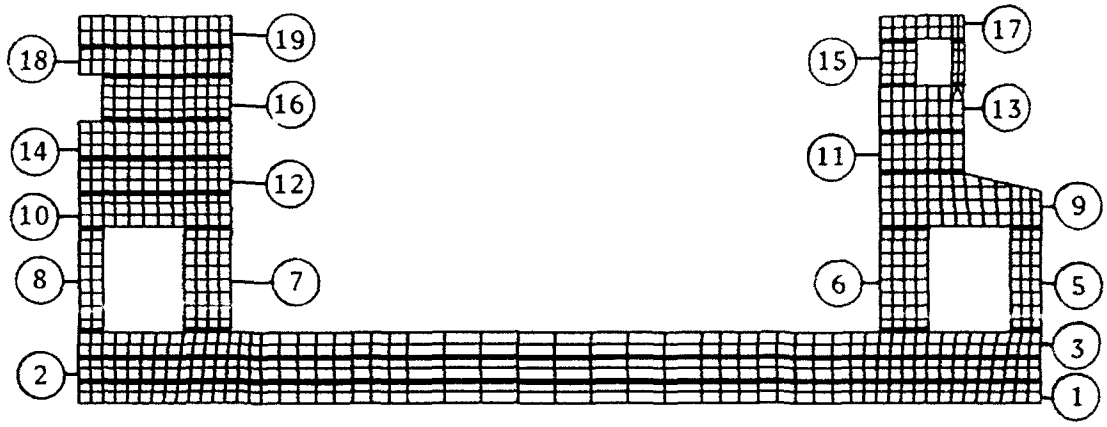

a. Strip placement

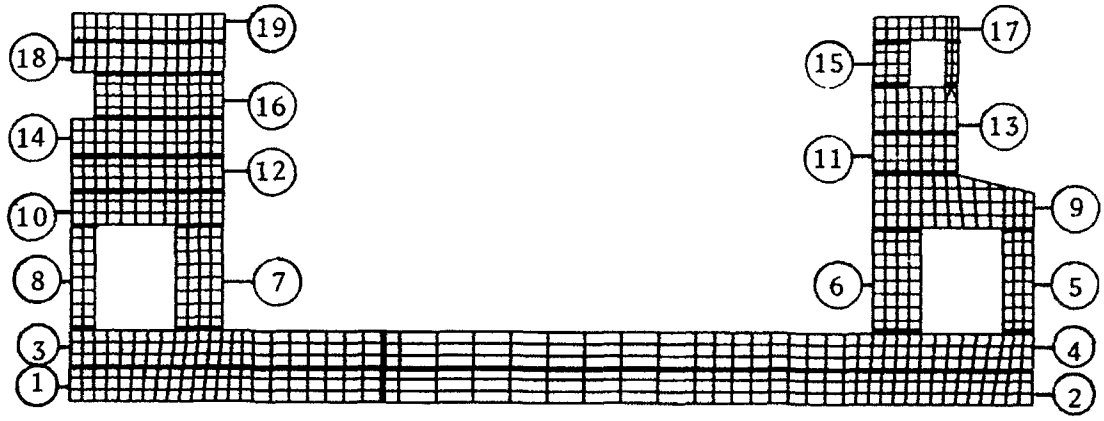

b. Block placement

Figure 9. Lift numbering

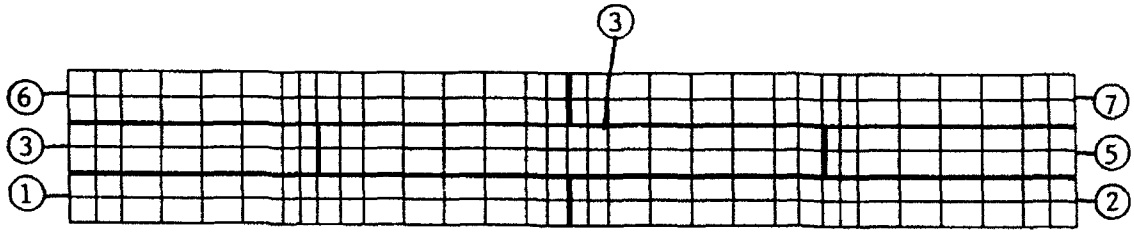

Figure 10. Lift numbering, strip placement scheme, out-of-plane floor only

49. The minimum lift placement interval for the analysis was 5 days. Longer placement intervals were used between some lifts in the analyses to allow gaps in time for the placement of lifts not modeled in the 2-D and 3-D grids. Lift placement times used in all analyses are shown in Table 9. Other lift placement sequences and schedules are possible, some may even be more critical. However, in accordance with ETL 1110-2-324 (Headquarters, Department of the Army, 1990) guidance on multidiscipline coordination, the USAED, Louisville, Construction and Engineering Divisions, using their best engineering judgement, jointly devised the strip and block placement schemes along with their placement schedules.

Table 9

Lift Placement Schedule

Lift Number	Strip Placement Method, days	Block Placement Method, days
1	0	0
2	10	5
3	20	15
4	*	20
5	30	30
6	35	35
7	40	40
8	45	45
9	65	65
10	70	70
11	75	75
12	80	80
13	85	85
14	90	90
15	95	95
16	100	100
17	105	105
18	110	110
19	115	115

* To have corresponding wall lift numbers for both placement methods, no model lift 4 was included in the strip placement method.

Ambient Temperatures

50. Ambient air temperatures used in the thermal analyses were obtained from the National Oceanic and Atmospheric Administration (NOAA) Service for the weather station located nearest the construction site at Paducah, KY. Air temperatures actually used are the expected mean daily temperatures.

Figure 11 shows a plot of these data. The time of the year origin shown is the date of placement for a summer construction start on 20 June.

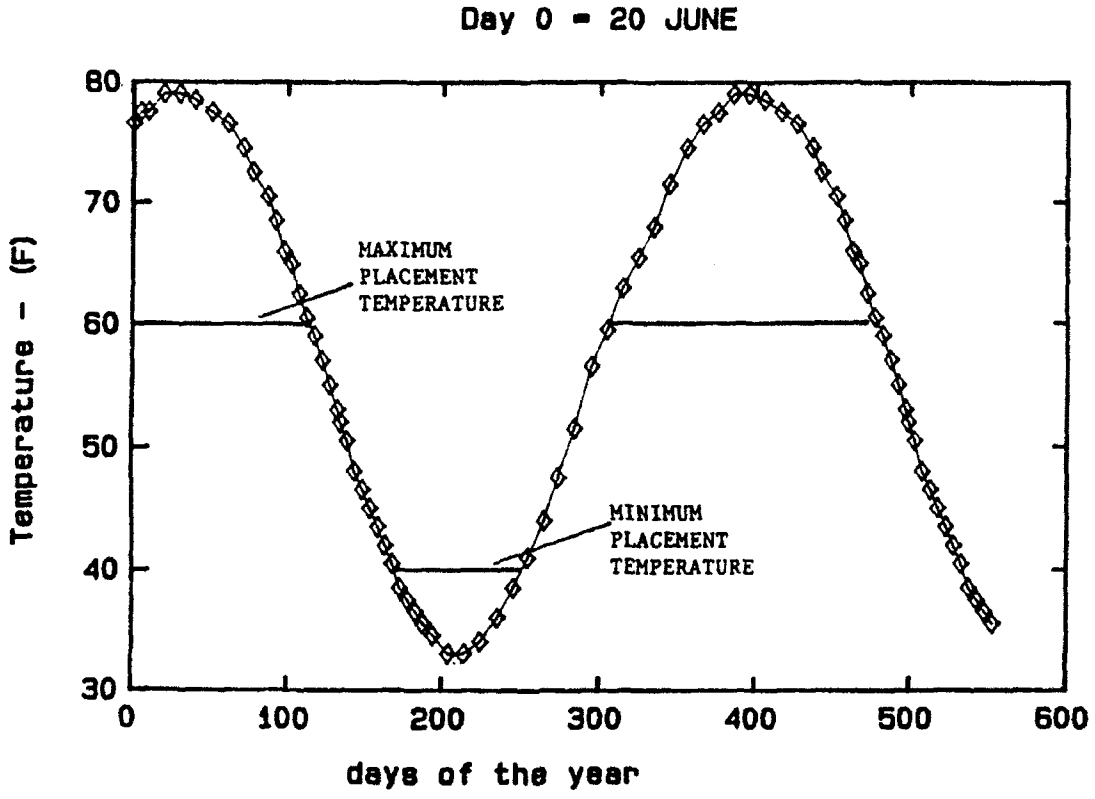

Figure 11. Daily mean temperature, Paducah, KY

Additional provisions

51. Three additional provisions were specified by the USAED, Louisville: (a) a maximum 60 °F placement temperature, (b) no insulation, and (c) a start-of-construction date of June 21. These provisions limited the scope of this investigation to construction which could be concluded prior to the earliest possible onset of freezing temperatures.

52. By the end of the construction period, ambient temperature was approximately 60 °F. To ensure that placement temperatures remained below ambient temperatures, a 60 °F placement temperature was used in the floor. Wall placement temperatures were varied from 60 °F to 50 °F to guarantee that placement temperatures remained below a decreasing ambient temperature until the minimum placement temperature was reached. An additional analysis with a 60 °F placement temperature for all lifts (OMSTDS2) was run for comparison. Placement temperatures and average daily ambient temperatures are shown in Figure 12.

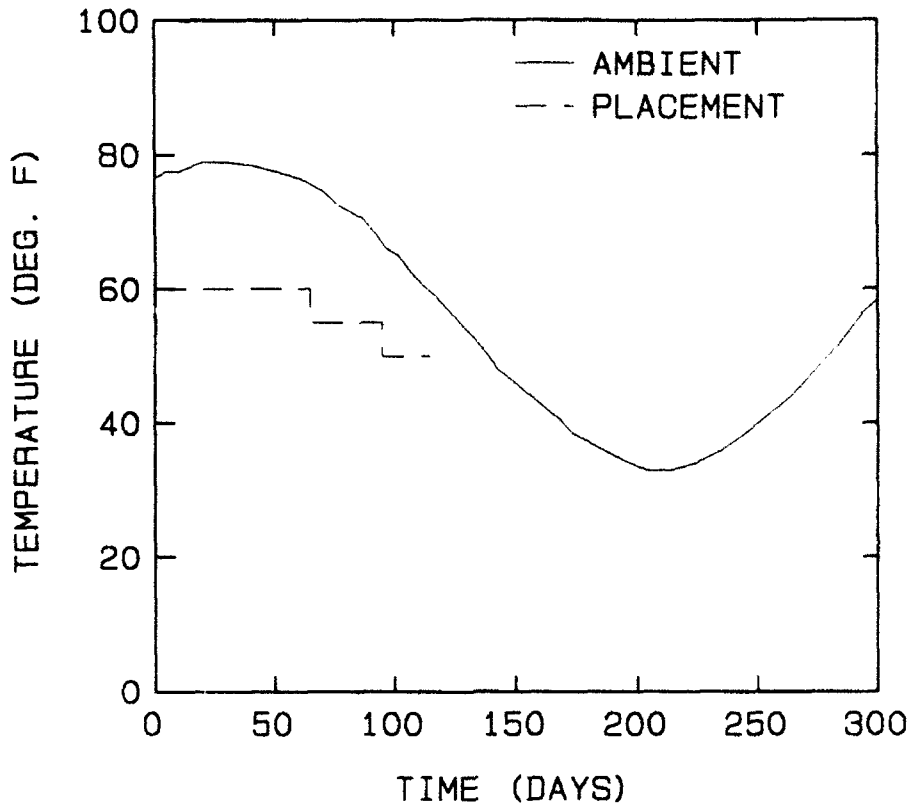

Figure 12. Placement and ambient temperatures

Thermal boundary conditions

53. The lower boundary of the foundation material at a depth of 20 ft was fixed at 57.2 °F which is the mean yearly temperature for the construction site. Temperature distribution in the soil up to the surface is dependent upon the air temperature-time history before construction begins. The initial vertical distribution of temperatures in the foundation was computed by exposing the foundation surface to 2 years of ambient temperature variation. Calculated temperatures from the surface downward at the selected construction start date computed in the second year were used as the starting foundation temperature distribution. This process accounts for the thermal momentum in the foundation and is the most realistic method for obtaining the starting temperatures.

54. No horizontal heat flow was permitted through vertical model boundaries at symmetric monolith center lines in 2-D analyses, at planes of symmetry in 3-D analyses, or through vertical soil boundaries.

55. All other heat flow from the surface is a function of the surface heat transfer coefficients which control heat exchange between the structure

or foundation and the ambient air. A film coefficient is used which is composed of a convection coefficient that defines heat exchange with surrounding air as a function of wind velocity and a conduction heat transfer coefficient which defines the heat flow through formwork and/or surface insulation. The following general equation is used to compute the composite film coefficient

$$h = \frac{1}{\frac{1}{h_{air}} + \frac{1}{C_{formwork}} + \frac{1}{C_{insulation}}}, \quad (Btu/ft^2\text{-}h\text{-}^\circ F) \tag{13}$$

where

h_{air} = convection coefficient

$C_{formwork}$ = conductance of formwork (when in use)

$C_{insulation}$ = conductance of insulation (when in use).

56. The surface conductance was computed by the following equation (Jurges 1924) for a wind velocity less than or equal to 16.5 ft/s and a surface with a rough texture

$$h_{air} = 1.086 + 0.225V \quad (Btu/ft^2\text{-}hr\text{-}^\circ F) \tag{14}$$

where V is wind velocity in ft/s.

57. Wind velocity for which the surface heat transfer coefficients are partially based were obtained from NOAA for Paducah, KY. It was observed that the mean wind velocity varies with season of the year; however, velocities are nearly constant over the summer and winter months with a transitional period during the spring and fall months. This pattern of wind velocities was selected to simplify the input of surface heat transfer coefficients during thermal analyses. Wind velocity data used are listed in Table 10.

Table 10

Mean Wind Velocity Used in Thermal Analyses

Time Period	Mean Wind Velocity mi/h	Mean Wind Velocity ft/s
June - September	5.30	7.777
October	6.80	9.974
November - April	9.43	13.831
May	6.50	9.534

58. Formwork was assumed to be 0.75-in. plywood with a conductance of 1.07 Btu/ft^2-h-°F. For temperature calculations when insulation may be simulated, a conductance of 0.37 Btu/ft^2-h-°F (R value = 2.7 h-ft^2-°F/Btu) was used. Vertical formwork was assumed to be removed 2 days after placement of a lift. Horizontal formwork as used in ceilings of culverts was removed 5 days after concrete placement. The surfaces of culverts were assumed to be exposed to the same wind velocity as other exterior surfaces, although, guide specification requires that the culverts be closed during construction. This variation provides a "worst case" condition for stresses in the walls. Table 11 shows the values used for surface heat transfer film coefficients given the variation in wind velocities presented earlier.

Table 11

Surface Heat Transfer Film Coefficients Used in Thermal Analyses

Time Period	Mean Wind Velocity mi/hr	Mean Wind Velocity ft/s	Film Coefficient, h, Btu/day-in^2-°F Wind Only	Wind + Forms**	Wind + Insul.†	Wind+Form +Insul.
June - Sept	5.30	7.777	0.4727	0.1295	NA	NA
Oct	6.80	9.974	0.5552	0.1350	NA	NA
Nov-April	9.43	13.831	0.6998	0.1421	0.05672	0.04305
May	6.50	9.534	0.5387	0.1340	NA	NA

Note: NA indicates not applicable.
* h_{wind} = 1.086 + 0.255 V; Wind velocity, V on ft/s; h in Btu/h-ft^2-°F.
** Forms = 3/4-in. fir plywood; Conductance, C = 1.07 Btu/h-ft^2-°F.
† Insulation = 3/4-in. blanket; Resistance, R = 2.7 h-ft^2 -°F/Btu, for C = 0.37 Btu/h-ft^2-°F.

Boundary conditions for stress analyses

59. For the stress analyses, no elements were included to model the soil. The finite element grids were supported at their axis of symmetry with rollers and at the base with vertical and lateral springs applied at the corner and midside nodes.

60. The pile layout for both placement schemes, shown in Figure 13, was generated from information provided by the USAED, Louisville. All piles are HP 14 by 117, 708 in. in length, and are vertically oriented. Battered piles in previous preliminary plans were deleted and new equally spaced piles, 75 in. in the transverse and longitudinal directions, were provided.

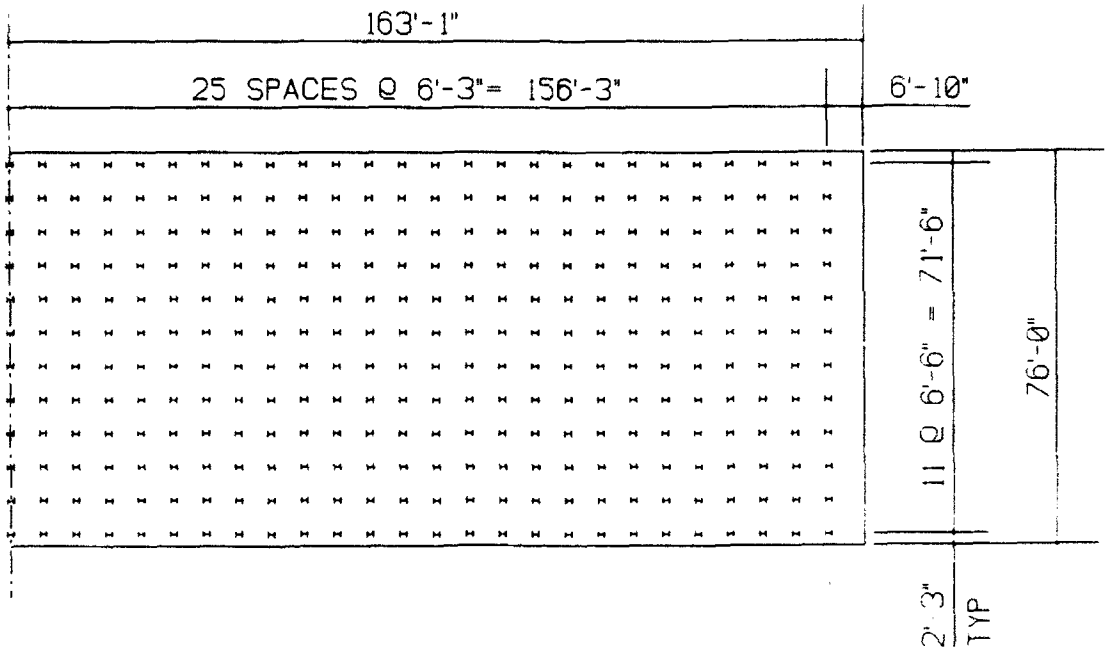

Figure 13. Typical lock monolith pile layout

61. For the 2-D models, the pile stiffness must be modified to represent the average stiffness of each row of piles parallel to the flow axis per inch thickness into the model. Based on pile tests conducted at the site and experience, the vertical pile stiffness was calculated using $k = 1.25(AE)/L$. This resulted in a stiffness of 1,761,300 lb/in./pile. This stiffness was then modified by dividing it by the pile spacing in the transverse direction (75 in.) to obtain 23,500 lb/in./in., which is the average stiffness of each pile row transverse to the flow axis.

62. The lateral pile stiffness is more difficult to obtain and is highly dependent on the soil surrounding the pile, especially the upper 10 ft. Two typical soil profiles, Figures 14 and 15, were developed from boring logs along the center line of the lock structure. These profiles were used as input for the COM624G computer program (1984) which automatically generated the pile p-y curve for each soil profile. Experience and previous studies have shown that pile stiffness for strong soil pile support induces higher

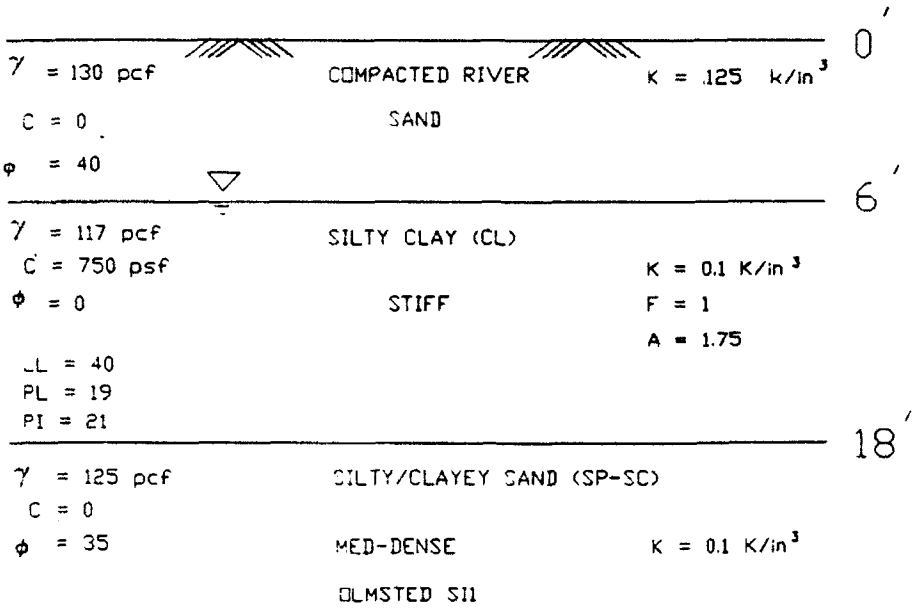

Figure 14. Lock soil profile 1

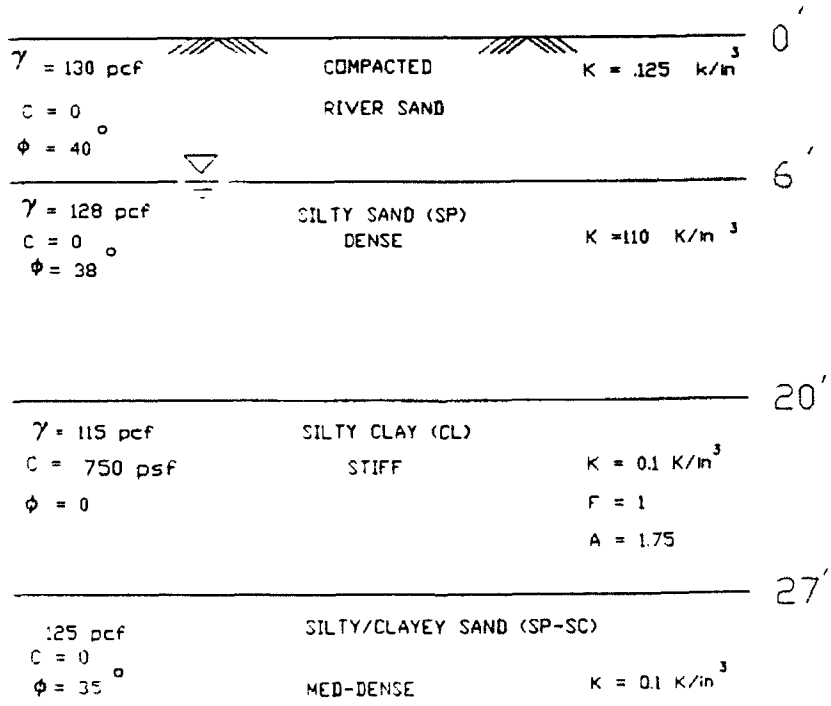

Figure 15. Lock soil profile 2

stresses in the structure. Therefore, soil profile 2 was used since it showed the least displacement for a given load. The soil profile 2 p-y curve was then modified, using the same procedure as the vertical pile stiffness, to obtain the average lateral stiffness of each row of piles parallel to the flow axis. Lateral pile stiffness, unlike vertical pile stiffness, is affected by

pile group behavior. Since the pile spacing was approximately five times the pile section depth, 75 in. versus 14.4 in., guidance contained in TR K-83-1, "Basic Pile Group Behavior," (CASE Task Group On Pile Foundations 1983), recommends a pile group reduction factor of 0.55. This factor was then applied to the average pile lateral stiffness. The maximum displacement for these types of two-dimensional analyses are normally on the order of 0.2 in. Since the p-y curve is nearly linear in this range of displacements, the nonlinear lateral pile stiffness was replaced using a linear spring based on 0.2 in. of displacement. Similar approximations were used in the Lock and Dam 26R study (Bombich, Norman, and Jones 1987).

63. Pile stiffness calculations and computer analysis results are provided in Appendix A.

64. In addition to the vertical support provided by the piles, a vertical soil stiffness of 300 psi per inch was applied at all nodes located along the base of the models. This is a fairly low value for a well-compacted sand (Hough 1969). Although soil support is normally neglected in pile design, including some support from the soil is a more realistic condition for a finite element analysis. These additional spring supports are especially important during the early phases of construction when the concrete still has a fairly low modulus and is primarily supported by the soil. This additional support should be adequate to support the dead load of the concrete. Therefore, since vertical stresses in a floor are normally extremely small in a thermal stress analysis, and little lateral restraint is offered by the piles, small changes in pile spacing should have little effect on stresses calculated in the analyses.

65. At times prior to the removal of formwork, gravity loads were represented by an equivalent uniform pressure loading placed on the existing concrete of previous lifts. Gravity loads, in the form of body forces in the newly placed concrete, replaced this uniform pressure representation 2 days after placement for most lifts and 5 days after placement for lifts containing roof sections. This was done to allow the newly placed concrete sufficient time to gain strength to resist the body force applied gravity load without cracking. In lifts spanning openings, the initial pressure loading was applied to the existing concrete using tributary area.

Heat Transfer Analyses

General

66. The results of the analyses are discussed in terms of maximum temperatures and temperature differentials across an entire section corresponding to an absolute time, with respect to the start of construction. Although temperature differentials are convenient for quantifying the results of heat transfer analyses, they are not the only important factor for the development of stresses and cracking. Monolith geometry, boundary conditions, shrinkage, and the mechanical properties of the concrete also affect stresses developed during construction.

67. Four sections, shown in Figure 16, were used to compare temperature differences between analyses in the XY plane. In addition, mixture 11 considered three sections, shown in Figure 17, to compare temperatures across the floor in the out-of-plane analyses.

Mixture 11 analyses

68. A summary of all 2-D heat transfer analyses using the mixture 11 properties is given in Table 12. The XY and ZY planes are oriented as shown in Figures 16 and 17. Unless otherwise noted, contour plots just prior to the placement of each new lift are presented in Appendix B. Current ambient temperature is given on each plot for reference.

69. Strip placement analysis 1 (OMSTDT1). The temperature contour plots included in Appendix B indicate that heat flow throughout most of the floor was 1-D as expected. This means that temperatures at a given time and elevation were constant for the width of the floor.

70. A plot of nodal temperatures across section 3 is shown in Figure 18. The maximum temperature in the floor occurred in lift 3 and was approximately 92 °F. This temperature rise of 32 °F was reached at 9 days after placement. The maximum temperature differential in the entire floor was 26 °F and occurred at 200 days after the start of construction. Until that time, temperatures at the base of the structure decreased very slowly, while temperatures closer to the upper floor surface tended to decrease with ambient temperature. At approximately 200 days the yearly low was reached, and ambient temperature began to increase, decreasing the temperature differential. The maximum temperature at section 4 (see Figure 19) was 88 °F and was reached at approximately 9 days after placement of lift 12. For the first 30 days after placement, temperatures throughout section 4 were affected by the

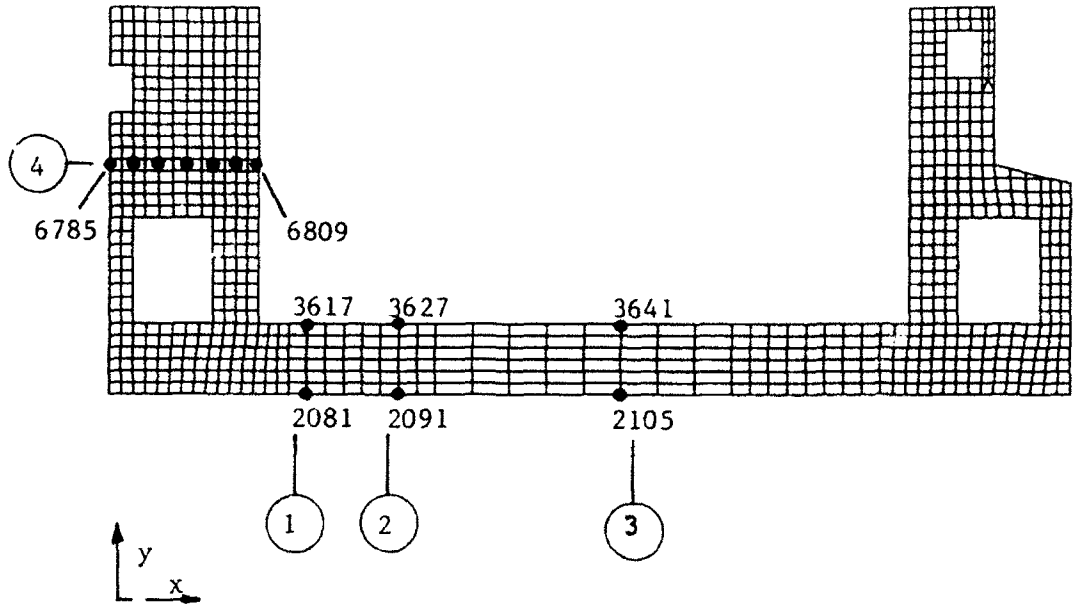

Figure 16. Nodes and sections for 2-D temperature versus time plots

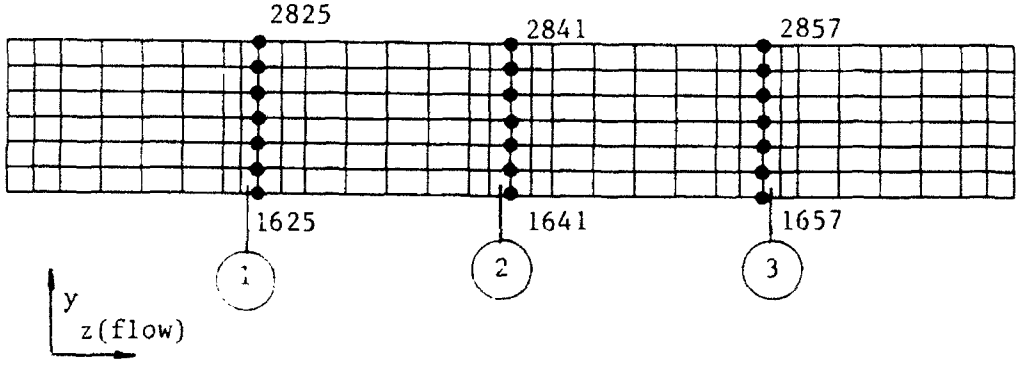

Figure 17. Nodes and sections for 2-D out-of-plane temperature versus time plots

Table 12

Summary of 2-D Heat Transfer Analyses for Mixture 11

Name	Mixture	Notes
OMSTDT1	11	Strip placement, 60 °F placement in floor, walls varying from 60 to 50 °F, XY plane
OMSTDT2	11	Strip placement, 60 °F placement throughout, XY plane
OMSTDT4	11	Block placement, 60 °F placement in floor, walls varying from 60 to 50 °F, XY plane
OMSTDT5	11	Strip placement, floor only 60 °F placement, ZY plane

placement of subsequent lifts. After that time temperatures across section 4 tended to decrease at about the same rate, and a constant differential of roughly 21 °F was maintained until the average daily ambient temperature began to rise. Temperatures in the relatively thin culvert walls became fairly uniform and approached ambient temperature shortly after placement.

71. Strip placement analysis 2 (OMSTDT2). The increase in placement temperature in the walls resulted in a maximum temperature difference in the center of section 4 at node 6785 of only 3 °F (Figure 20). Temperature differentials in the OMSTDT2 analysis were slightly greater than those in the OMSTDT1 analysis until approximately 200 days. Temperatures and temperature differentials were similar in the two analyses after 200 days.

72. Block placement analysis 3 (OMSTDT4). Even though heat flow was 1-D throughout most of the floor, temperatures varied slightly across the floor at any given elevation due to the placement scheme.

73. The maximum temperature in the floor was 96.8 °F and occurred 4 days after the placement of lift 4, resulting in a temperature differential of 15 °F across the top lift. Even though maximum temperature was higher in the OMSTDT4 than in the OMSTDT1 analysis, this was a short-lived phenomenon. The high interior temperature was reduced quickly at early times by conduction of cooler temperatures from both the base and the surface. As can be seen in Figure 21, after 50 days temperature differentials in the strip and block analyses were similar. The maximum temperature differential was 27 °F at

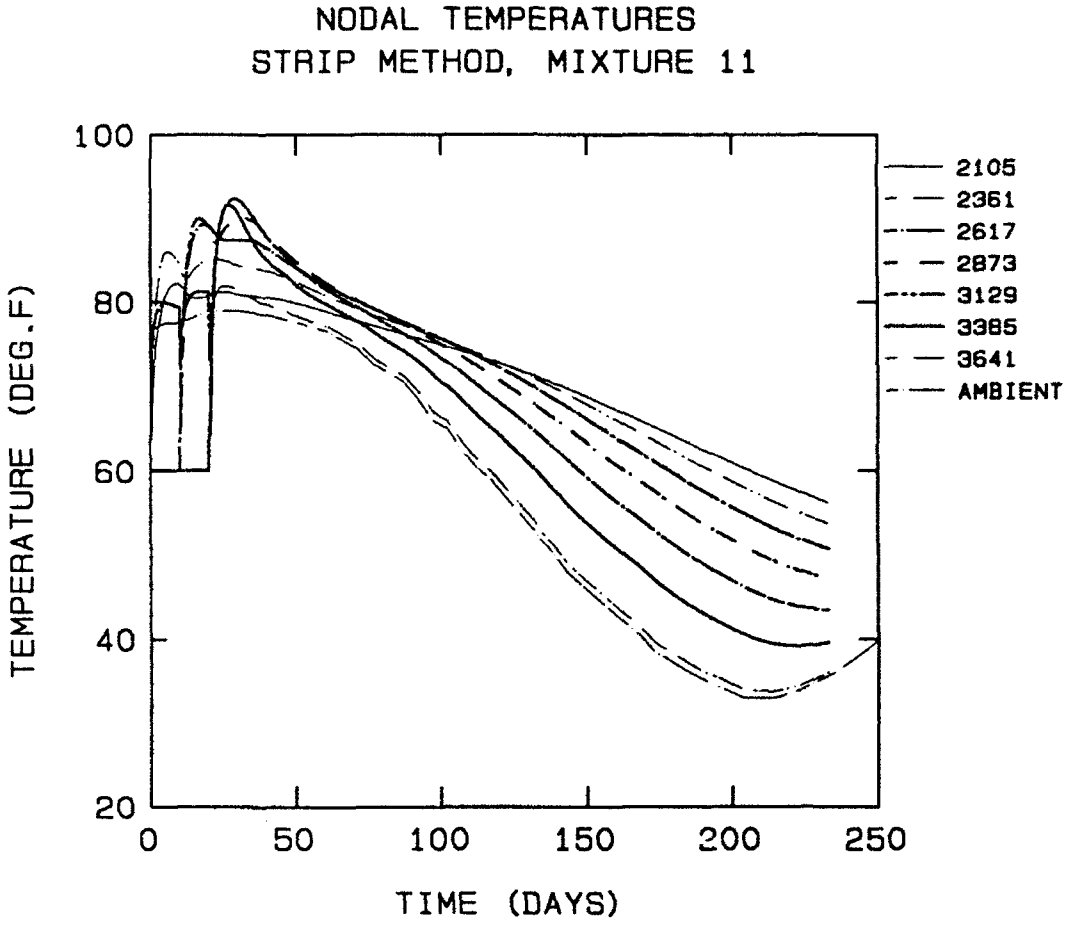

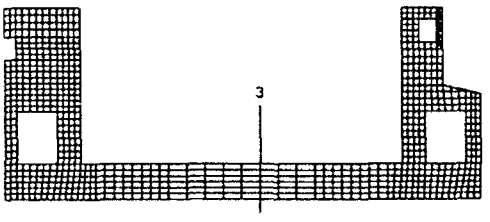

Figure 18. Nodal temperatures at section 3, OMSTDT1

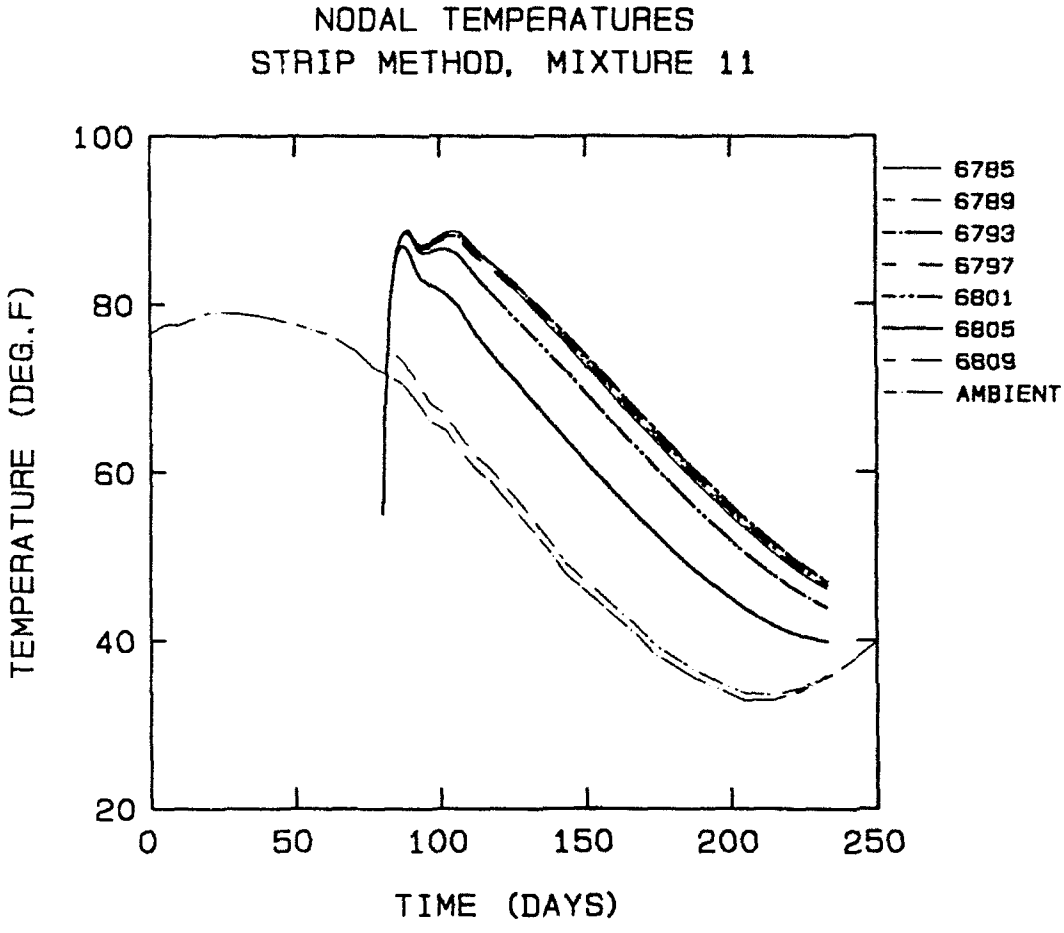

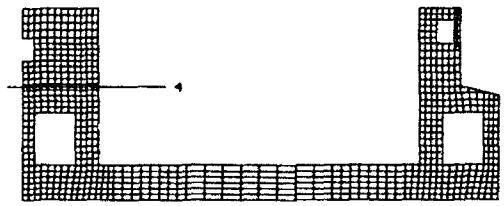

Figure 19. Nodal temperatures at section 4, OMSTDT1

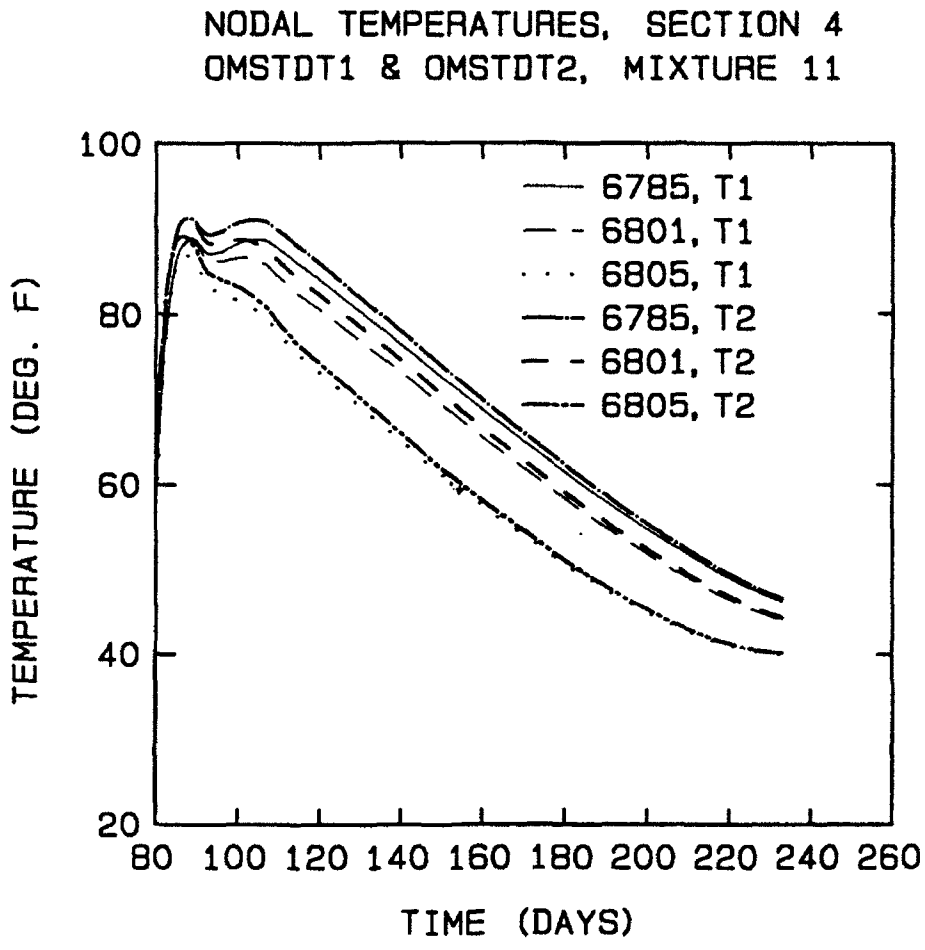

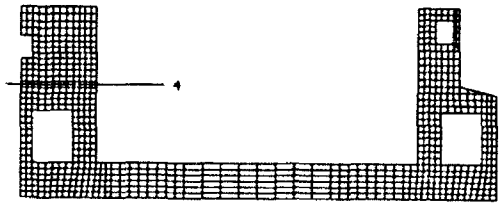

Figure 20. Nodal temperatures at section 4, OMSTDT1 and OMSTDT2

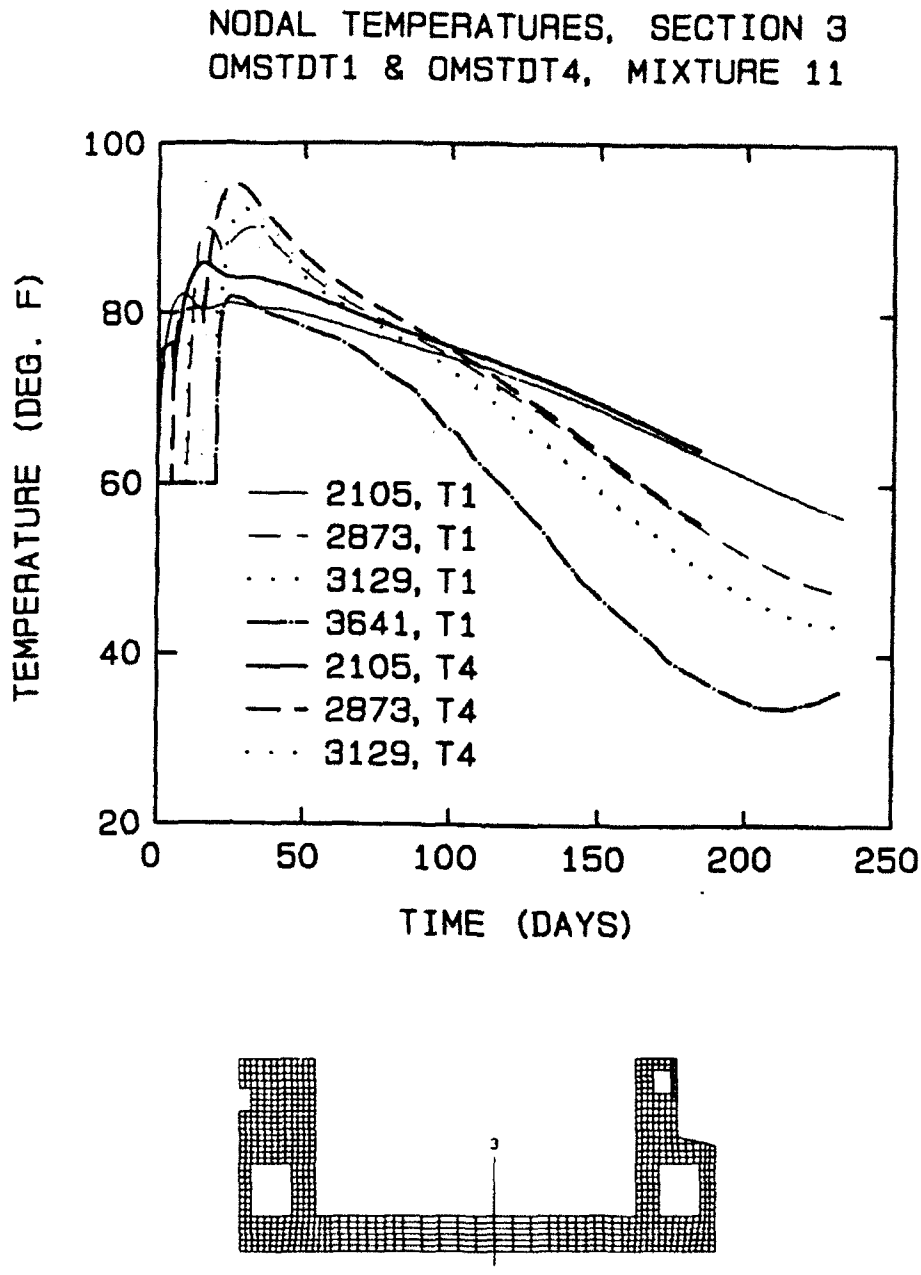

Figure 21. Nodal temperatures at section 3, OMSTDT1 and OMSTDT4

200 days. Wall temperatures varied slightly from those in the OMSTDT1 analysis due to the exclusion of interface elements. Very small differences in temperatures at the interface between lifts 10 and 12 in the two analyses can be seen in Figures 22 and 23. Temperatures across sections 1 through 4 are plotted against ambient temperatures in Figures 24 through 26.

74. Strip placement analysis 3 (OMSTDT5). Heat flow within each lift was 1-D except near vertical lift interfaces and vertical exterior faces. However, because of the placement scheme, temperatures at a given elevation across the structure did not become uniform until almost 50 days after the start of placement. The maximum temperature occurred at the interface between lifts 3 and 6 and was 93.2 °F. The maximum temperature differential across the sections presented in Figures 27 through 29 was 27 °F at 200 days after the start of placement. This differential results when the concrete temperature at the surface is exposed to ambient temperatures dropping at a faster rate than temperatures in the interior of the slab. This can seen from the relative steepness of the slope of the temperature time history curves, Figures 27 through 29, for the surface compared to those for the interior and base.

Mixture 6 analyses

75. Heat transfer analyses were performed using mixture 6 properties for both the strip placement method and the block placement method. For both methods, a 60 °F placement temperature was used throughout the slab and the wall placement temperatures varied from 50 °F to 60 °F. Temperature contours are shown in Appendix C.

76. Strip placement method. Temperature contour plots show the direction of heat flow was predominantly vertical, except near the edges. This is reflected by the near horizontal temperature contours in the slab shown in Appendix C. The maximum temperature in the slab was approximately 90 °F and occurred at the interface of lifts 2 and 3 at 28 days for section 3. The minimum temperature was approximately 33 °F at 214 days, and the maximum late time temperature differential in section 3 was 23 °F at 20 days. The nodal temperature versus time plot for section 3, Figure 30, shows that after about 20 days, the concrete temperature becomes more dependent on the ambient temperature than that temperature produced by hydration. This is reflected in the temperature curves tending to parallel the ambient temperature curve with only a slight phase shift.

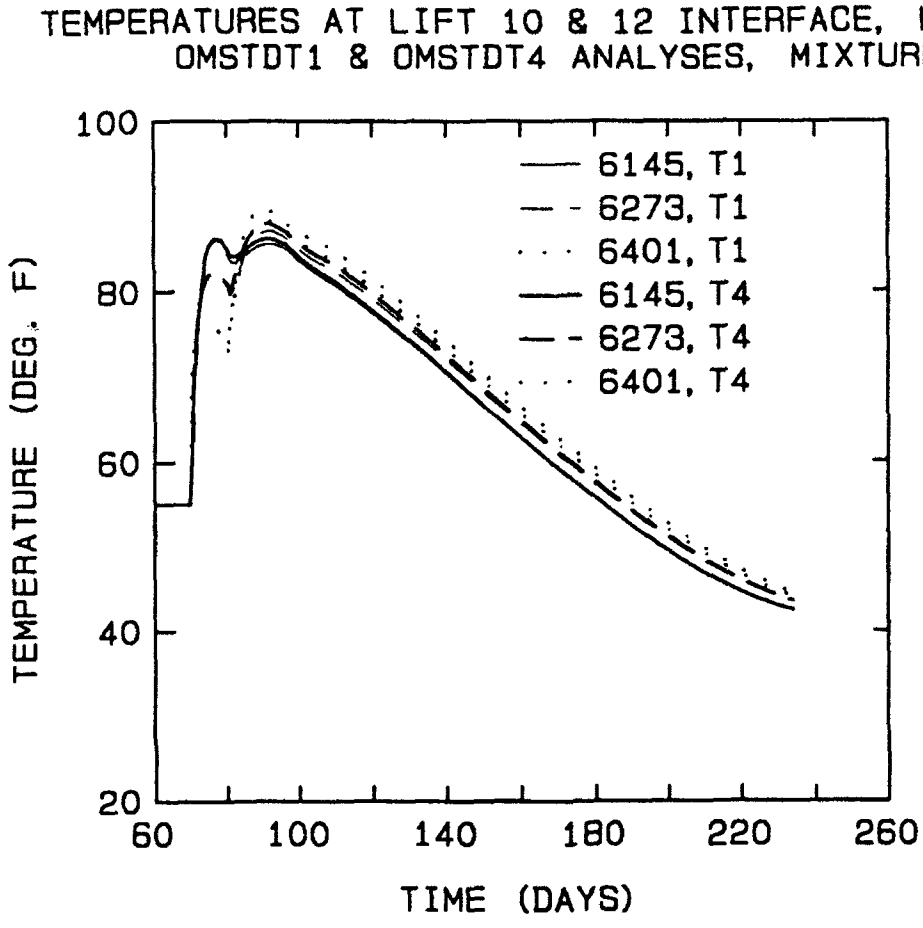

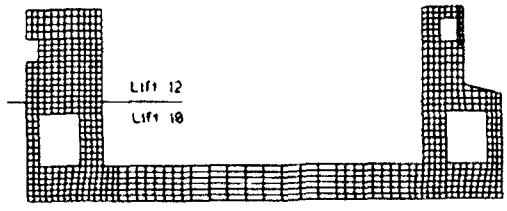

Figure 22. Nodal temperatures at lift 10 & 12 interface, OMSTDT1 and OMSTDT4

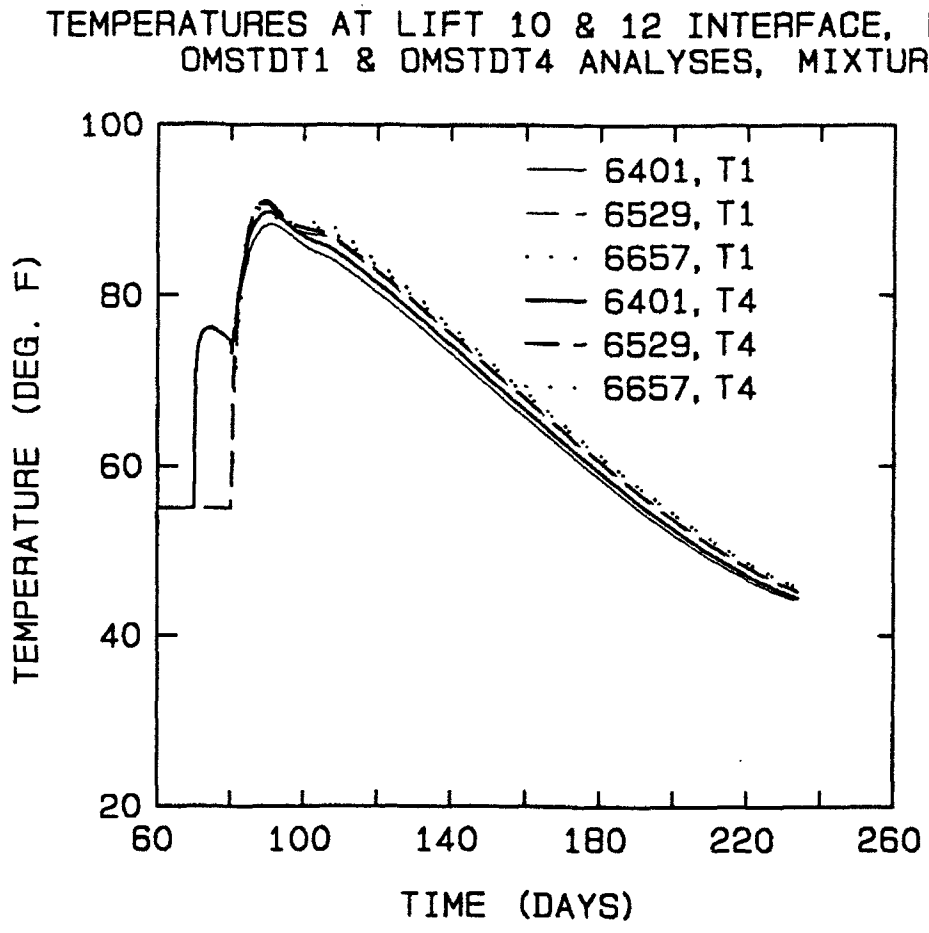

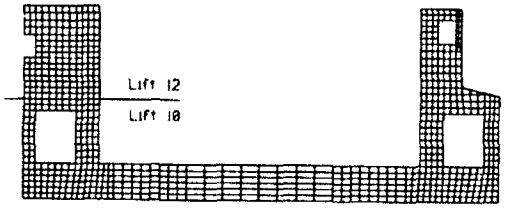

Figure 23. Nodal temperatures at lift 10 & 12 interface, OMSTDT1 and OMSTDT4

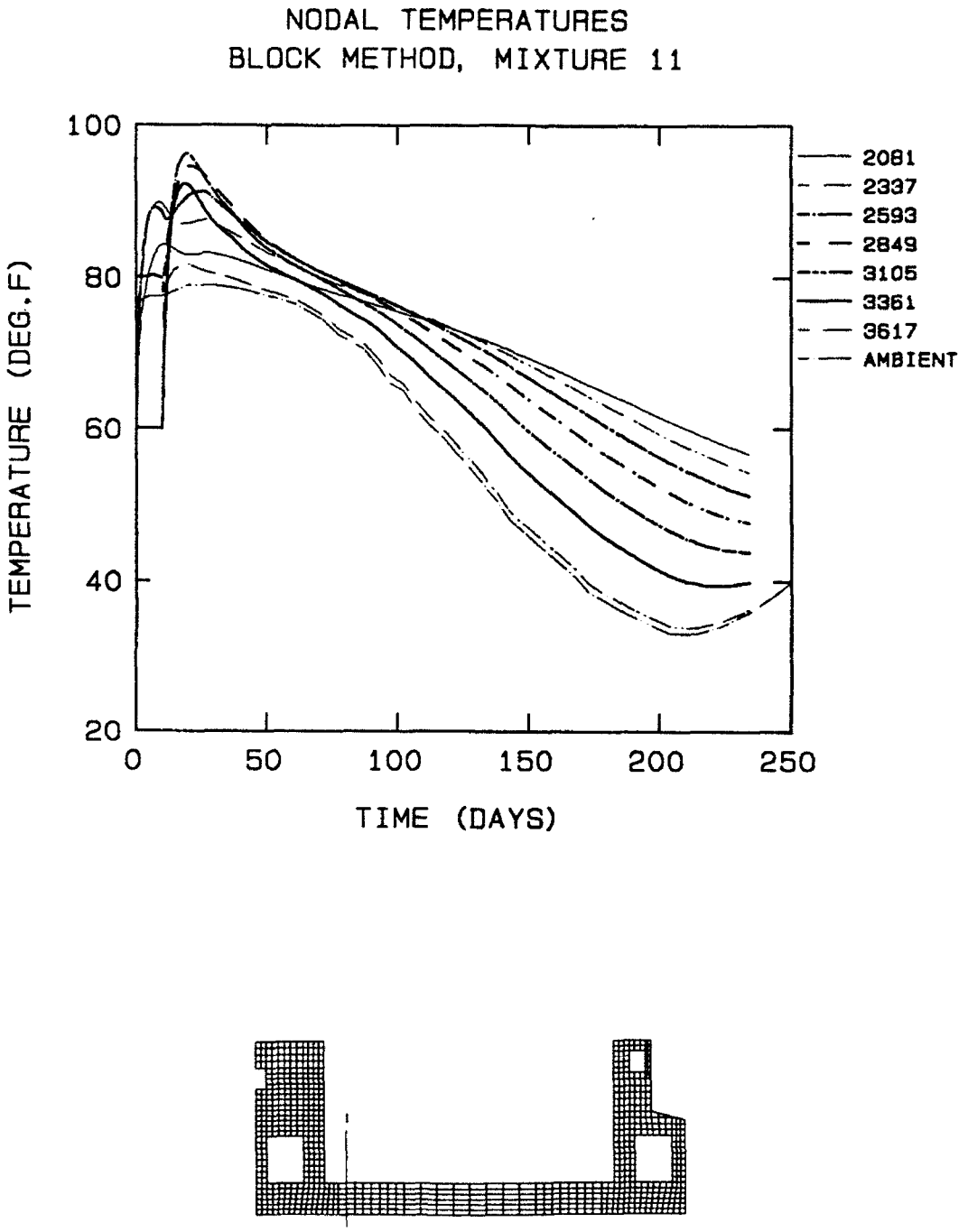

Figure 24. Nodal temperatures at section 1, OMSTDT4

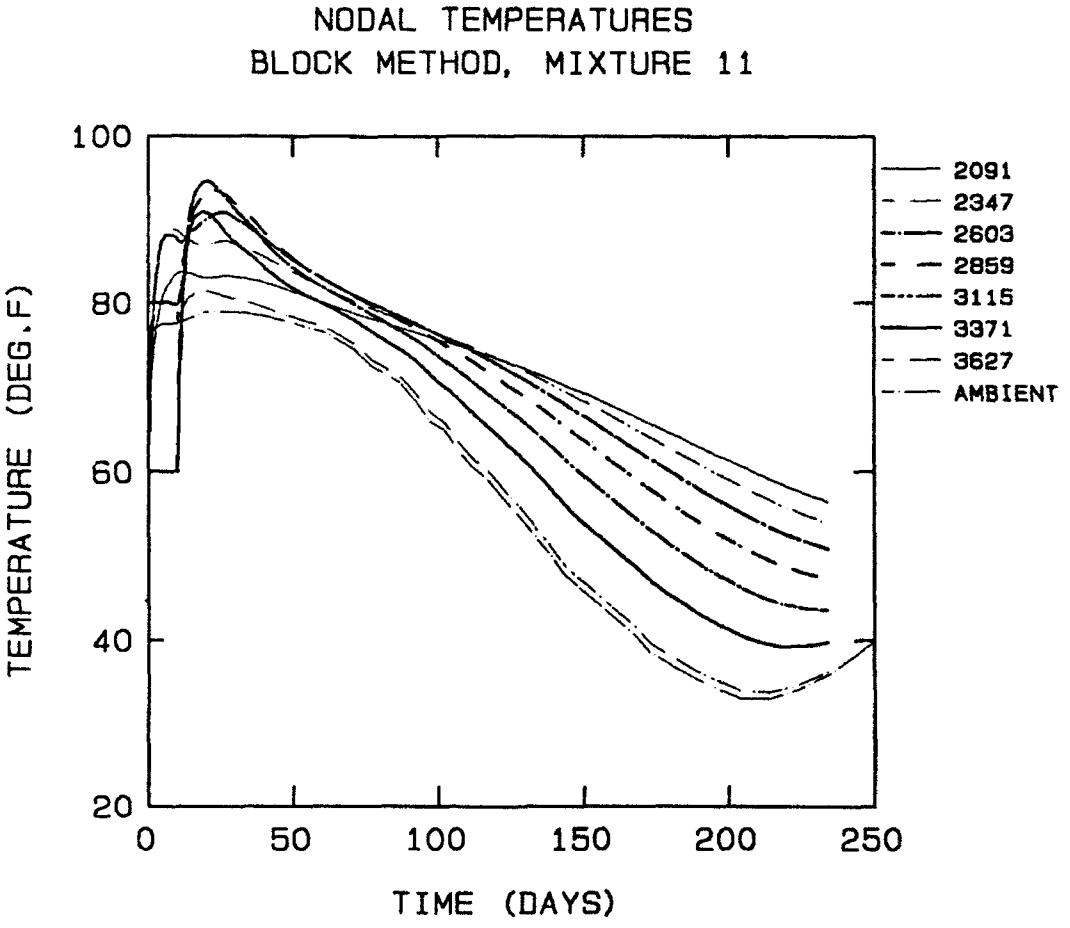

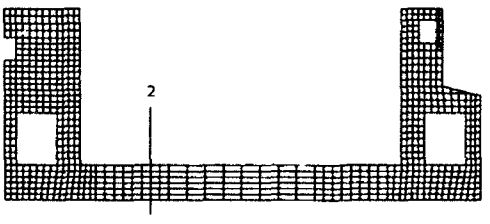

Figure 25. Nodal temperatures at section 2, OMSTDT4

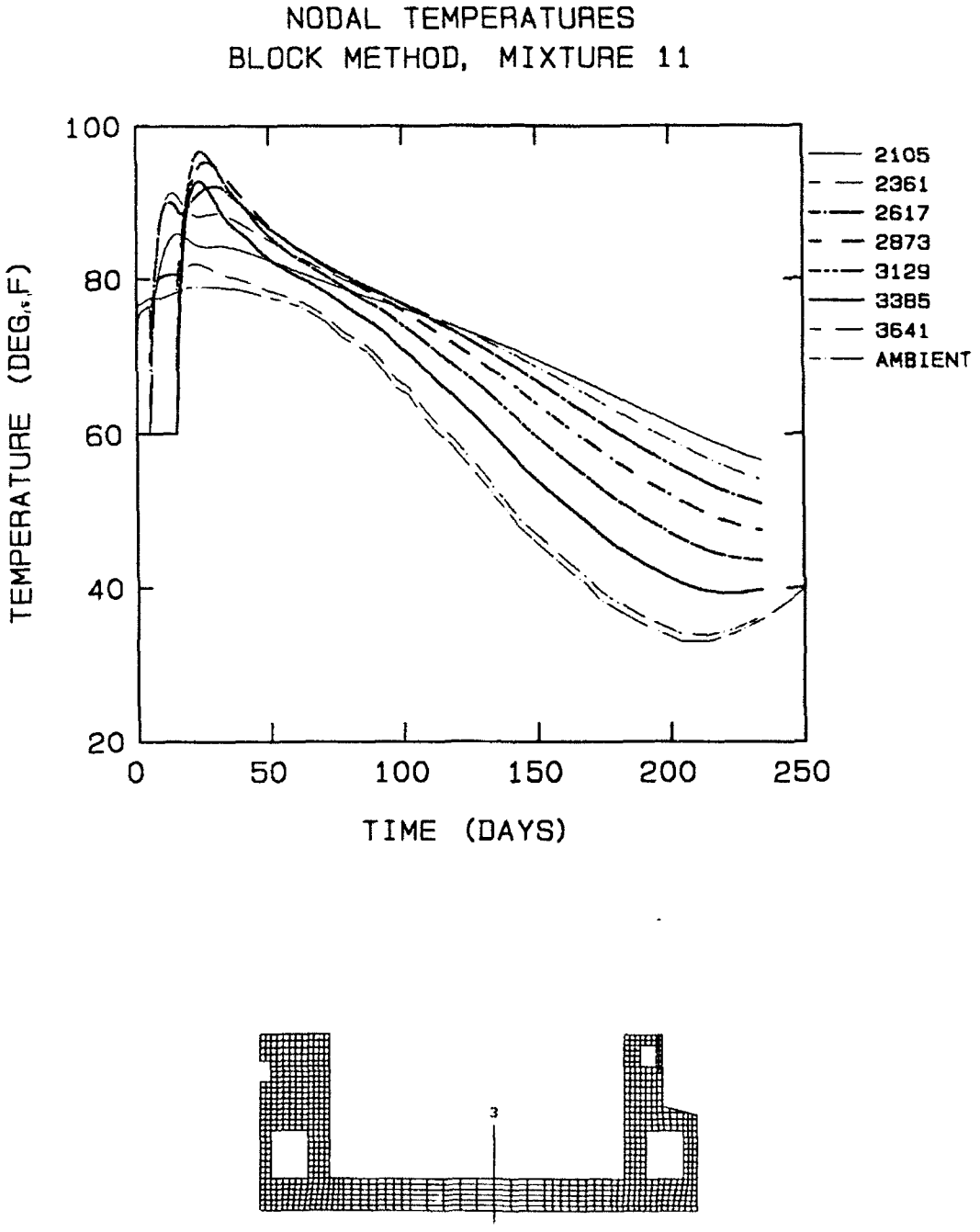

Figure 26. Nodal temperatures at section 3, OMSTDT4

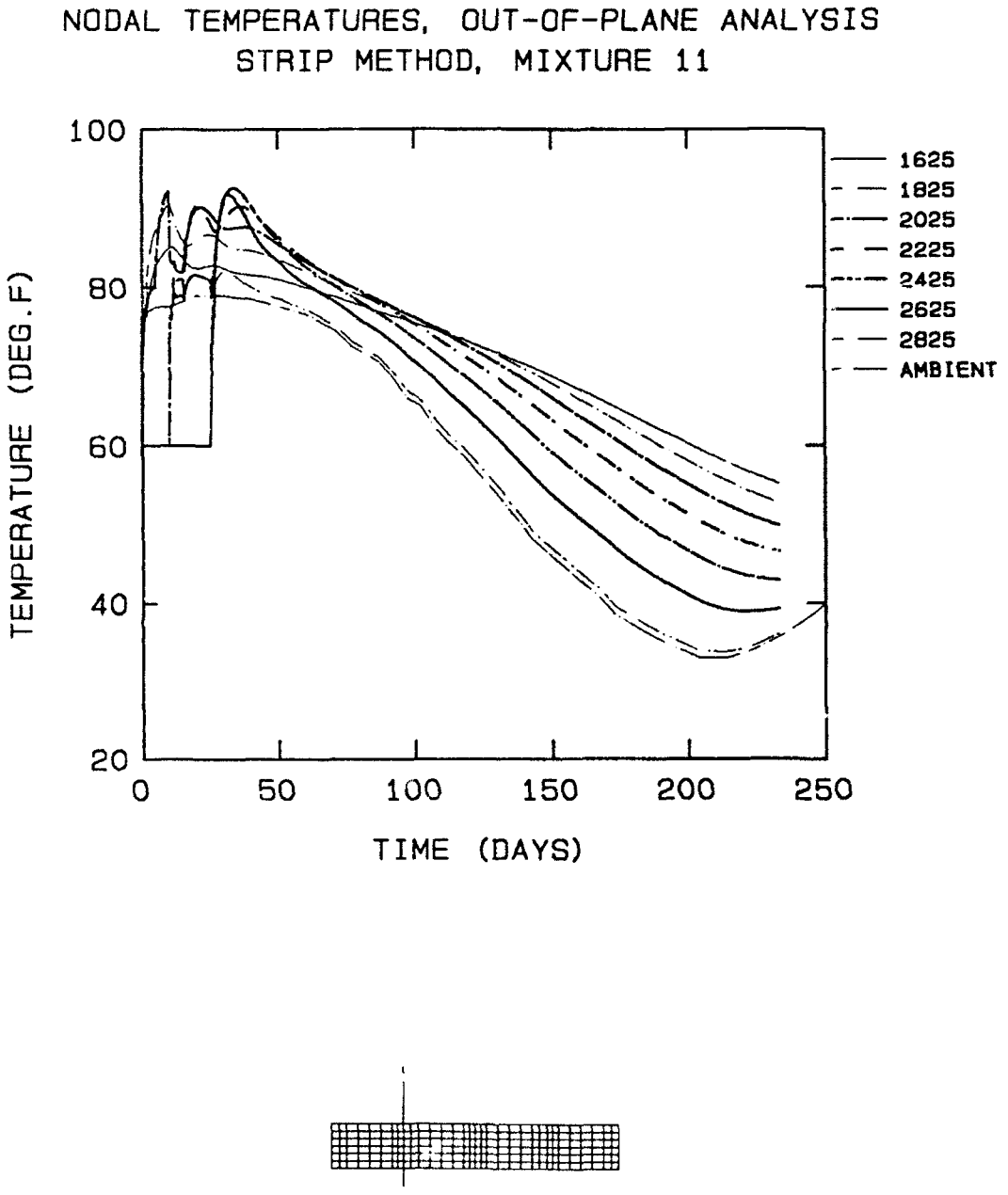

Figure 27. Nodal temperatures at section 1, OMSTDT5

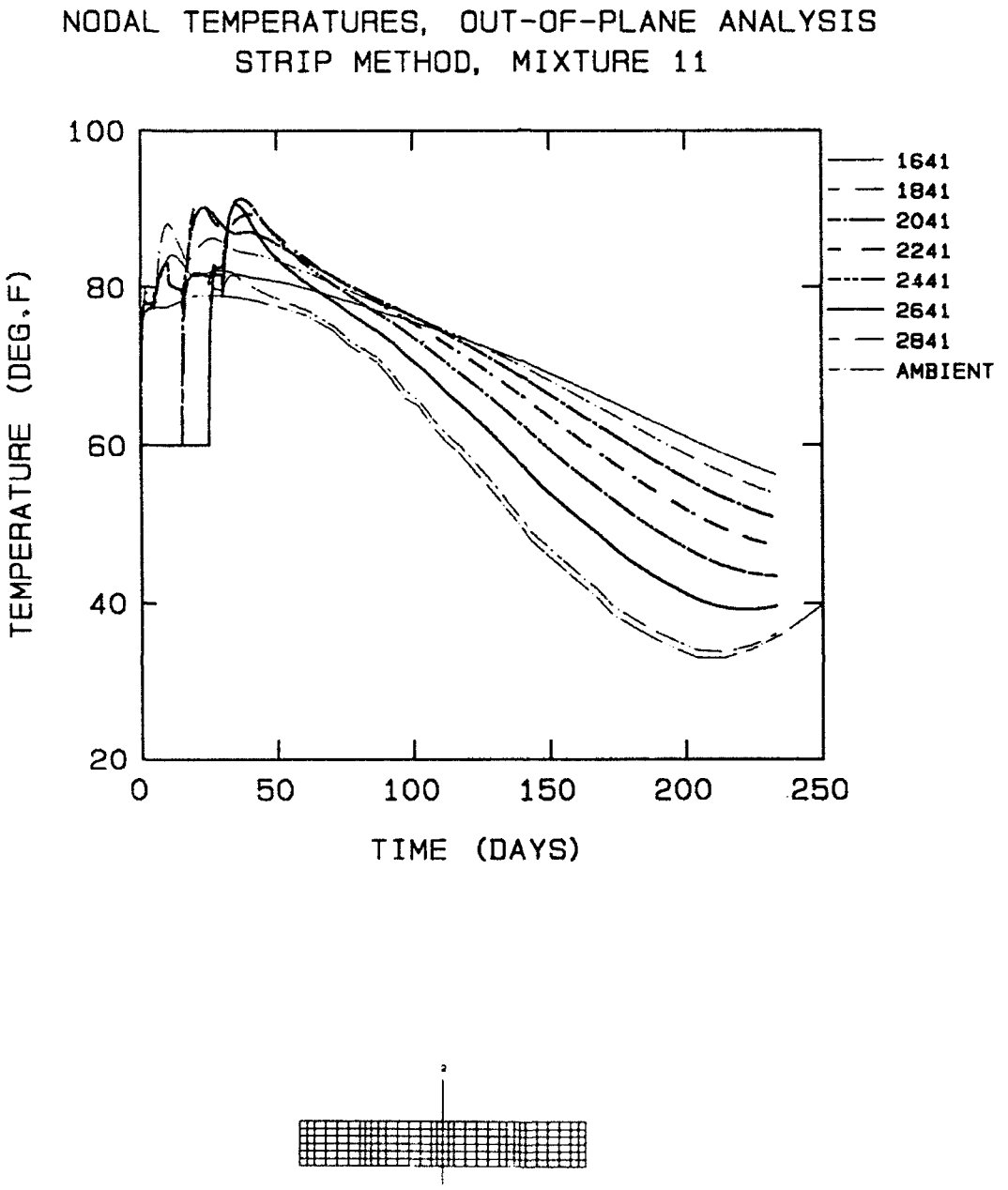

Figure 28. Nodal temperatures at section 2, OMSTDT5

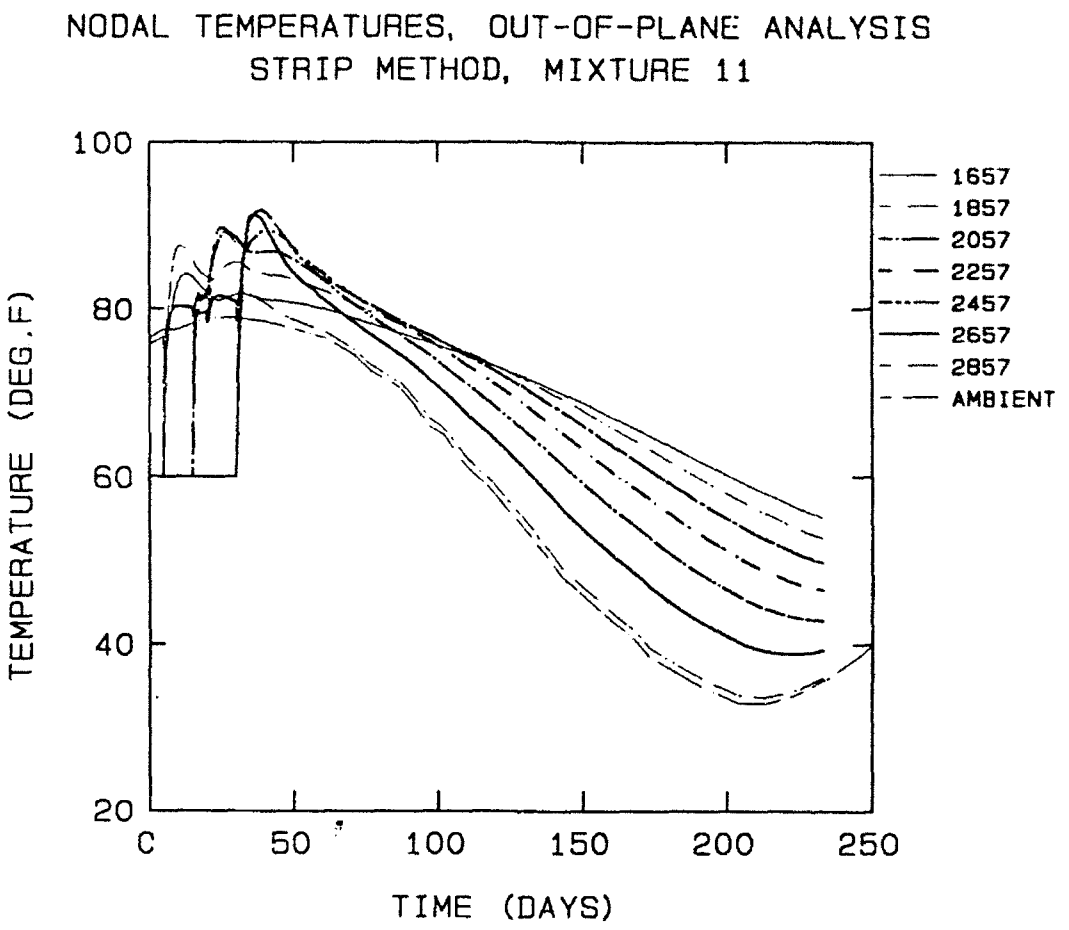

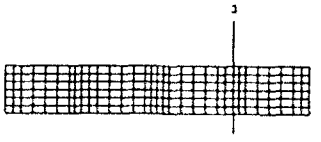

Figure 29. Nodal temperatures at section 3, OMSTDT5

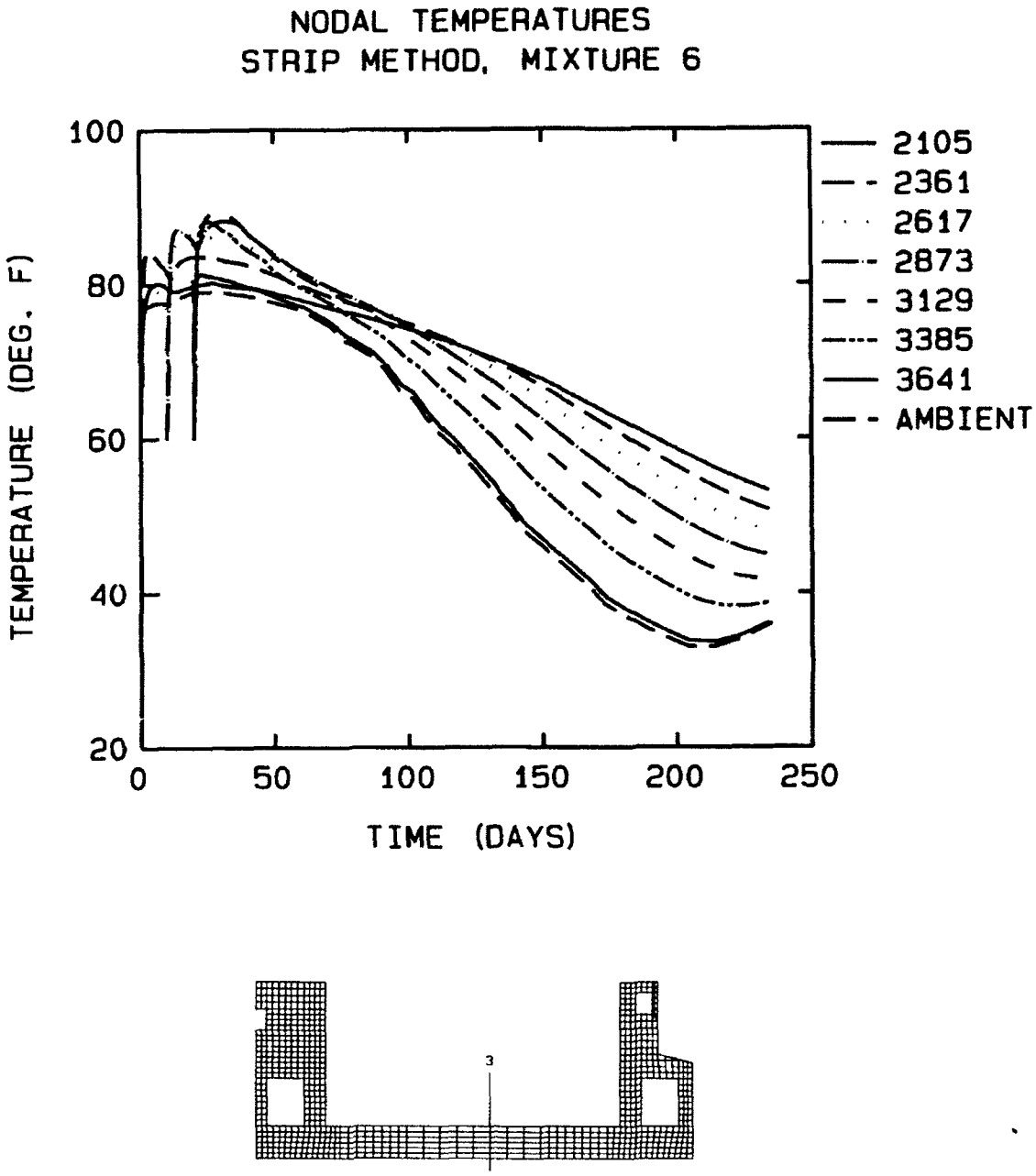

Figure 30. Nodal temperatures at section 3, mixture 6, strip method

77. For section 4 in the center wall, the maximum temperature was approximately 85 °F occurring at 76 days. The minimum temperature was approximately 33 °F at 214 days, and the maximum late time temperature differential was 9 °F at 214 days. Again, the nodal temperature versus time plot, Figures 31 and 32, for section 4 shows that after the initial heat of hydration temperature rise, the ambient temperature begins to predominantly influence the concrete temperatures.

78. Block placement method. Temperatures in the slab are somewhat higher than those predicted in the strip method due to the increased size of the lifts, but the same trend of vertical heat flow is observed except near the ends of the lifts (Appendix C). The maximum temperature along section 3 was near 95 °F at 24 days. The minimum temperature was near 34 °F at 214 days, and the maximum late time temperature differential was 26 °F at 214 days. The nodal temperature versus time plot, Figure 33, is similar to that for the strip placement method except for the higher temperatures due to the thicker lifts.

79. The center wall at section 4 had a somewhat higher maximum temperature, near 90 °F, than that for the strip method. This was due to effects resulting from different lift modeling techniques. The minimum temperature was near 34 °F at 214 days and the maximum late time temperature differential was 8 °F at 214 days. Figures 34 and 35 show the nodal temperature versus time plots for section 4. The same trend of paralleling the ambient temperature after the initial heat rise is also apparent in these curves.

3-D analysis

80. The quarter symmetrical 3-D grid (block construction method) is shown in Figure 36 with the planes of symmetry indicated. In the plane of symmetry transverse to the axis of flow, no heat flow parallel to the axis of flow is allowed. Because of the length of the monolith, no heat flow occurs normal to that plane. This is the same condition that exists in a 2-D analysis, i.e. heat flow in only the x and y directions. This means that predicted temperatures at the transverse center plane of the 3-D model should be the same as those in a 2-D analysis of the structure under the same conditions. Nodes located at sections 1 through 4 along this plane are indicated in Figure 36. Temperatures at these nodes are plotted versus ambient temperatures in Figures 37 through 40. As can be seen in the plots, after reaching some initial peak temperatures, all points through the thickness of the slab

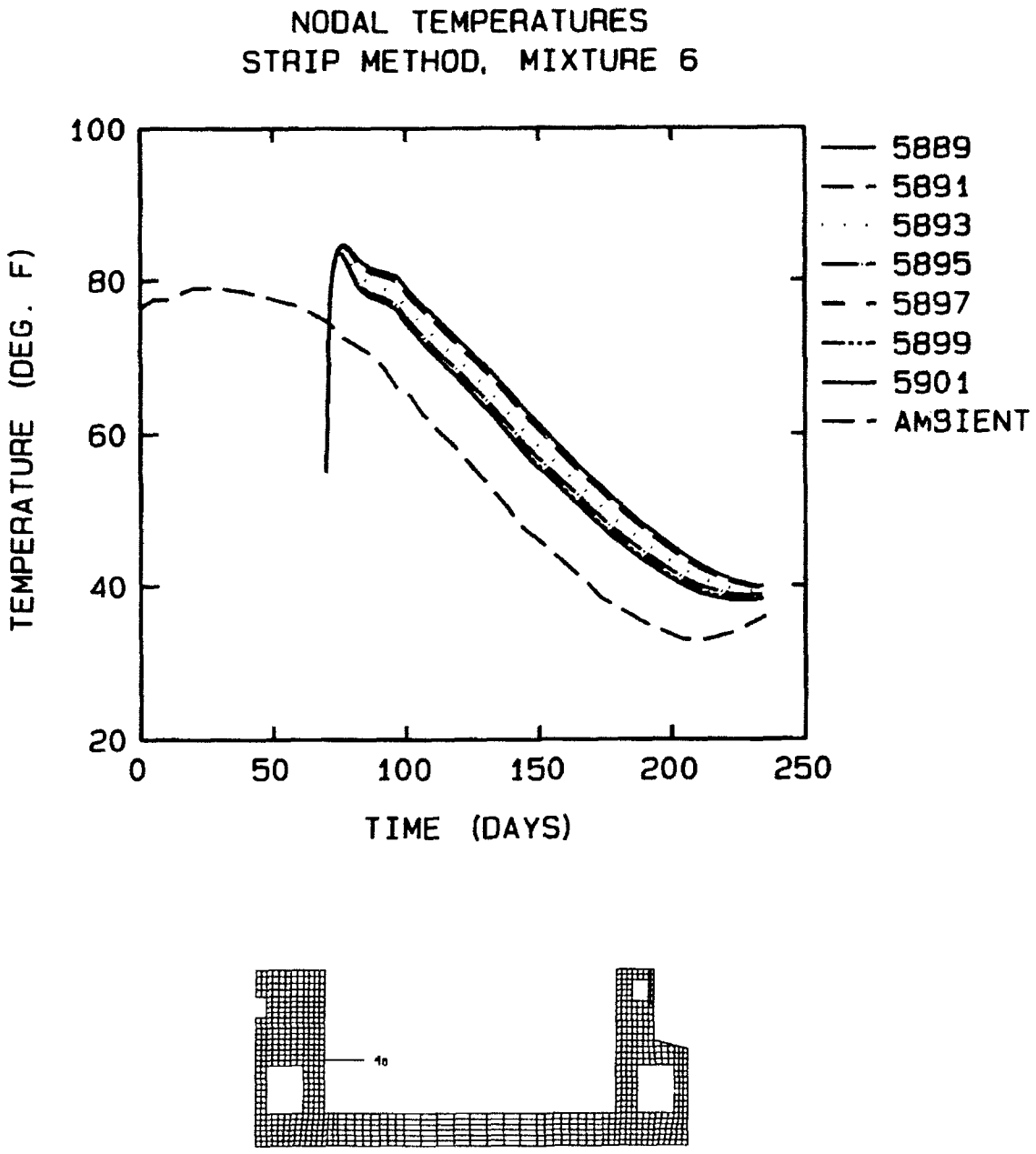

Figure 31. Nodal temperature at section 4a, mixture 6, strip method

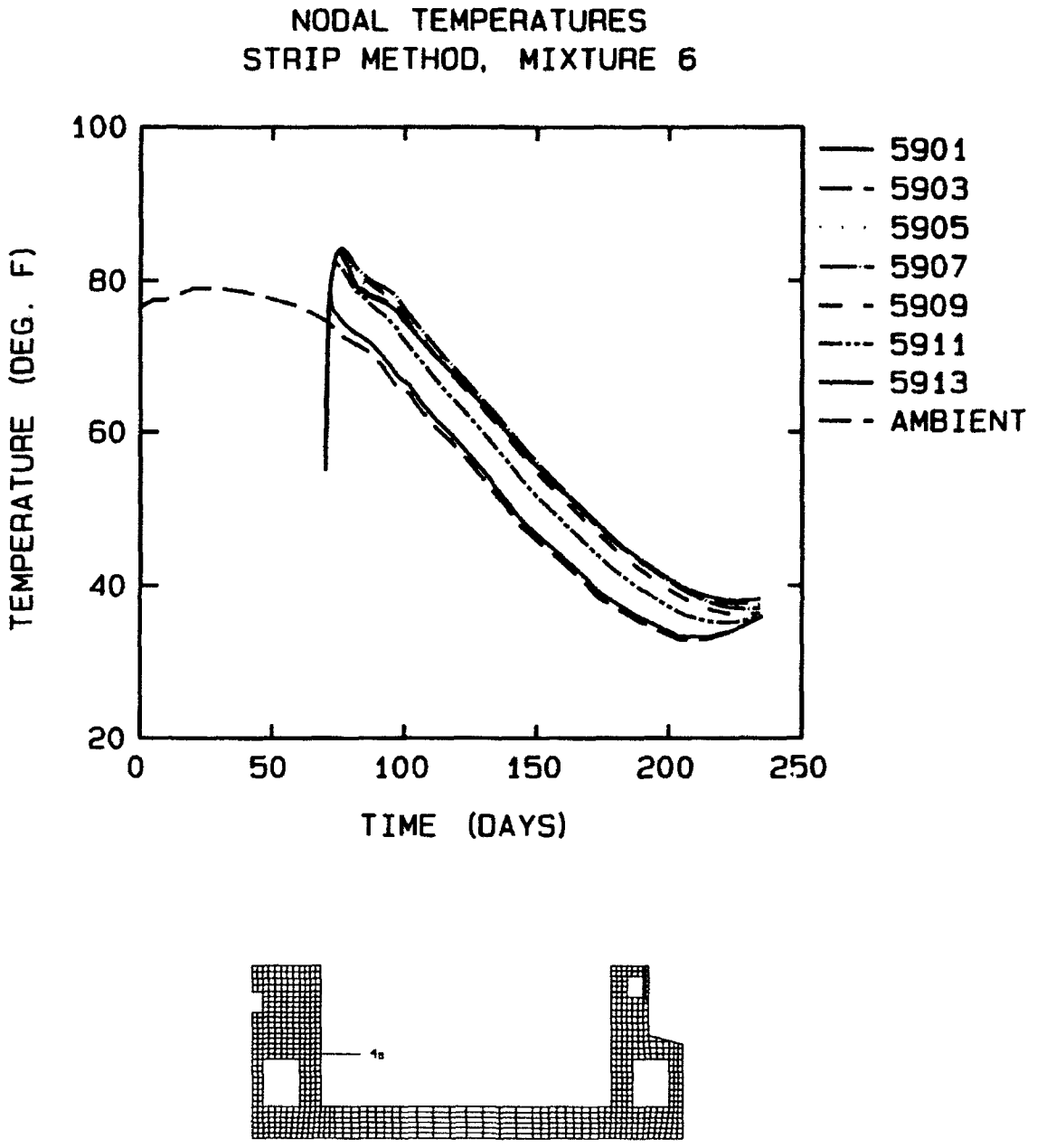

Figure 32. Nodal temperatures at section 4a, mixture 6, strip method

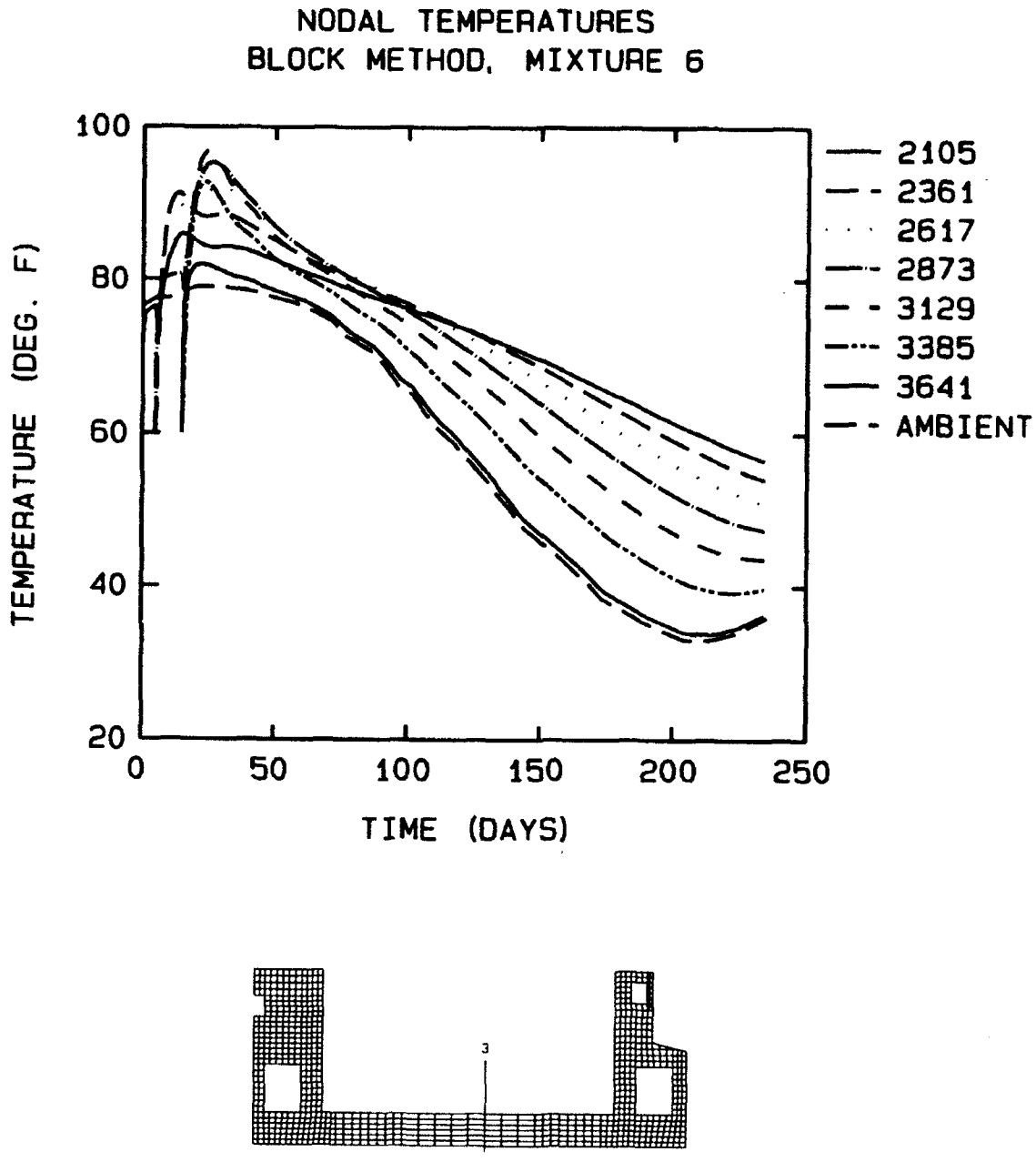

Figure 33. Nodal temperatures at section 3, mixture 6, block method

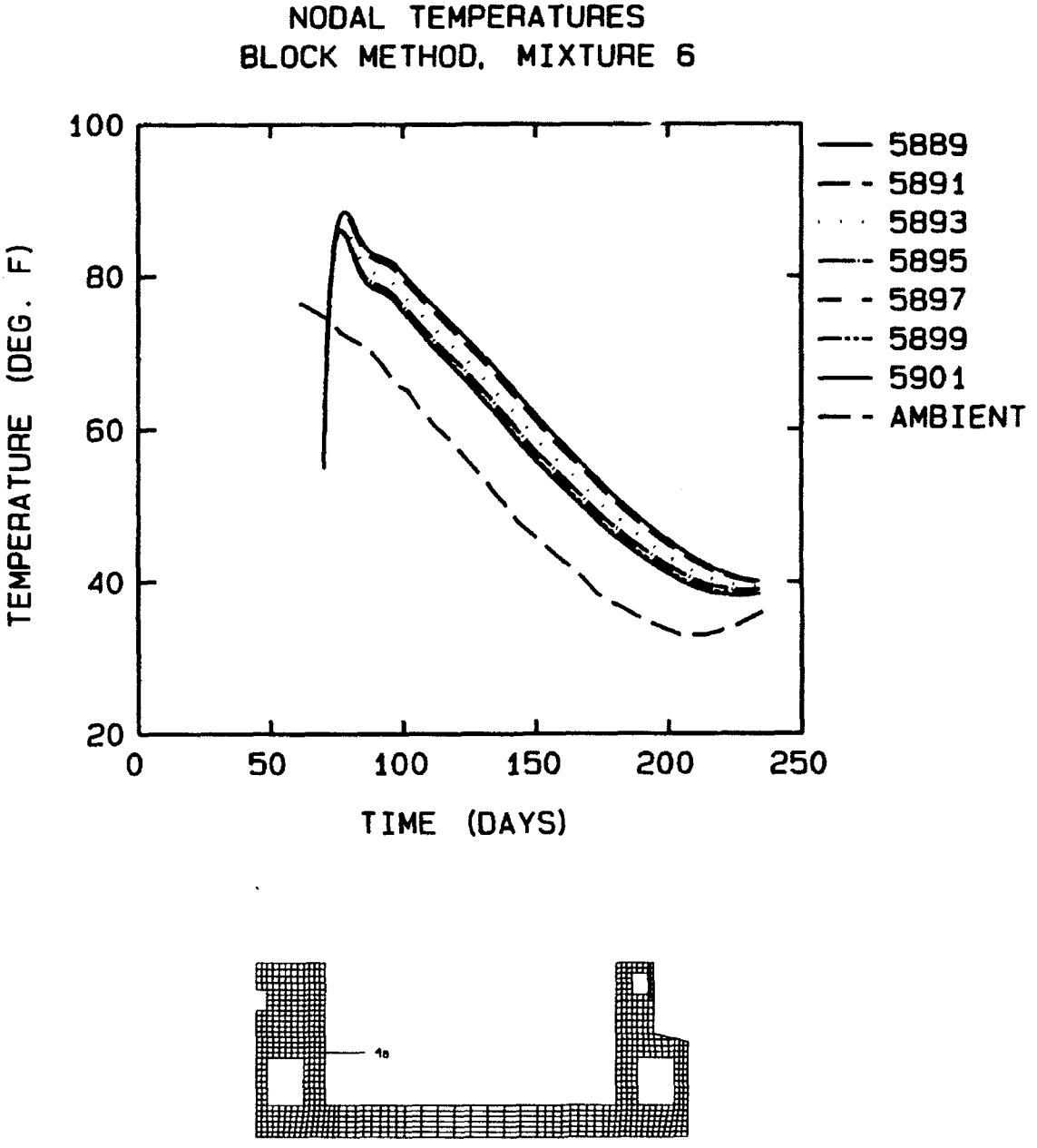

Figure 34. Nodal temperatures at section 4a, mixture 6, block method

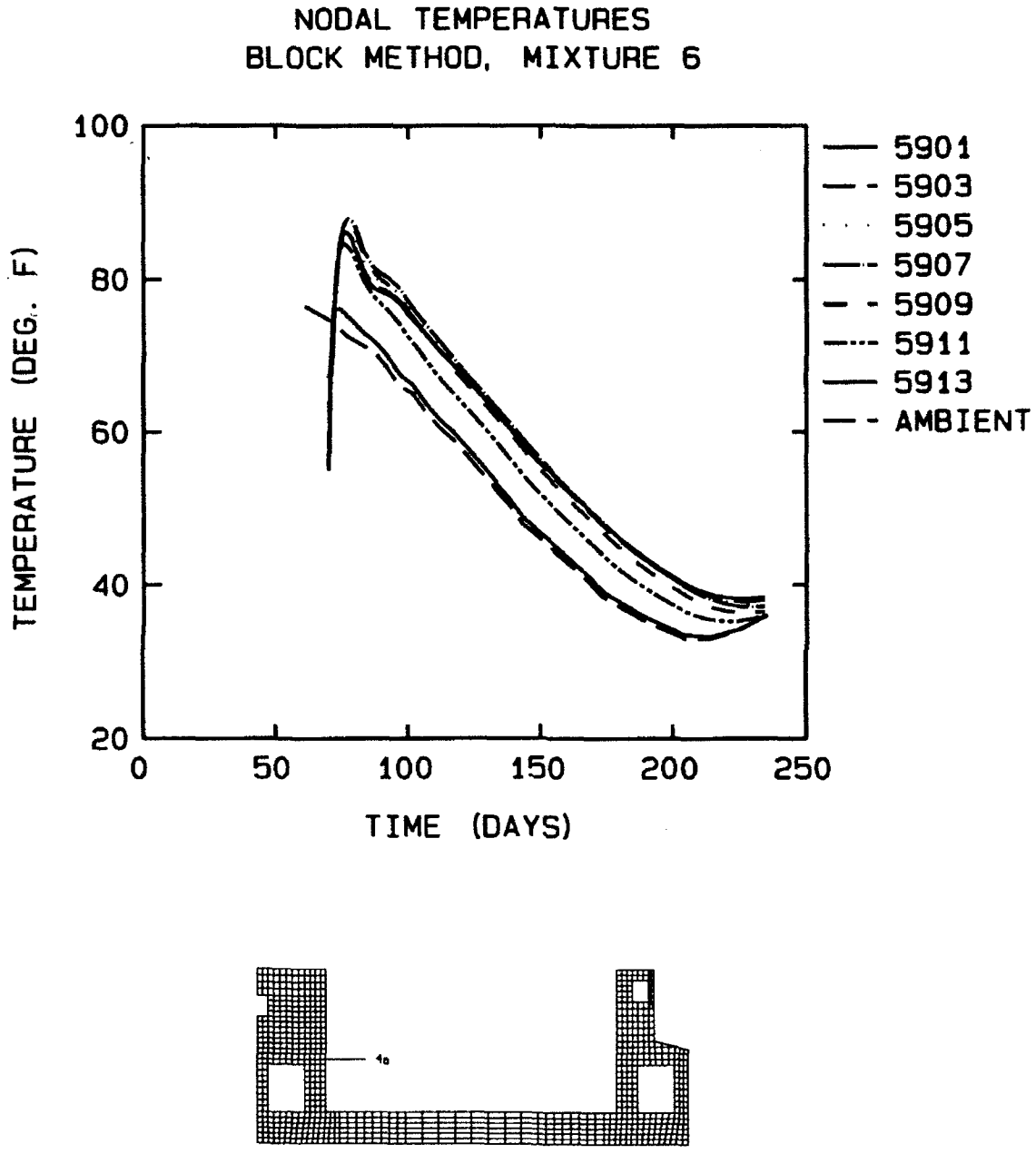

Figure 35. Nodal temperatures at section 4a, mixture 6, block method

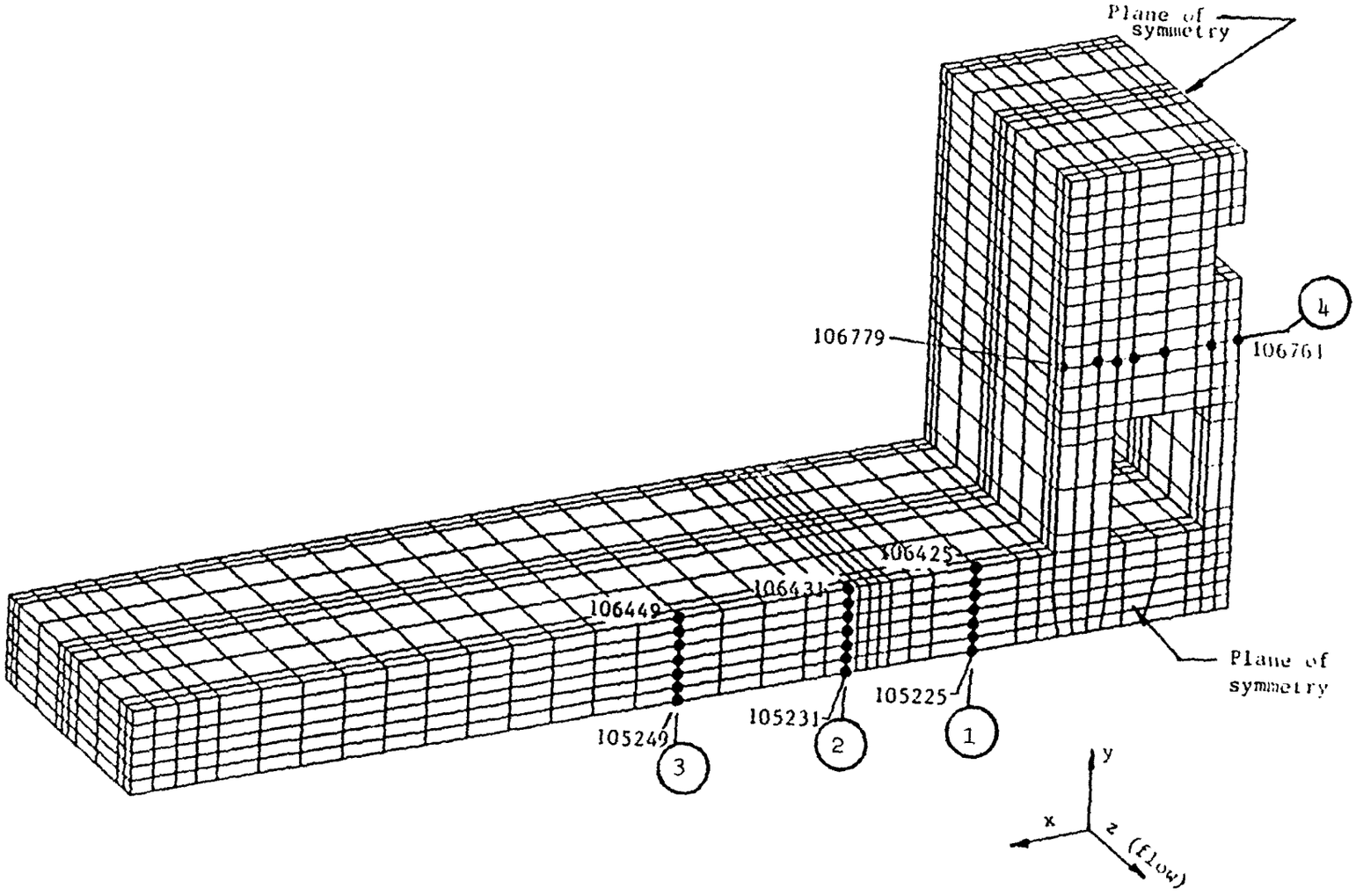

Figure 36. Nodes for temperature/time plots, 3-D heat transfer analysis

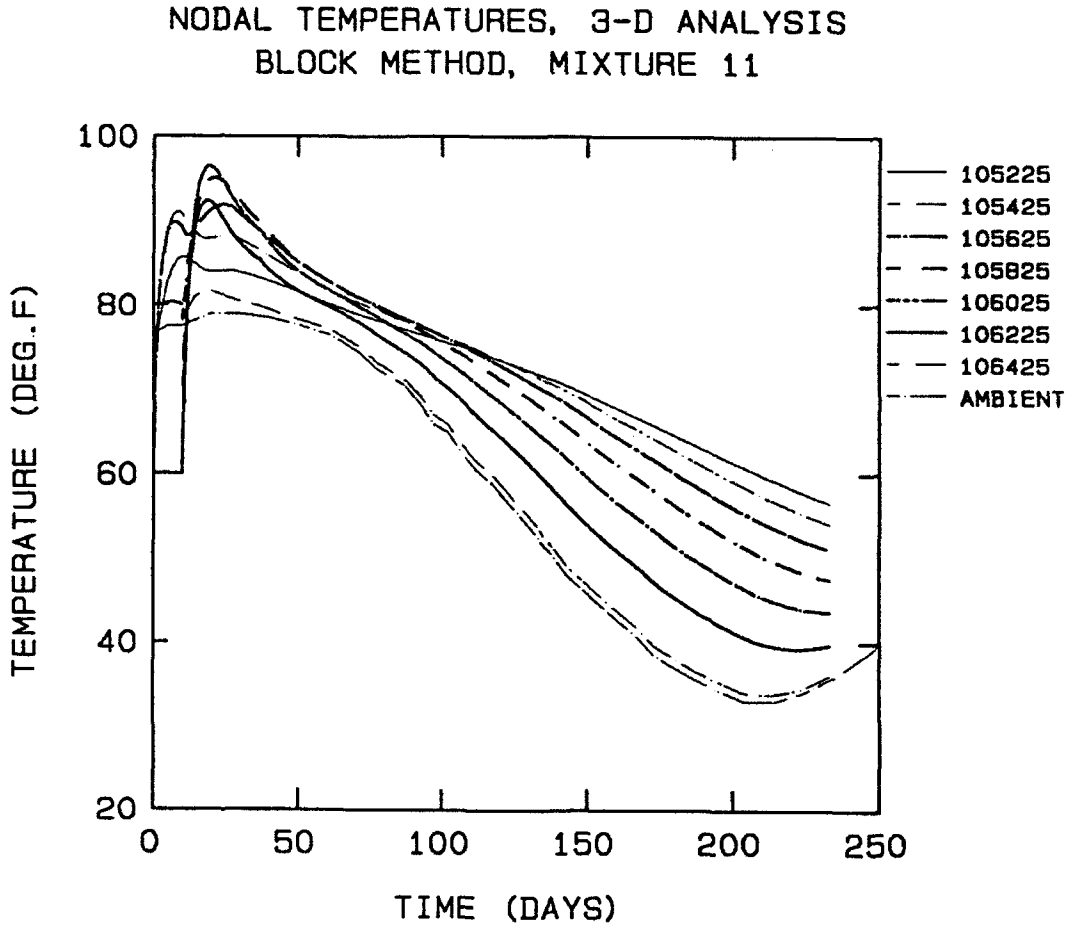

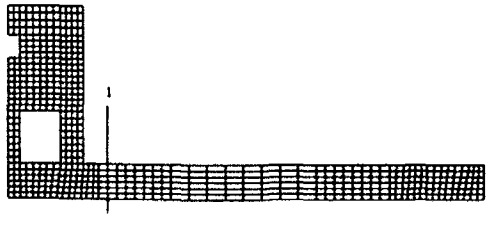

Figure 37. Nodal temperatures at section 1, 3-D analysis

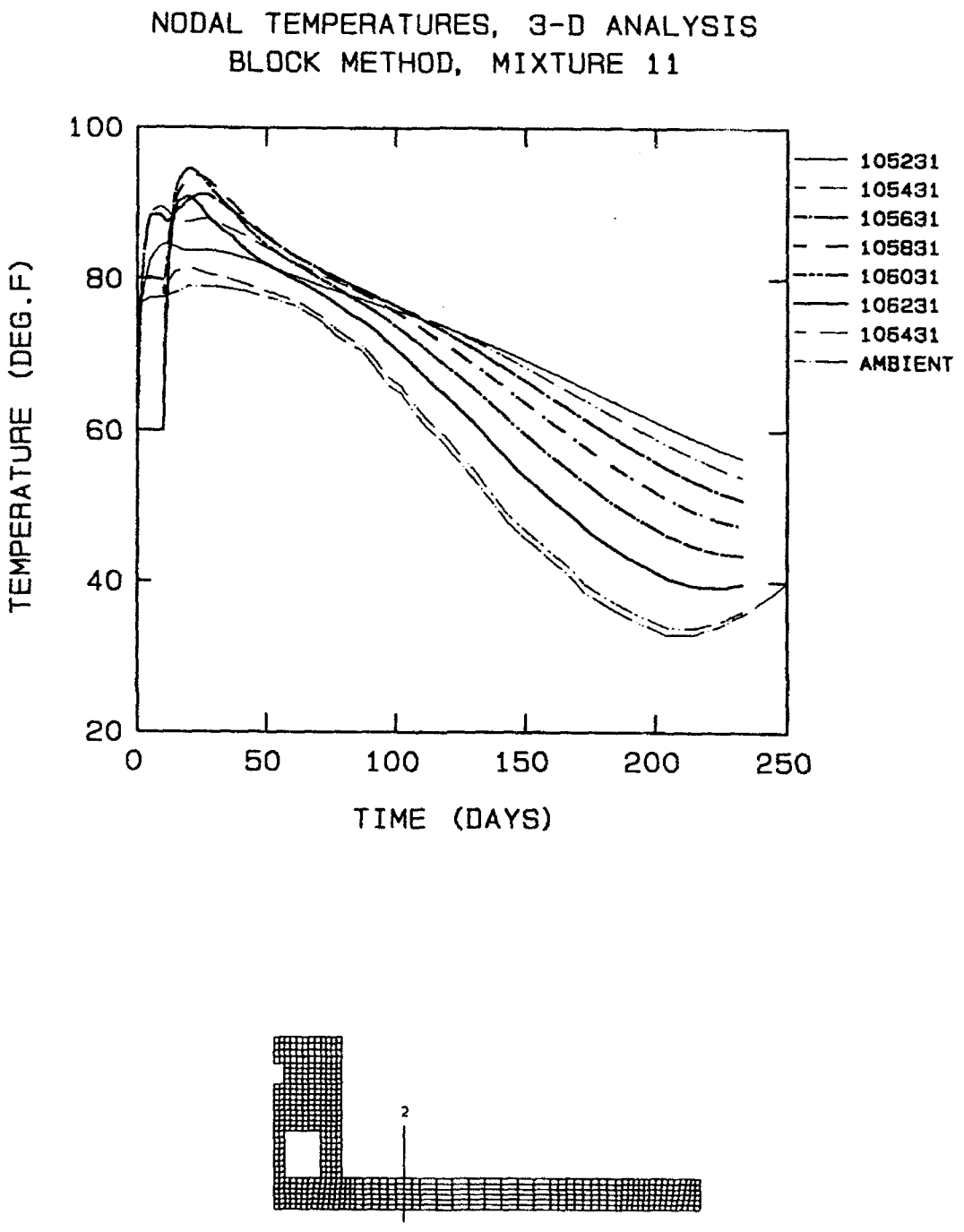

Figure 38. Nodal temperatures at section 2, 3-D analysis

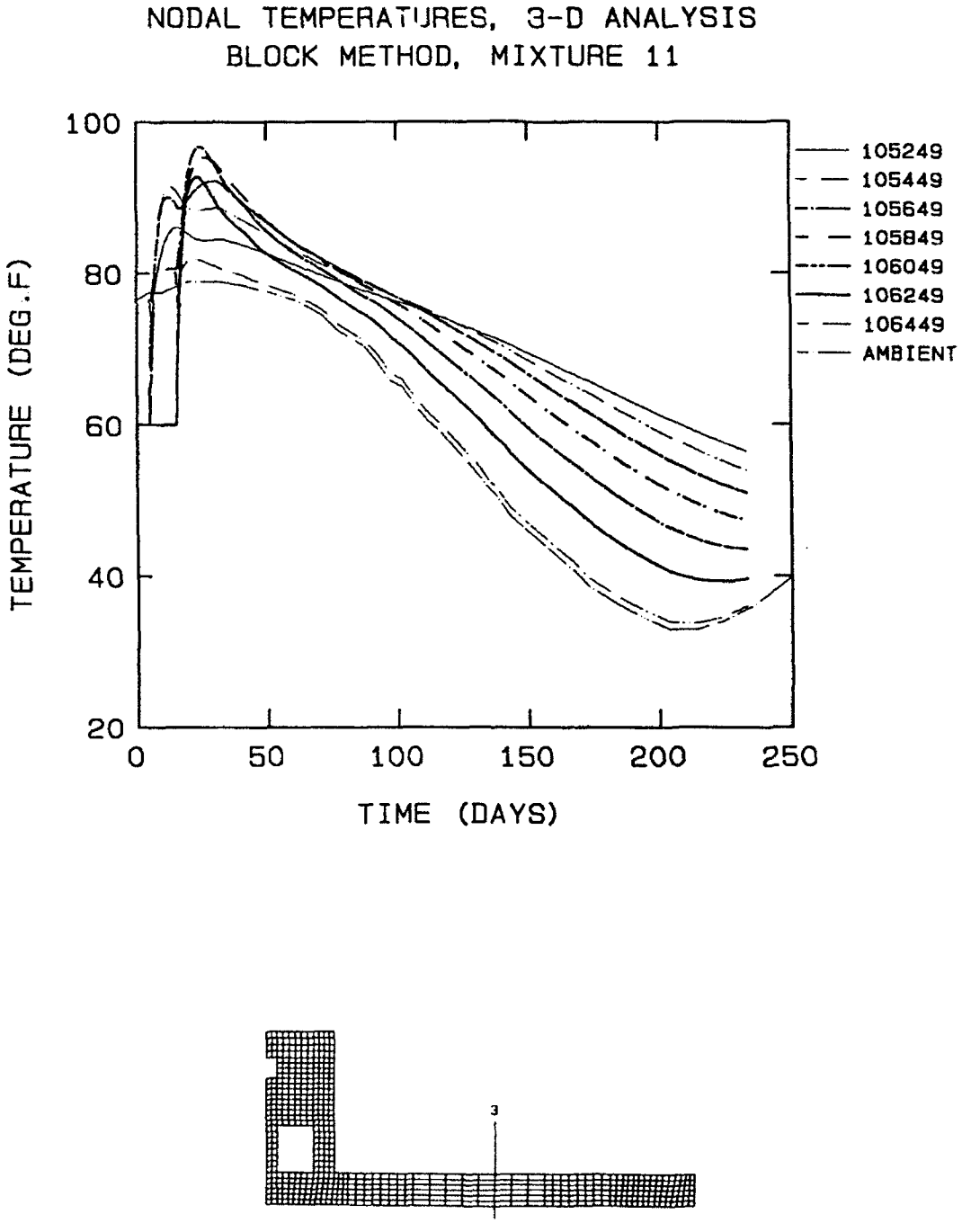

Figure 39. Nodal temperatures at section 3, 3-D analysis

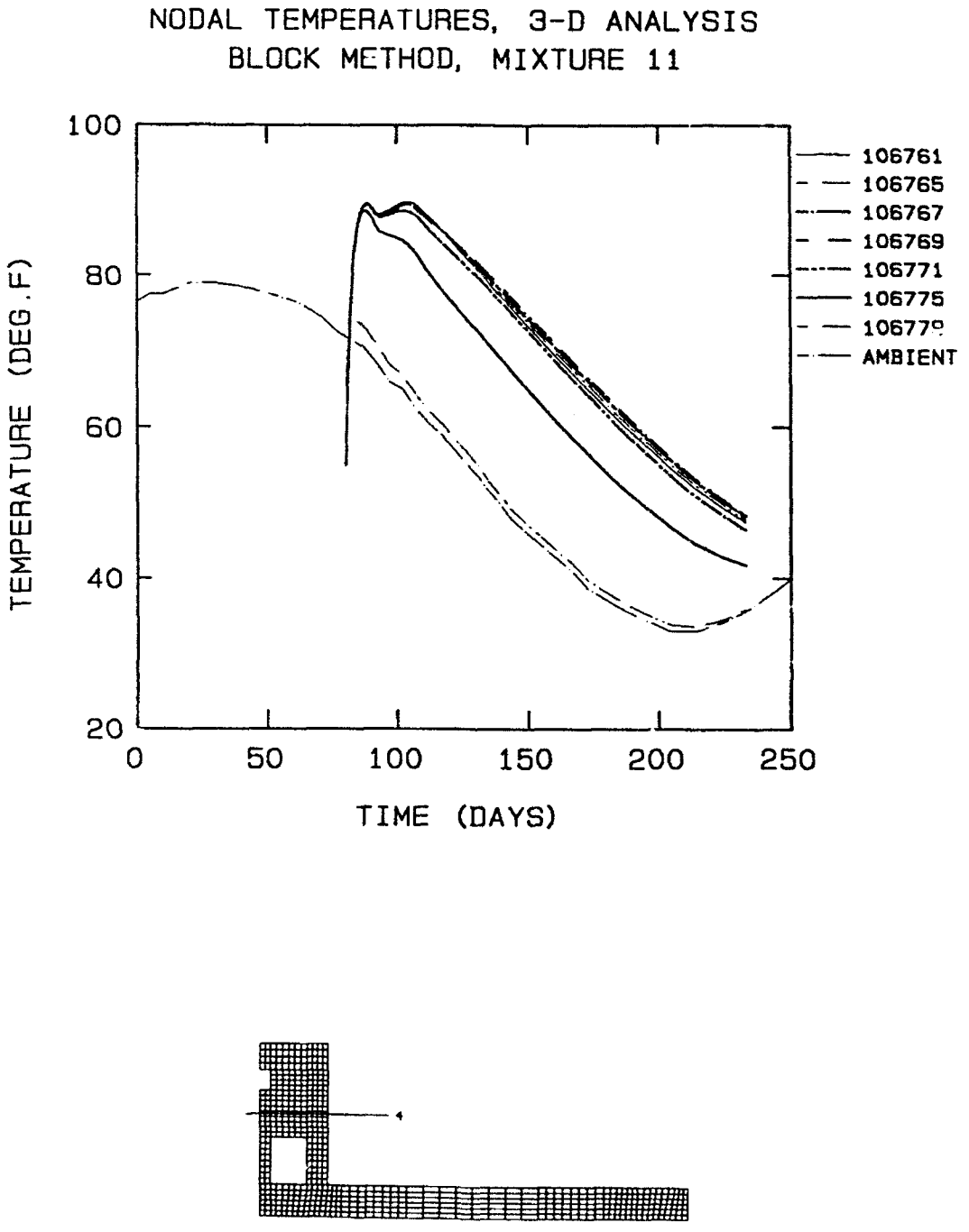

Figure 40. Nodal temperatures at section 4, 3-D analysis

begin to decrease along with the decrease in the ambient temperature. Temperatures in the nodes closest to the top of the floor decrease at a much faster rate than those in the bottom of the floor, and as the ambient temperature begins to rise, the nodes in the bottom of the floor do not immediately respond to this positive change as quickly as nodes near the top of the floor. This is a result of the poor conductivity of concrete.

81. In Figures 41 through 45, temperatures from the OMSTDT4 analysis are compared to the temperatures resulting from the 3-D analysis. Close examination of these plots reveals that temperatures in the 3-D analysis varied only slightly from those in the 2-D analysis. This can most clearly be seen in Figure 41 by comparing the time history for node 2081 in the 2-D analysis to node 105225 in the 3-D analysis. These nodes located at the bottom of the floor exhibited the largest difference between the two analyses, approximately 2 °F. This difference can be attributed to the use of the larger elements which had to be used in the soil for the 3-D analysis. Predicted temperatures at this node converged at approximately 120 days, and temperature differentials across the floor at times prior to that were only slightly greater than those in OMSTDT4. The maximum temperature differential was the same in both analyses.

82. Temperatures at the external face approximate ambient temperature after an initial period (about 50 days in this case) and have not been plotted.

83. Contour plots included in Appendix D are at the transverse center plane, at the vertical interface between floor lifts, and at the center plane in the direction of flow. These plots indicate that the area of 1-D heat flow along the length of the structure extended through the center one-half of the structure.

Stress Analyses

Mixture 11, 2-D analyses

84. All 2-D stress analyses using mixture 11 mechanical properties are listed in Table 13. In general, for the chamber monolith structure, results of stress analyses are discussed in terms of maximum stresses transverse to the direction of heat flow. This is possible because the dimensions and placement scheme of the structure are such that heat flow in the analyses was

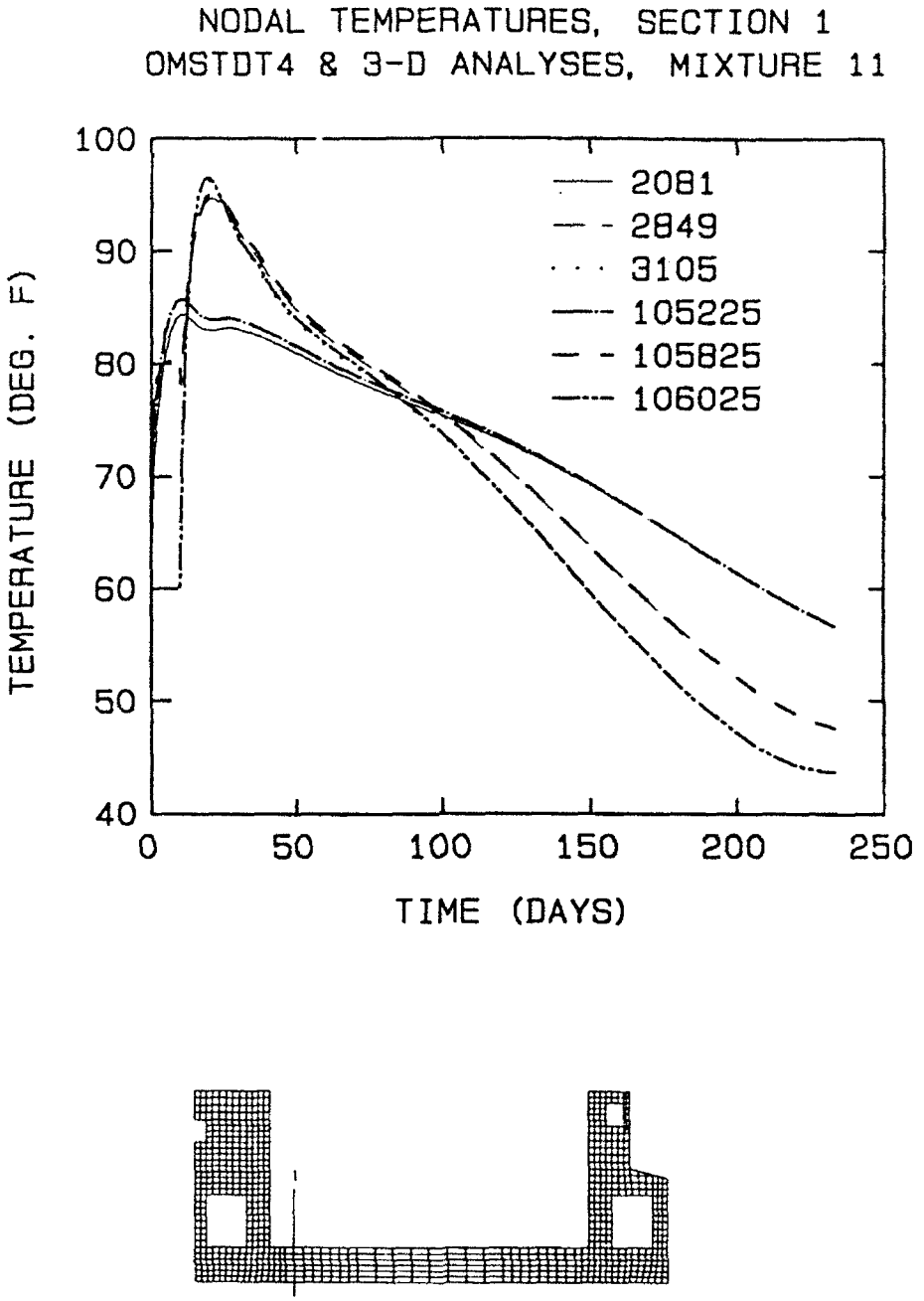

Figure 41. Nodal temperatures at section 1, OMSTDT4 and 3-D analyses

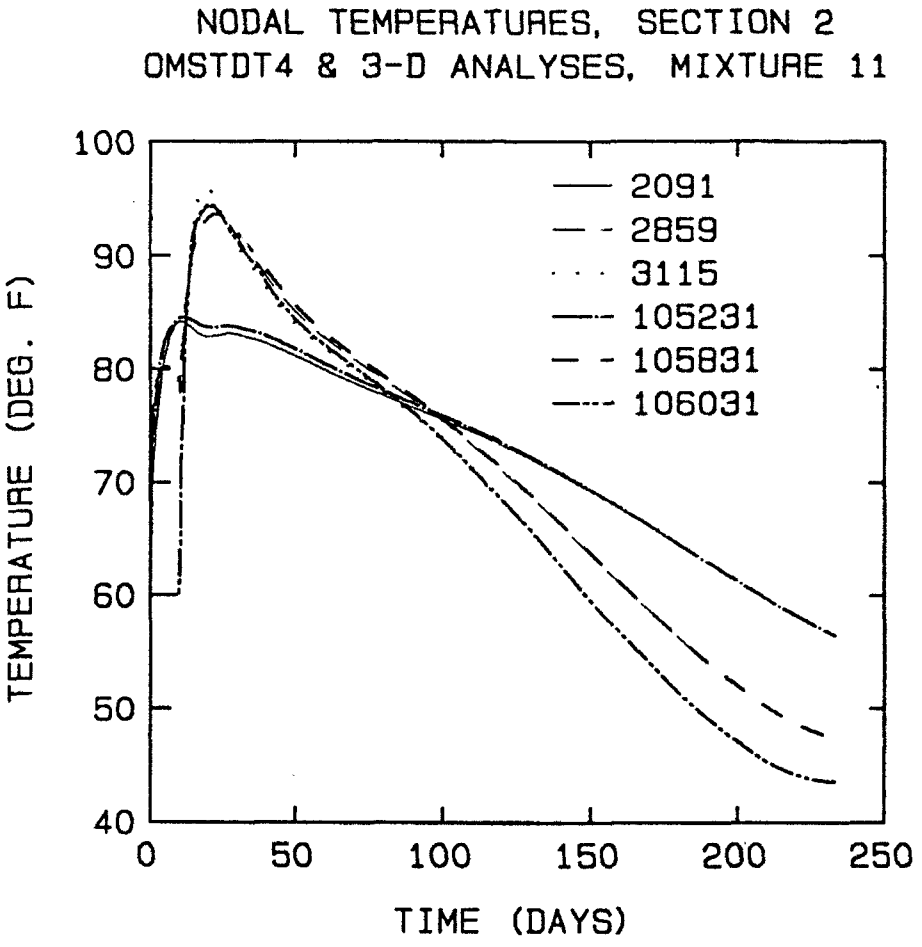

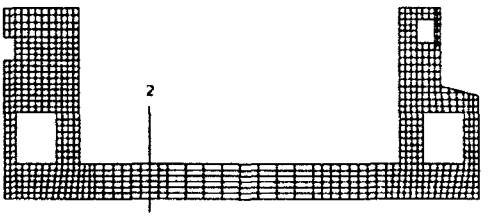

Figure 42. Nodal temperatures at section 2, OMSTDT4 and 3-D analyses

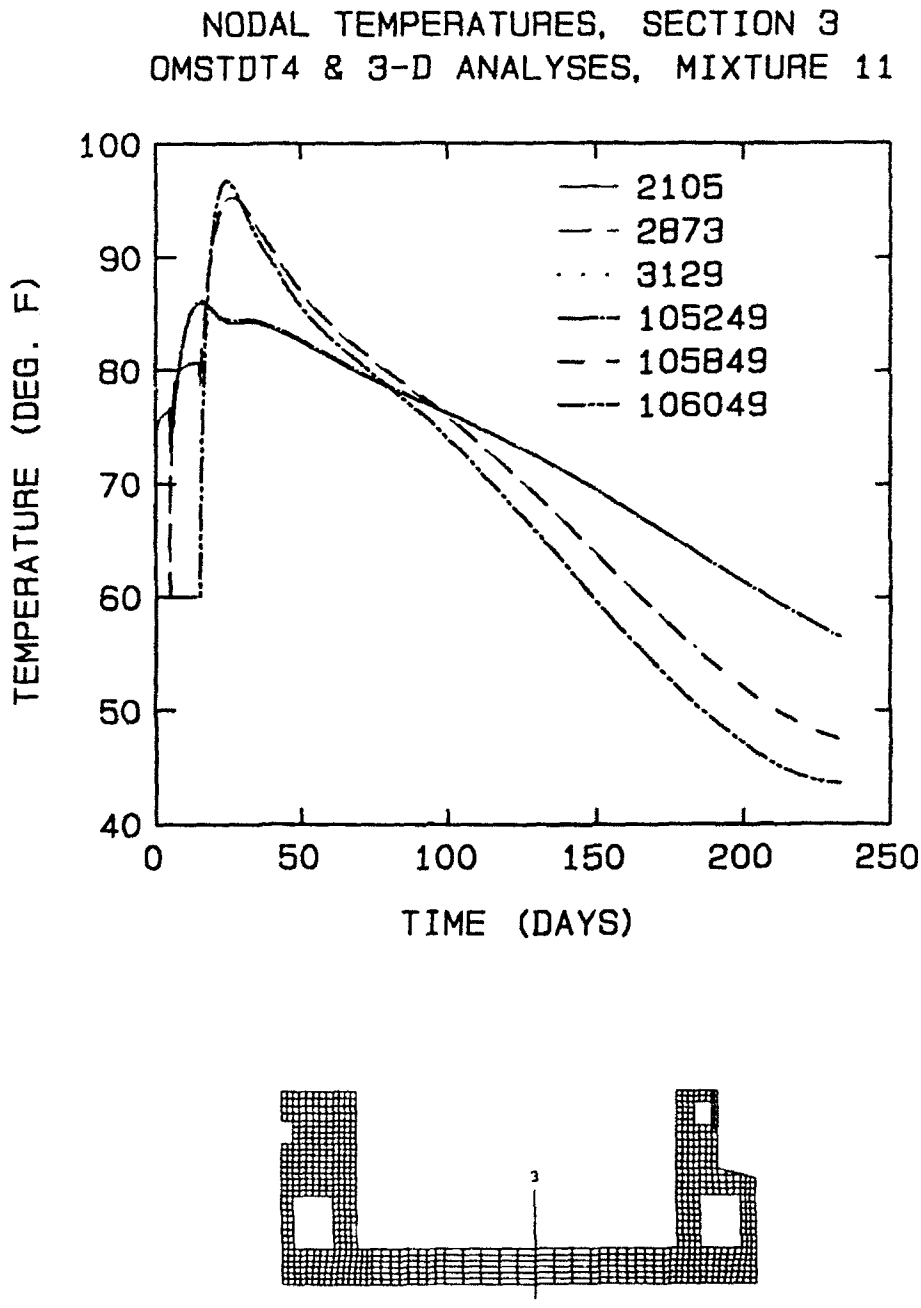

Figure 43. Nodal temperatures at section 3, OMSTDT4 and OMSTDT4 and 3-D analyses

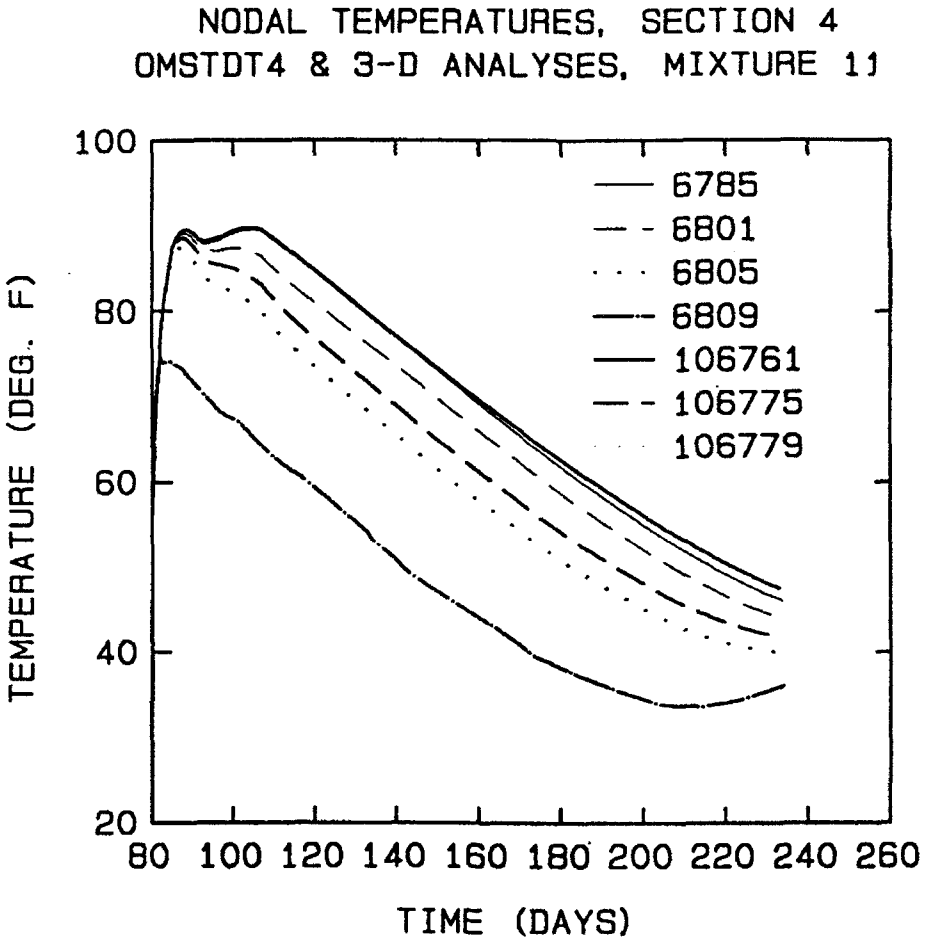

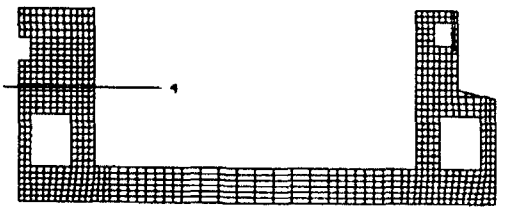

Figure 44. Nodal temperatures at section 4, OMSTDT4 and 3-D analyses

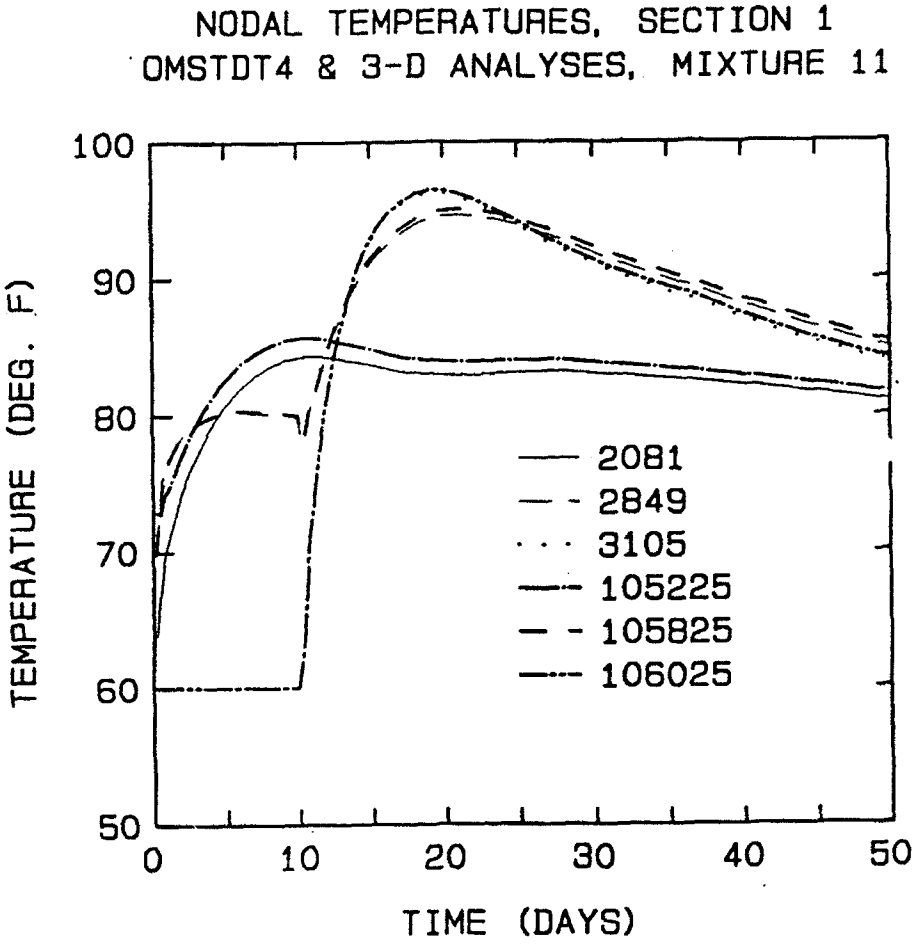

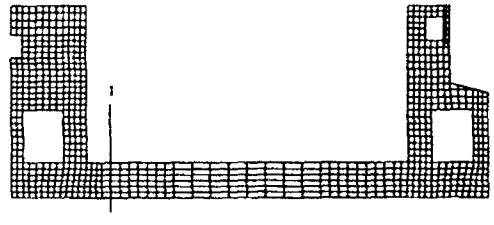

Figure 45. Early-time nodal temperatures at section 1, and 3-D analyses

Table 13

Summary of 2-D Stress Analyses

Name	Heat Transfer Analyses for Loading	Floor Placement Method	Notes
OMSTDS1	OMSTDT1	Strip	Varying placement temperatures in walls; plane stress; XY plane
OMSTDS1A	OMSTDT1	Strip	Varying placement temperatures in walls; plane strain; XY plane
OMSTDS2	OMSTDT2	Strip	Constant 60 °F placement temperature; plane stress; XY plane
OMSTDS3	OMSTDT1	Strip	Varying placement temperatures in walls; mixture 6 shrinkage curve; plane stress; XY plane
OMSTDS4	OMSTDT4	Block	Varying placement temperature in walls; plane strain; XY plane
OMSTDS4A	OMSTDT4	Block	Varying placement temperature in walls; plane stain; XY plane
OMSTDS5	OMSTDT5	Strip	Floor only; 60 °F placement temperature; plane stress; ZY
OMSTDS5A	OMSTDT5	Strip	Floor only; 60 °F placement temperature; plane strain; ZY plane

largely 1-D. Even in the center wall, where significant heat flow could be expected to occur at wall faces, lifts were 4 to 6 ft high and 52 ft long, and heat flow was initially 1-D. In these areas, shear stresses and tensile stresses parallel to the primary direction of heat flow were negligible. Maximum principal stress was out-of-plane stress in plane strain problems and the stress transverse to the direction of heat flow in plane stress problems. The exception to this rule was at corners of wall openings, where significant stresses were induced in all directions due to bending. In these areas, maximum principal stress may not be in the vertical or horizontal directions.

85. Stress contour plots at specific intervals throughout the analyses have been included in Appendix E. Only the plots appropriate to the problem have been included. In plane strain problems, maximum principal stress as calculated by ABAQUS is often dominated by out-of-plane stress and cannot be used to determine areas of high in-plane stress. Therefore, only horizontal and vertical stress contour plots have been included for plane strain problems. Plots of maximum principal stress have been added for comparison with horizontal and vertical stresses in plane stress problems.

86. Displacement plots have been included in Appendix F for the plane strain analyses, OMSTDS1A and OMSTDS4A, only. The differences between the plots from the two analyses reflect the different methods used to account for displacements occurring prior to the placement of each lift. However, these plots are useful because they show the general trend of volumetric change with time and temperature. Current ambient temperature and elapsed time are given on all stress contour and displacement plots for reference.

87. Strip placement analyses 1 and 2 (OMSTDS1 and OMSTDS1A). In both the plane stress and plane strain analyses, the highest tensile stresses occurred at the top center of the floor (element 763), the top of the center wall culvert (element 993), and at the lower corner of the top center wall opening (element 1216). These elements are identified in Figure 46. The typical horizontal stress distribution across the floor, shown in Figure 47, displays slope discontinuities at the lift interfaces. This is not uncommon and similar stress distributions have been observed in the NISA conducted for Melvin Price Locks and Dam. This is due to the fact that each lift was placed separately imparting a different state of stress in each lift. Vertical and shear stresses in the floor were low, and horizontal stresses were primarily compressive for the first 50 days after the start of construction. Maximum horizontal tensile stresses at the top of the floor occurred at approximately 170 days and were 241 psi in the plane stress analysis and 275 psi in the plane strain analysis. Stresses across the section in the OMSTDS1 analysis at 173 days are presented in Figure 48. Tensile stresses in the floor decreased after 200 days. This drop in stress can be attributed to the fact that the minimum average ambient temperature occurs at approximately 200 days. At this time, the temperature gradient across the floor is at a maximum. As warming occurs, the temperature gradient is reduced, reducing stresses. This means that for the floor, maximum tensile stresses during construction are

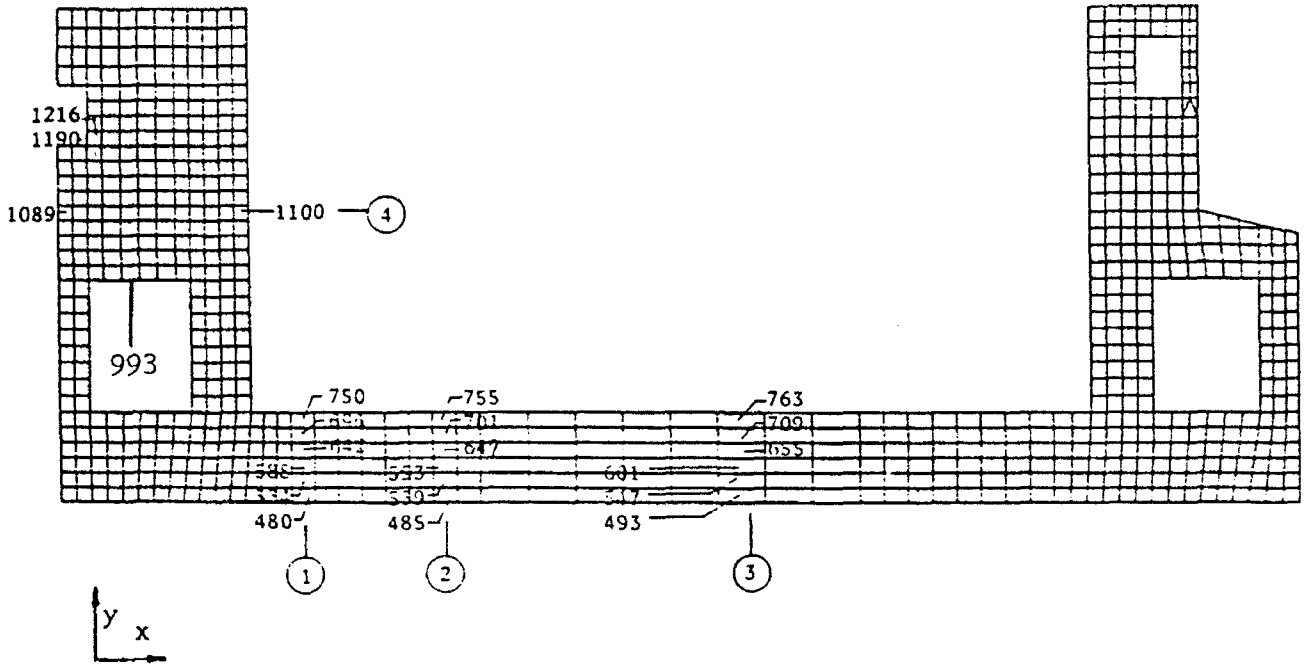

Figure 46. Sections and elements for stress/time plots

controlled by fluctuations in the average ambient temperature. Stresses in lift 3, section 3 for the OMSTDS1A analysis are shown in Figure 49. Wall stresses are shown in Figures 50 through 54. Wall stresses were relatively low except at openings. Stress contour plots indicate that stresses in the culvert walls were low. This justifies ignoring the changes in material properties that result when maximum aggregate size is limited to 1-1/2 in. The maximum horizontal stress in the center wall occurred at the top of the center wall culvert in element 993 (Figure 50) and was 129 psi in the plane stress analysis and 146 psi in the plane strain analysis at 110 days (40 days after placement). Vertical and shear stresses in this area were negligible, and tensile stresses decreased after 144 days. High tensile stresses at the corner of the upper opening also decreased after 144 days. High tensile stresses at openings occurred relatively early after placement of the concrete. In general, a sharp rise in tensile stresses at openings occurred at about 10 to 20 days after placement. The maximum principal stress in element 1216, point 1 was 132 psi by 20 days after placement in OMSTDS1. Horizontal and vertical stresses around openings are plotted in Figures 51 through 54. Figures 51 and 52 show large drops in stress from approximately 105 to 110 days. As can be seen from Table 9, new lifts are being placed above this location during these times. When a new lift is placed on an existing lift, the new lift attempts

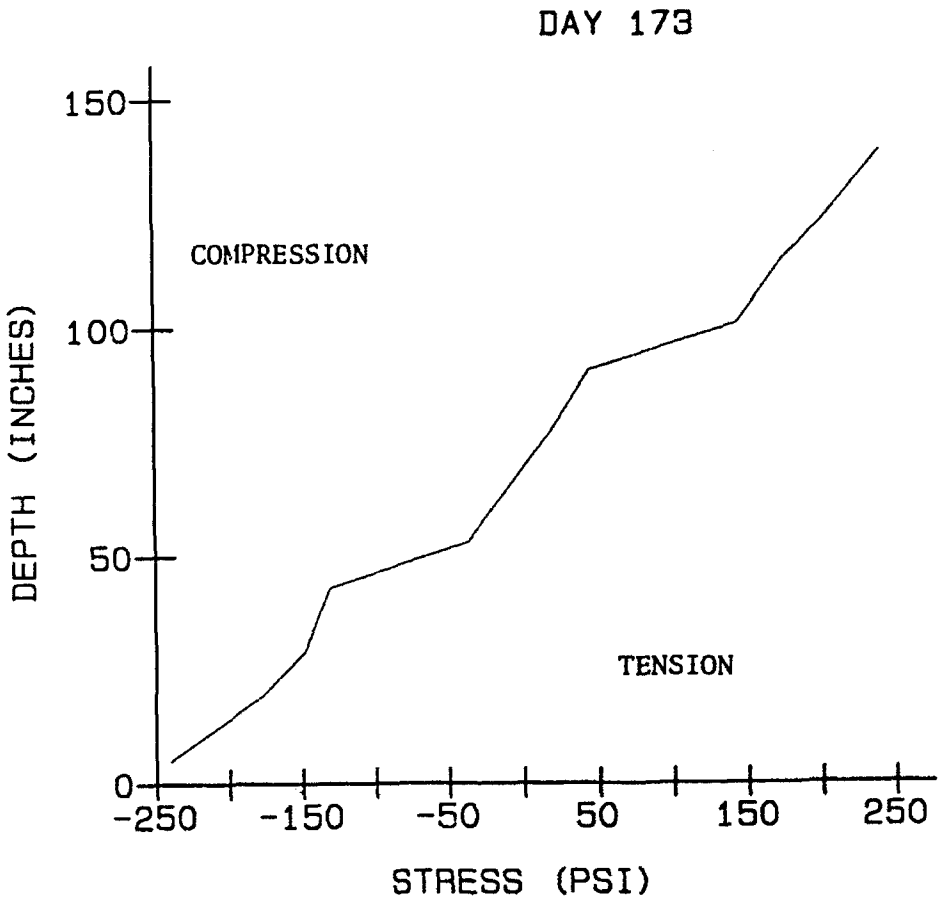

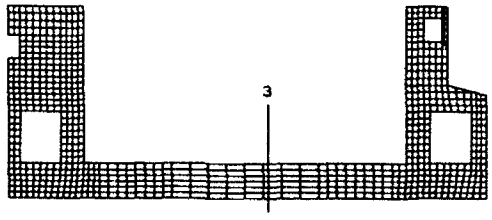

Figure 47. Stress distribution at section 3, OMSTDS1

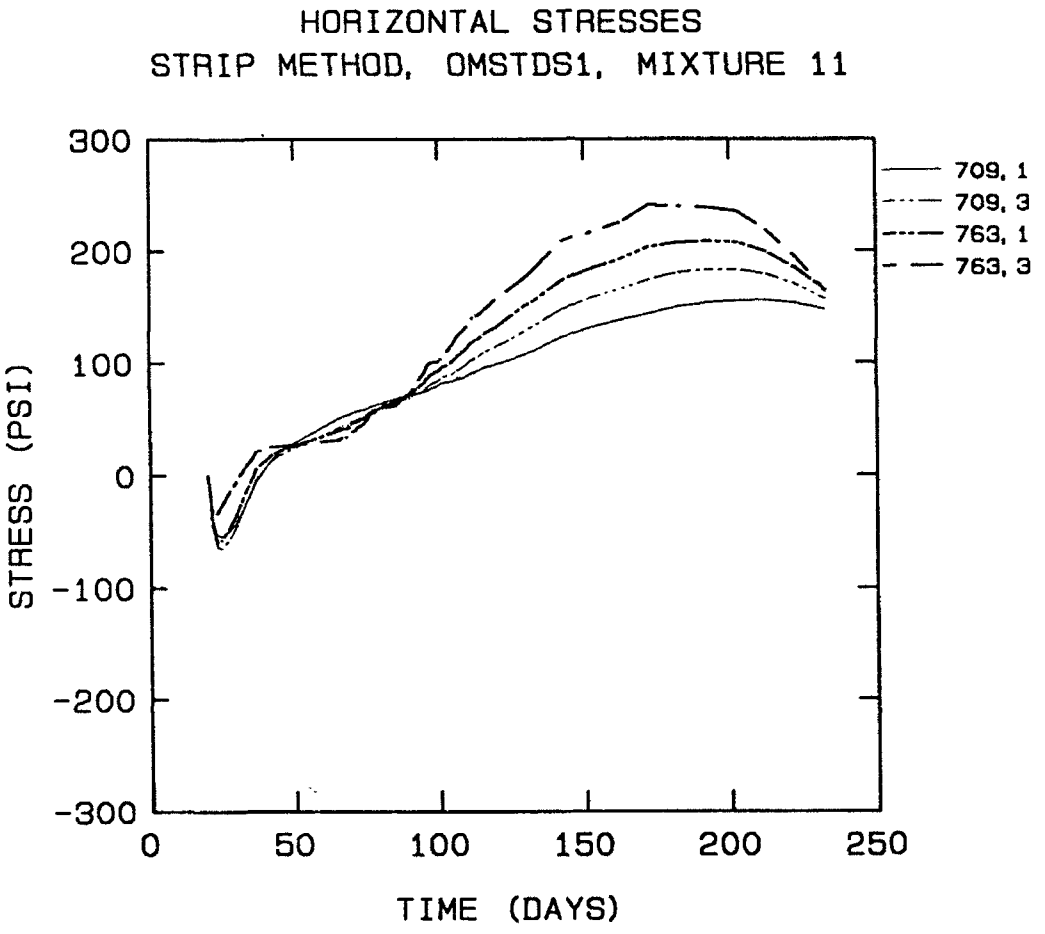

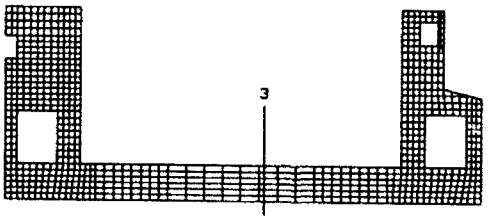

Figure 48. Horizontal stress at lift 3, section 3, OMSTDS1

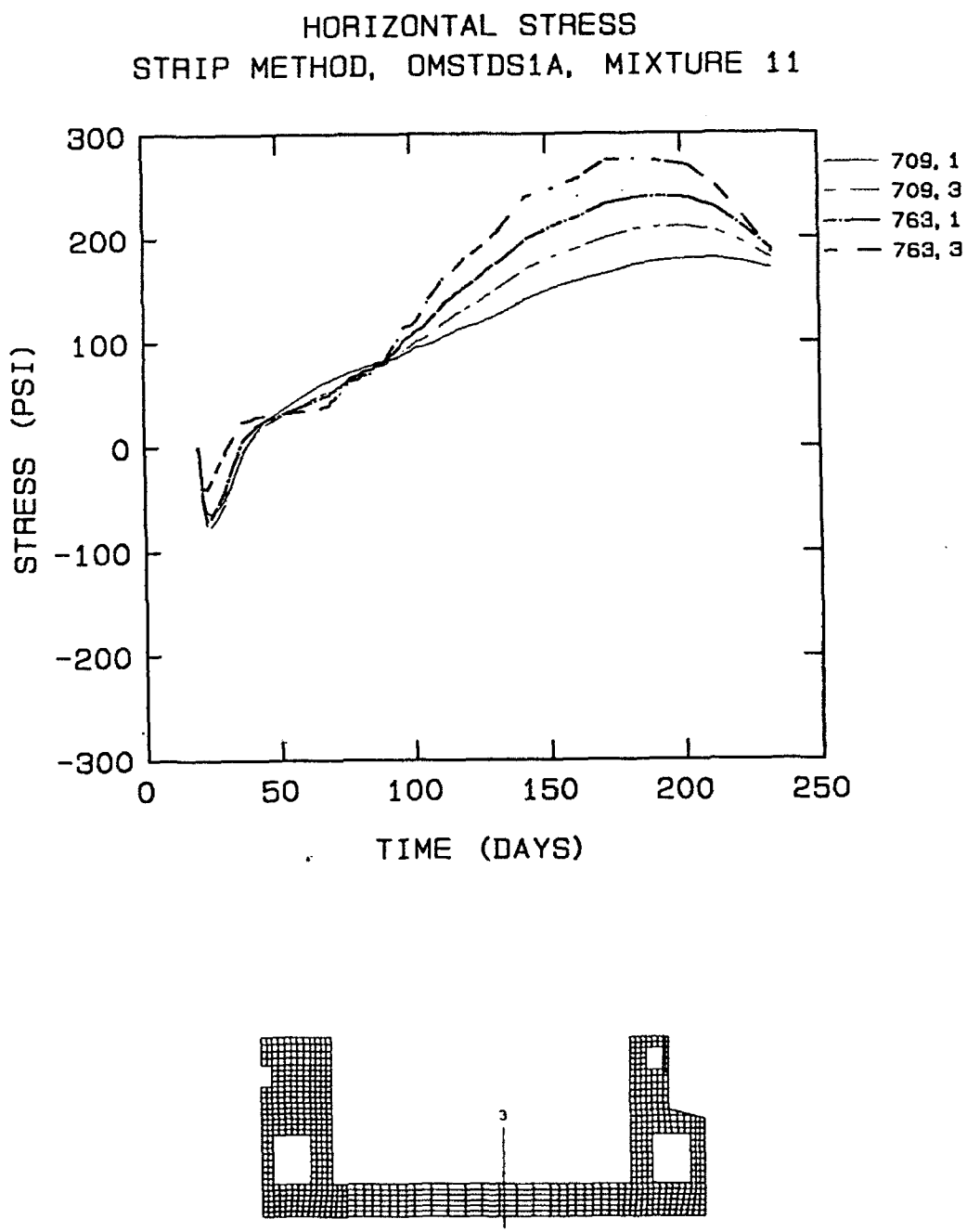

Figure 49. Horizontal stress at lift 3, section 3, OMSTDS1A

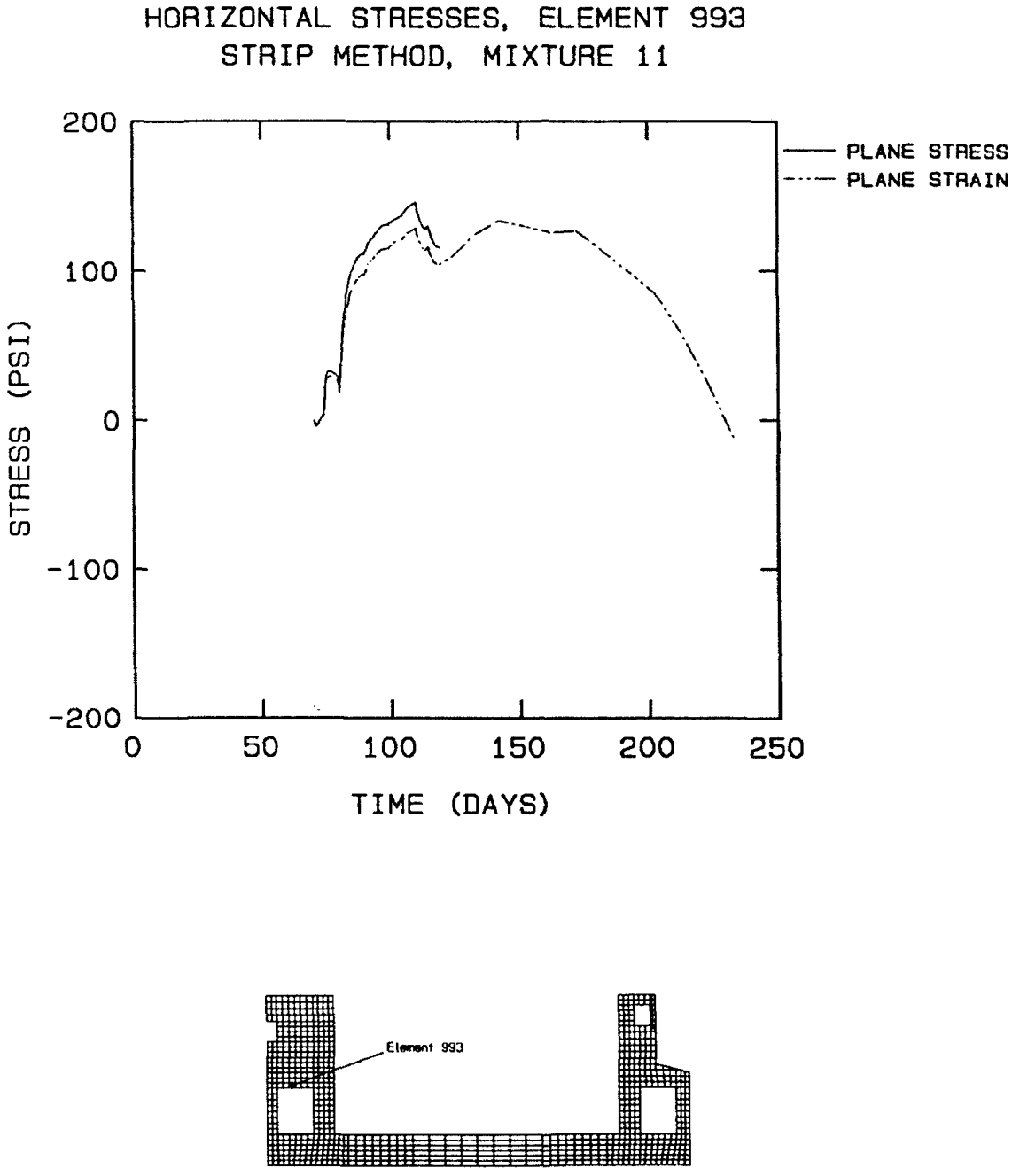

Figure 50. Horizontal stress at element 993, OMSTDS1 and OMSTDS1A

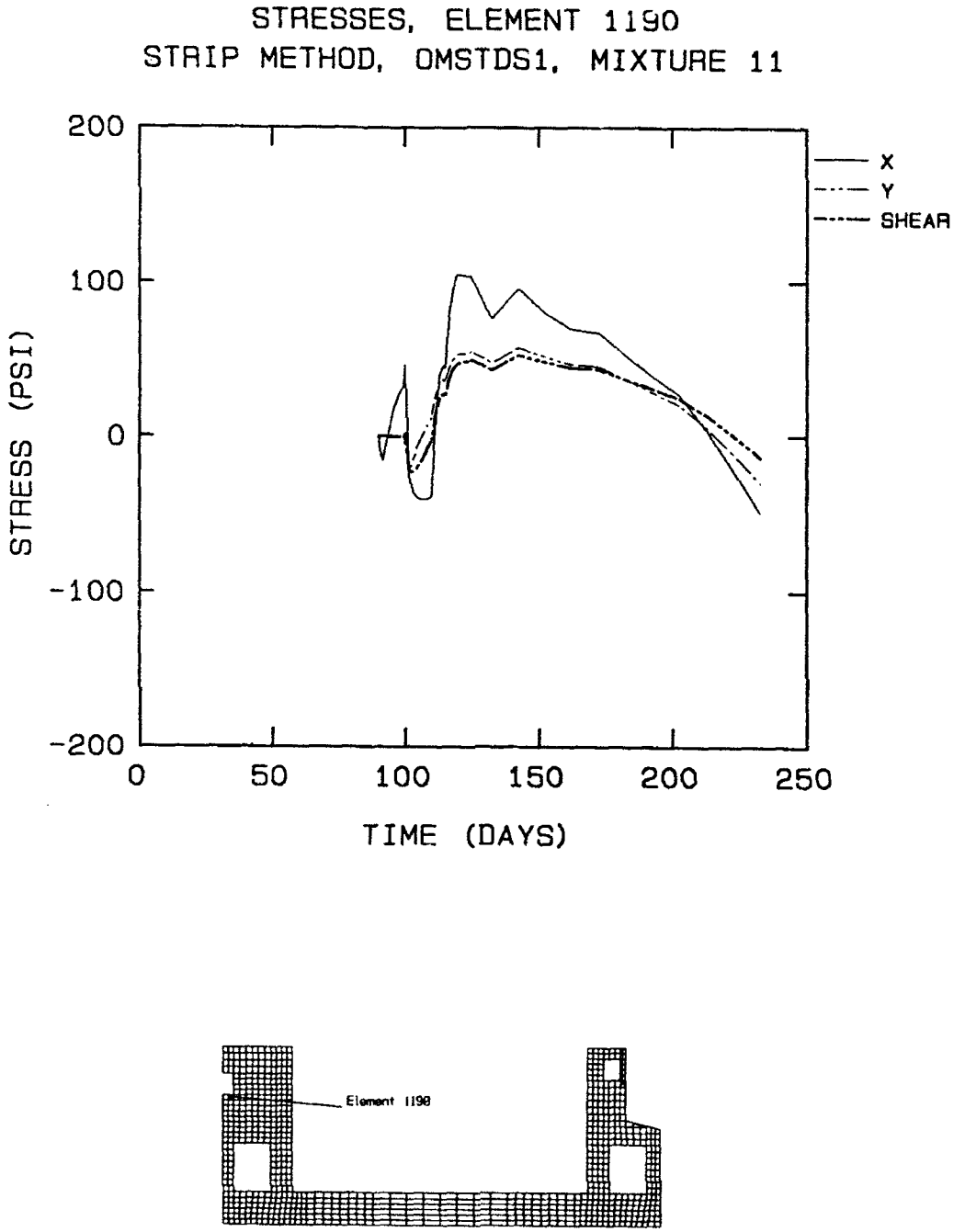

Figure 51. Stresses at element 1190, OMSTDS1

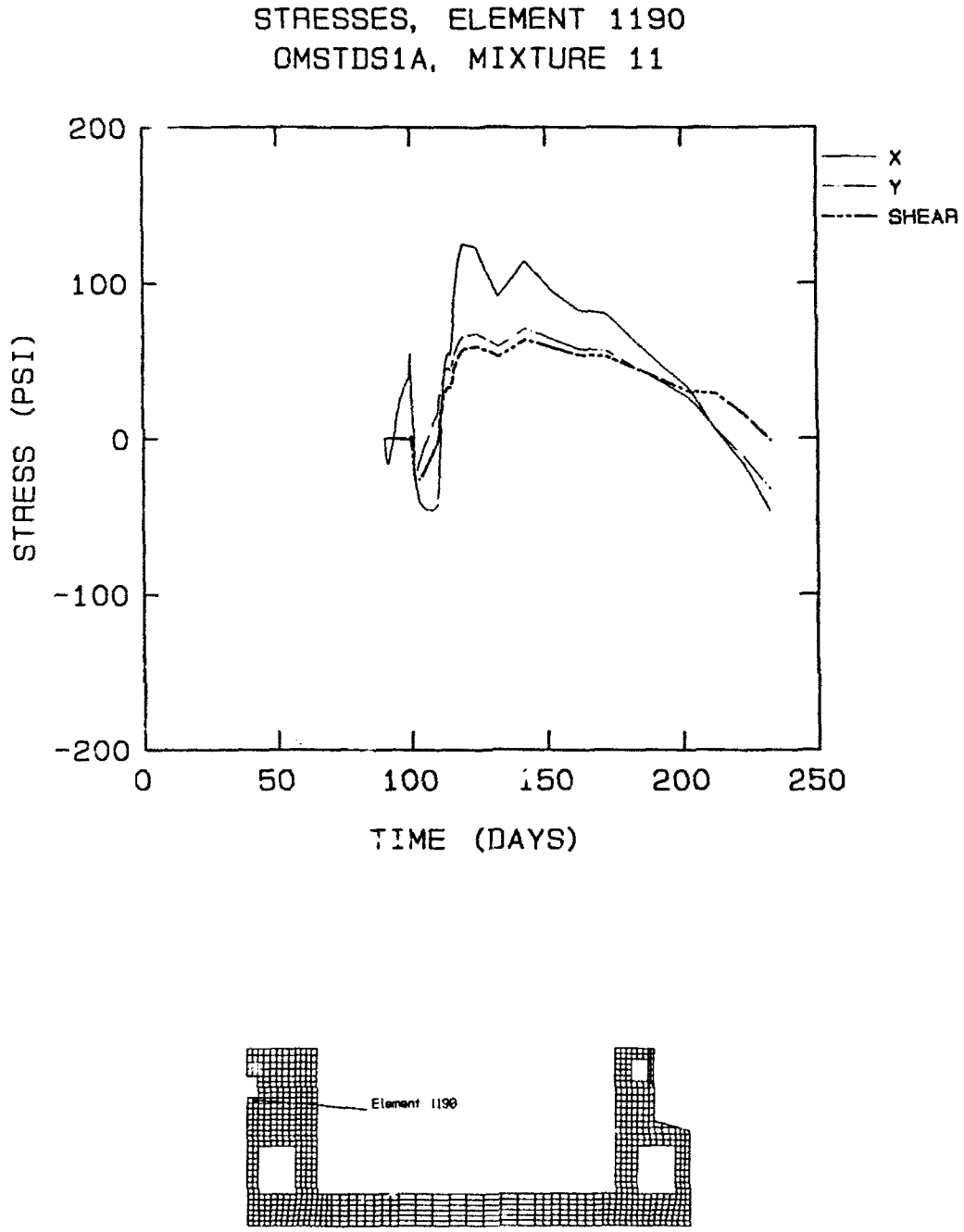

Figure 52. Stresses at element 1190, OMSTDS1A

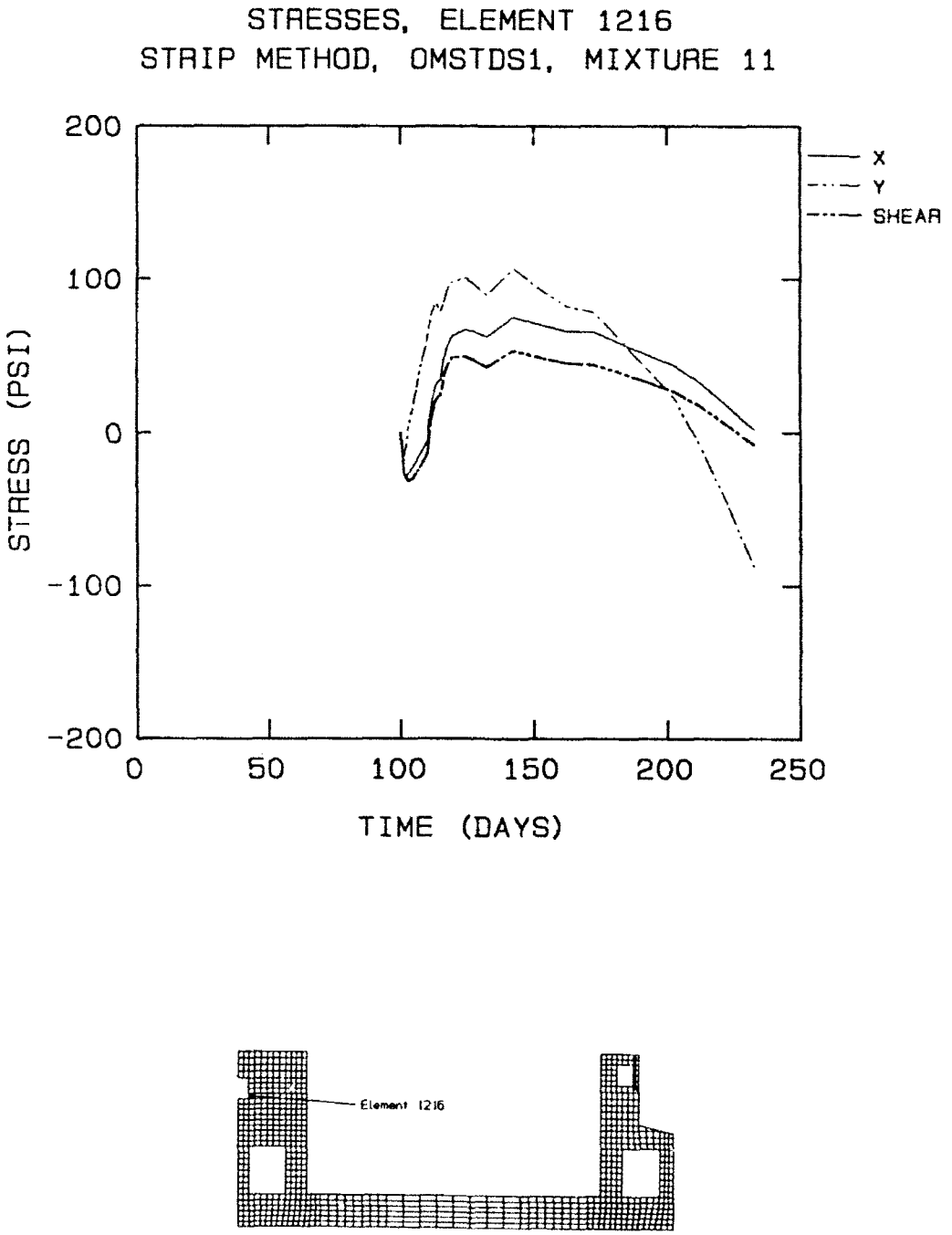

Figure 53. Stresses at element 1216, OMSTDS1

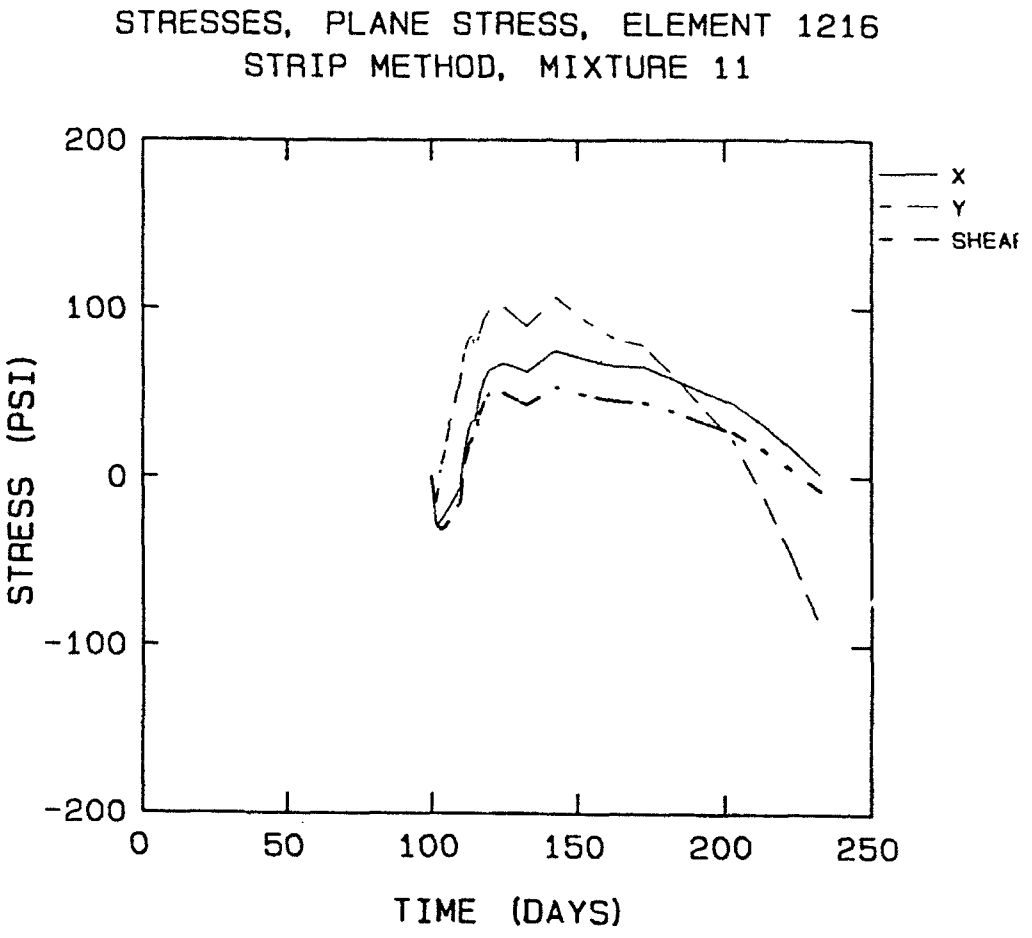

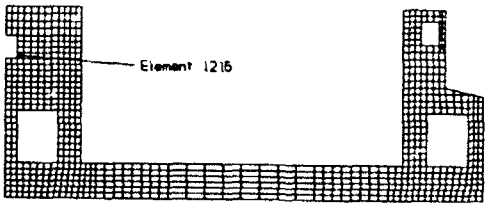

Figure 54. Stresses at element 1216, OMSTDS1A

to expand but is restrained and forced into compression by the existing lift. At the same time, horizontal stresses in the old lift become tensile. Thus, the sharp increases occur in tensile stress at 10 and 20 days after placement of this lift (Lift 14). As the new lift attempts to contract but is restrained by the existing lift, stresses in the new lift become tensile and those in the existing lift become compressive. Hence, sudden drops in stress result as shown in Figures 51 and 52.

88. Maximum lateral displacement due to volumetric expansion in the OMSTDS1 analysis was 0.134 in. at node 2669 and occurred at 5 days after the placement of lift 3. The maximum lateral displacement due to volumetric contraction was 0.332 in. at node 3437 at the end of the analysis. Both of these points are located at the outer edge of the floor.

89. No cracking occurred in the plane stress analysis. In the plane strain analysis, cracking due to out-of-plane stresses was initiated in the floor at 101 days. The out-of-plane cracking occurred randomly throughout the structure and resulted in nonconvergence at several time increments, probably affecting the accuracy of predicted stresses in some areas of the structure.

90. Strip placement analysis 3 (OMSTDS2). Due to problems encountered in the previous plane strain analysis, this analysis used plane stress elements. Stresses in the floor were identical to those in the OMSTDS1 analysis. Stress plots across each lift at section 3 are presented in Figures 55 through 57. As can be seen from these plots, when a new lift was placed on existing concrete, expansion due to the rise in temperature in the new lift was restrained by the older concrete. Initial stresses in the new concrete were due to this restraint and were compressive. At the same time, stresses in the existing lift were tensile. When the new lift began to cool and contract, the tensile stresses in the previous lift were reduced as it provided restraint to contraction in the new lift. This restraint resulted in tensile stresses in the new lift.

91. Stresses in the walls are compared with those from OMSTDS1 in Figures 58 through 62. As expected, horizontal tensile stresses at section 4 were higher in the OMSTDS2 analysis (see Figure 58). Placement temperatures were higher in this analysis, and the vertical direction is the primary direction of heat flow at early times. Stresses at openings (Figures 58 through 62) are a result of moments induced by differential displacements and cannot be as readily linked to differences in temperature as can those in the more massive sections.

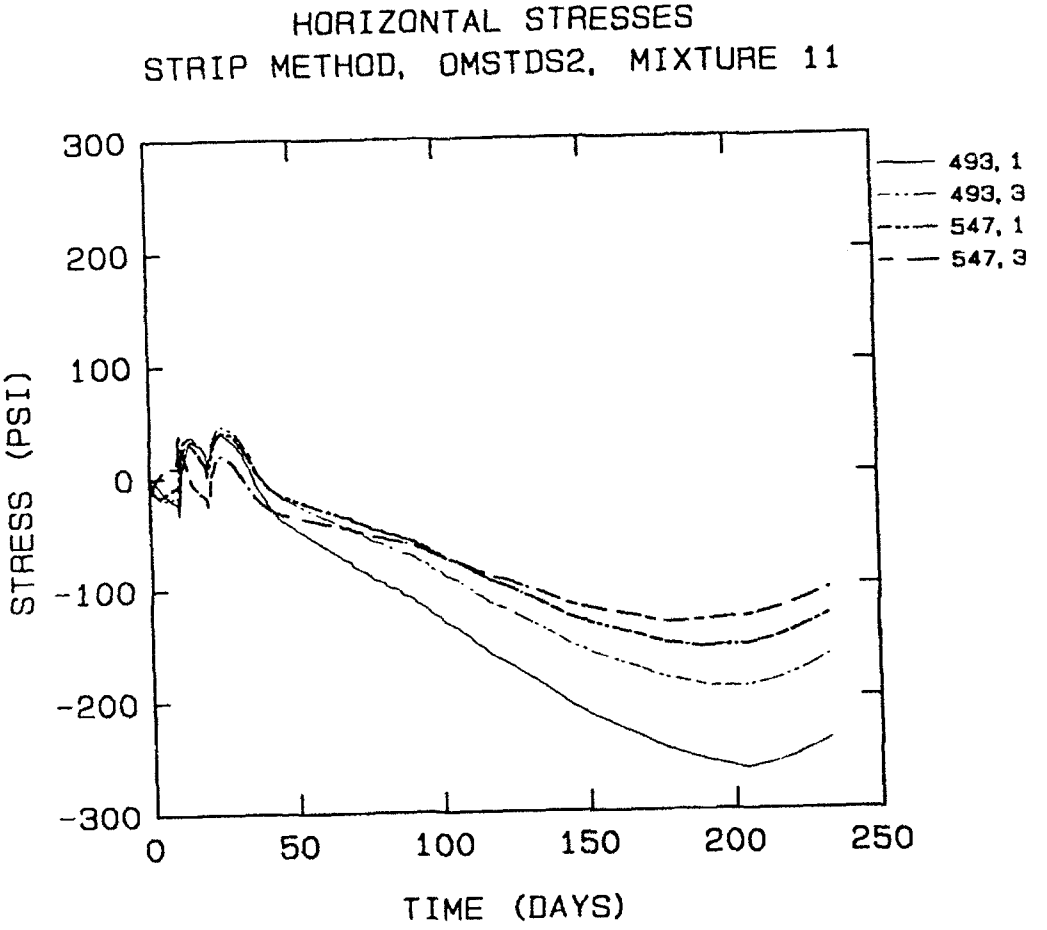

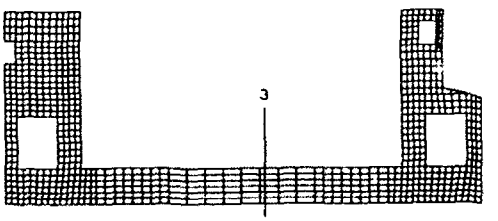

Figure 55. Horizontal stress at lift 1, section 3, OMSTDS2

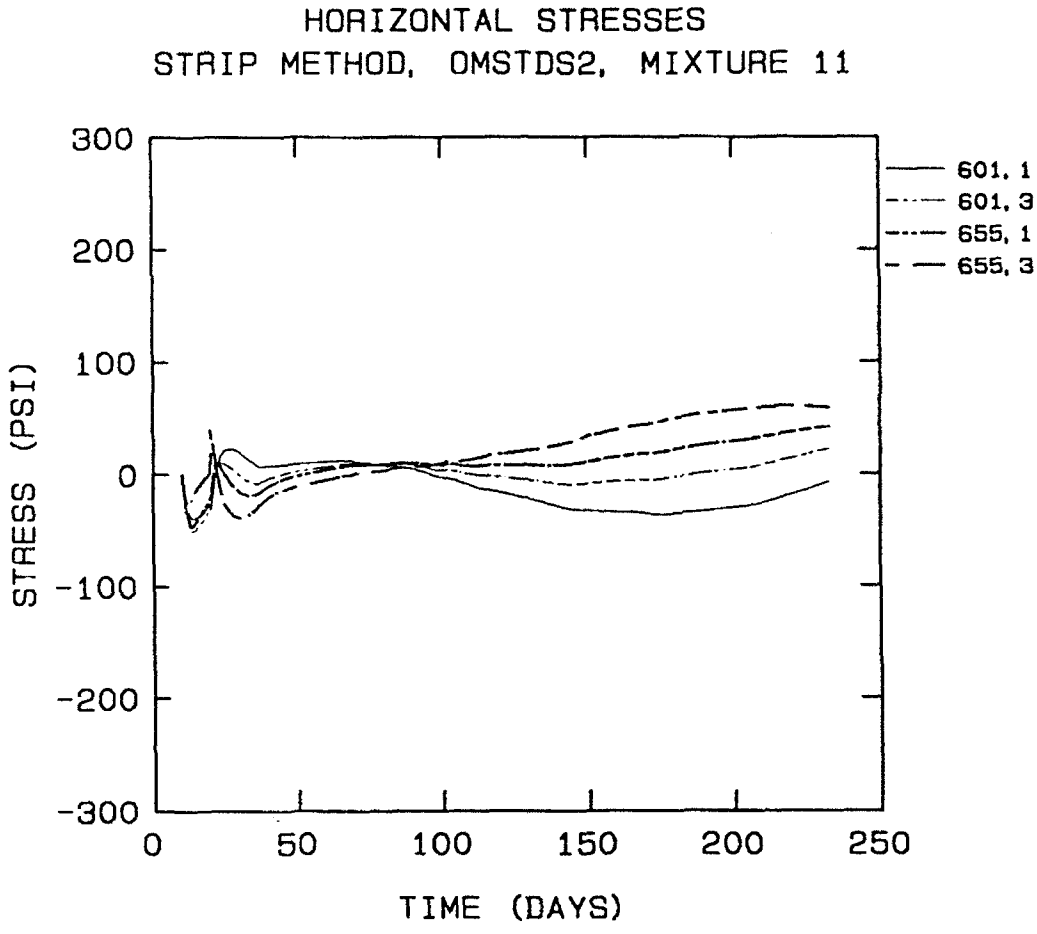

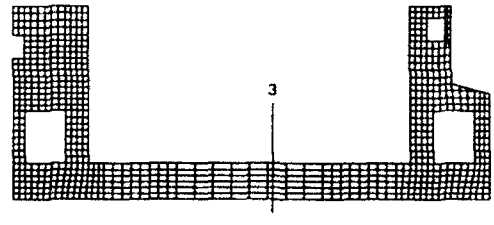

Figure 56. Horizontal stress at lift 2, section 3, OMSTDS2

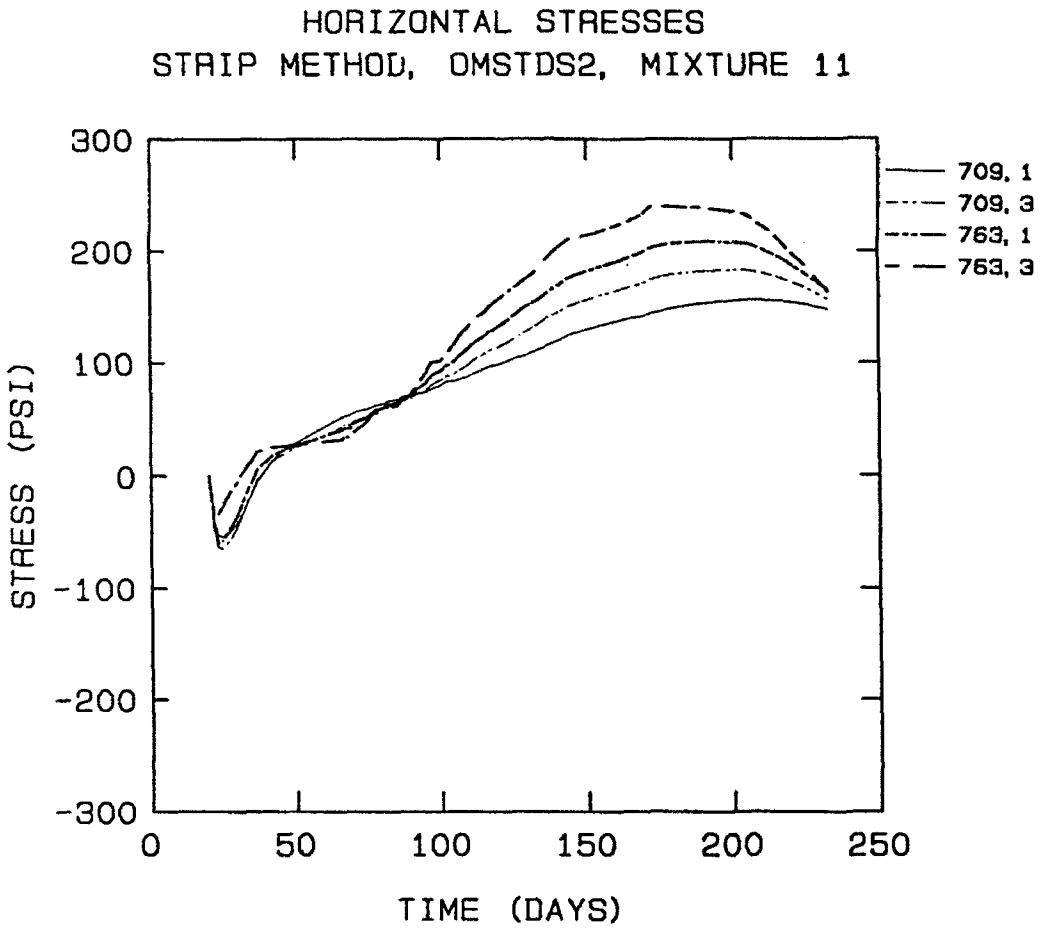

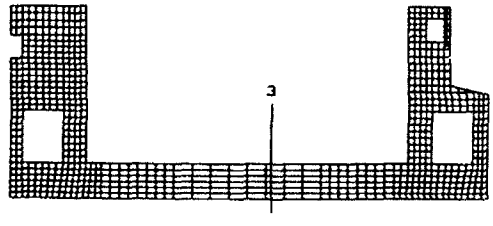

Figure 57. Horizontal stress at lift 3, section 3, OMSTDS2

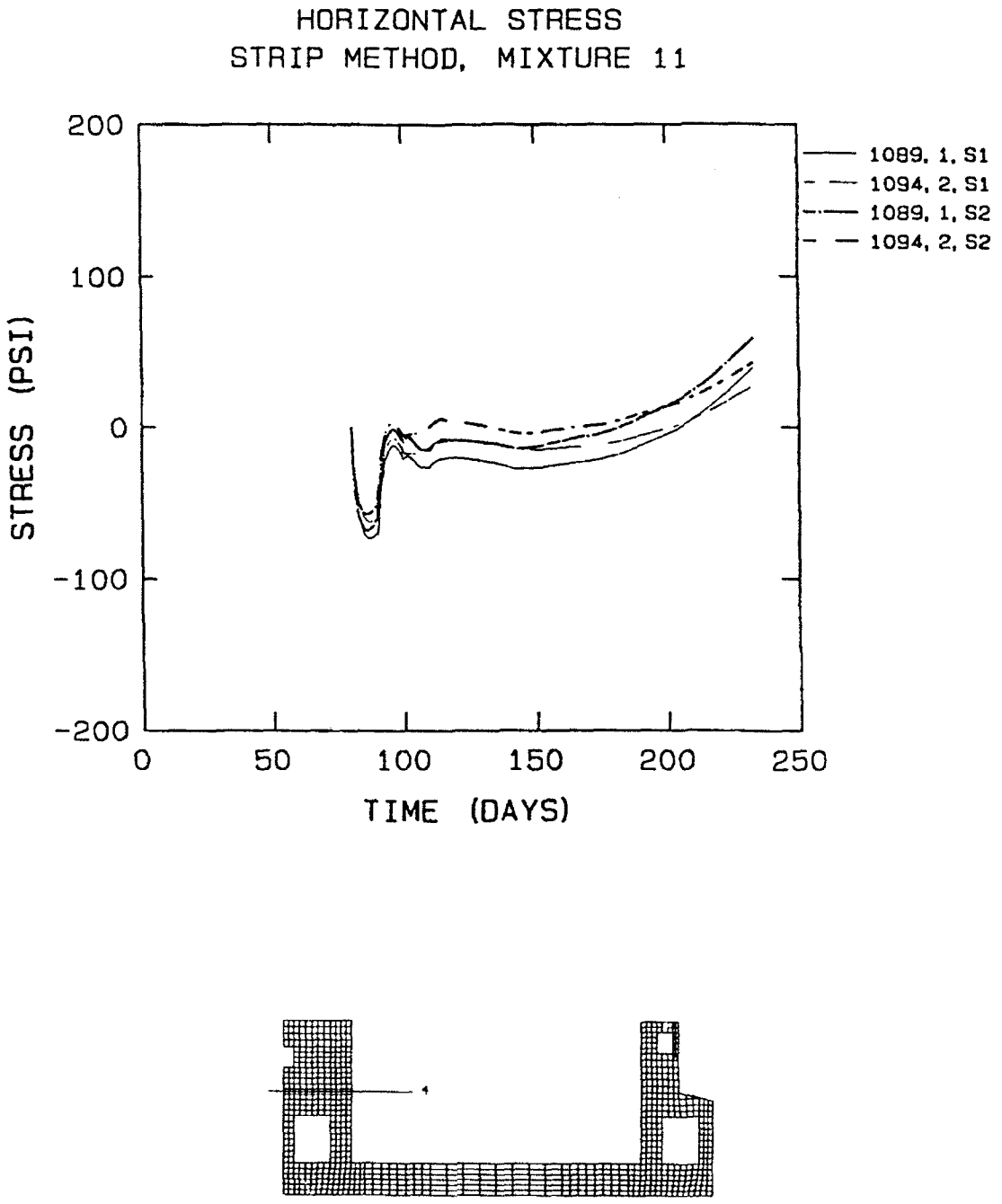

Figure 58. Horizontal stress at section 4, OMSTDS1 and OMSTDS2

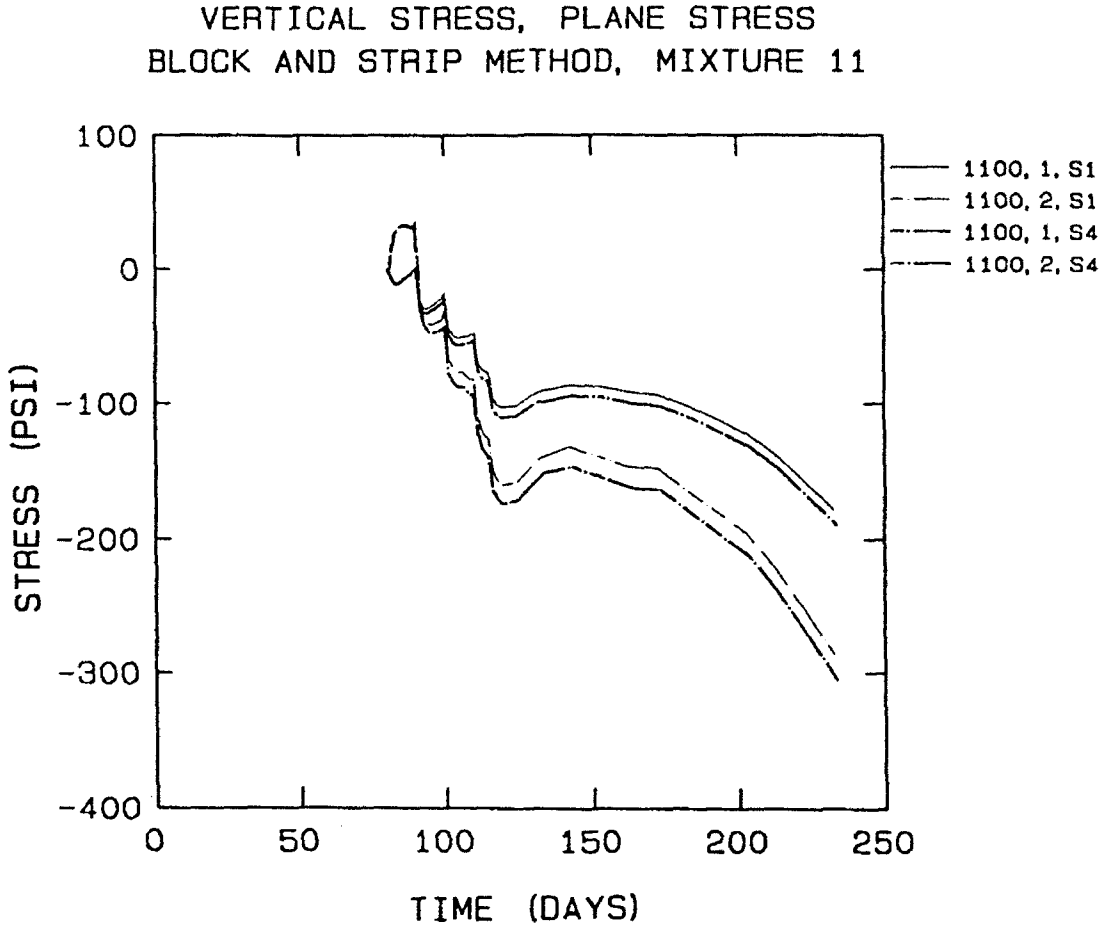

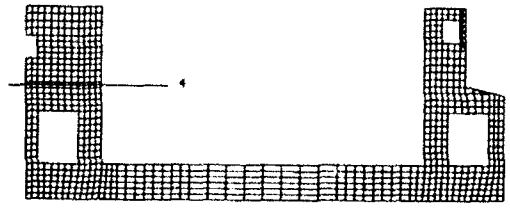

Figure 59. Vertical stress at section 4, OMSTDS1 and OMSTDS2

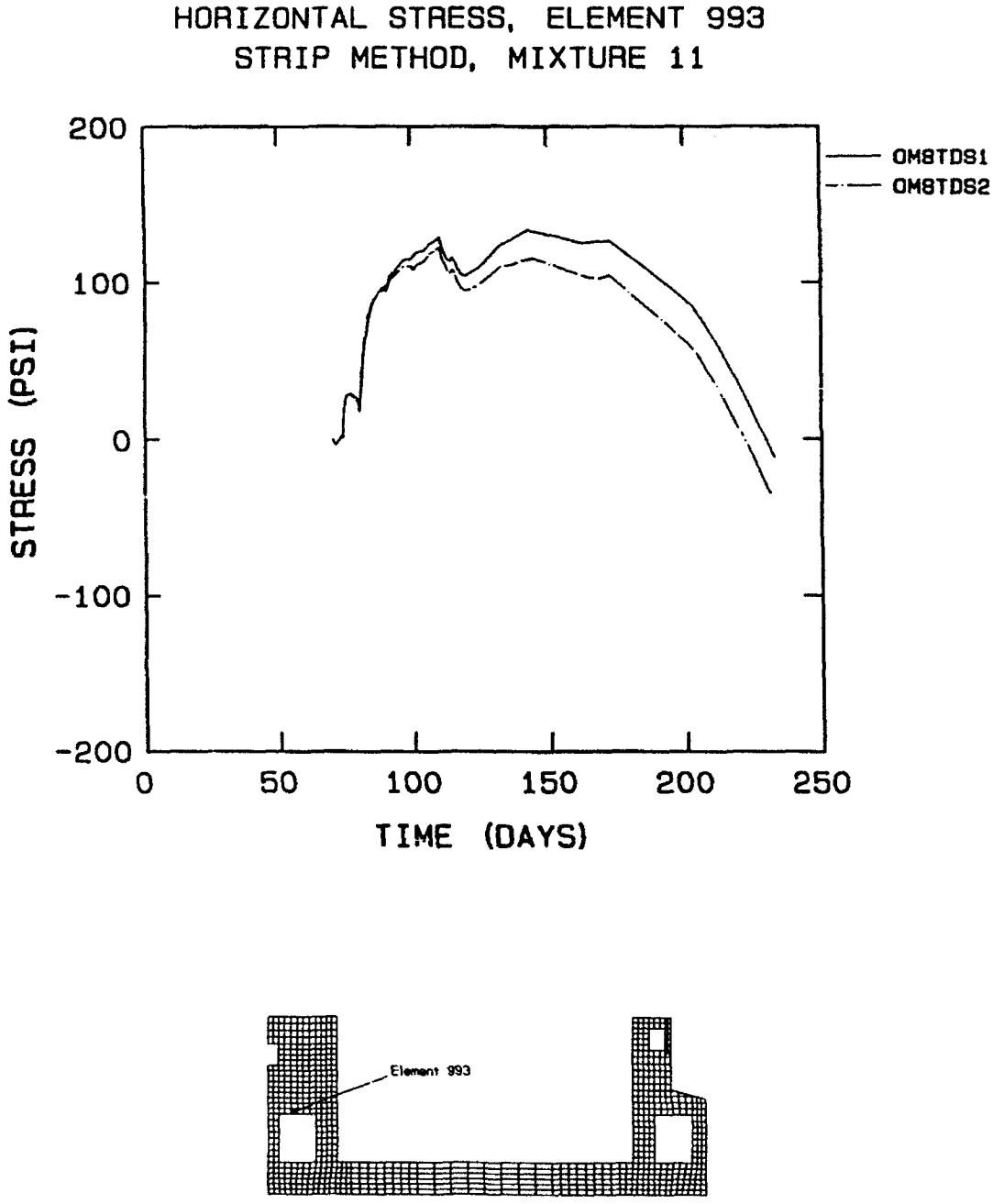

Figure 60. Horizontal stress at element 993, OMSTDS1 and OMSTDS2

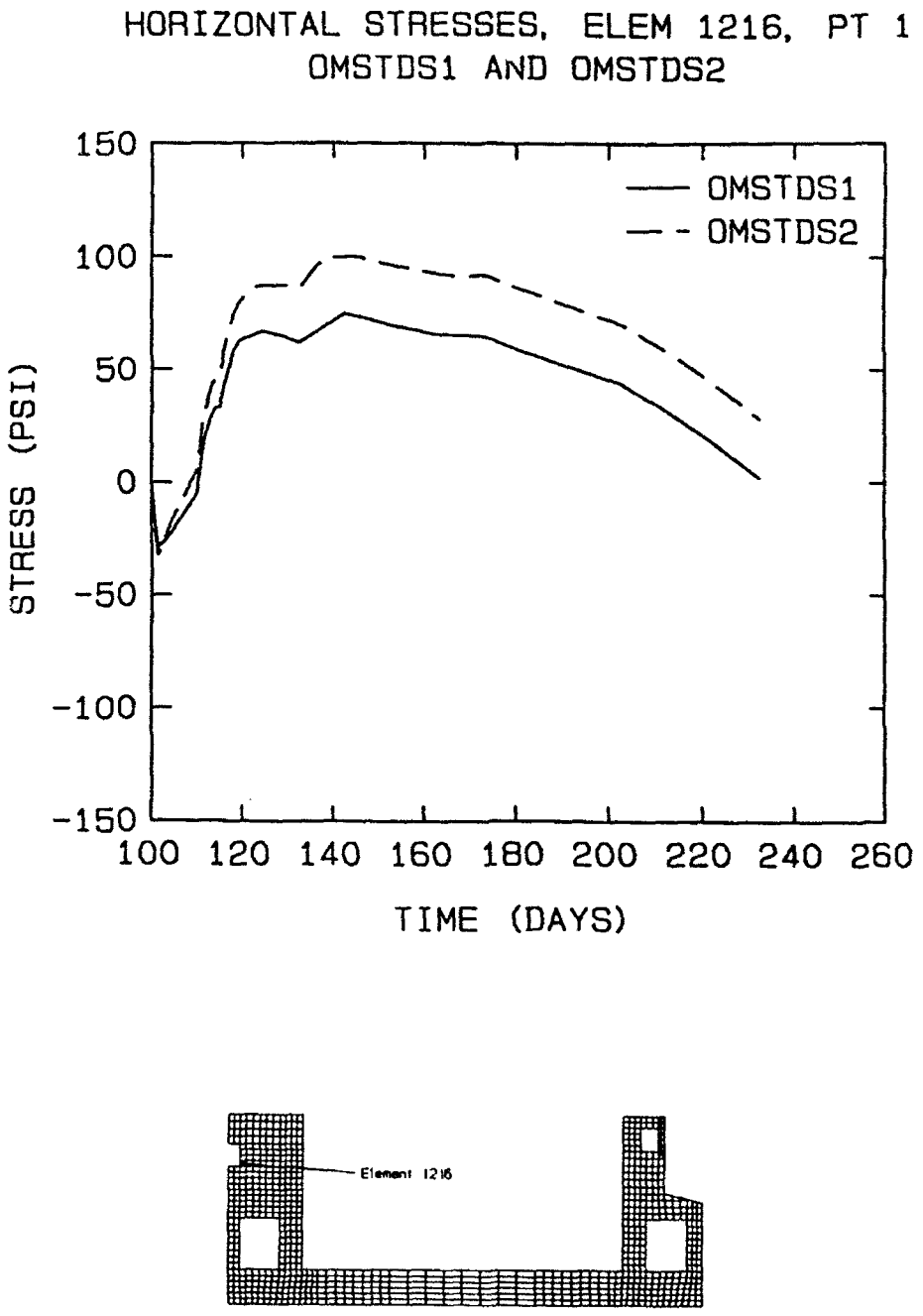

Figure 61. Horizontal stress at element 1216, OMSTDS1 and OMSTDS2

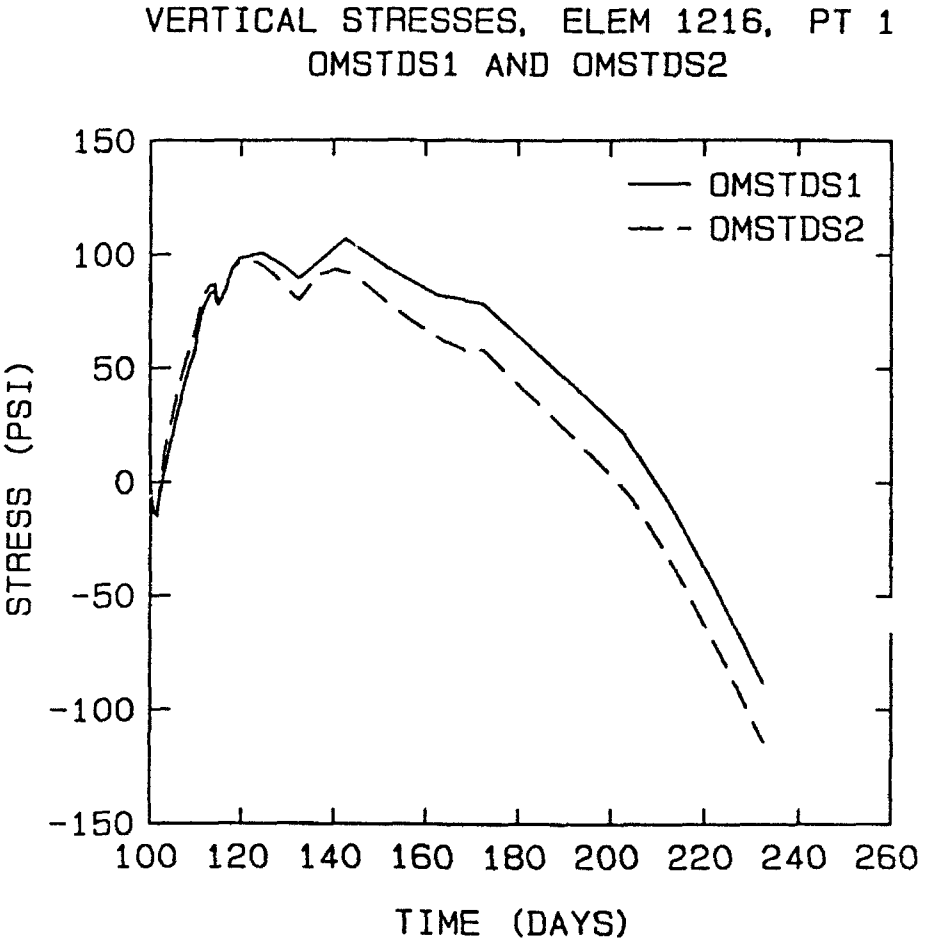

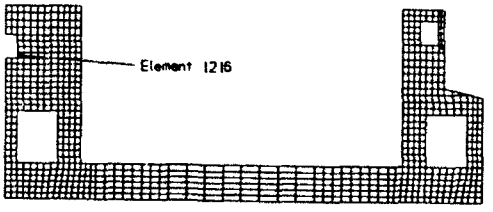

Figure 62. Vertical stress at element 1216, OMSTDS1 and OMSTDS2

92. Stress contours from this analysis were similar to those from the first plane stress analysis, and no stress contour plots for this analysis have been included in the Appendices.

93. Strip placement analysis 4 (OMSTDS3). Since the low shrinkage characteristic of mixture 11 was due to the composition of the particular cement and fly ash used, an analysis was run using the mixture 6 shrinkage curve. All other variables remained the same as in the OMSTDS1 analysis. That horizontal stress behavior at lift 3, section 3, in the slab similar to that seen in previous analyses is apparent in Figure 63. Stresses from this analysis are compared to those from the OMSTDS1 analysis in Figures 64 through 68. Maximum tensile stresses in the floor were approximately 20 psi larger than those in the OMSTDS1 analysis. This represents only a 7-percent increase in stress. As was expected, horizontal tensile stresses and vertical compressive stresses were larger at section 4 in this analysis than in the OMSTDS1 analysis. Stresses at openings were similar to those in the OMSTDS2 analyses.

94. The same trends found in the OMSTDS1 and OMSTDS1A analyses are apparent in the OMSTDS3 analysis. The structure is responding in similar manner as in the OMSTDS1 and OMSTDS1A analyses, so similar conclusion as to fluctuations in stress can also be made.

95. Stress contour plots for this analysis were similar to those from the OMSTDS1 analysis and have not been included in the Appendices.

96. Block placement analyses 1 and 2 (OMSTDS4 and OMSTDS4A). These analyses differed from the OMSTDS1 and OMSTDS1A analyses in only two ways: (a) the placement scheme in the floor was different, and (b) the STEP=AMP parameter was used in place of intermediate nodes to isolate new lifts from existing displacements. As would be expected, areas of high stress were the same as in the OMSTDS1 and OMSTDS1A analyses.

97. Horizontal stresses at sections 2 and 3 are shown in Figures 69 through 71. As in the other analyses, vertical and shear stresses in the floor were negligible and have not been plotted. Maximum horizontal stress at the top of the floor was 203 psi in the plane stress analysis and 221 psi in the plane strain analysis. These values were slightly less than those in the strip placement analyses. Since the higher temperatures in the OMSTDT4 analysis occurred during the first 50 days when the w-frame floor was largely in compression, differences in temperatures between the two analyses probably had very little effect on stresses. The lower tensile stresses in the block placement analyses were probably due to the relative stiffness of the new and

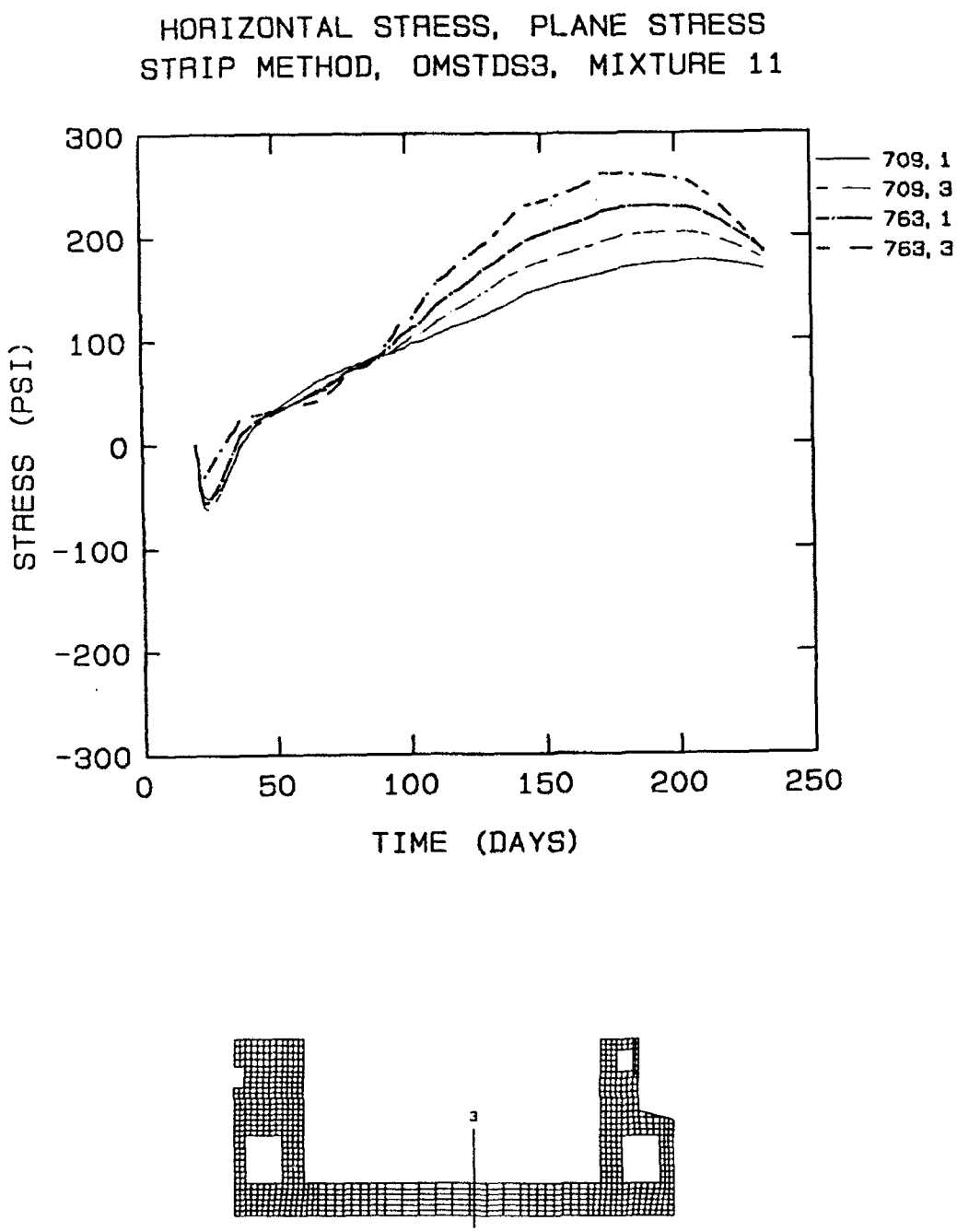

Figure 63. Horizontal stress at lift 3, section 3, OMSTDS3

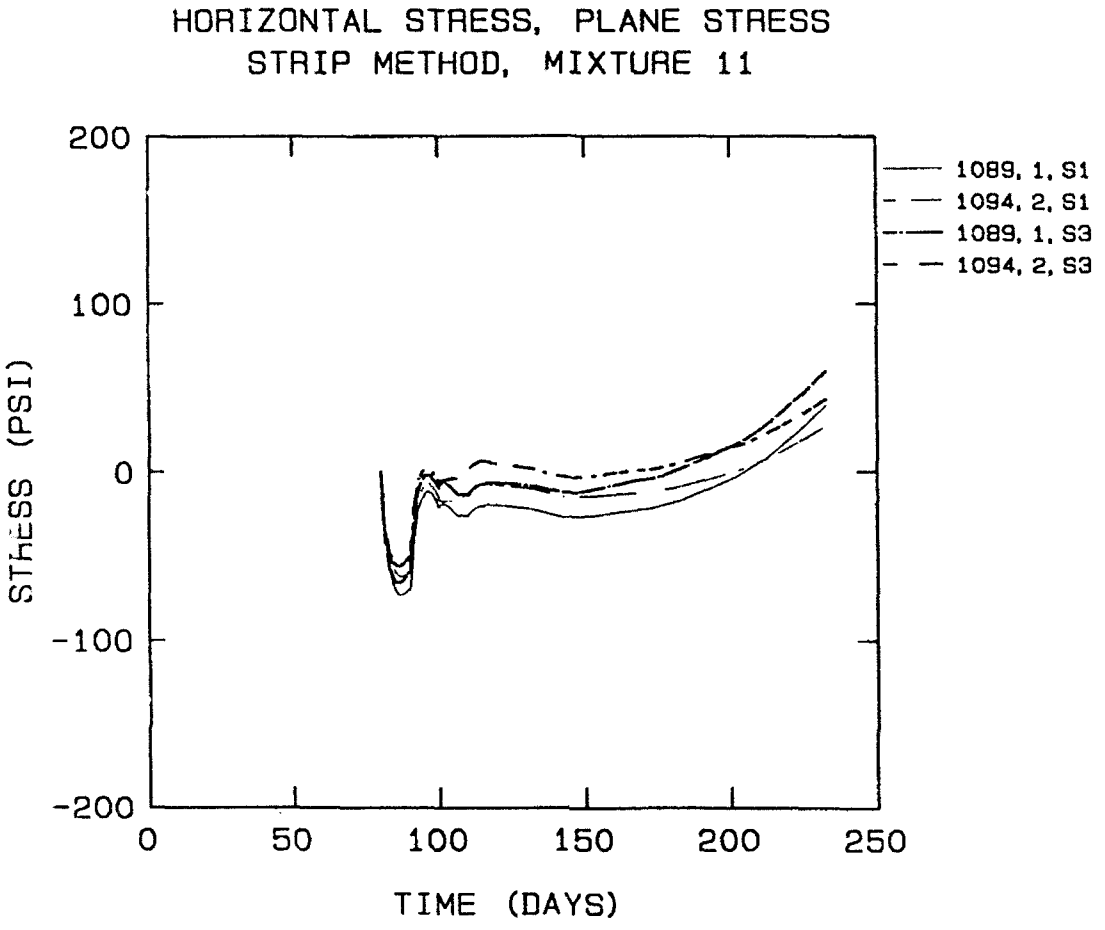

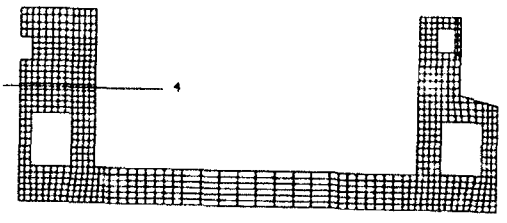

Figure 64. Horizontal stress at section 4, OMSTDS1 and OMSTDS3

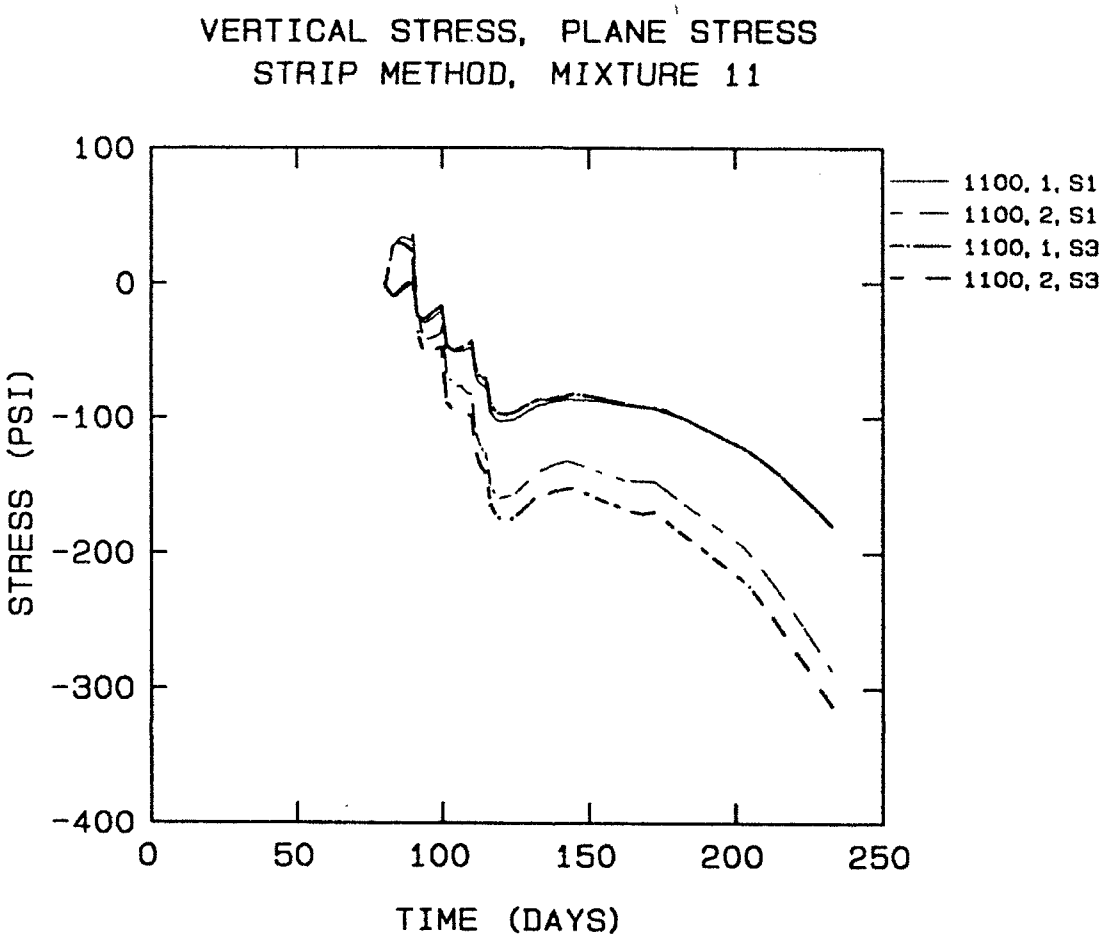

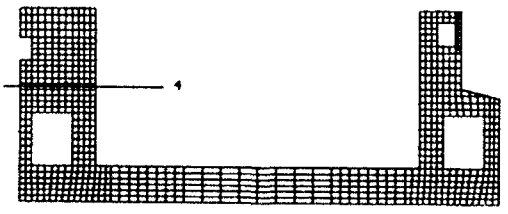

Figure 65. Vertical stress at section 4, OMSTDS1 and OMSTDS3

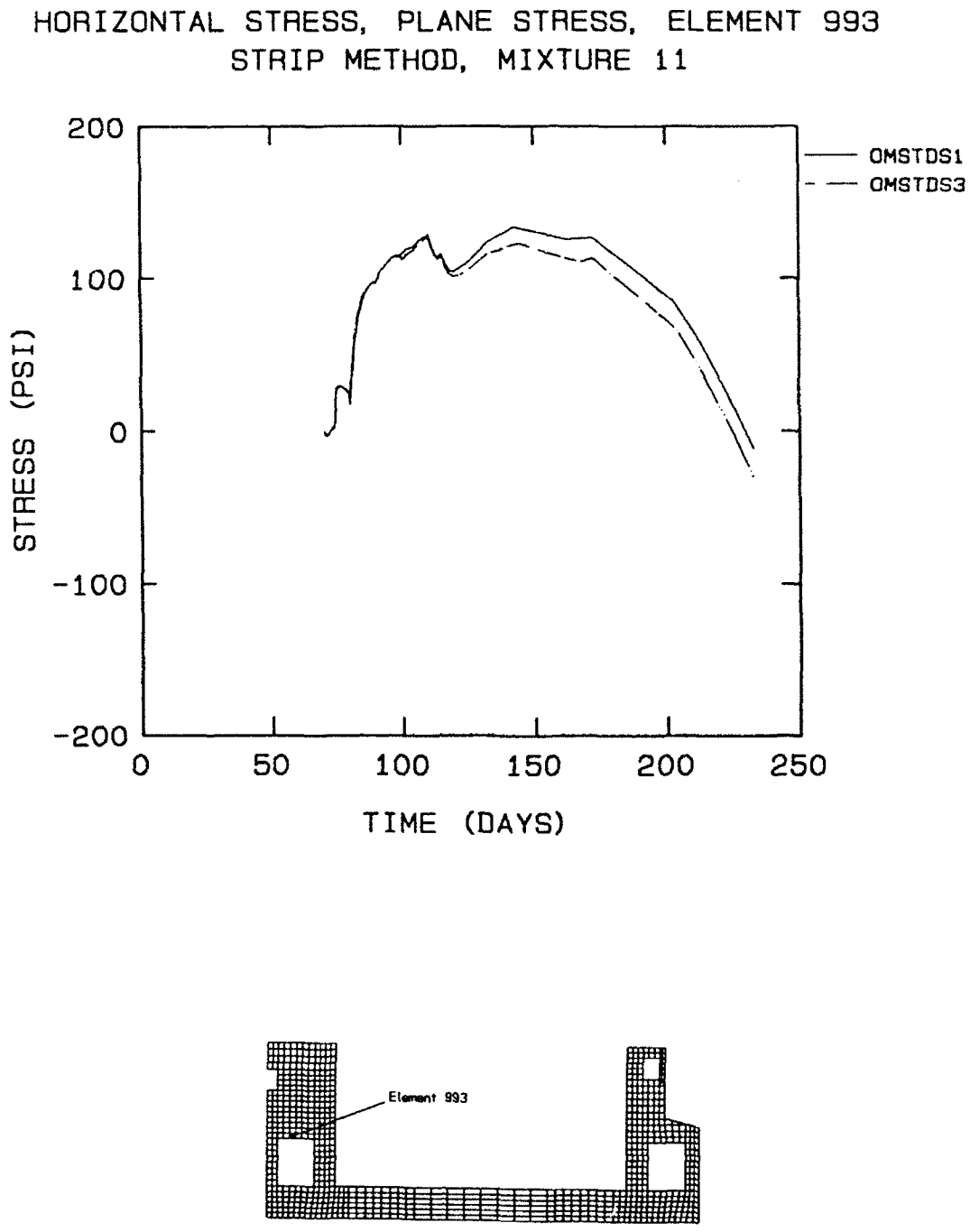

Figure 66. Horizontal stress at element 993, OMSTDS1 and OMSTDS3

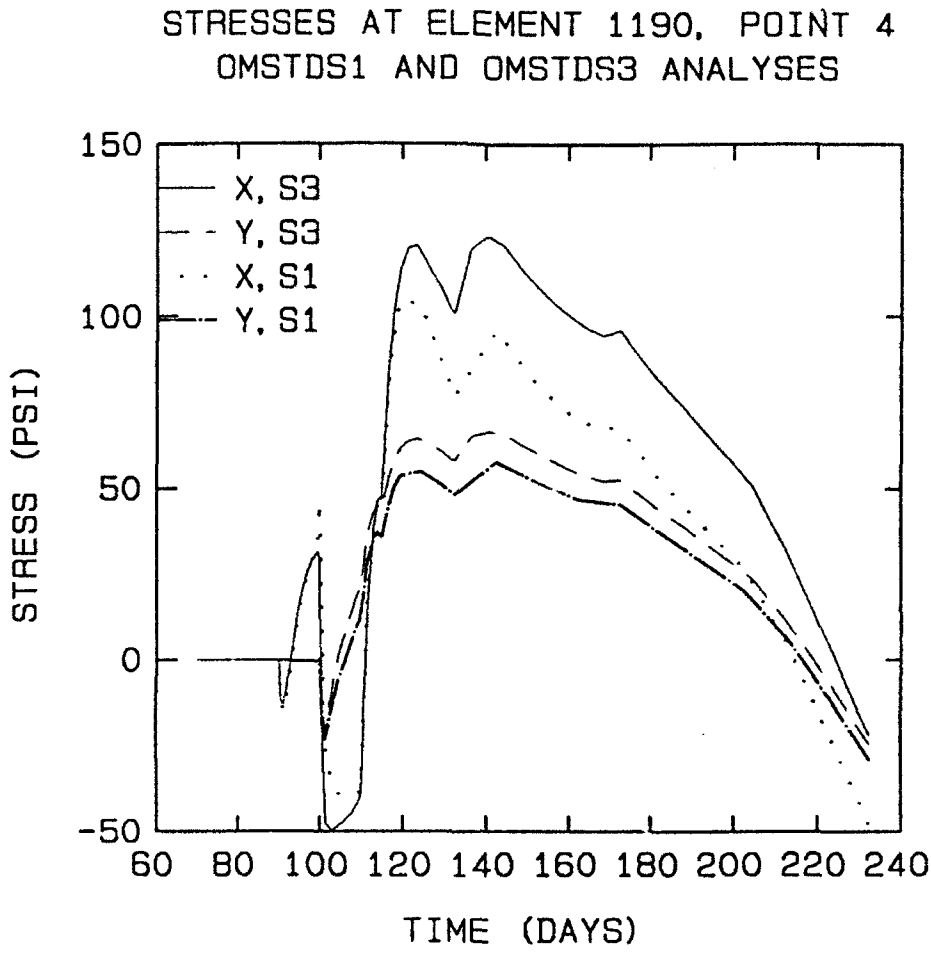

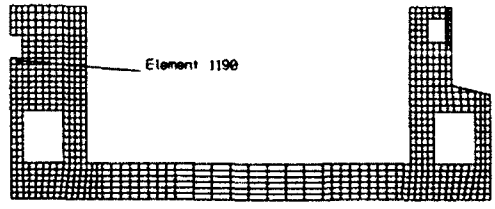

Figure 67. Stress at element 1190, OMSTDS1 and OMSTDS3

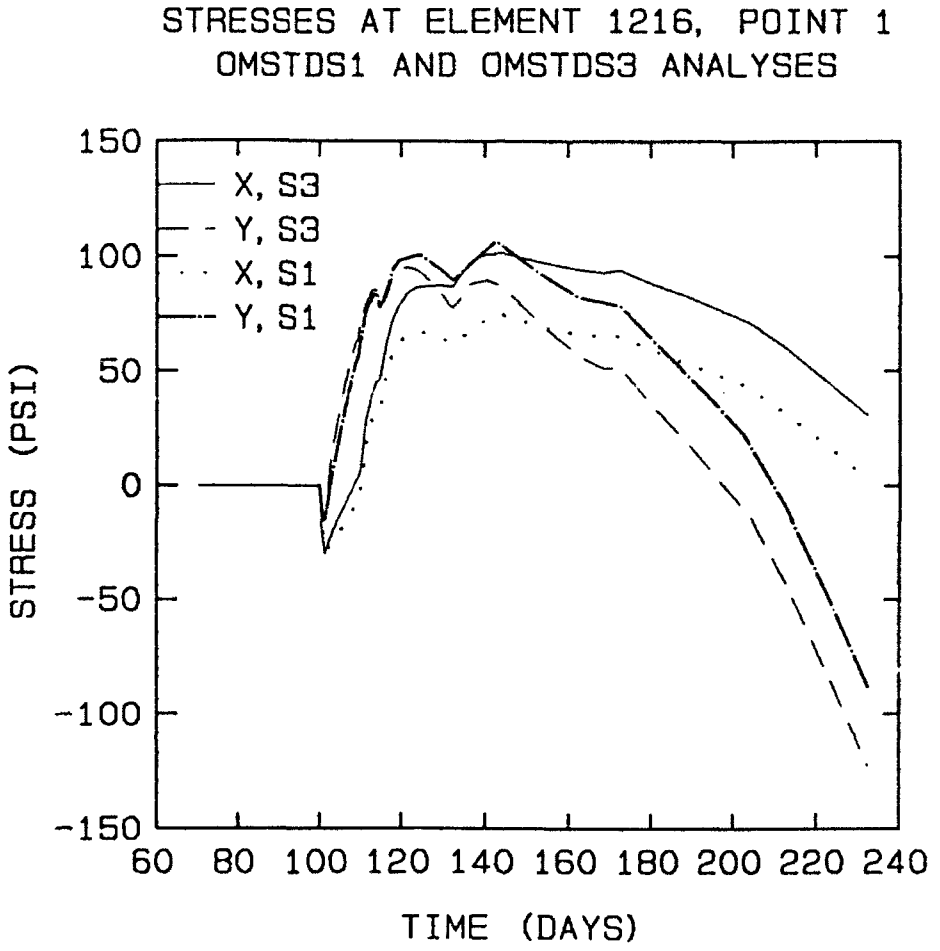

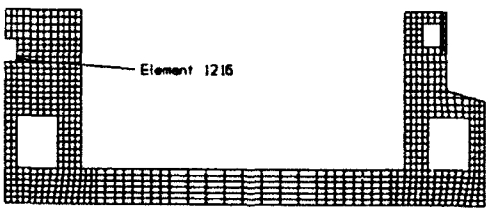

Figure 68. Stress at element 1216, OMSTDS1 and OMSTDS3

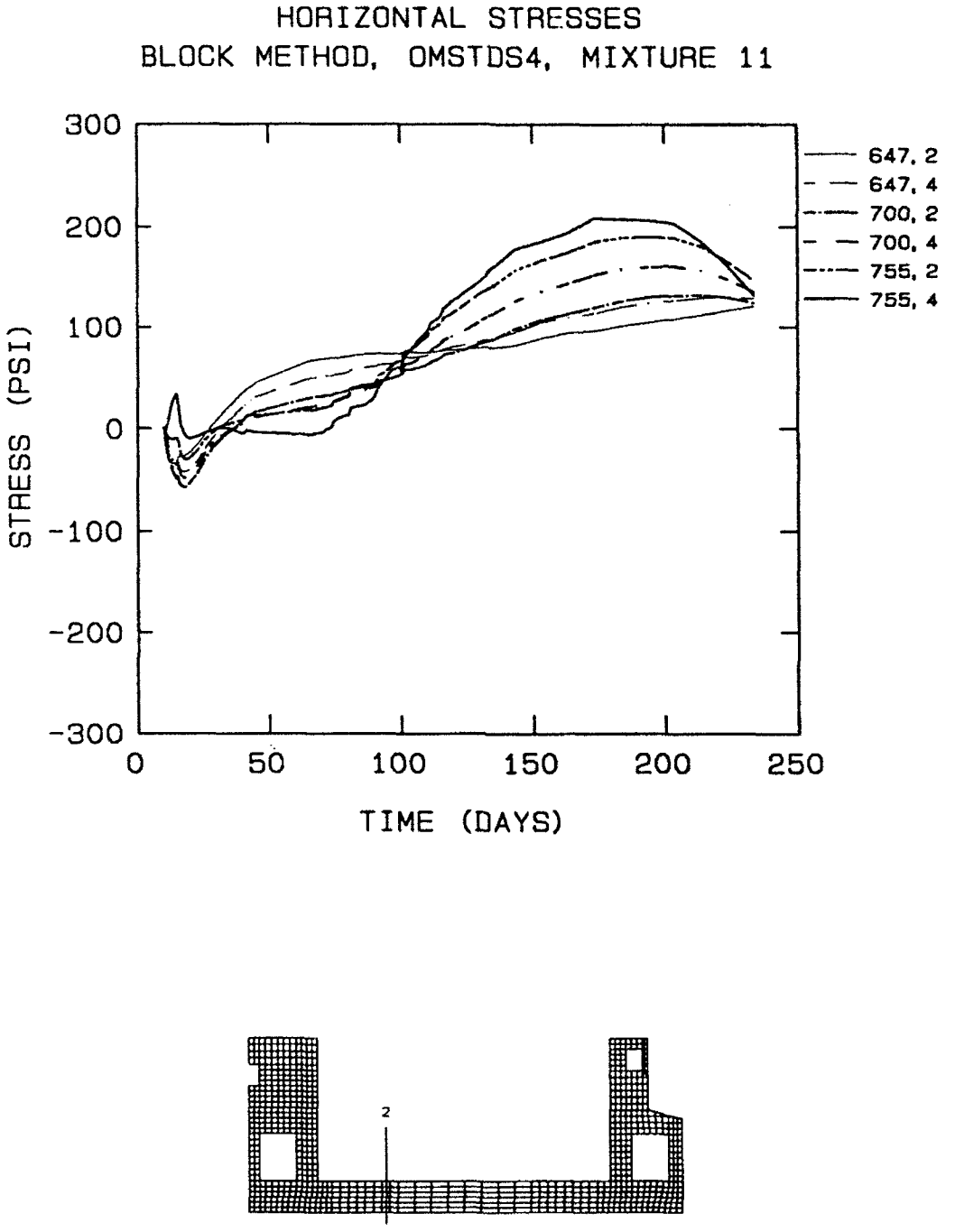

Figure 69. Horizontal stress at lift 3, section 2, OMSTDS4

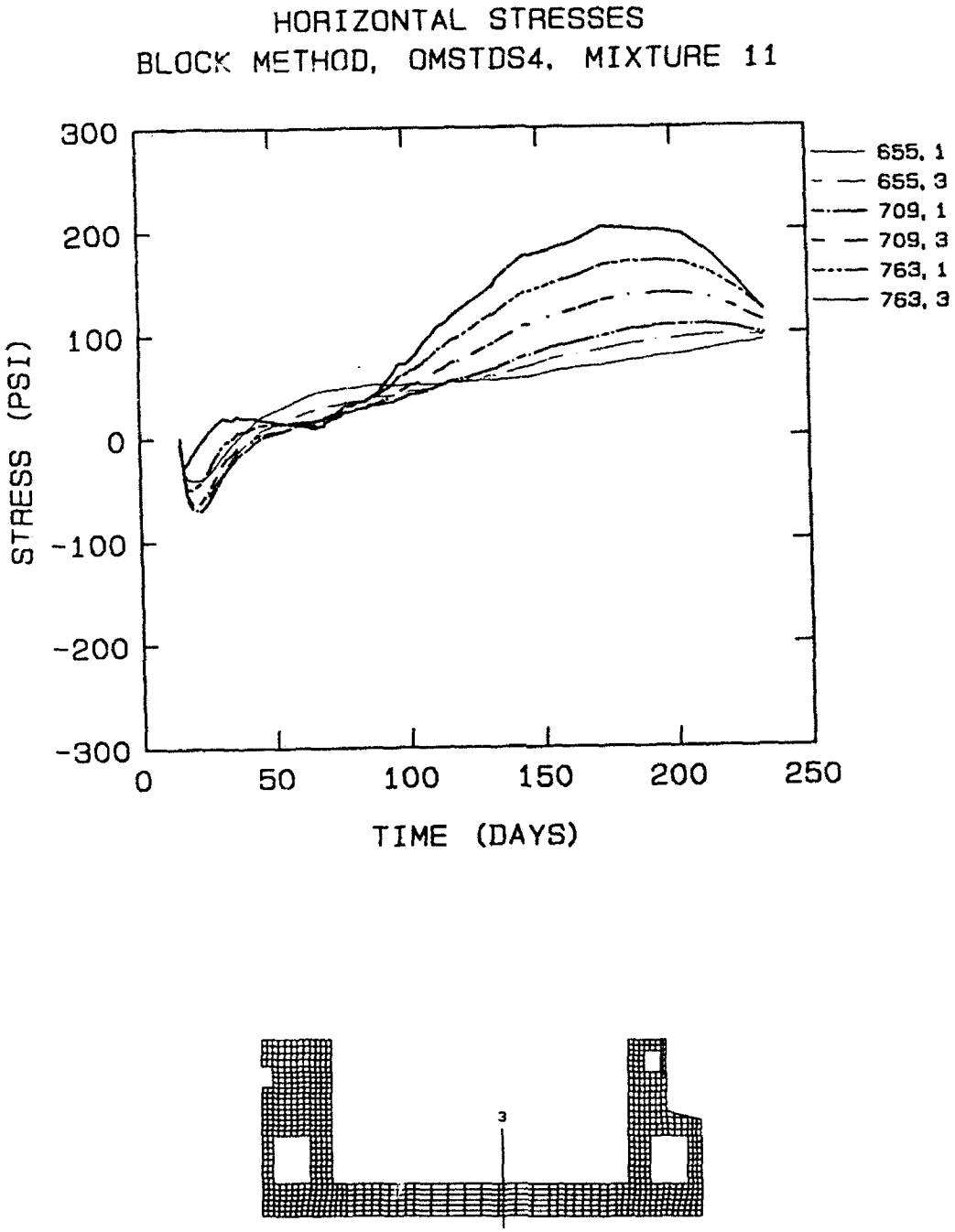

Figure 70. Horizontal stress at lift 4, section 3, OMSTDS4

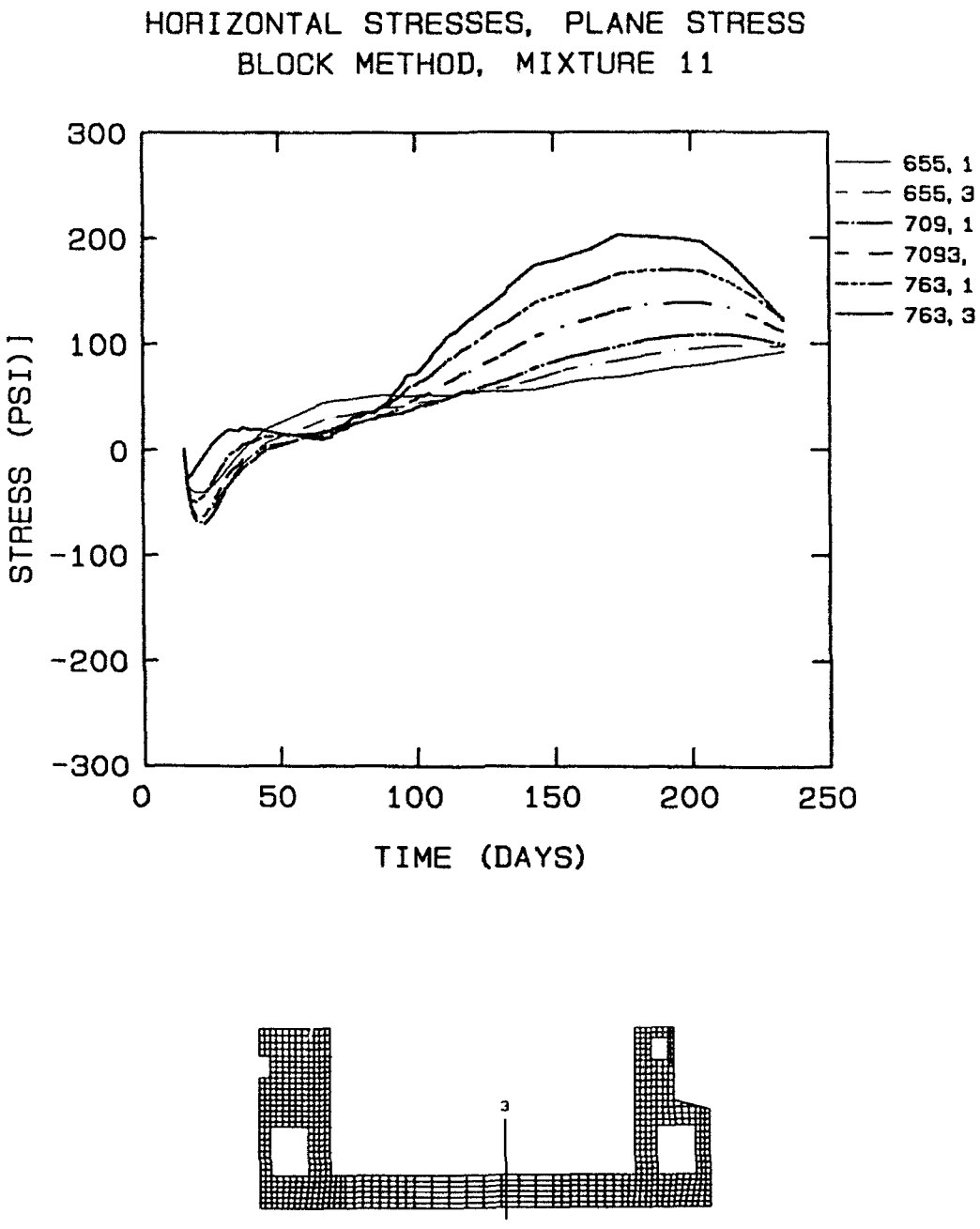

Figure 71. Horizontal stress at lift 4, section 3, OMSTDS4

existing concrete sections in each analysis. In the block placement method, the existing concrete section was only 6 ft high and had been in place for only 10 days at the start of placement of the top section. In the strip method, the existing concrete section was 8 ft high, and the bottom lift had been in place for 20 days at the start of placement of lift 3. This means that more restraint was provided to volumetric changes in the new lift in the strip placement method analyses than in the block placement analyses in the plane under consideration.

98. Even though placement times and temperatures and boundary conditions are the same in the walls as in the first two analyses, predicted stresses vary slightly between similar analyses. This is due to the different methods used to isolate new concrete from existing displacements in the strip and block placement analyses. In general, predicted stresses from comparable analyses are within 5 percent except at the top wall opening, where maximum differences between similar analyses are approximately 10 percent. Stresses at section 4, at the top of the center wall culvert and at the corner of the upper opening are compared with those from the previous analyses in Figures 72 through 76. The dramatic change in stress in OMSTDS4A curves at 180 days in Figure 76 is a result of nonconvergence in the analysis rather than any real phenomenon. This demonstrates the problems that can occur in a plane strain analysis. Cracking due to out-of-plane stresses can cause nonconvergence resulting in unrealistic in-plane stresses and even in-plane cracking. Cracking due to out-of-plane stresses was initiated in the OMSTDS4A analysis at 65 days. No cracking occurred in the OMSTDS4 analysis.

99. Strip placement analyses 5 and 6 (OMSTDS5 and OMSTDS5A). These analyses were of the floor only in a plane parallel to the direction of flow. The strip placement method was used in both analyses since it was the only placement method with construction joints in the plane of the model. Sections 1 through 3, Figure 77, were used for the comparison of stresses across the floor and are located near vertical lift interfaces. Lift numbers refer to the placement scheme shown in Figure 10.

100. The maximum stress in the z-direction occurred near the vertical interface of the top two lifts (at section 2) and were 127.4 psi in the plane strain analysis and 109 psi in the plane stress analysis. High tensile stresses in the top two lifts tended to decrease with time after 180 days. All other vertical interfaces were in lower lifts, and stresses normal to the interface were primarily compressive. Stresses in the z-direction in section

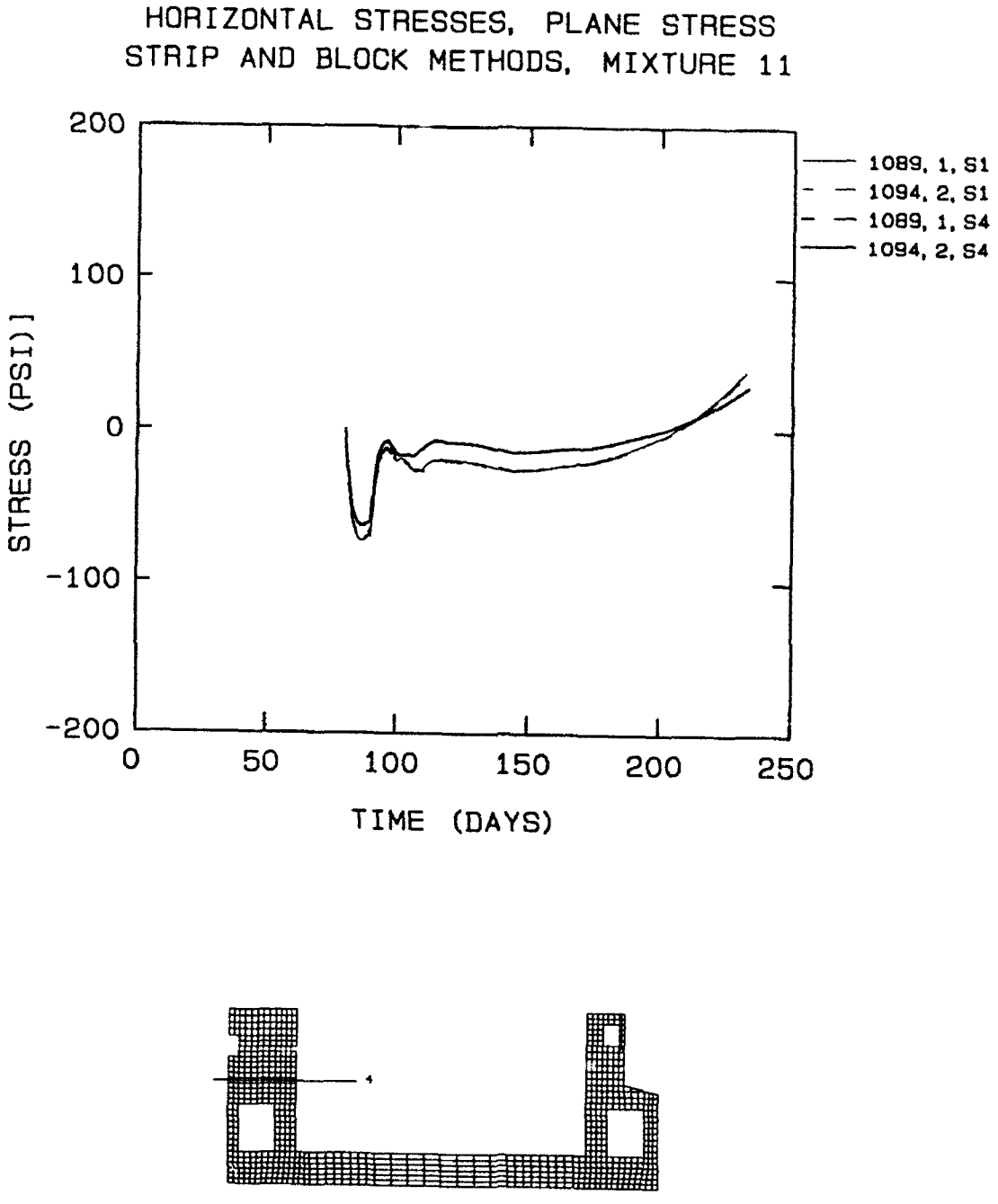

Figure 72. Horizontal stress, section 4, OMSTDS1 and OMSTDS4

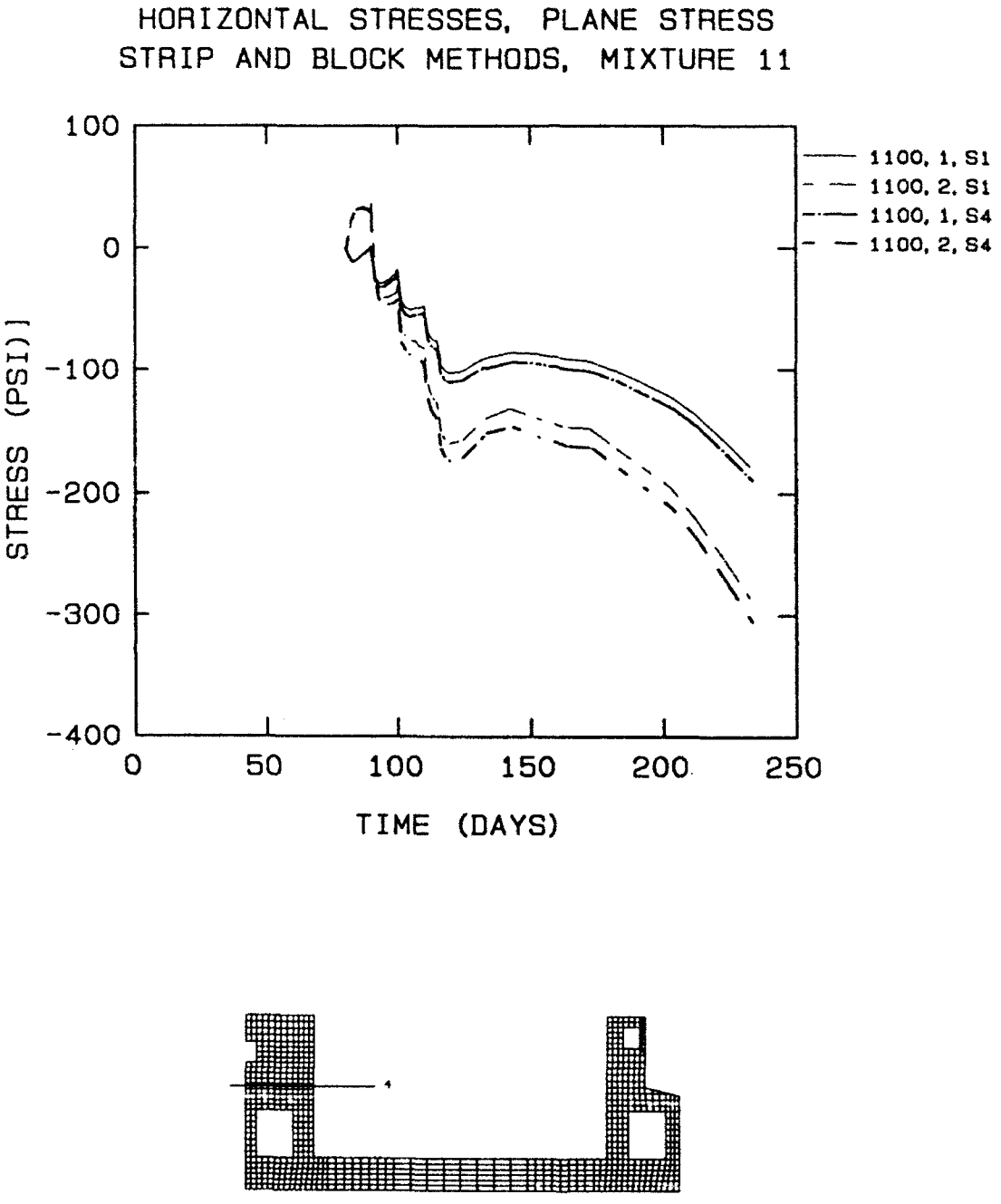

Figure 73. Vertical stress, section 4, OMSTDS1 and OMSTDS4

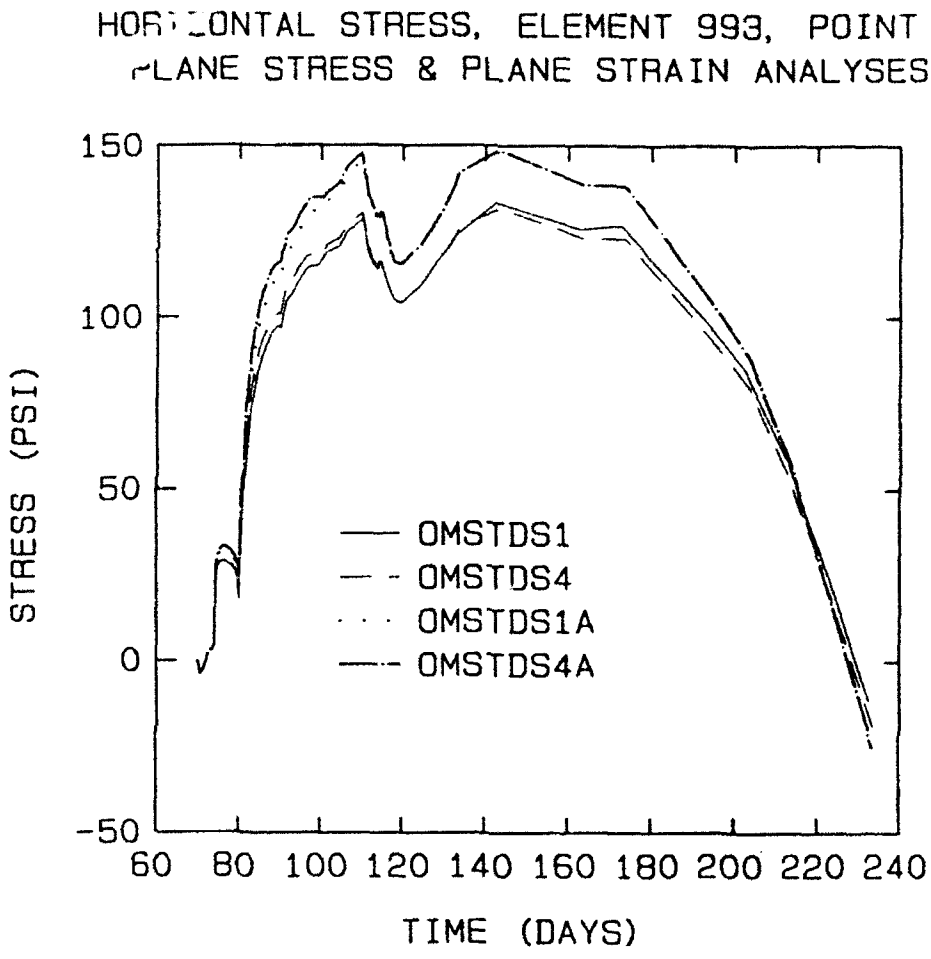

Figure 74. Horizontal stress, element 993, plane stress and plane strain analyses

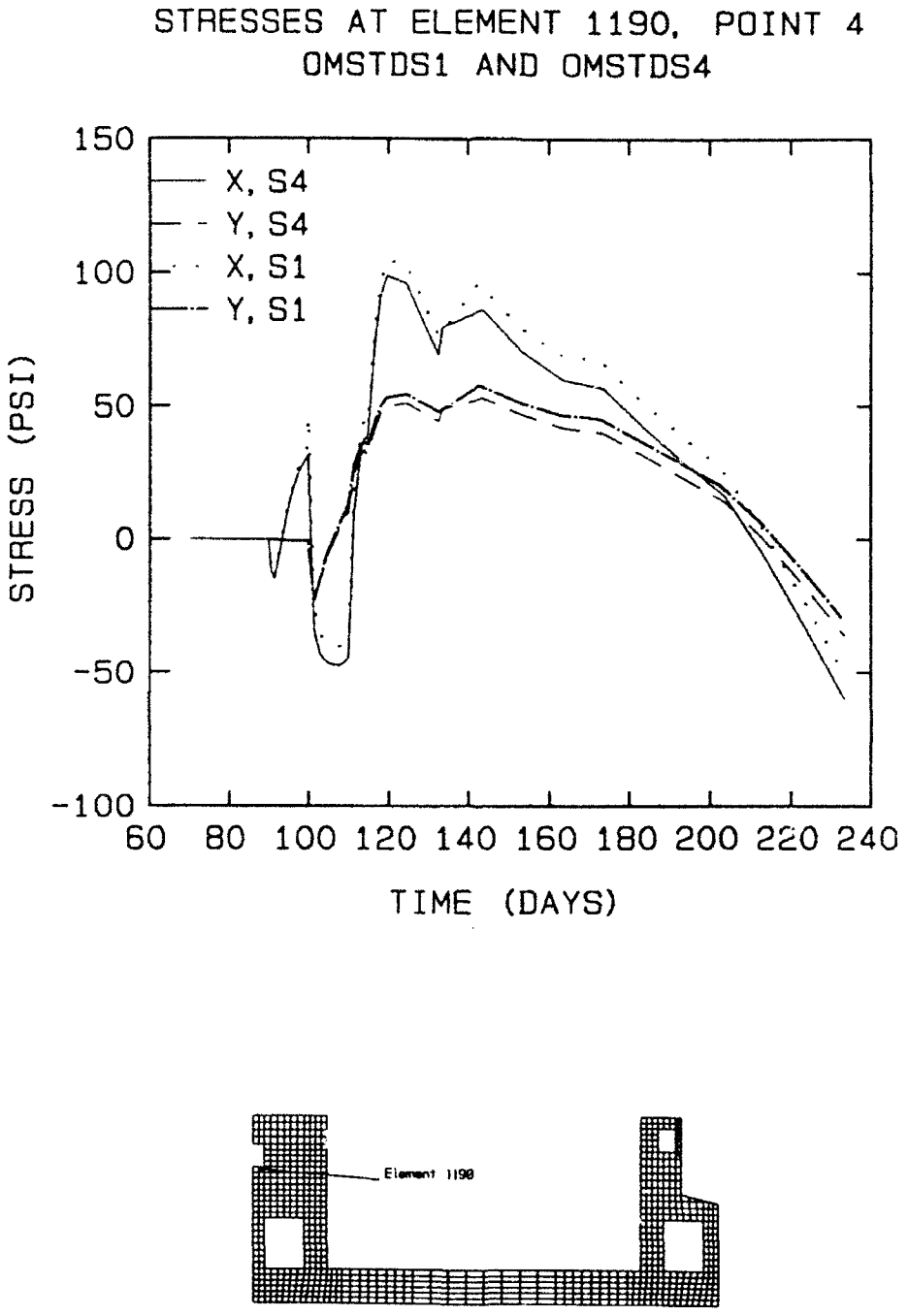

Figure 75. Stress at element 1190, OMSTDS1 and OMSTDS4

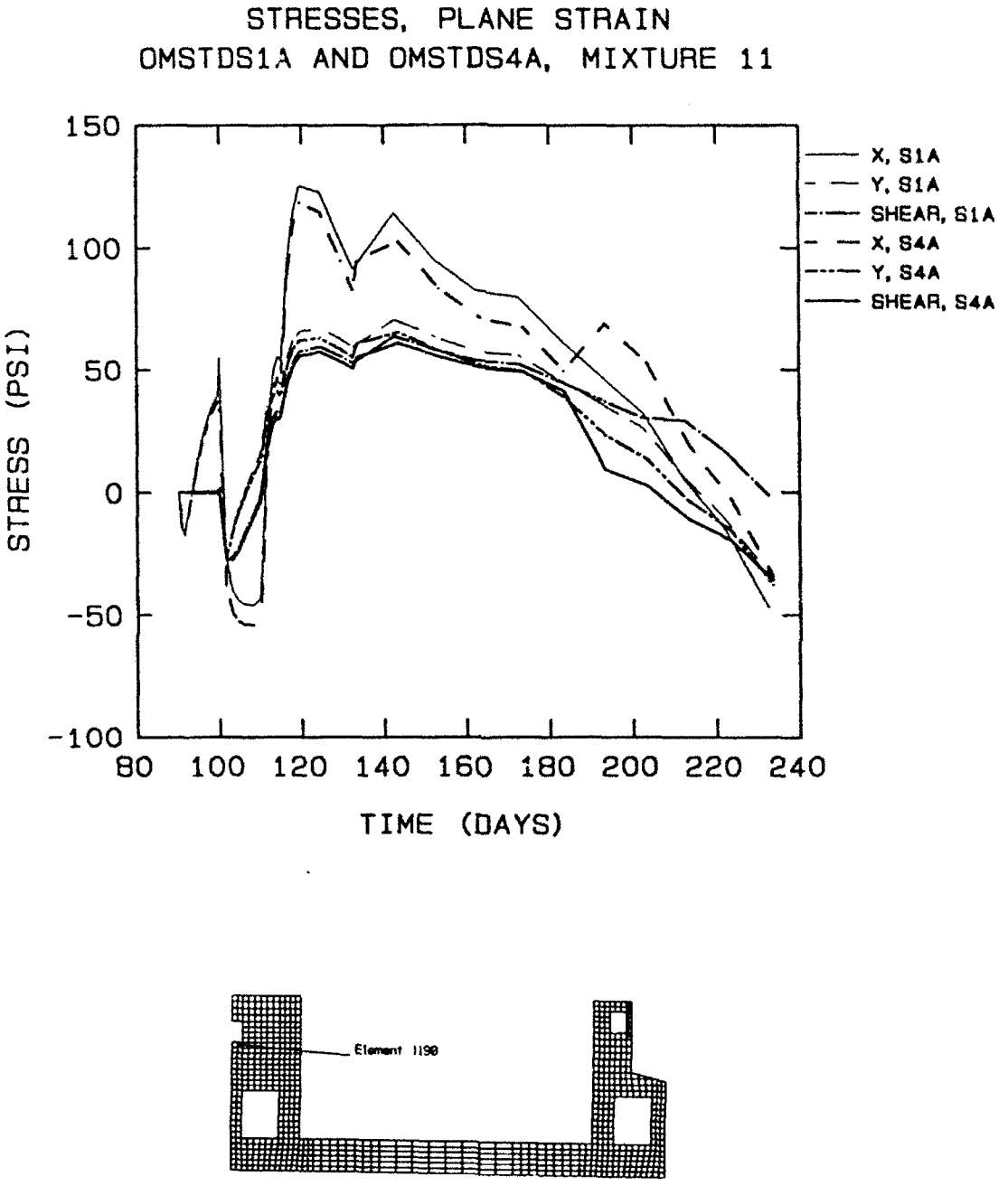

Figure 76. Stress at element 1190, plane strain analyses

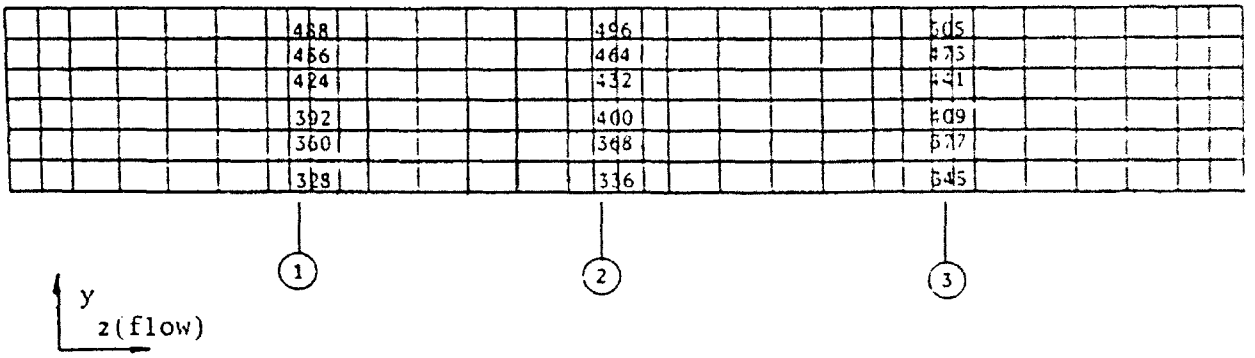

Figure 77 Sections and elements for stress/time plots, out-of-plane grid

2 are plotted in Figures 78 through 83. Stresses in the top lifts only at sections 1 and 3 are plotted in Figures 84 through 87.

101. Initial fluctuations in horizontal stress in Figures 78 and 81 are due to the effects of adjacent lift placements. After approximately 50 days, stresses in upper lifts become tensile and those in lower lifts become compressive, as was seen in previous analyses. Figures 79 and 82, being near the center of the slab, expectedly show small stress levels. Due to the location of the elements shown in these figures, it should be expected that the element just above midslab would show small tensile stress while the element just below midslab would show small compressive stress. Results showing rising and falling tensile and compressive stresses are ambient temperature related and reasons for this conclusion have previously been discussed in the OMSTDS1 and OMSTDS1A presentation. Figure 84, presenting results of a plane strain analysis, shows discontinuities just after 150 days. These result from stress redistributions due to the effects of out-of-plane cracking of nearby elements which occur in the analysis. Figure 85 results show the same trends that have been discussed for slab section in models transverse to this section.

Mixture 6, 2-D analyses

102. Strip placement method. Data selected for presentation correspond to the same locations as for the mixture 11 portion of this report. This allows direct comparison of results for each mixture. Stress contour and deformed shape plots for mixture 6 are provided in Appendices G and H. Caution should be exercised when viewing the deformed shape plots. They show severely distorted elements at the lift interfaces. These are merely

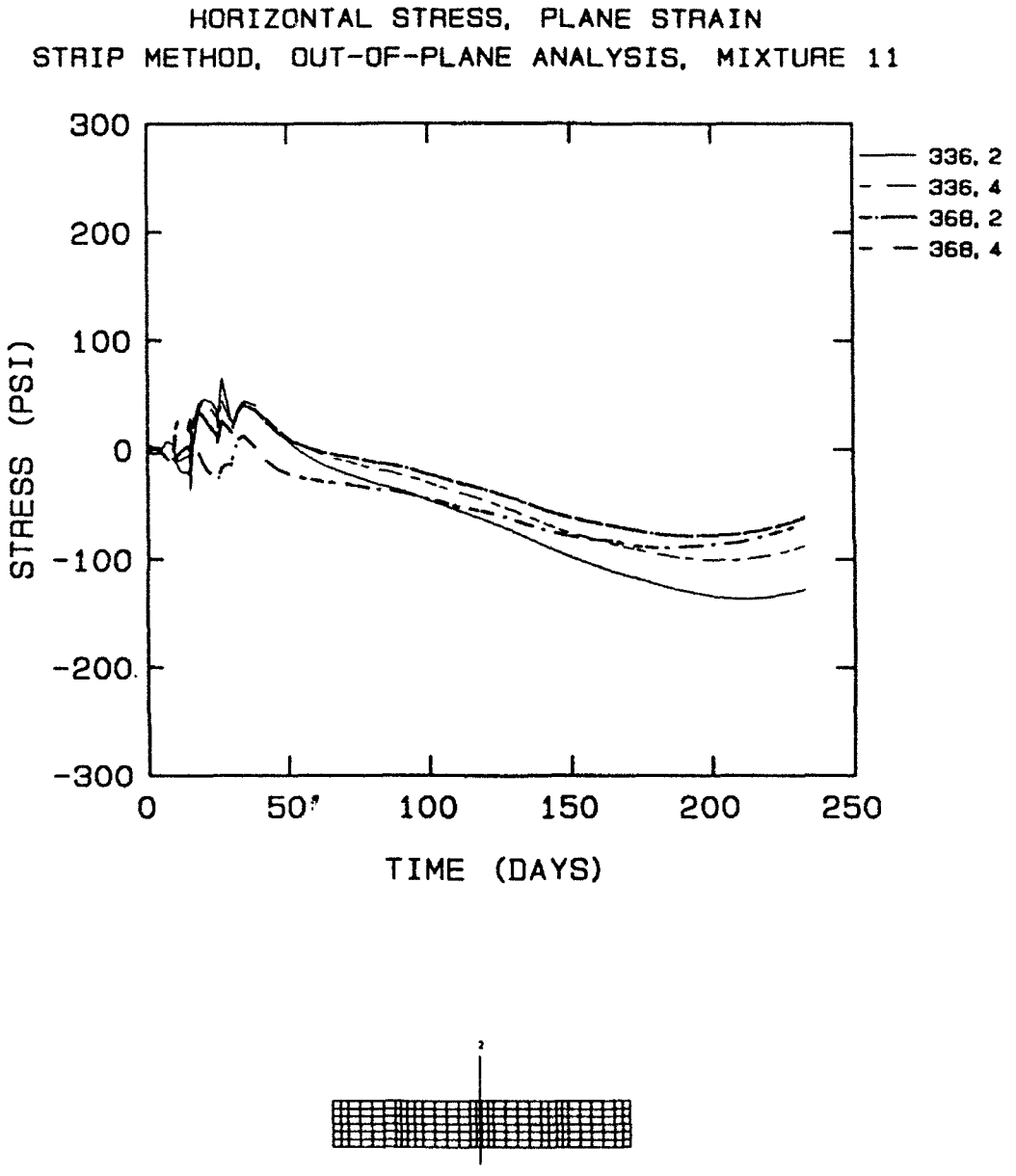

Figure 78. Horizontal stress at lift 1, section 2, OMSTDS5A

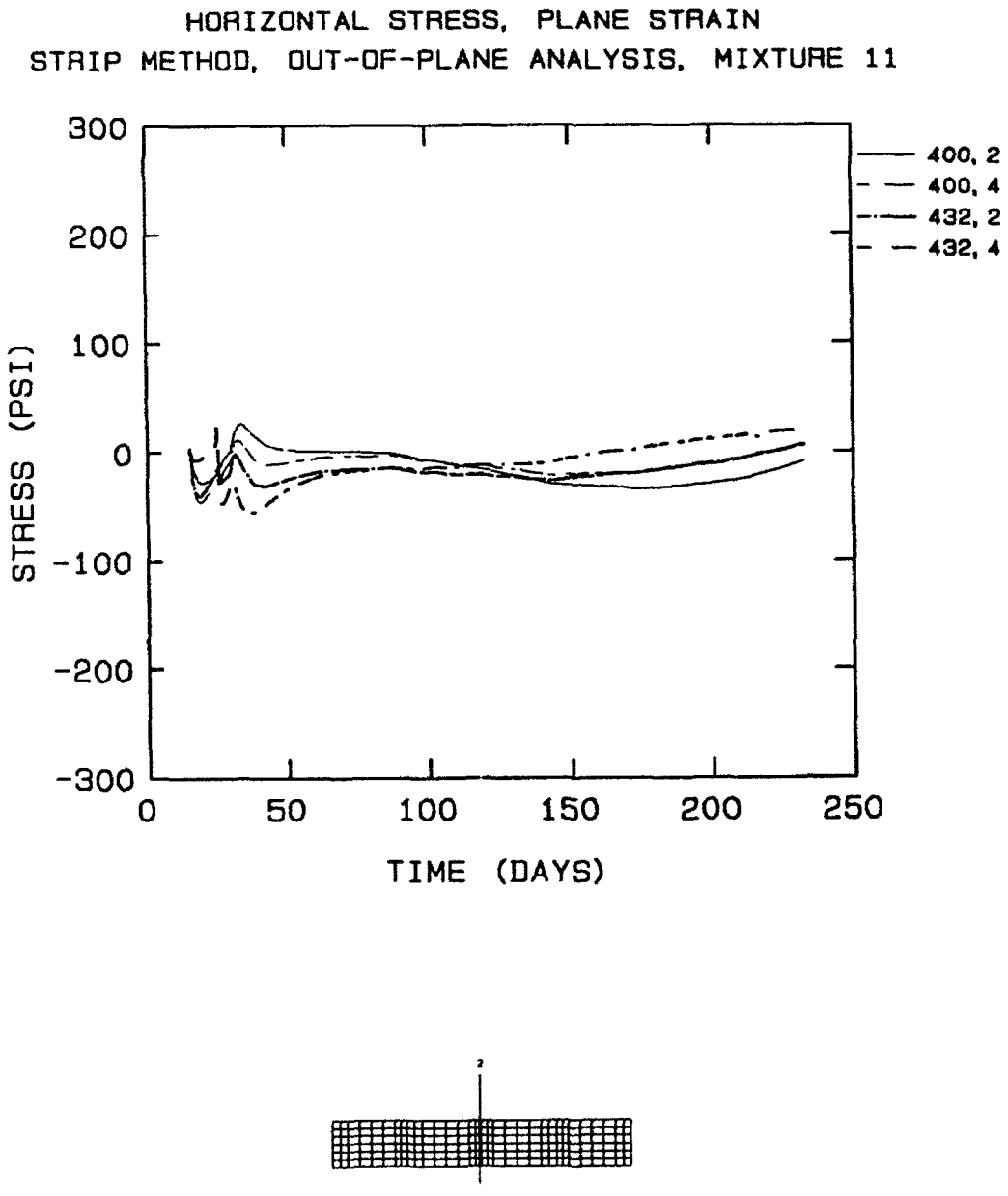

Figure 79. Horizontal stress at lift 4, section 2, OMSTDS5A

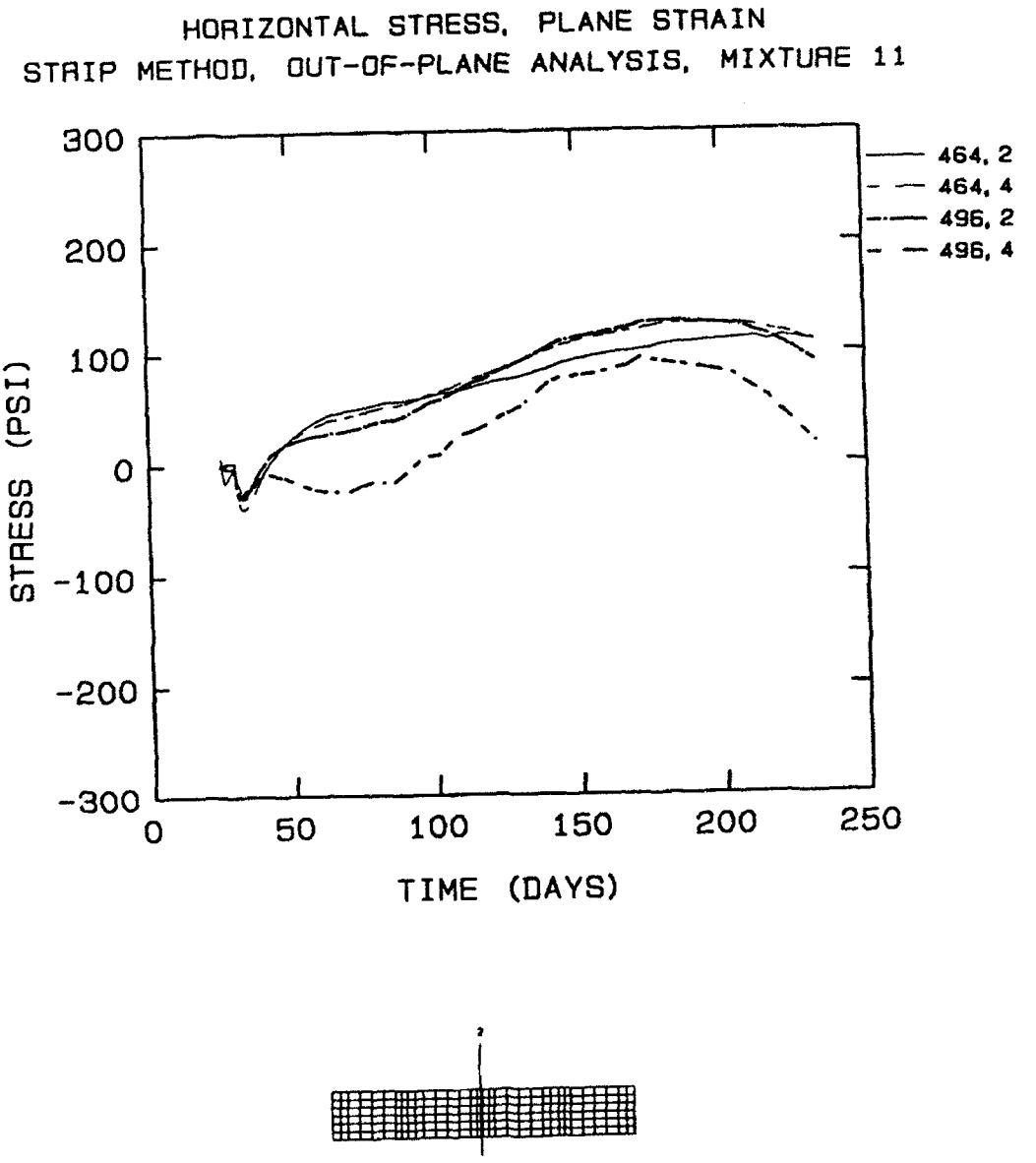

Figure 80. Horizontal stress at lift 6, section 2, OMSTDS5A

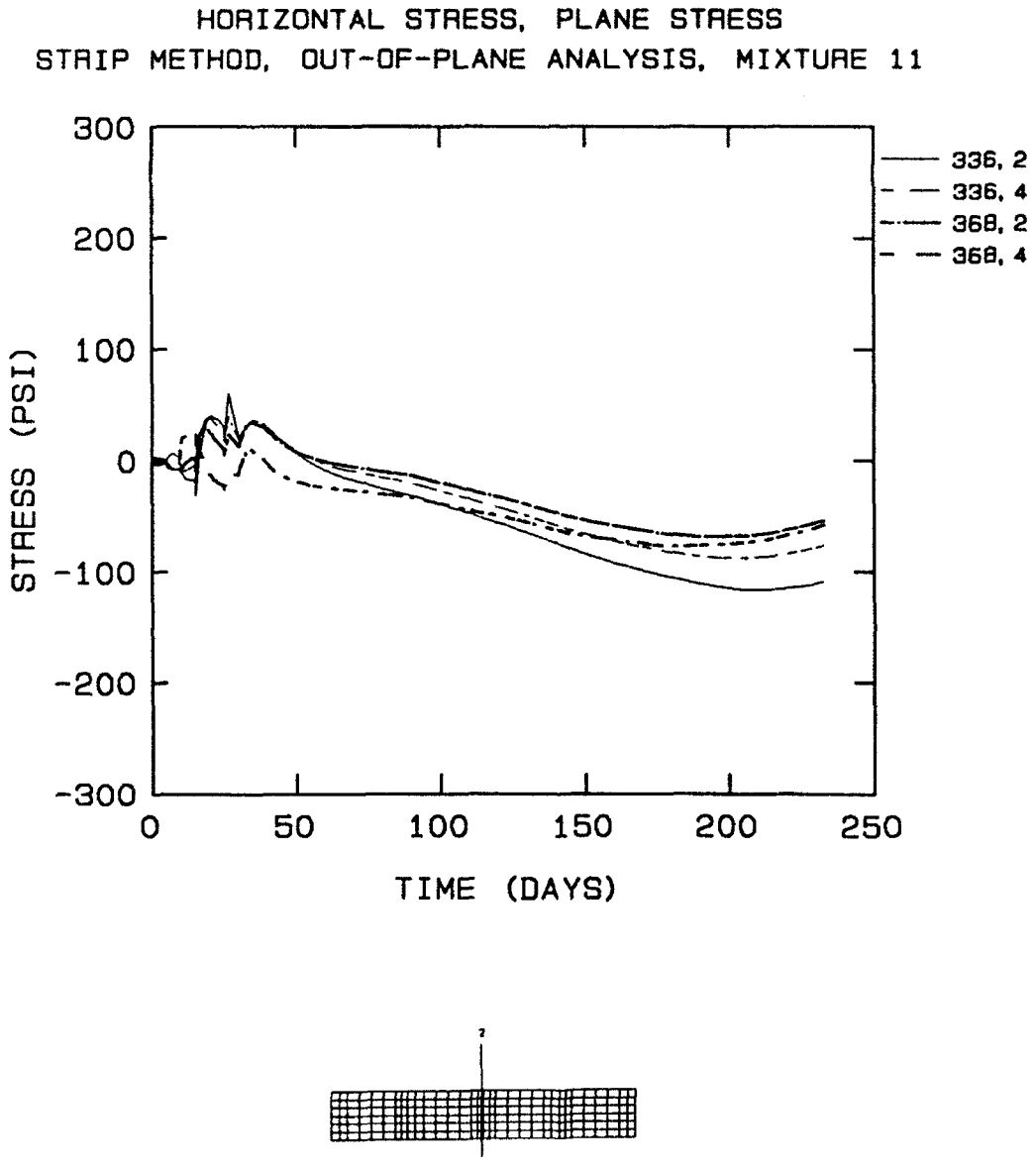

Figure 81. Horizontal stress at lift 1, section 2, OMSTDS5

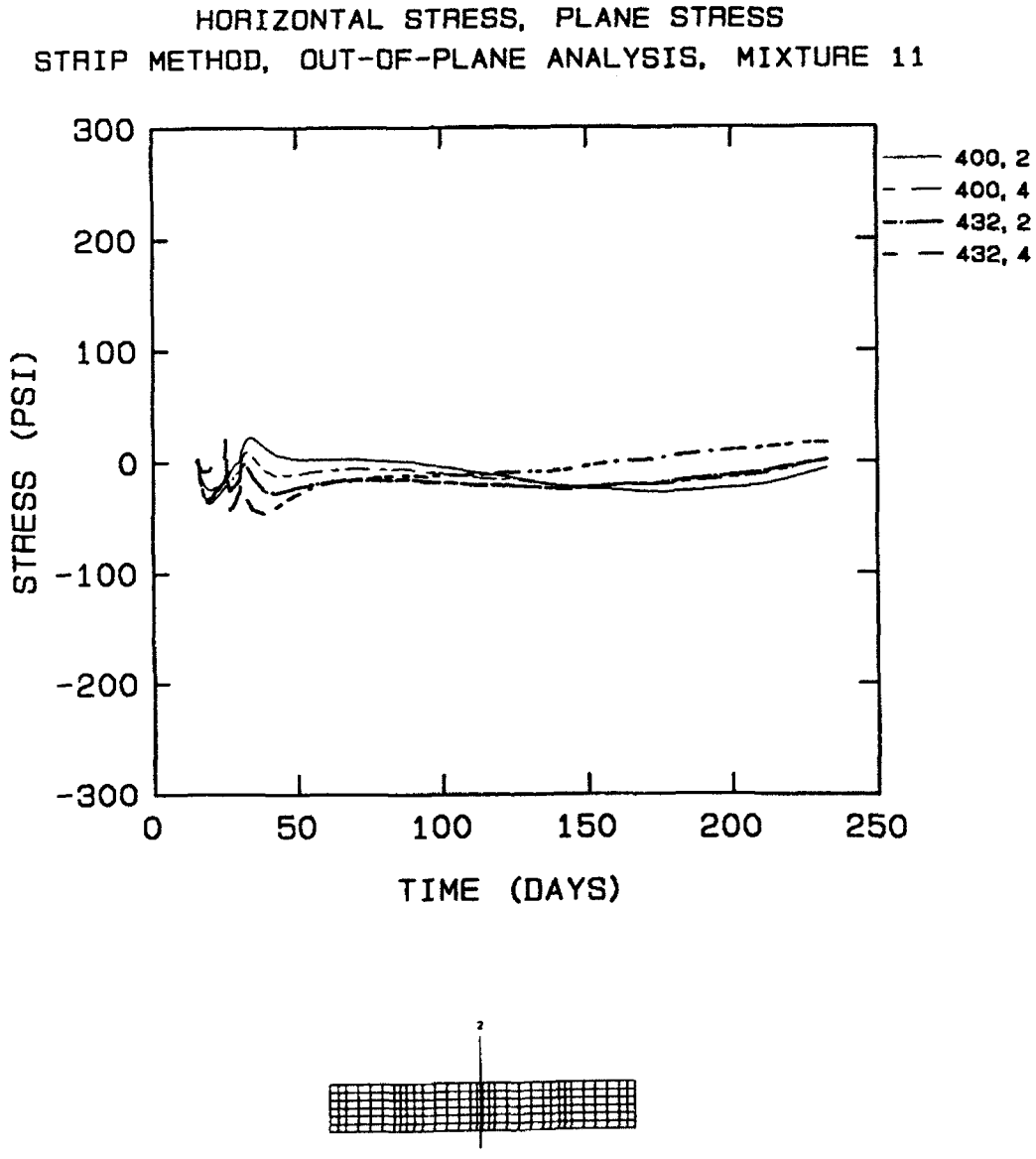

Figure 82. Horizontal stress at lift 4, section 2, OMSTDS5

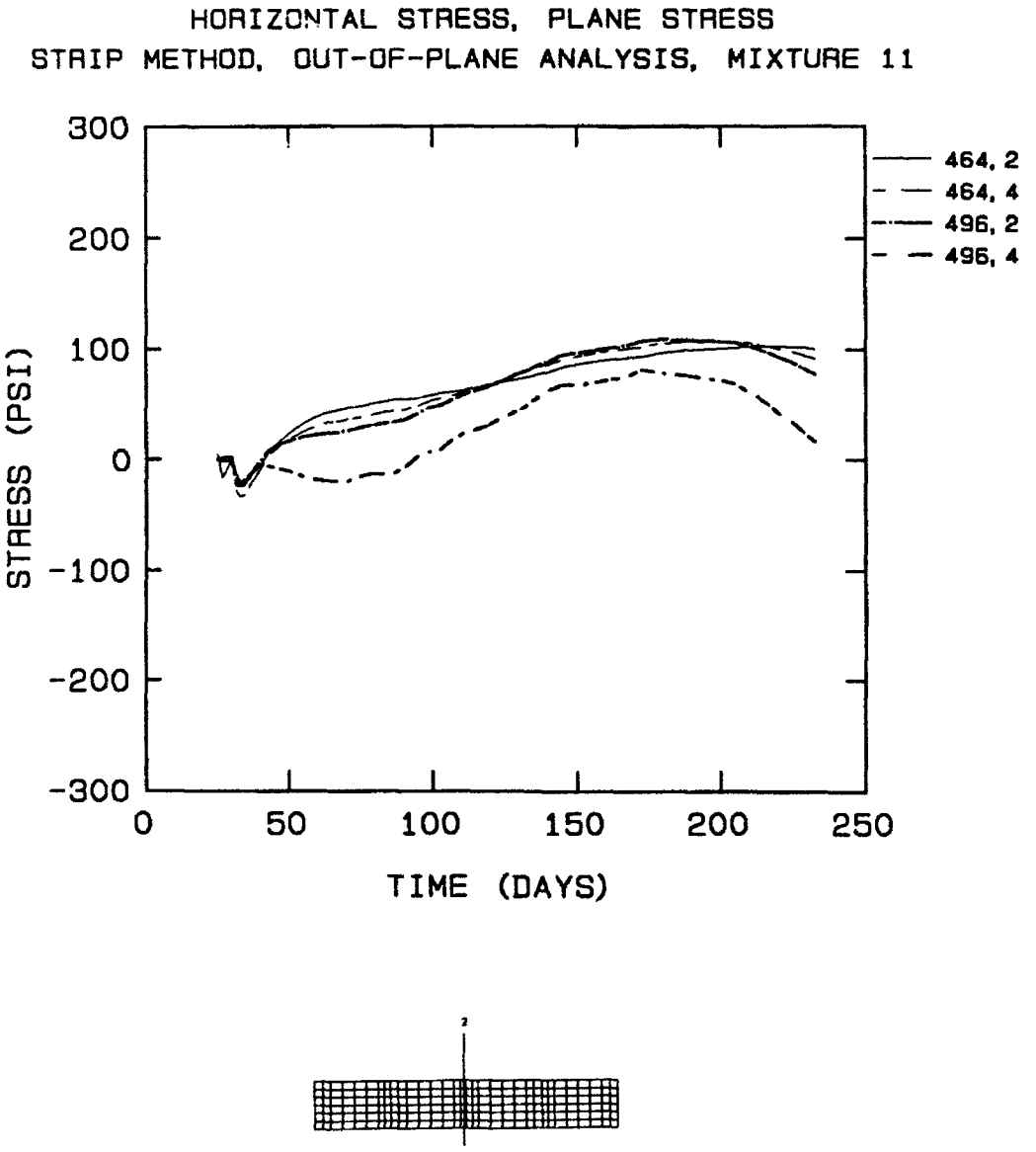

Figure 83. Horizontal stress at lift 6, section 2, OMSTDS5

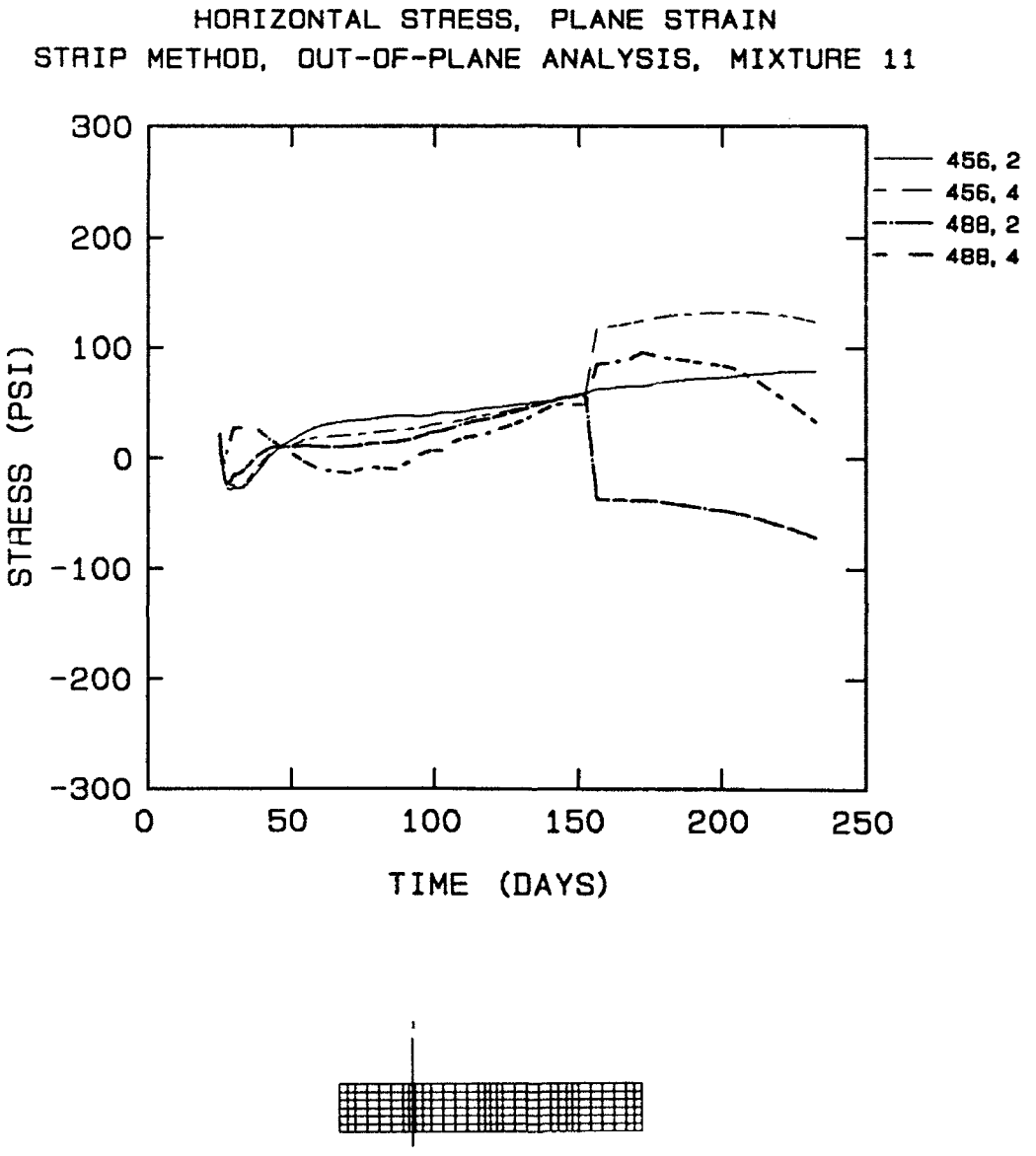

Figure 84. Horizontal stress at lift 6, section 1, OMSTDS5A

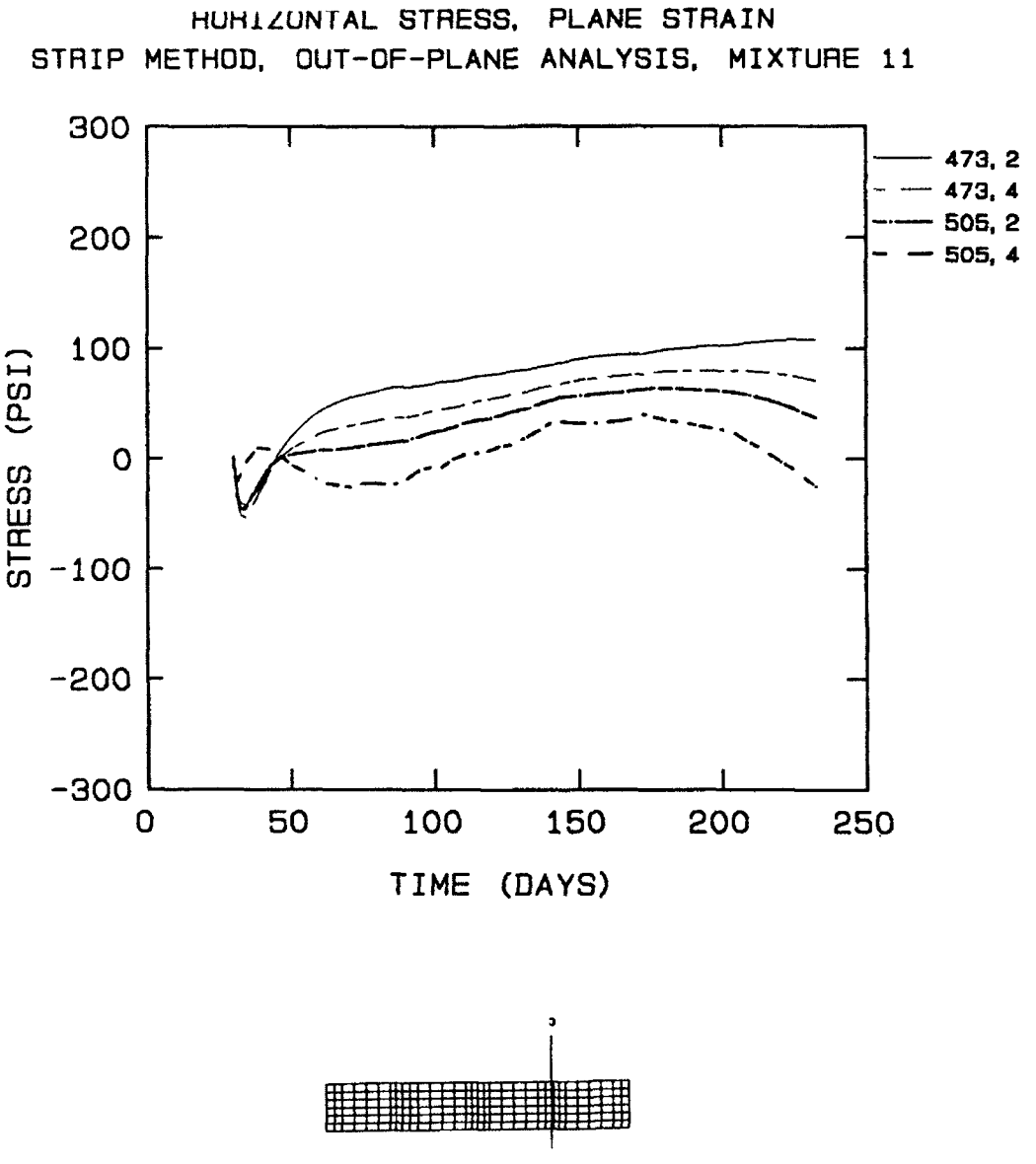

Figure 85. Horizontal stress at lift 7, section 3, OMSTDS5A

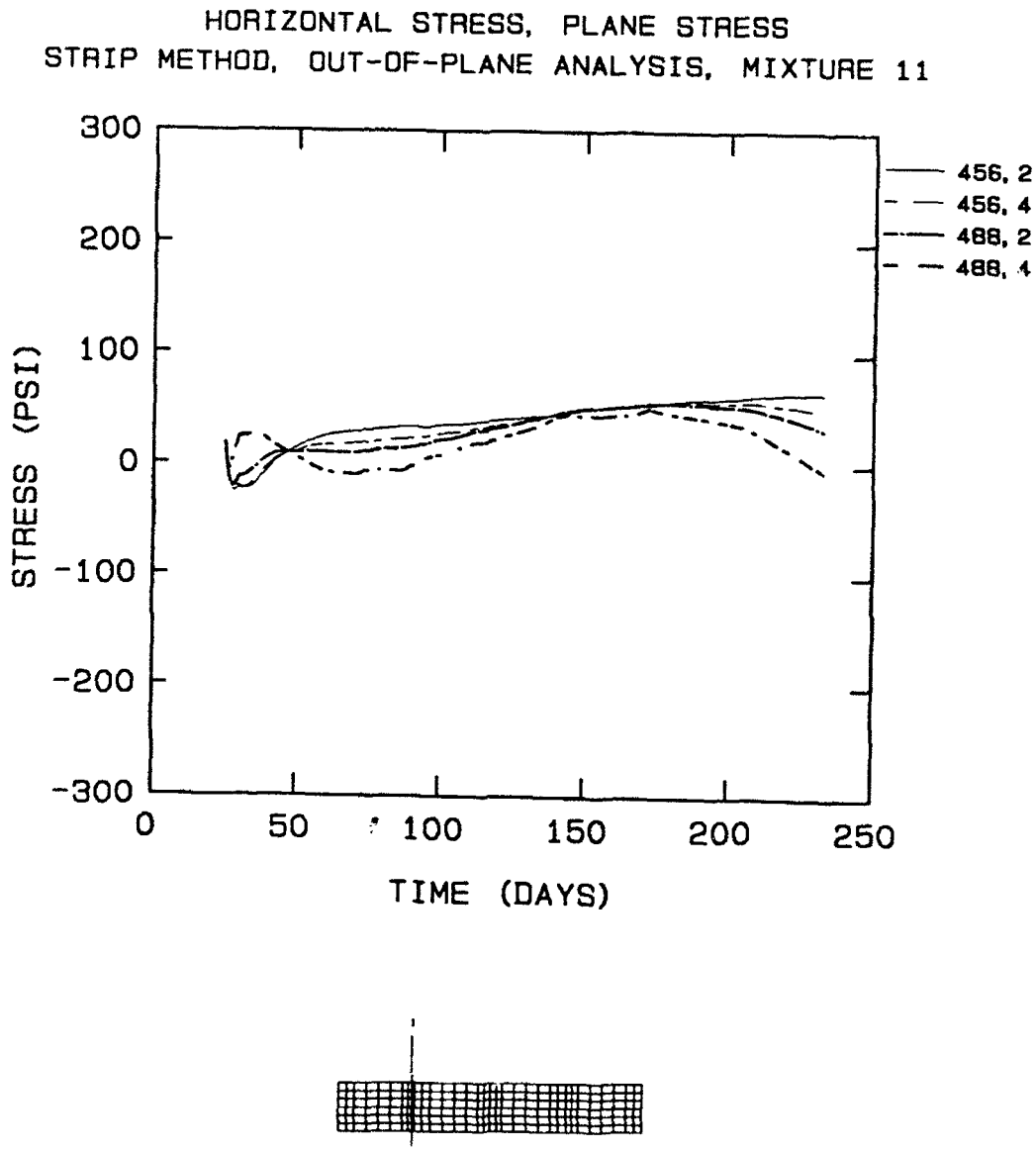

Figure 86. Horizontal stress at lift 6, section 1, OMSTDS5

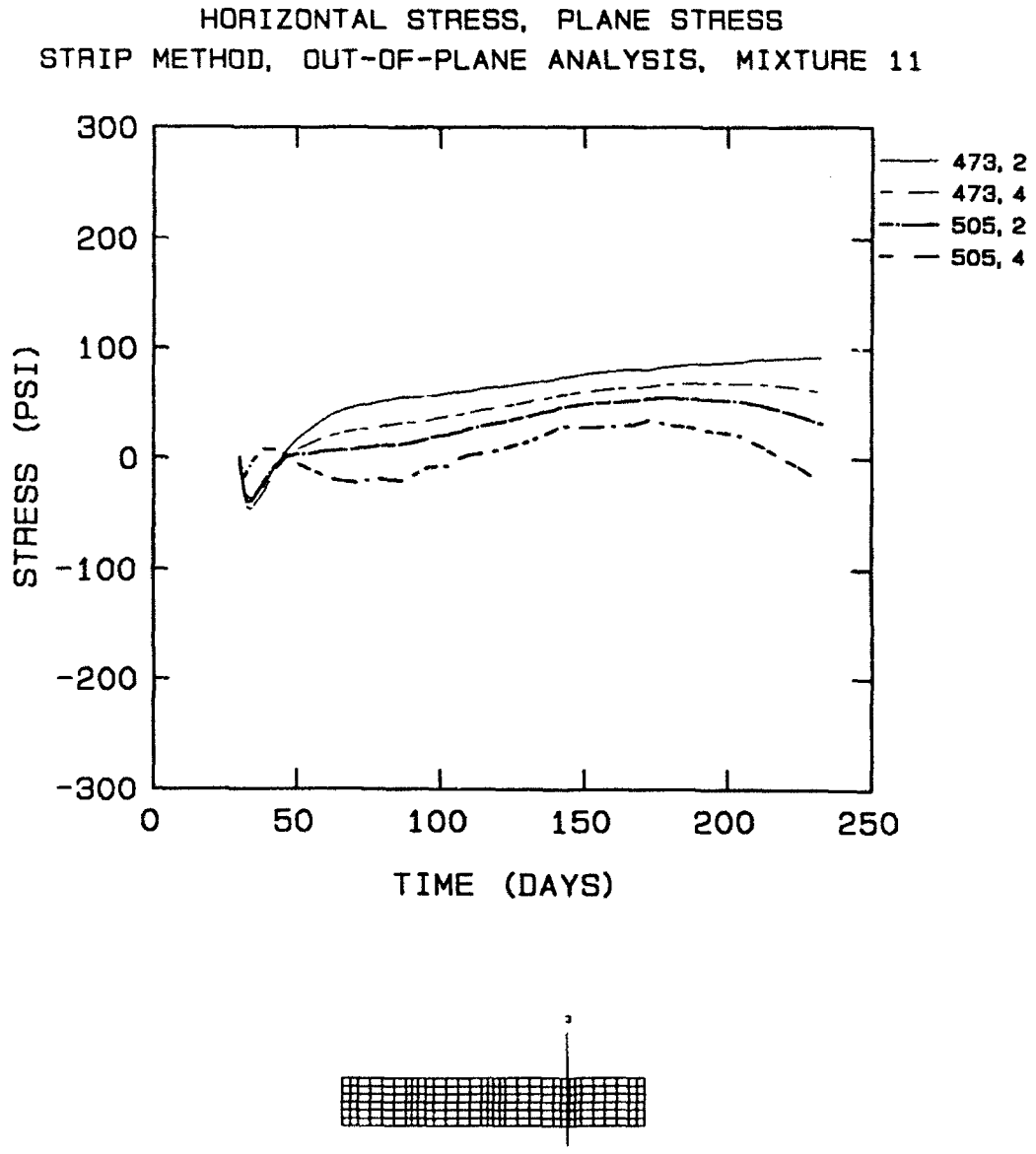

Figure 87. Horizontal stress at lift 7, section 3, OMSTDS5

illusions resulting from the manner in which ABAQUS draws the deformed shape plots.

103. Material properties listed in Table 4 were used for input into the user subroutine, UMAT, for plane stress and plane strain analyses for this placement method. Temperature data from the strip placement method heat transfer analysis were used for input into the plane stress and plane strain analyses for the strip placement model.

104. From stress contour plots in Appendix G, higher stressed zones are near the top of the slab in the middle of the lock chamber, at the upper and lower corners of the center wall culvert, and at the lower right corner of the center wall inspection gallery. Random pockets of stress concentrations occur in the plane strain stress contours around the areas where element cracking has initiated. Figures 88 and 89 show the stress variation for both analyses for the upper floor slab lift. Stresses for the plane stress model were somewhat higher at this location than the plane strain stresses, 210 psi versus 190 psi, respectively, but each analysis peaked at approximately 175 days and began to move toward compression. This trend is similar to behavior at the same location for analyses performed using mixture 11 properties. The fall in tensile stress at this section can be attributed to changes in ambient temperature. Figures 90 through 93 compare stresses at various elements in the other zones of higher stress. Stresses shown in these figures are slightly higher than stresses from the same location and comparable analyses using mixture 11 properties and show the same overall tendencies. For a more in-depth explanation of these tendencies and their causes, please refer to the section containing OMSTDS1 and OMSTDS1A results.

105. Maximum lateral displacement due to volumetric expansion at the edge of the slab was 0.0998 in. for node 2669, the interface between lifts 1 and 2, at 22.5 days for the plane stress analysis and was 0.1923 in. for the same node at 24.5 days for the plane strain analysis. Maximum lateral displacement due to volumetric contraction was 0.3728 in. for node 3437, middle of lift 3, at 234 days for the plane stress analysis and was 0.3378 in. for the same node at 234 days for the plane strain analysis.

106. No cracking occurred in the plane stress analysis. Cracking in the plane strain analysis was due to the large out-of-plane stress and began at 74 days.

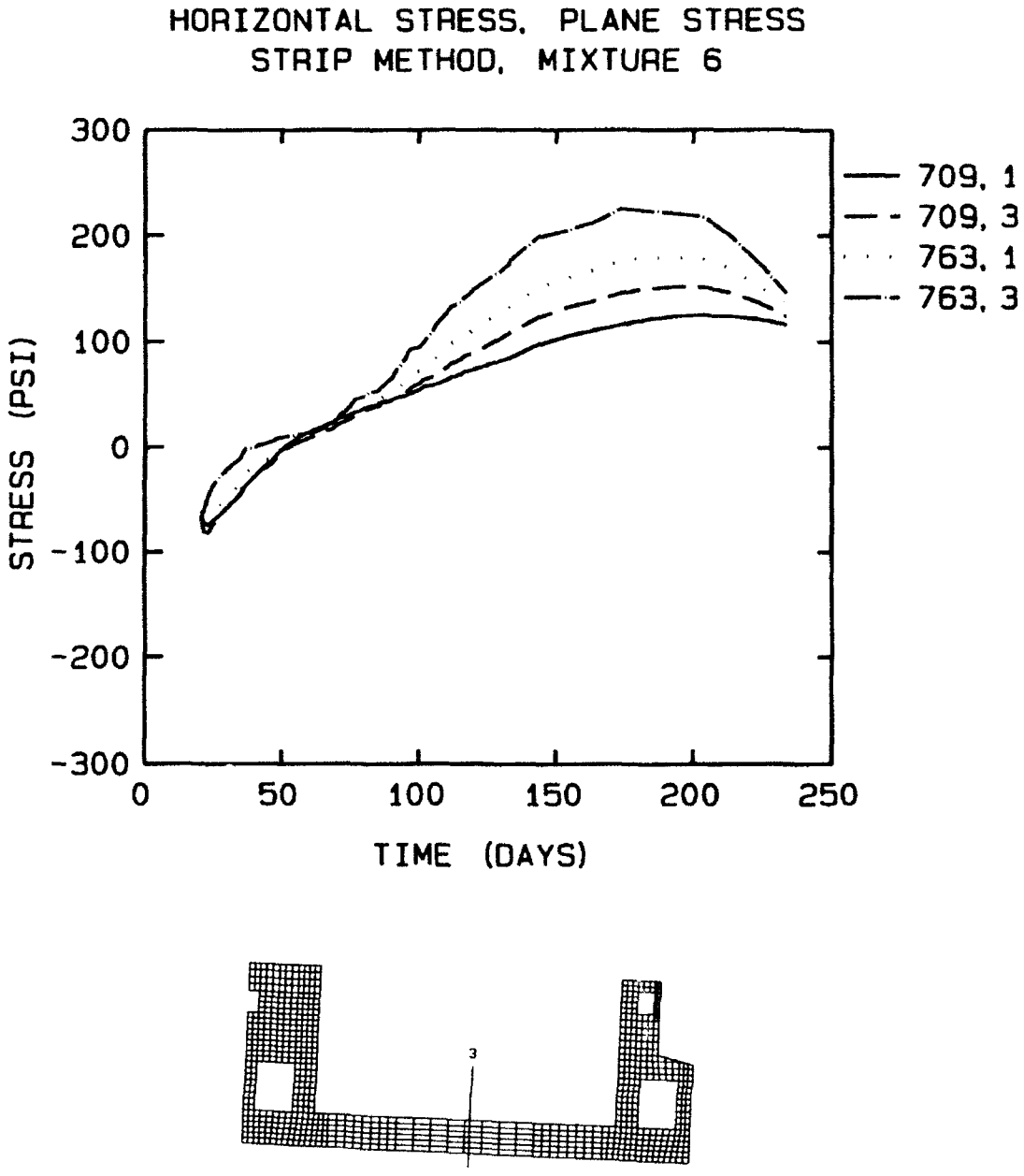

Figure 88. Horizontal stress at lift 3, section 3, strip method, plane stress analysis

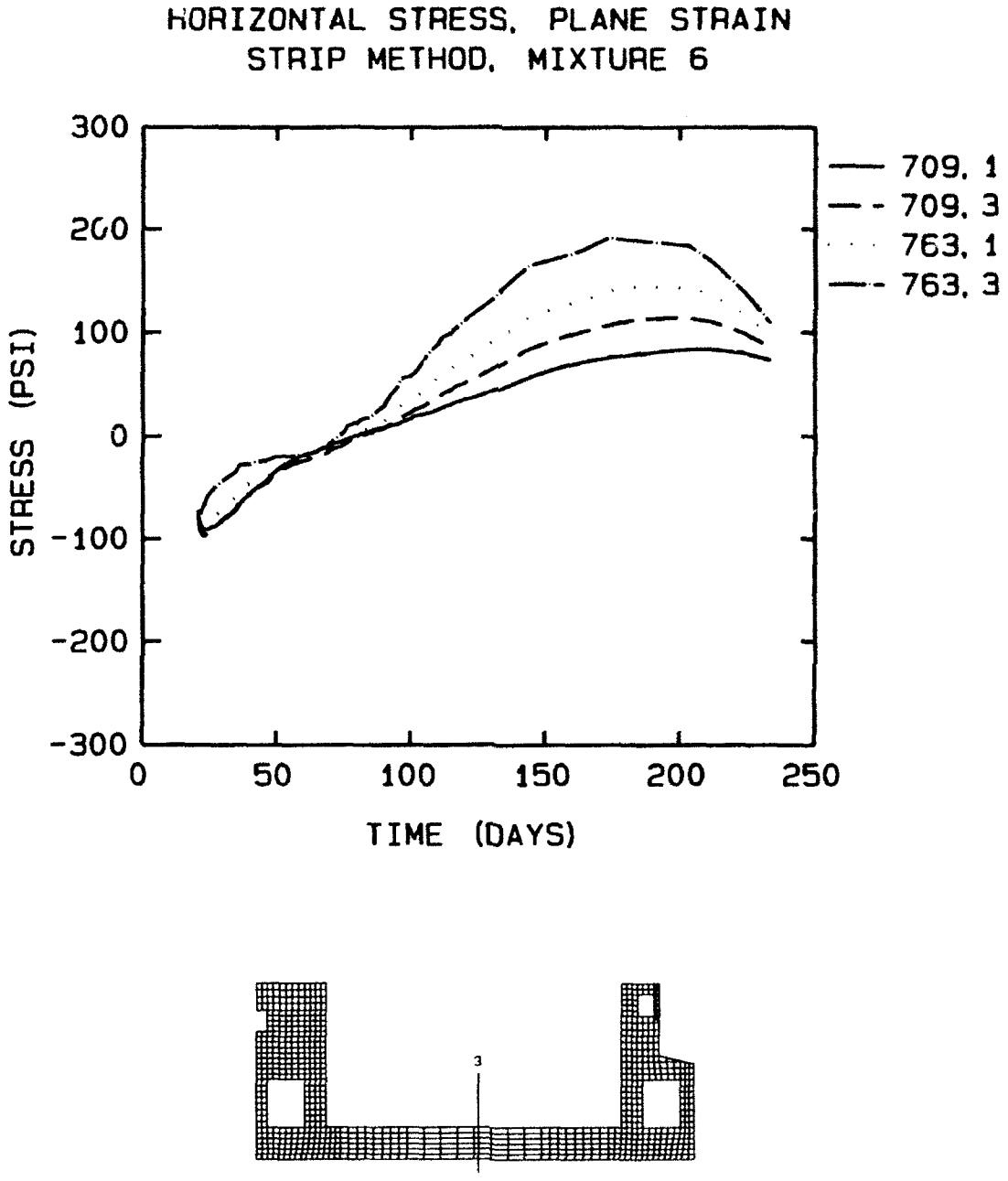

Figure 89. Horizontal stress at lift 3, section 3, strip method, plain strain analysis

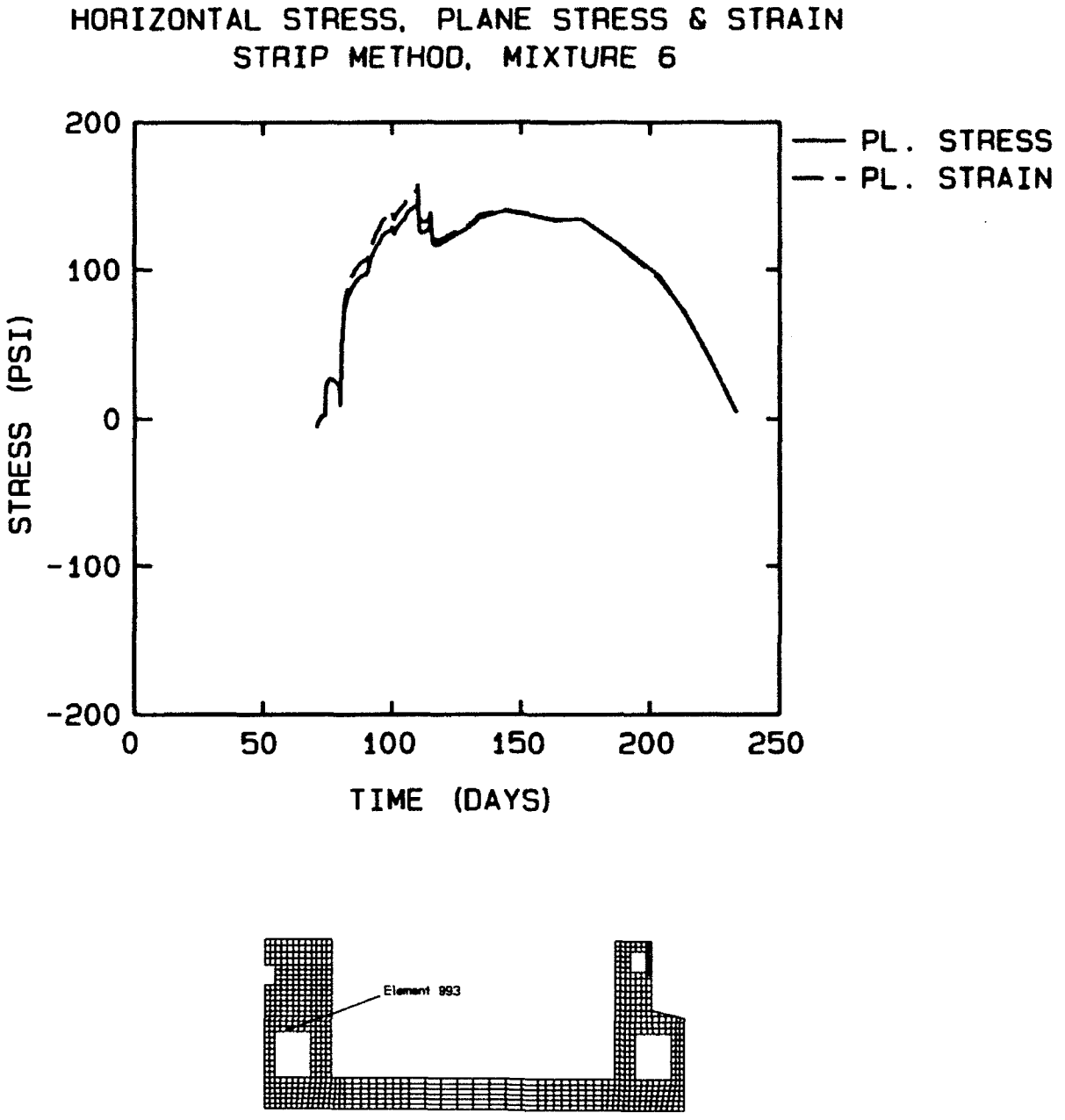

Figure 90. Horizontal stress at element 993, plane stress and plane strain analyses

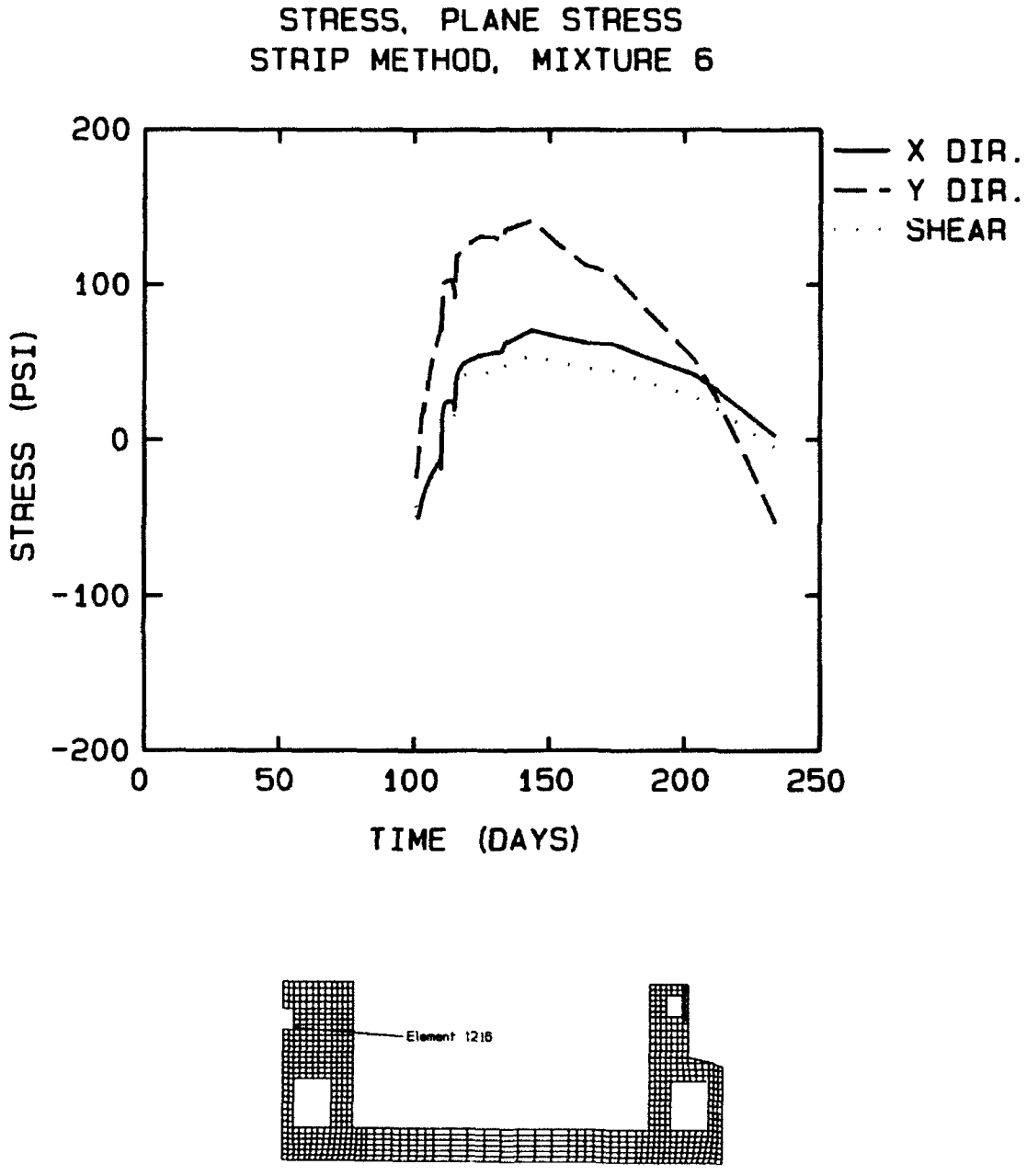

Figure 91. Stress at element 1216, mixture 6, plane stress analysis

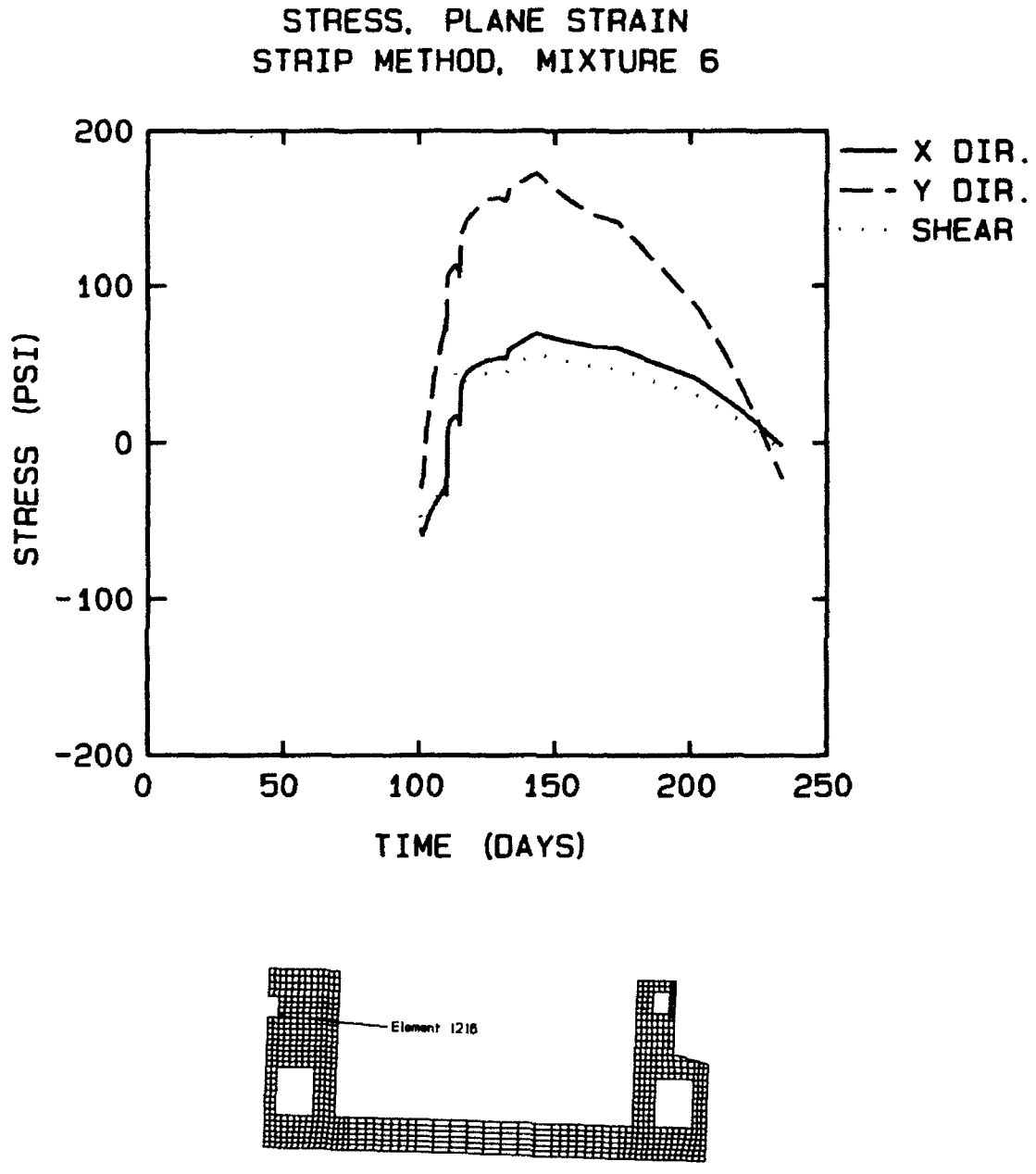

Figure 92. Stress at element 1216, mixture 6, plane strain analysis

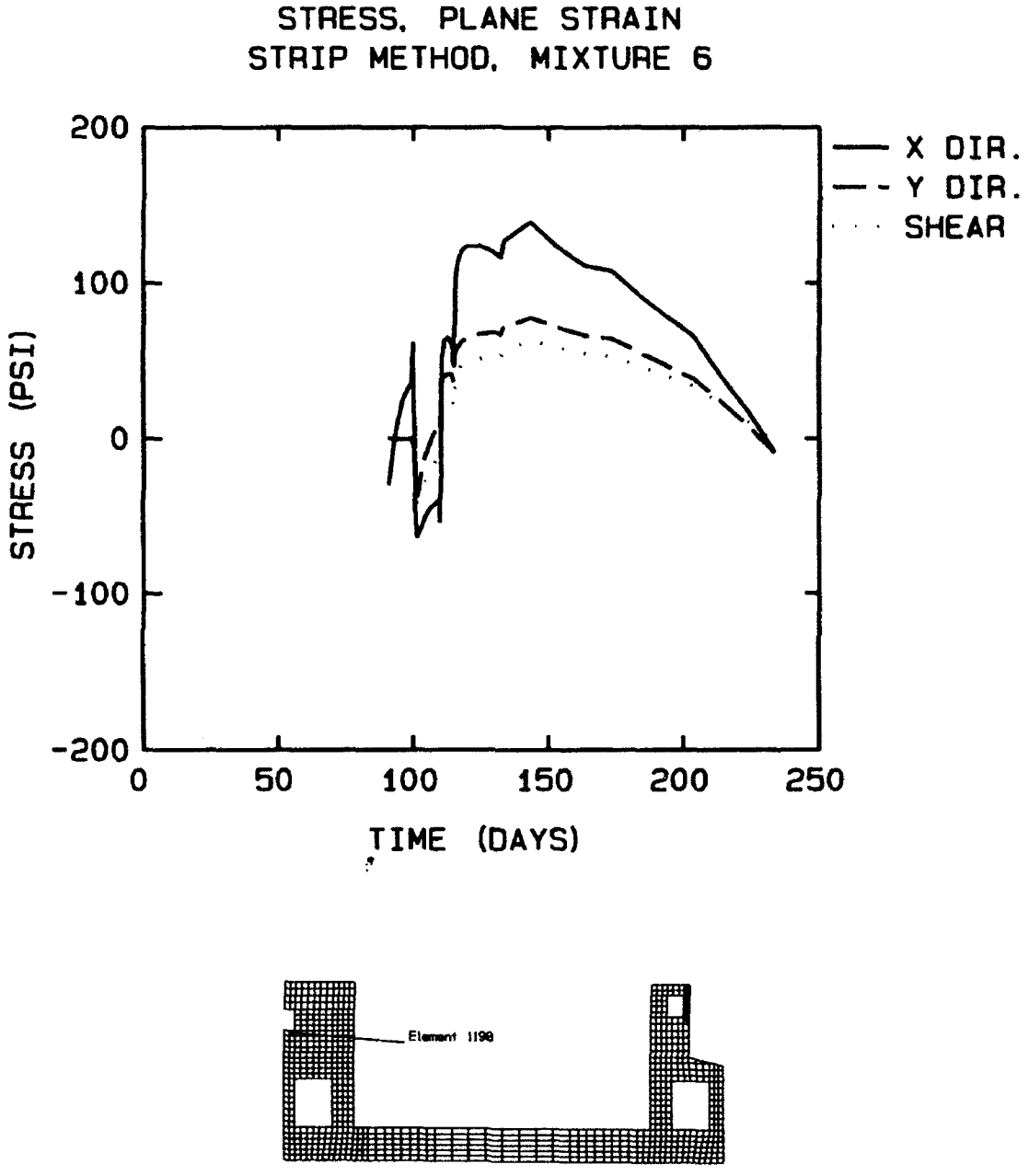

Figure 93. Stress at element 1190, mixture 6, plane strain analysis

107. Block placement method. Material properties listed in Table 4 were used for input into the user subroutine, UMAT, for plane stress and plane strain analyses for this placement method. Temperature data from the block placement method heat transfer analysis were used for input into the plane stress and plane strain analyses for the block placement model.

108. Stress contour plots in Appendix G indicate high stress zones in relatively the same areas as for the strip placement method. More random pockets of stress concentrations occur in the plane strain analysis near cracked elements. Figures 94 through 97 show results for plane stress and plane strain analyses for section 2 lift 3, section 3 lift 2, and section 3 lift 4. Results presented in these figures show the same tendencies as described in the mixture 6 plane stress discussion and are comparable to mixture 11 results. All but the plane stress results for section 3 lift 2 show initial compression for approximately 50 days and then tensile stresses which peak from 190 to 210 psi at 75 days. Section 3 lift 2 shows tensile stresses for the first 70 days and then compressive stresses which peak at 150 psi at 205 days.

109. Maximum lateral displacement due to volumetric expansion at the edge of the slab was 0.1124 in. for node 2925, the middle of lift 2, at 20.5 days for the plane stress analysis and was 0.1432 in. for the same node at 20.5 days for the plane strain analysis. Maximum lateral displacement due to volumetric contraction was 0.3867 in. for node 3181, the interface between lifts 2 and 3, at 234 days for the plane stress analysis and was 0.4199 in. for the same node at 224 days for the plane strain analysis.

110. No cracking occurred in the plane stress analysis. Cracking in the plane strain analysis was due to the large out-of-plane stress and began at 80 days. Figure 95 shows stress discontinuities, resulting from stress redistribution due to analyses induced out-of-plane cracking of nearby elements, occurring from approximately 160 to 200 days. Cracking in the plane strain analysis was so pervasive that numerical difficulties arose which prevented completion of the analysis for the last time-step.

111. Comparisons of the placement methods are provided in the stress plots shown in Figures 98 through 102. These figures show comparisons in the center wall. Except for element 993, integration point 1, the tensile stresses from the strip placement method show slightly higher values than those for the block placement method. Since wall placements are identical in both placement methods, the differences in stress can be attributed to the

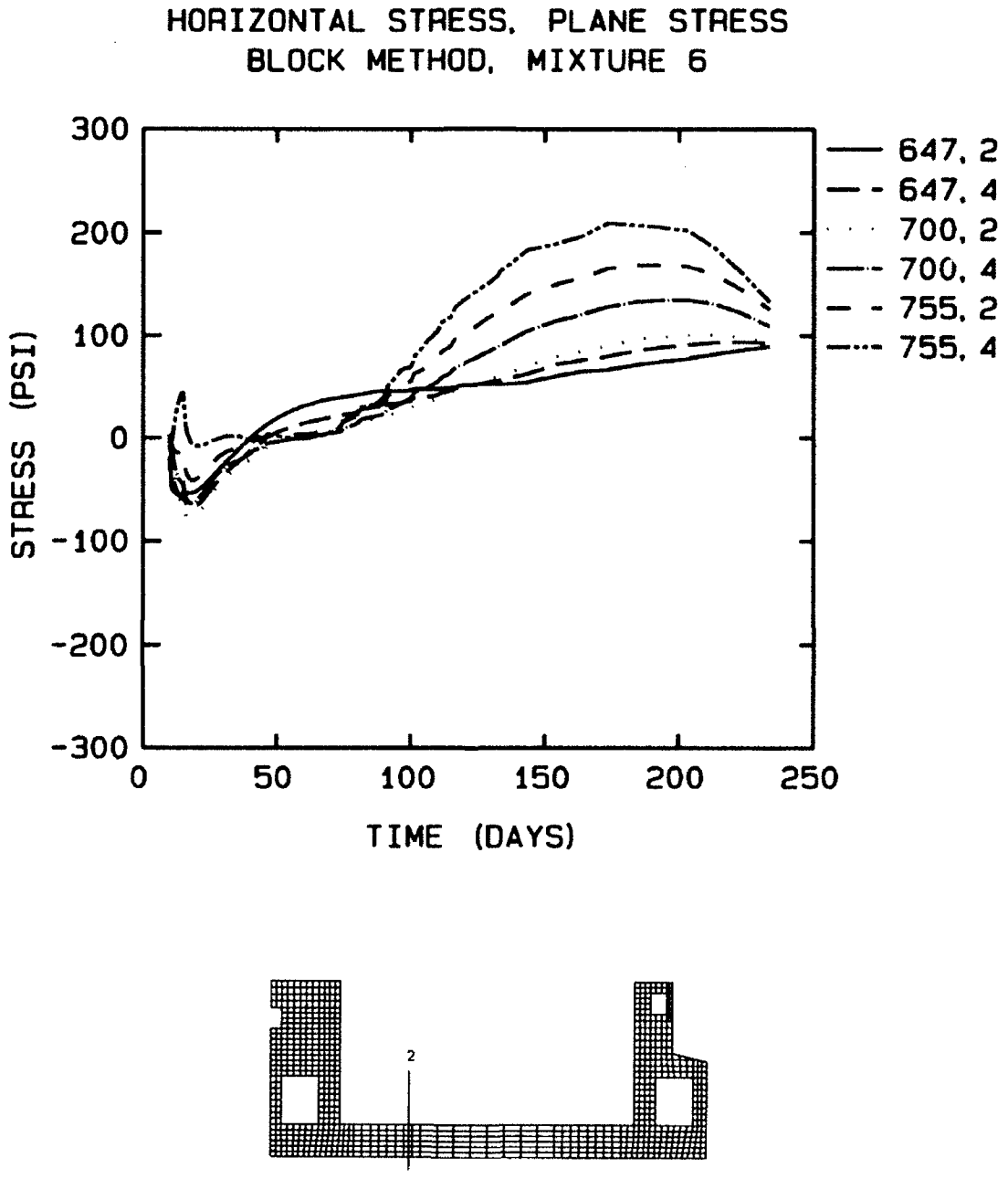

Figure 94. Horizontal stress at lift 3, section 2, block method, plane stress analysis

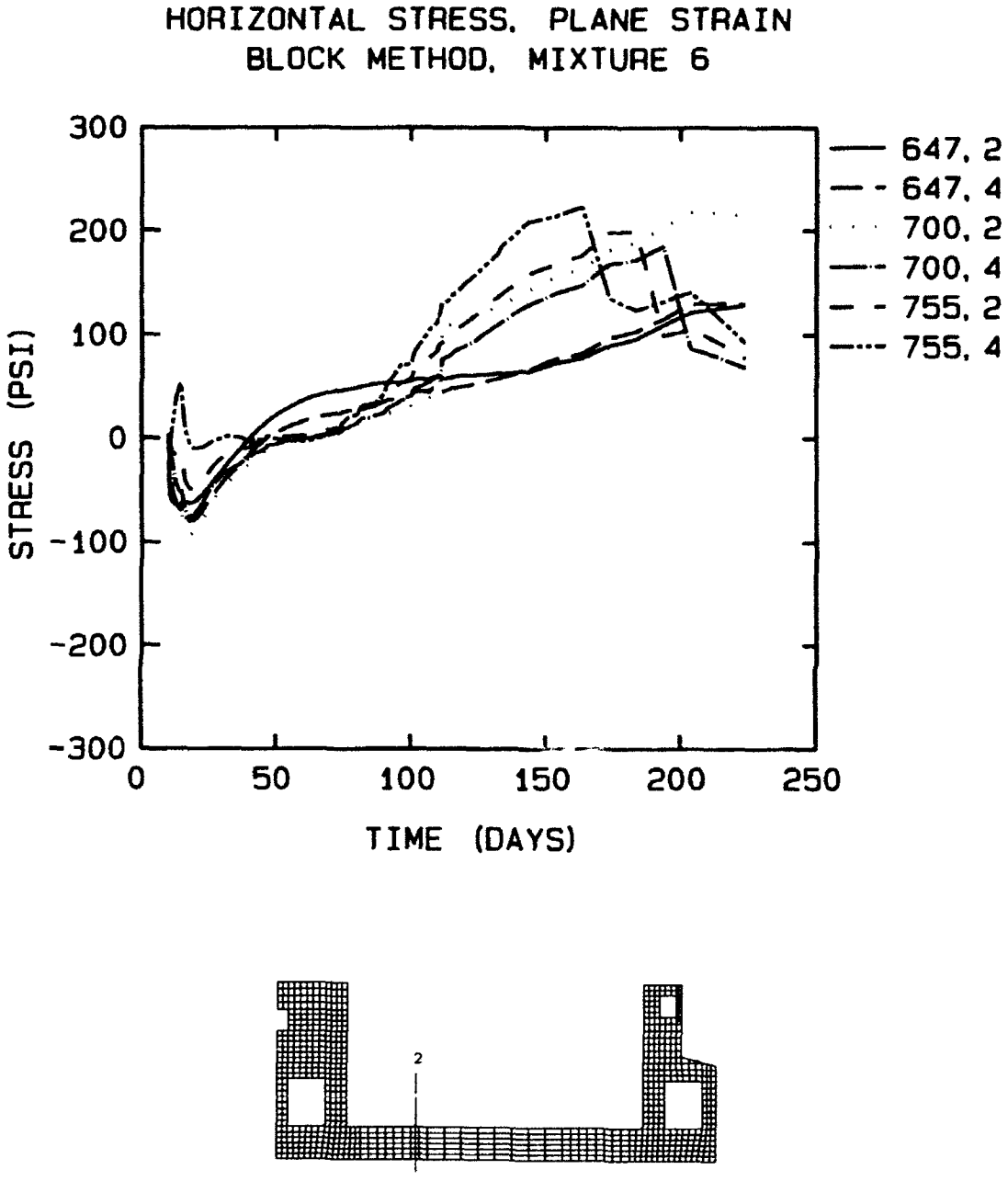

Figure 95. Horizontal stress at lift 3, section 2, block method, plane strain analysis

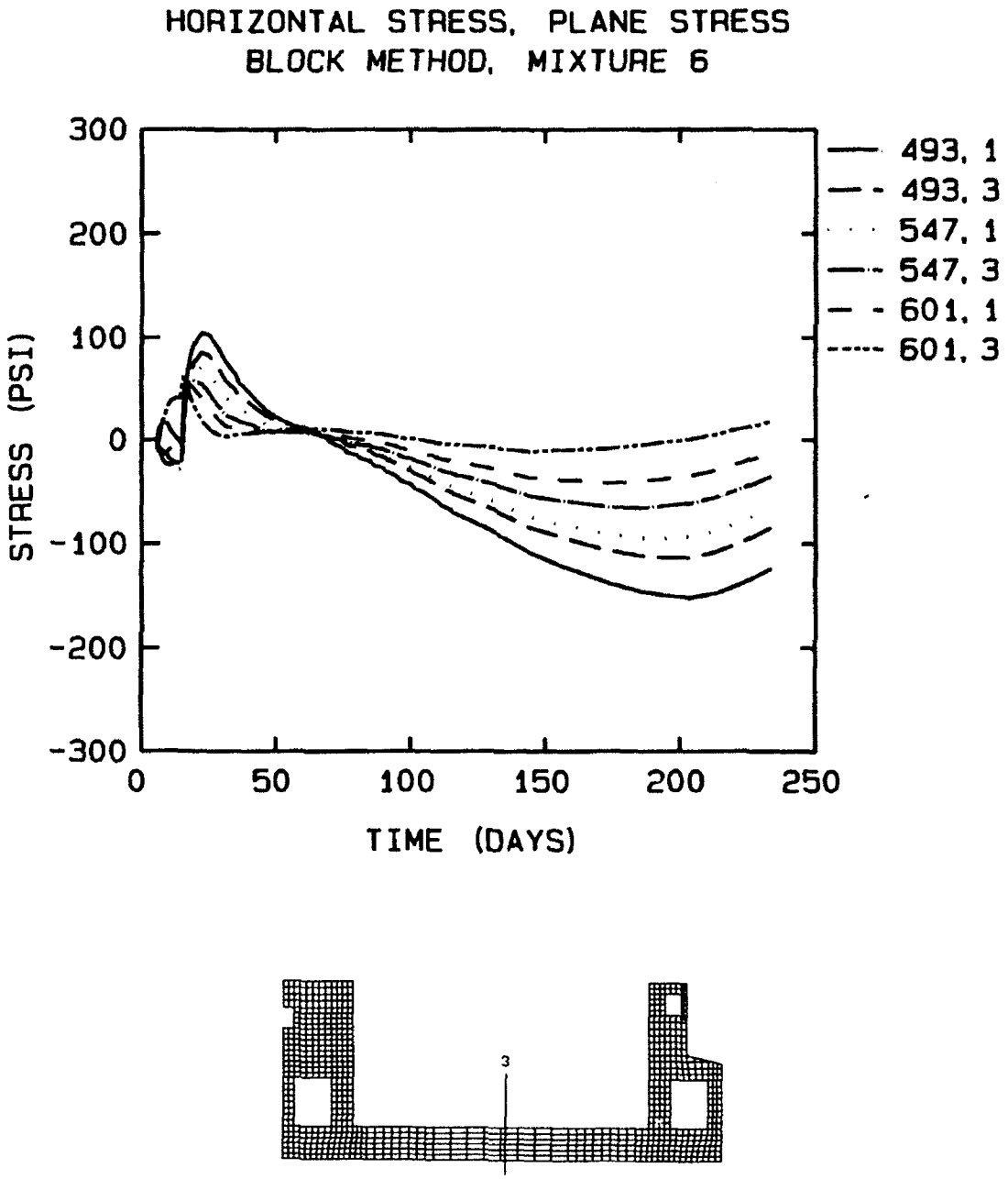

Figure 96. Horizontal stress at lift 2, section 3, block method, plane stress analysis

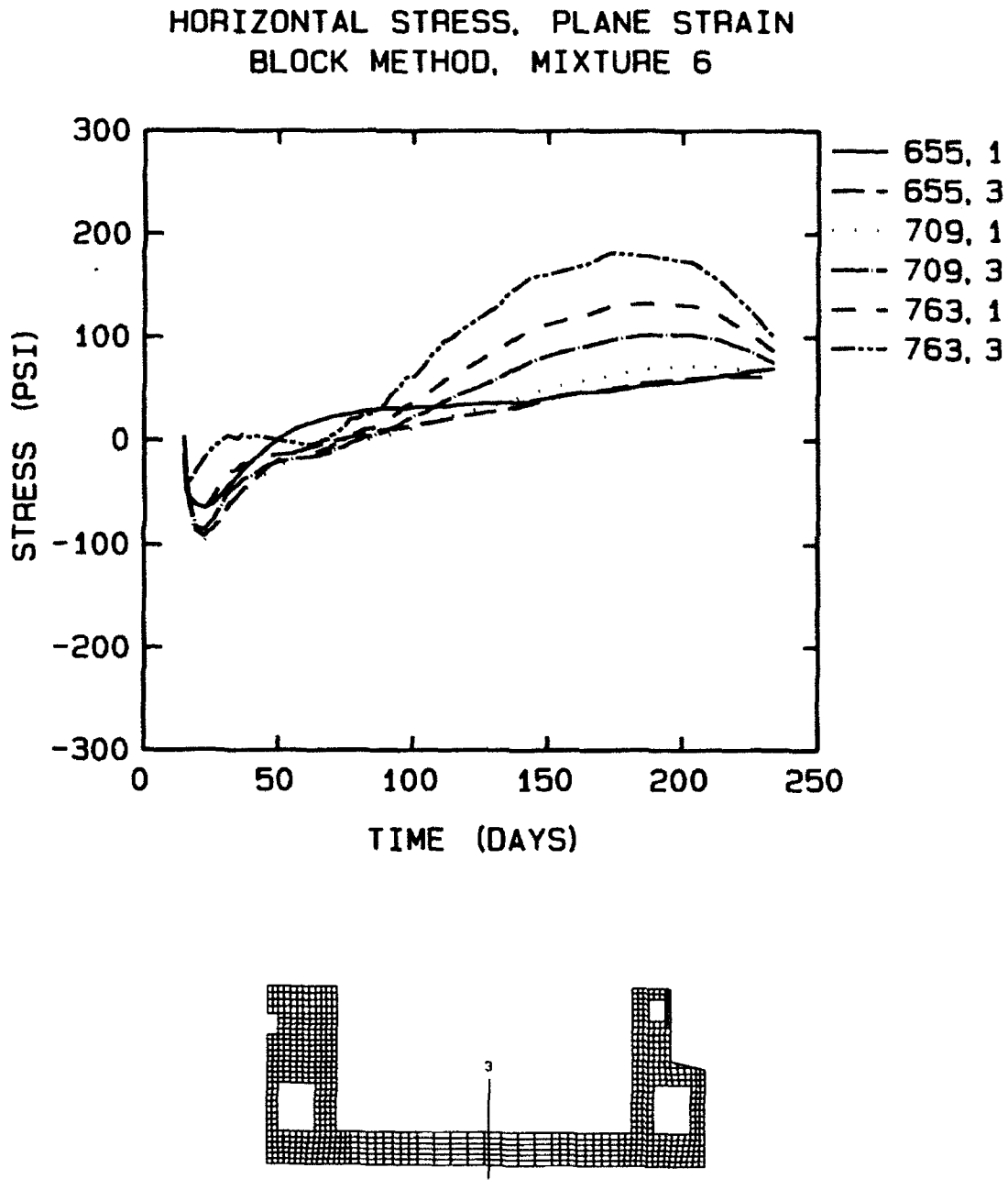

Figure 97. Horizontal stress at lift 4, section 3, block method, plane strain analysis

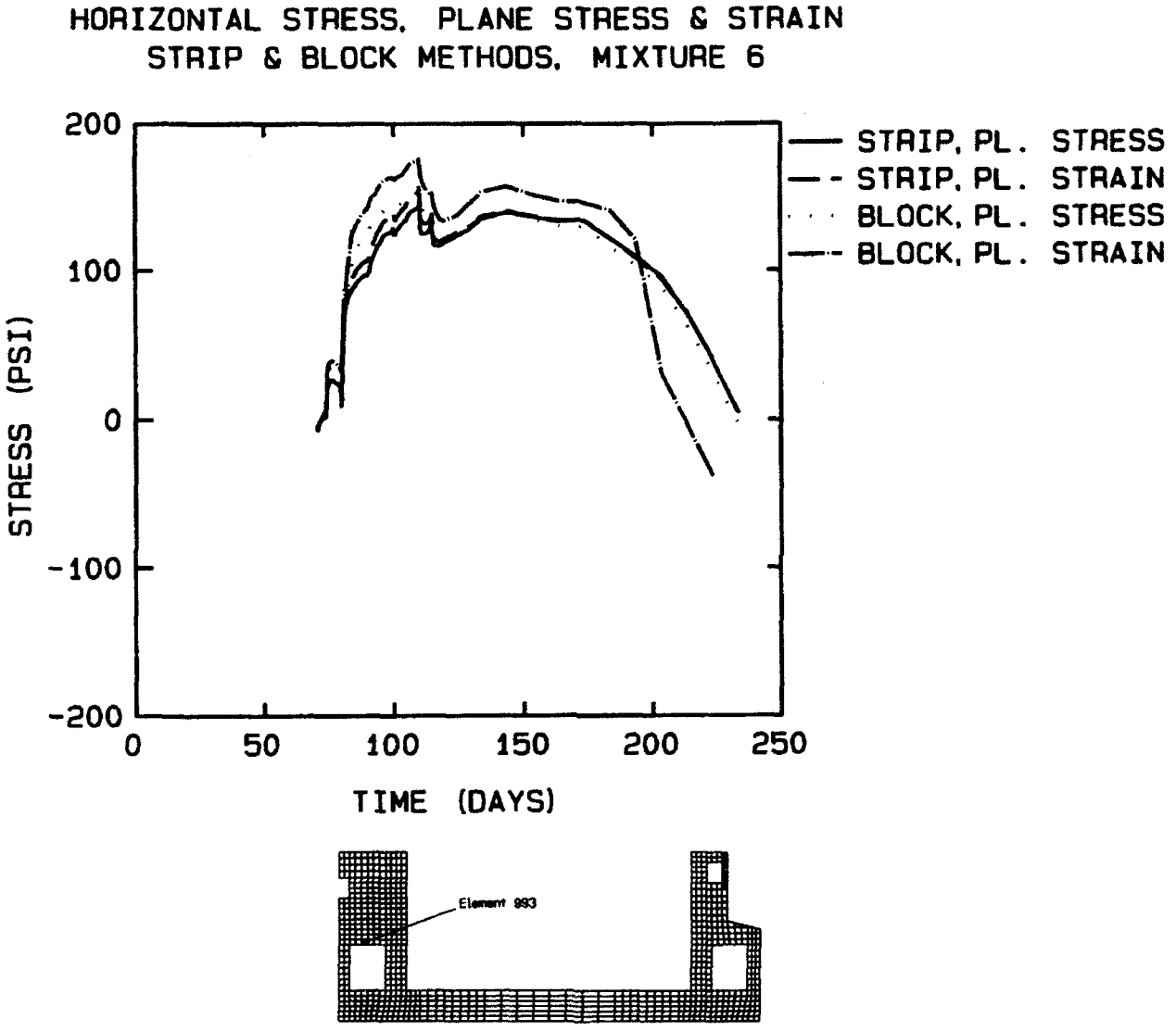

Figure 98. Horizontal stress at element 993, mixture 6 analyses

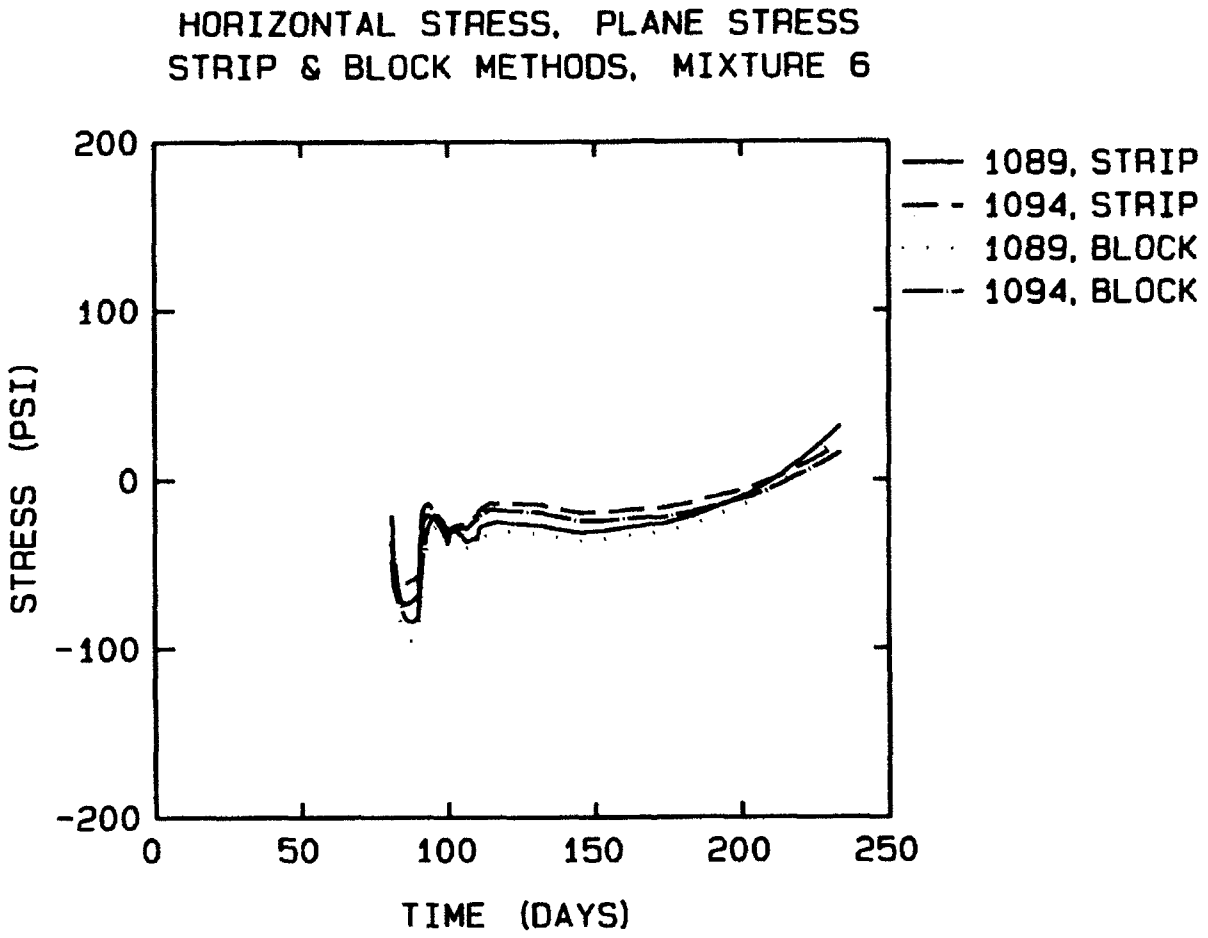

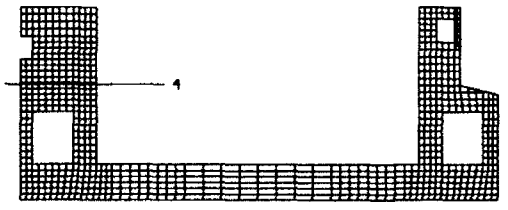

Figure 99. Horizontal stress at section 4, mixture 6 analyses

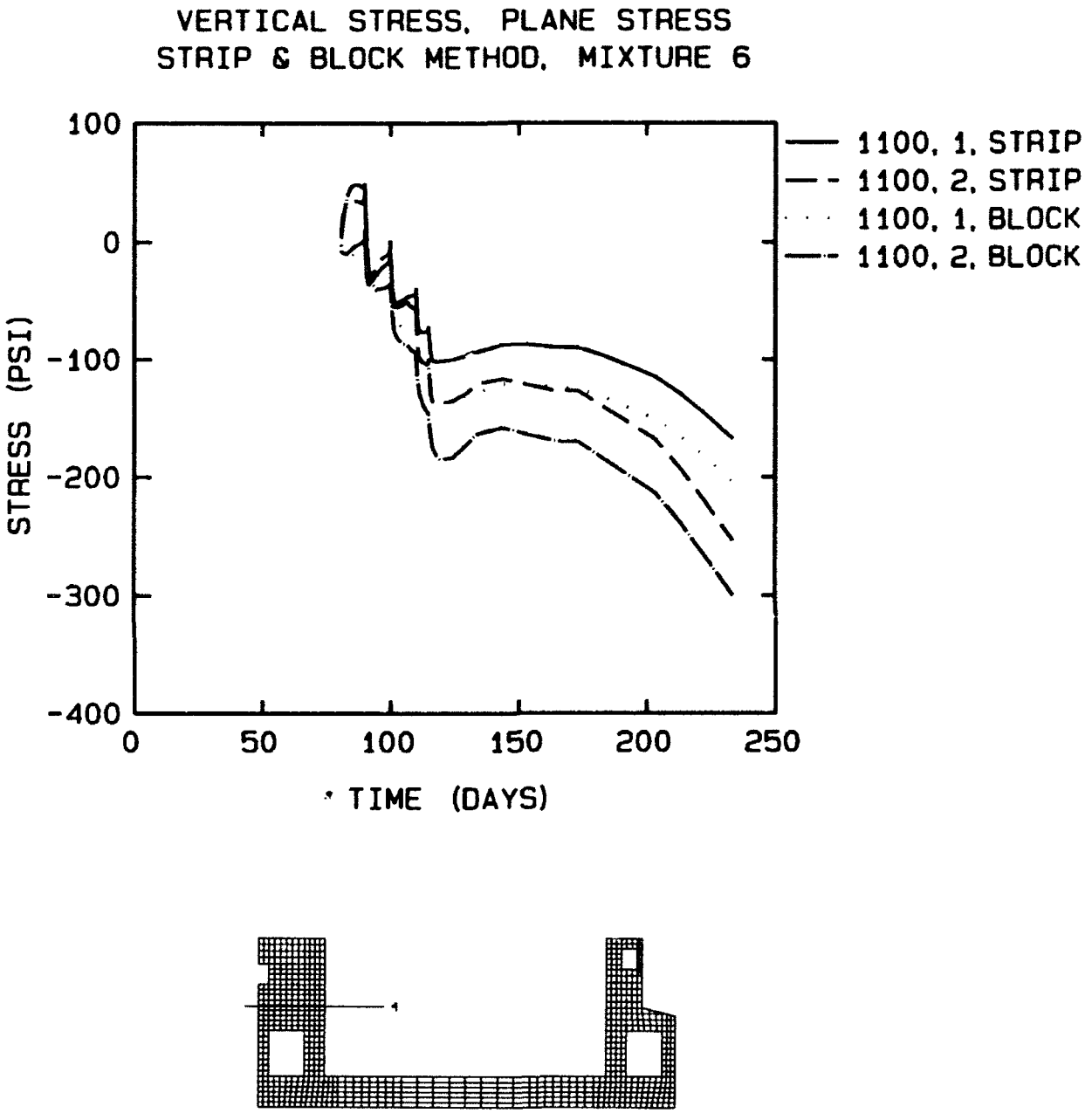

Figure 100. Vertical stress at section 4, mixture 6 analyses

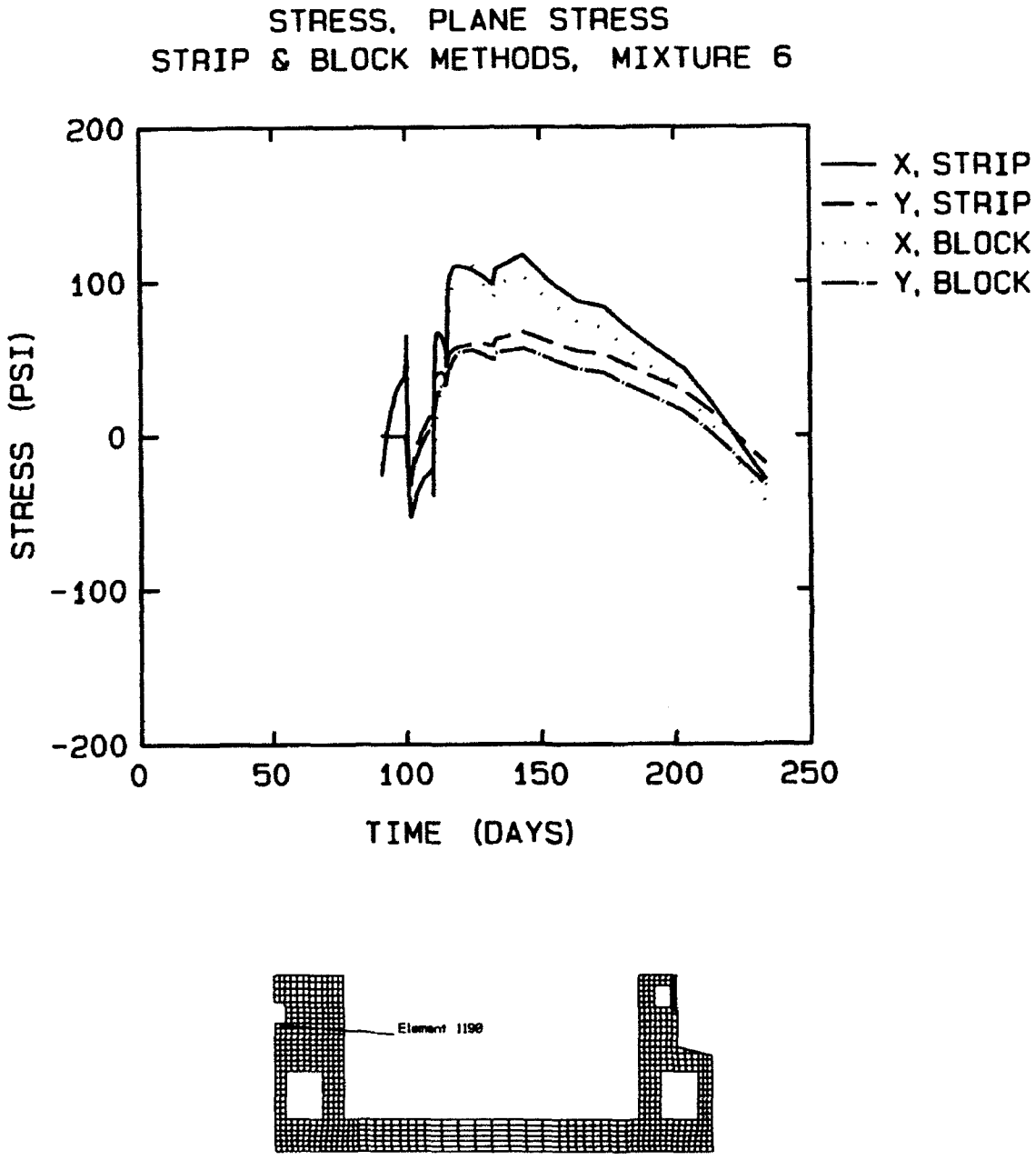

Figure 101. Stress at element 1190, mixture 6, plane stress analyses

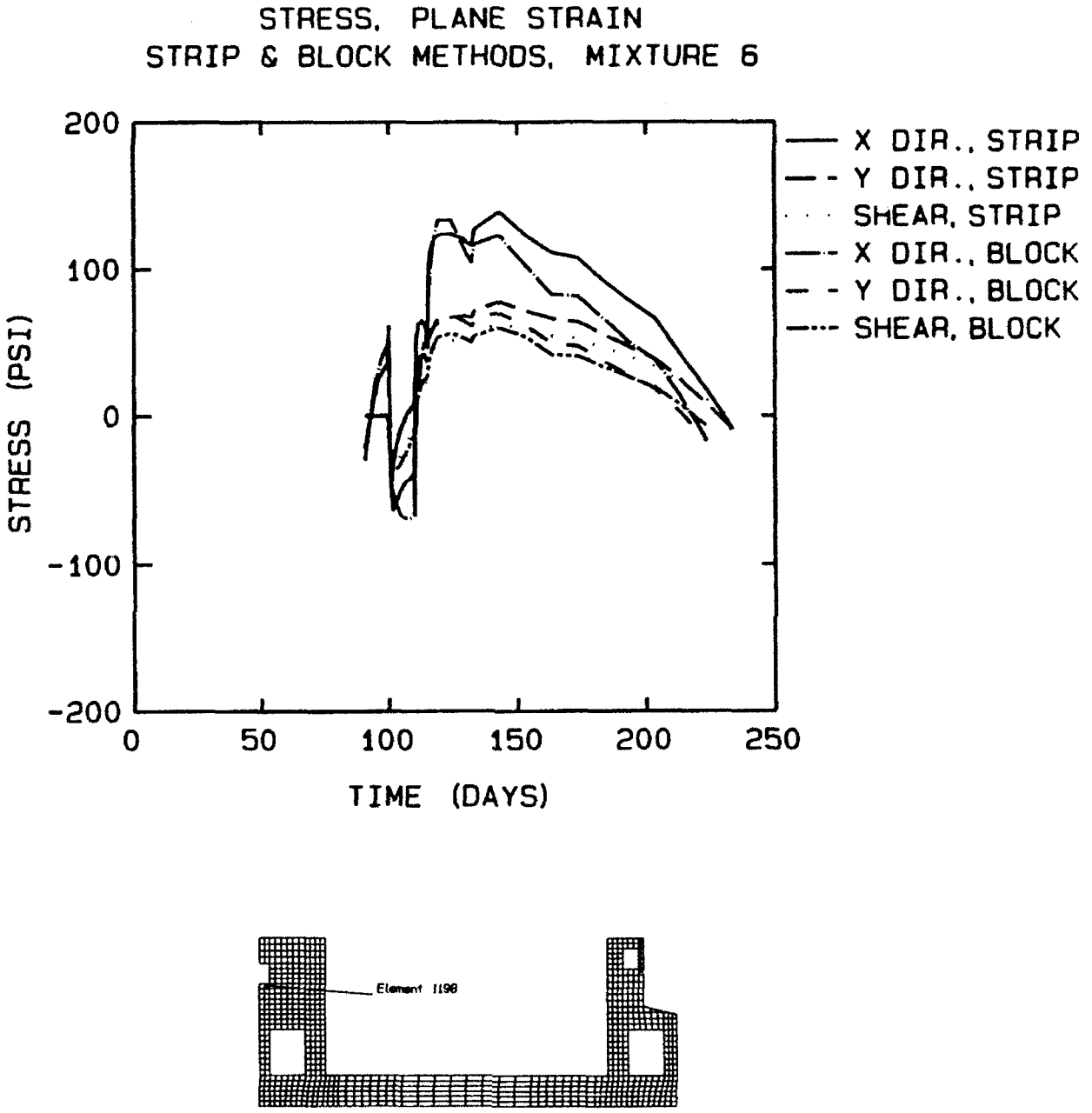

Figure 102. Stress at element 1190, mixture 6, plane strain analysis

different methods of modeling lift interfaces. Comparison of slab stresses at section 3 shows higher tensile stresses resulting from the strip placement method. These differences cannot be attributed solely to the different modeling techniques, but they reflect more volumetric restraint being applied to newer lifts in the strip placement method than in the block placement method. Although stresses were somewhat higher than in the block placement method, the strip placement models were better behaved and did not result in numerical instabilities. Numerical instabilities, in this case, arise from approximations made in the numerical model and solution convergence problems due to cracking, not from the physical model.

112. Except for the plane strain analyses, the block method yielded larger displacements than the strip method. This is consistent with larger lifts generating more heat for expansion and then contracting more during cooling. The plane strain anomaly is due to the numerical difficulties that resulted from excessive out-of-plane cracking during the plane strain analysis of the block placement method.

3-D analysis

113. The quarter-symmetrical grid used in the analysis is shown in Figure 103. Maximum tensile stresses should occur at the plane of symmetry transverse to the direction of flow (the front face in Figure 103). All time-history plots for comparison with 2-D analyses have been taken from elements in this section, and element numbers are indicated in the figure. Stress contour plots for specific times are included in Appendix I.

114. Horizontal stresses in lifts 3 and 4 at elements corresponding to 2-D elements at sections 1, 2, and 3 are shown in Figures 104 through 106. The maximum horizontal tensile stress in the floor section was 181 psi at approximately 170 days. As can be seen in Figure 107, this was slightly less than the maximums predicted in either the plane strain or plane stress block placement analyses. The reason for this becomes apparent when stresses parallel to the axis of flow in section 3 are compared with out-of-plane stresses at this location in the plane strain analysis (Figures 108 and 109). In the 2-D analysis, out-of-plane stress was not affected by interaction with previously existing concrete, but only by the restraints imposed by the plane strain formulation. Out-of-plane stress at section 3 in OMSTDS4A was induced by the total restriction of strain in the out-of-plane direction as discussed earlier in Part III and increased throughout the analysis to a maximum of approximately 800 psi. In the 3-D analysis, maximum stress in this direction

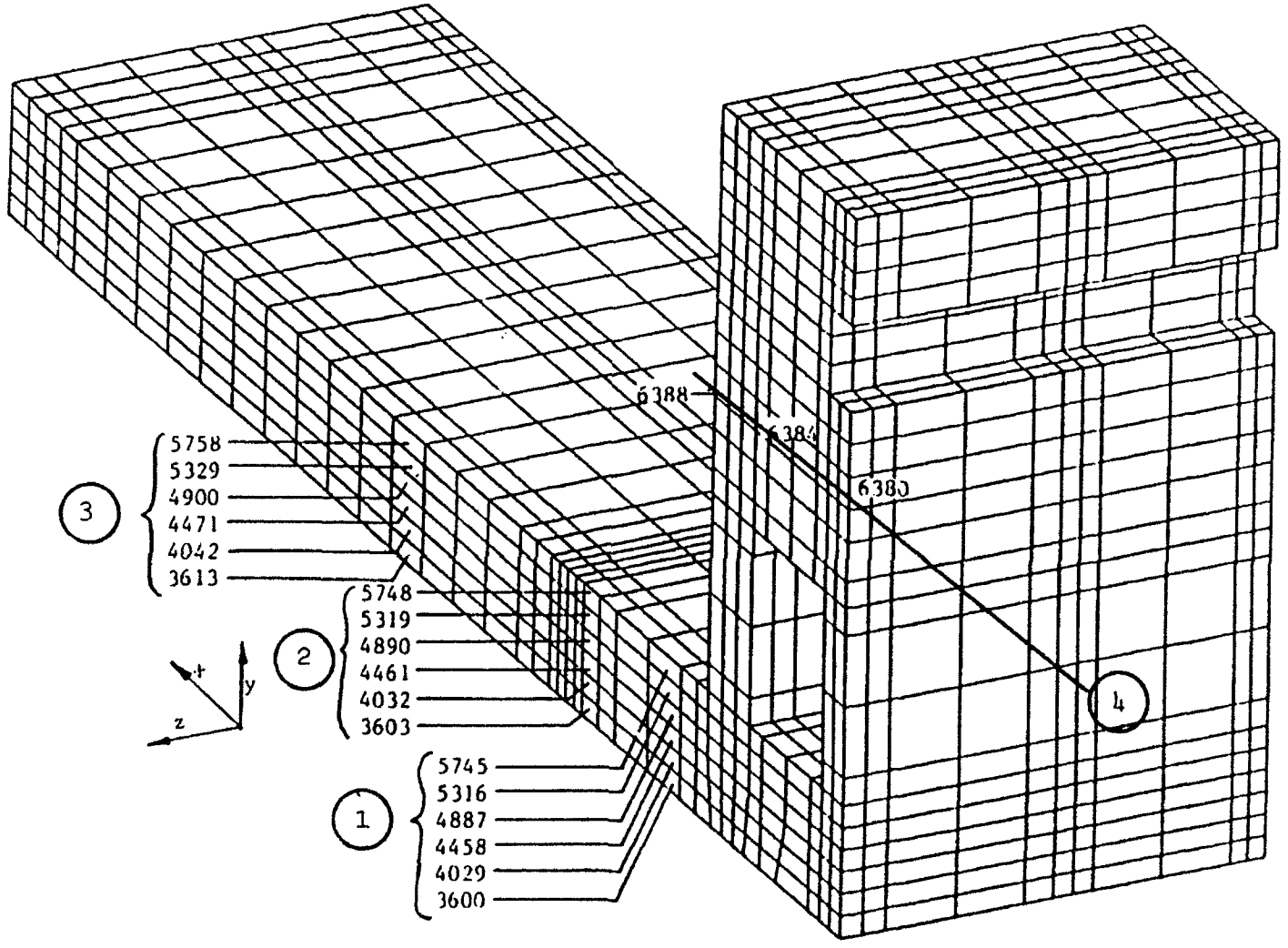

Figure 103. Elements for stress/time plots, 3-D analysis

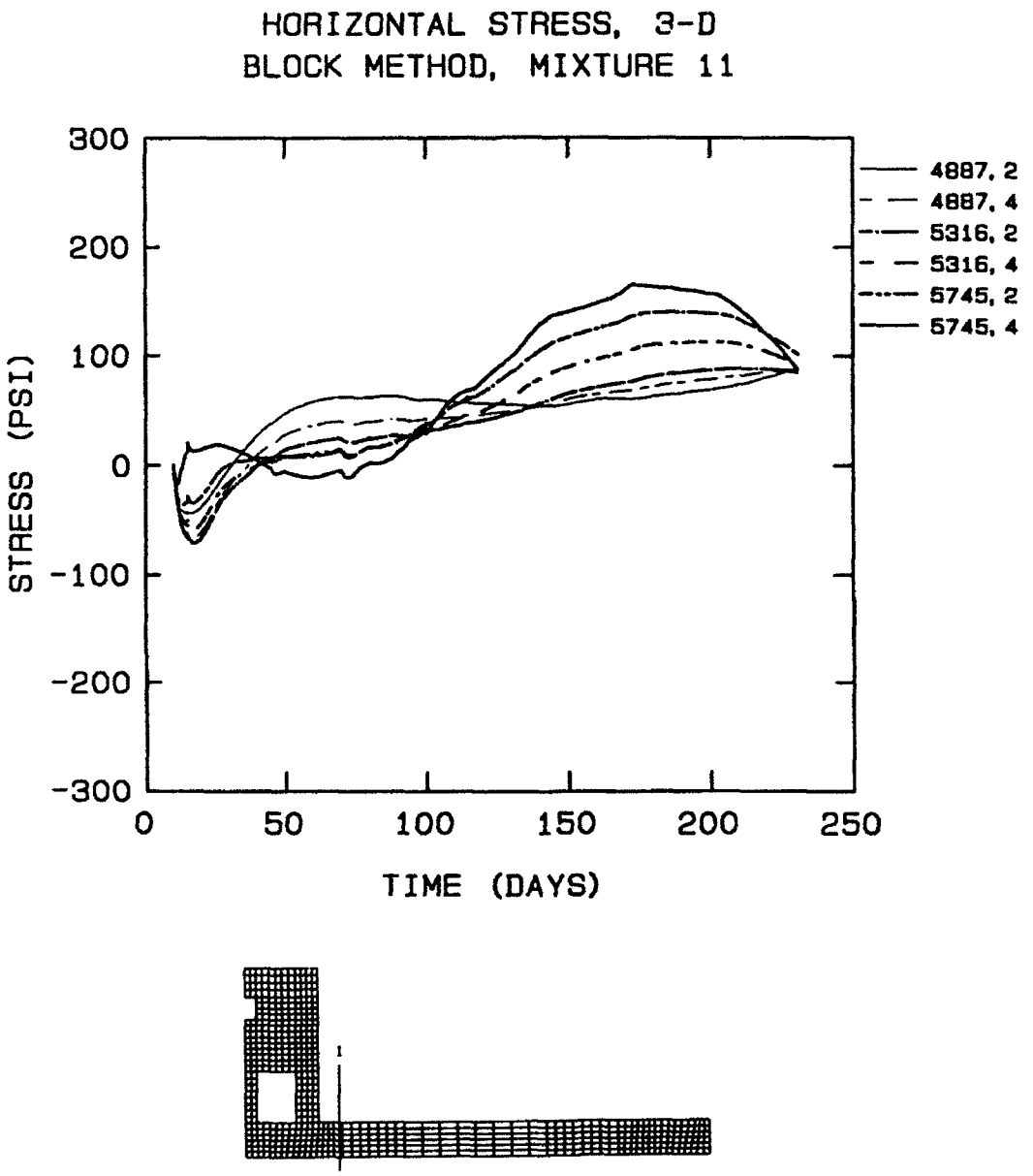

Figure 104. Horizontal stress at lift 3, section 1, 3-D analysis

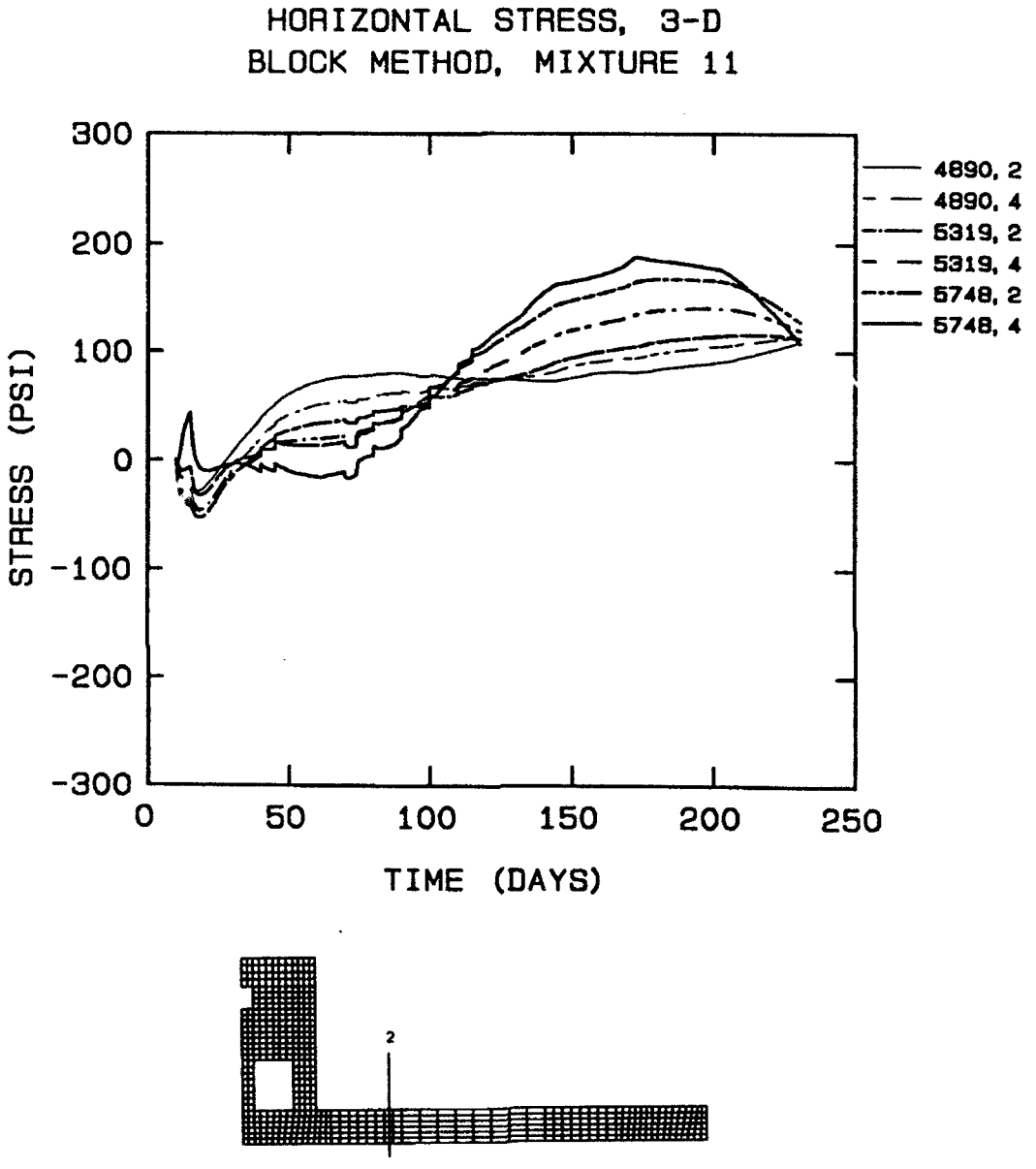

Figure 105. Horizontal stress at lift 3, section 2, 3-D analysis

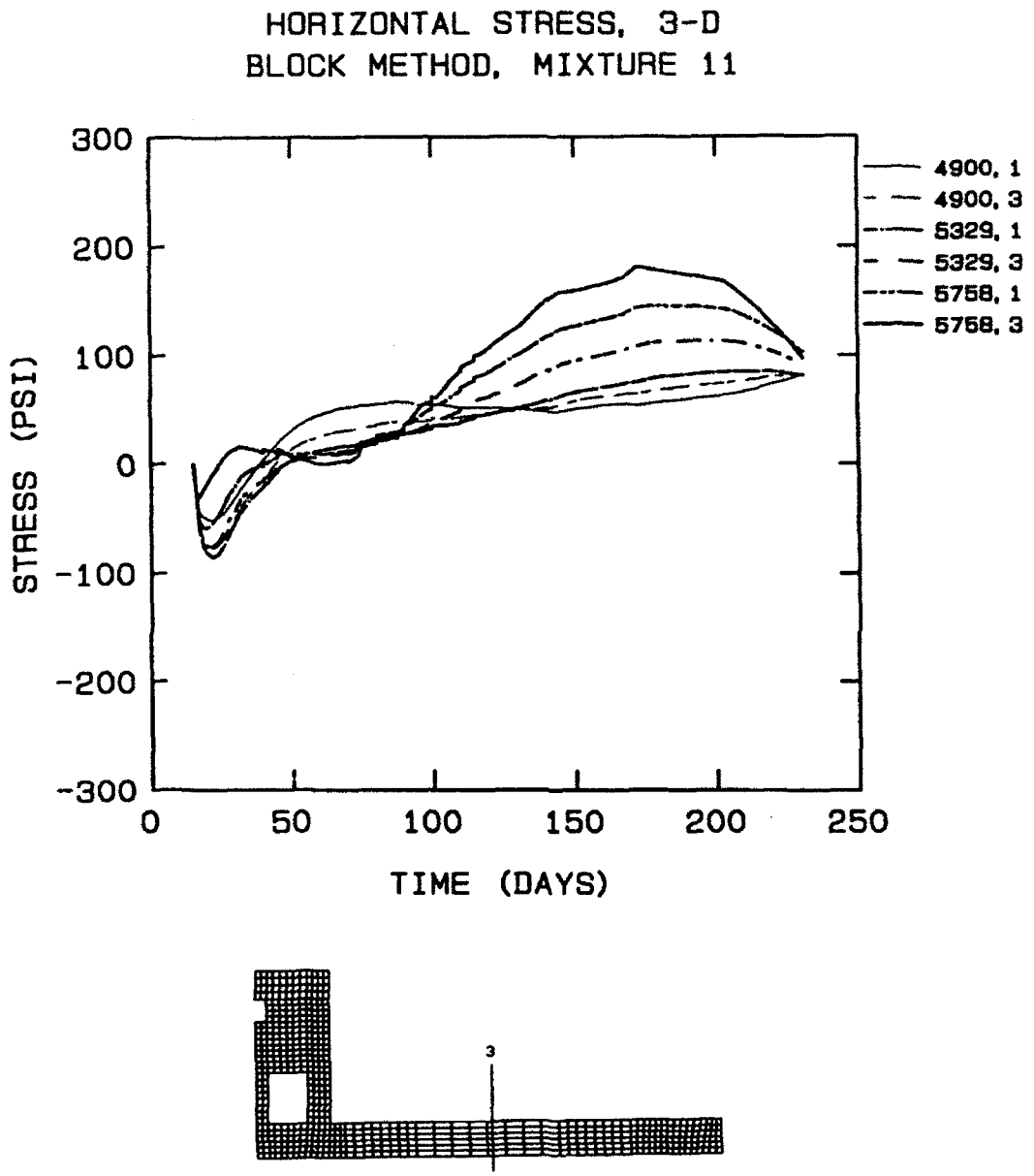

Figure 106. Horizontal stress at lift 4, section 3, 3-D analysis

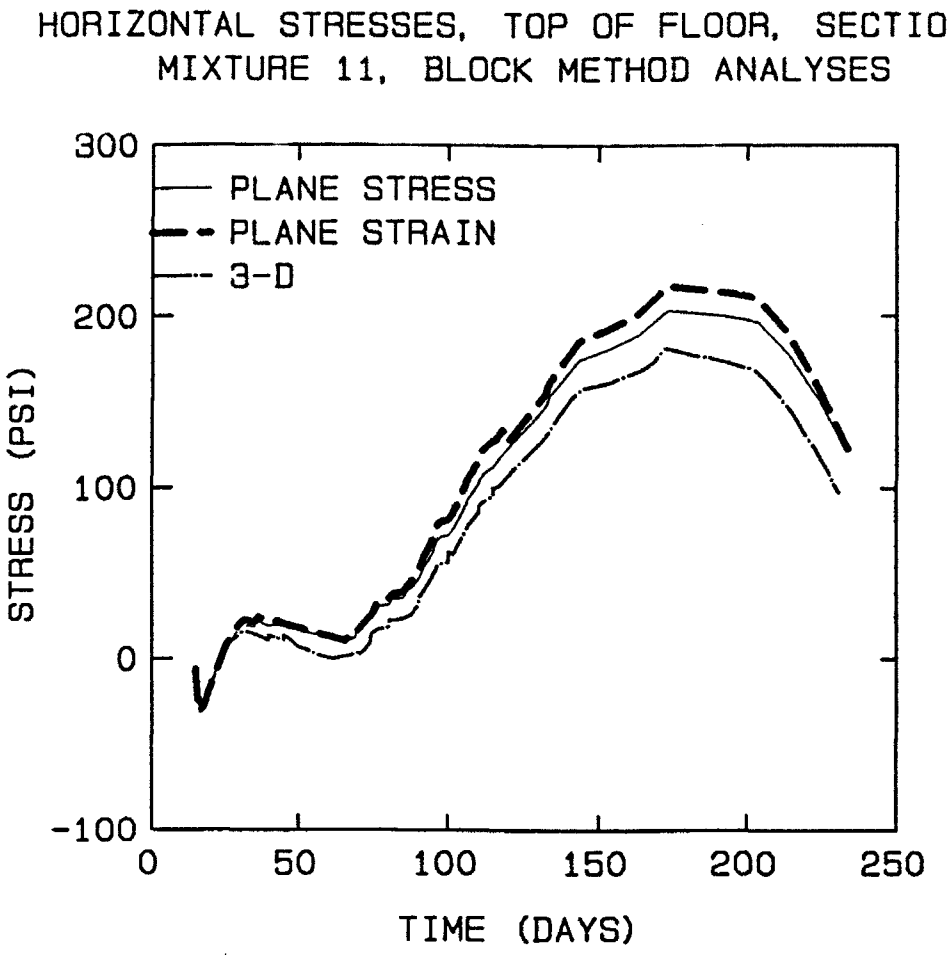

Figure 107. Horizontal stress at top of section 3, mixture 11, block method analysis

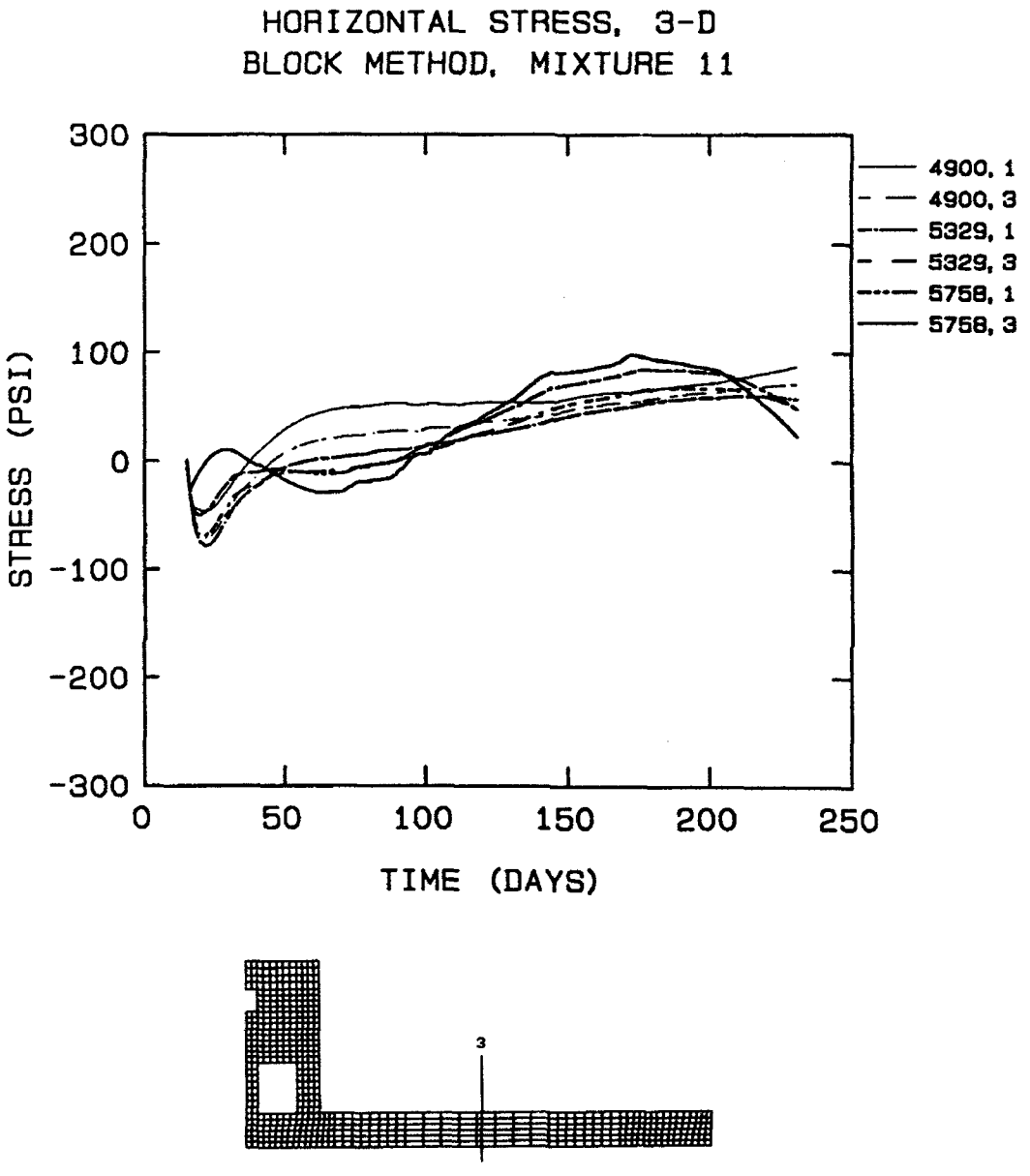

Figure 108. Stress parallel to axis of flow, lift 4, section 3, 3-D analysis

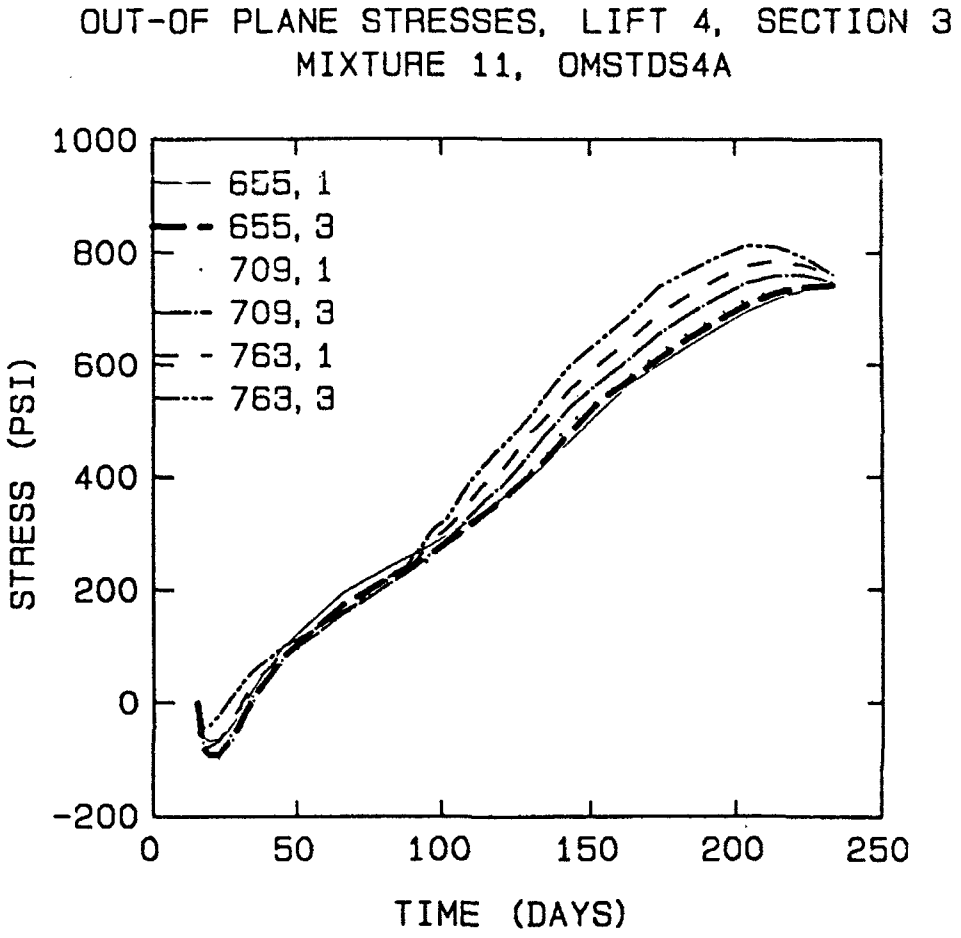

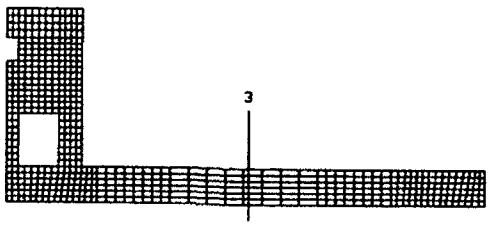

Figure 109. Out-of-plane stress at lift 4, section 3, OMSTDS4A

was induced by the restraint to volumetric contractions imposed by the existing concrete and was only 100 psi, and stresses at the top face were compressive for the first 100 days of the analysis. The Poisson's effect of these compressive stresses lowered horizontal tensile stresses in the plane of interest.

115. Since heat flow throughout much of the floor was 1-D, stresses tended to be fairly constant across a given elevation. Because of this, the maximum horizontal tensile stress was approximately the same at sections 1, 2, and 3. This means that concrete at the vertical joint will be under the same tensile stresses as the rest of the floor. Horizontal stresses at lift 2, section 2 remain compressive for approximately 30 days, but by 75 days tensile stresses normal to the vertical joint exist throughout the entire lift. Because of this, vertical joints must be carefully prepared prior to the placing of new concrete to ensure that the floor can act as a continuous member in tension. While reinforcing steel may act to limit the width of the crack if a joint opens, it cannot be expected to prevent a crack from forming.

116. Stresses at section 4 are shown in Figures 110 through 112. As expected, compressive horizontal stresses were larger in the 3-D analysis and tensile stresses were lower than in the plane stress or plane strain analyses. Maximum horizontal stresses at the top of the center wall culvert in the three analyses are compared in Figure 113. Stresses at the corner of the top opening are compared in Figures 114 through 116. Stresses in the 3-D analysis were slightly higher than those in the 2-D analyses in these areas, but the increase in stress did not result in cracking.

Conclusions

2-D analyses conclusions

117. In general, similar results were obtained from thermal stress analyses using both concrete mixtures. Mixture 11 analyses produced slightly higher stresses in the floor, and mixture 6 analyses produced slightly higher stresses in the walls. Both mixtures exhibited low early-time modulus and low shrinkage. However, specific creep strains for cylinders loaded at 1 to 3 days were much larger for mixture 11 than for mixture 6. For a structure under tension at relatively early times, this high early-time creep is usually advantageous. Due to the low placement temperature and low shrinkage, stresses in the top of the W-frame floor were compressive for the first 20 to

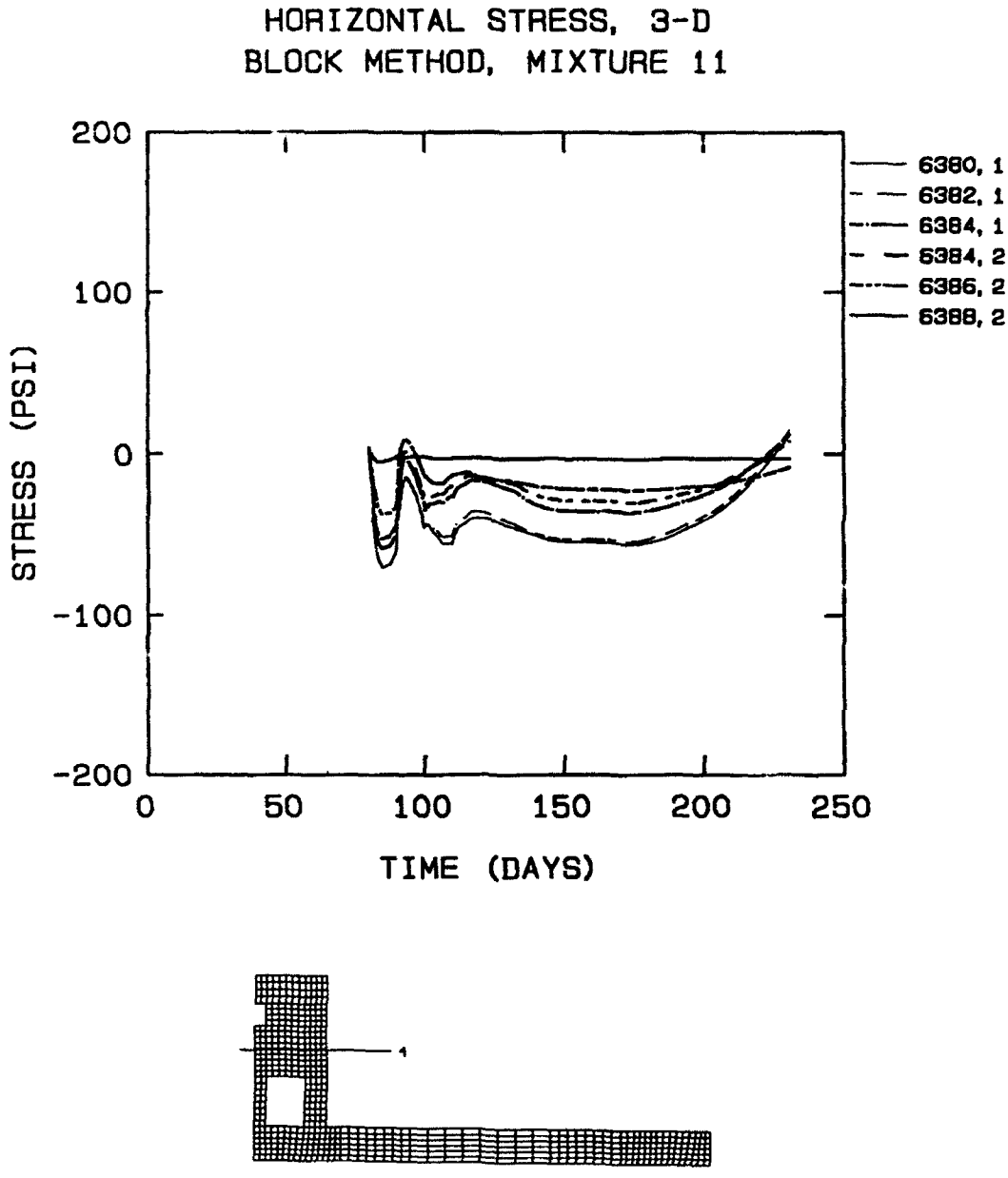

Figure 110. Horizontal stress at section 4, 3-D analysis

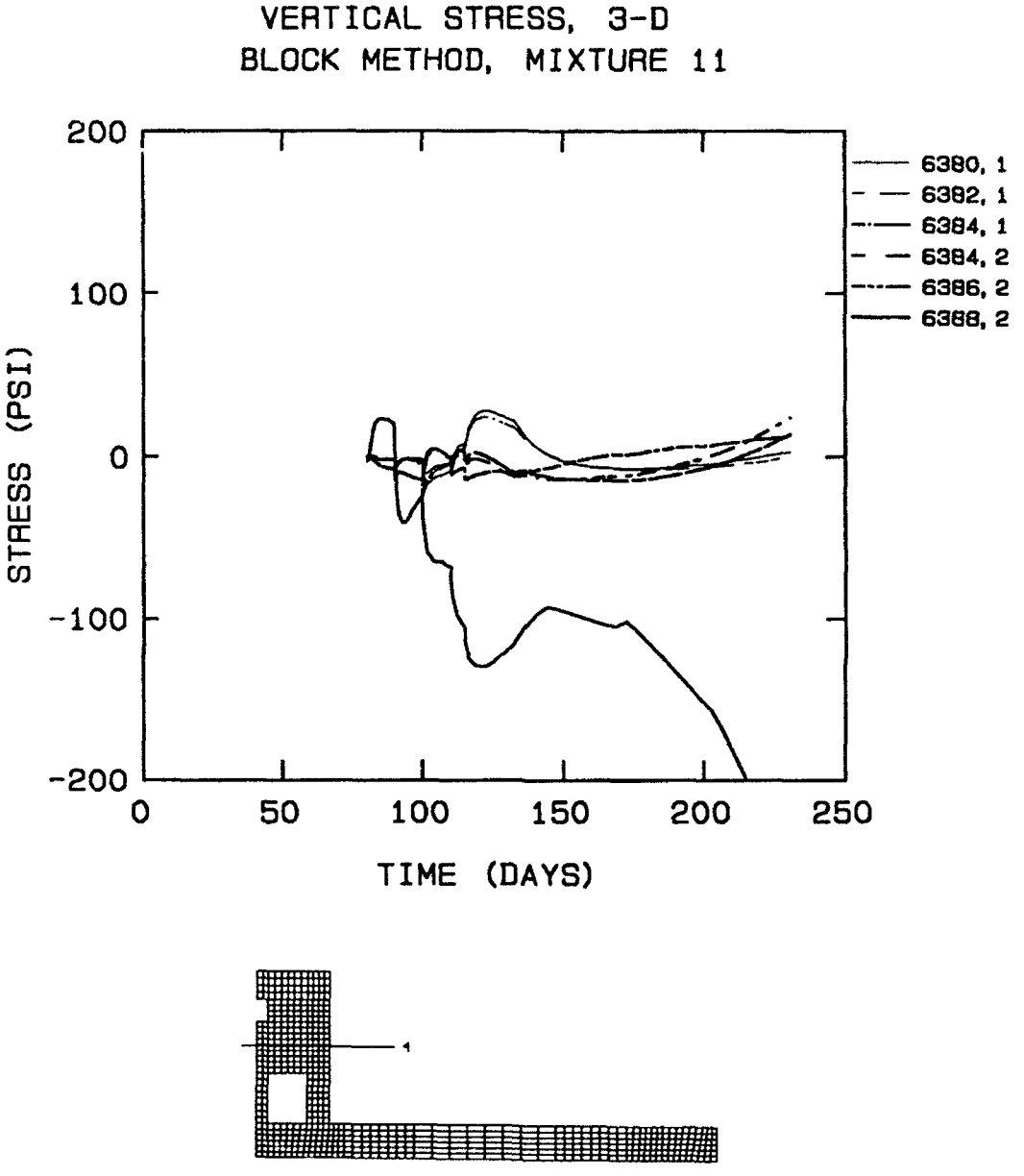

Figure 111. Vertical stress at section 4, 3-D analysis

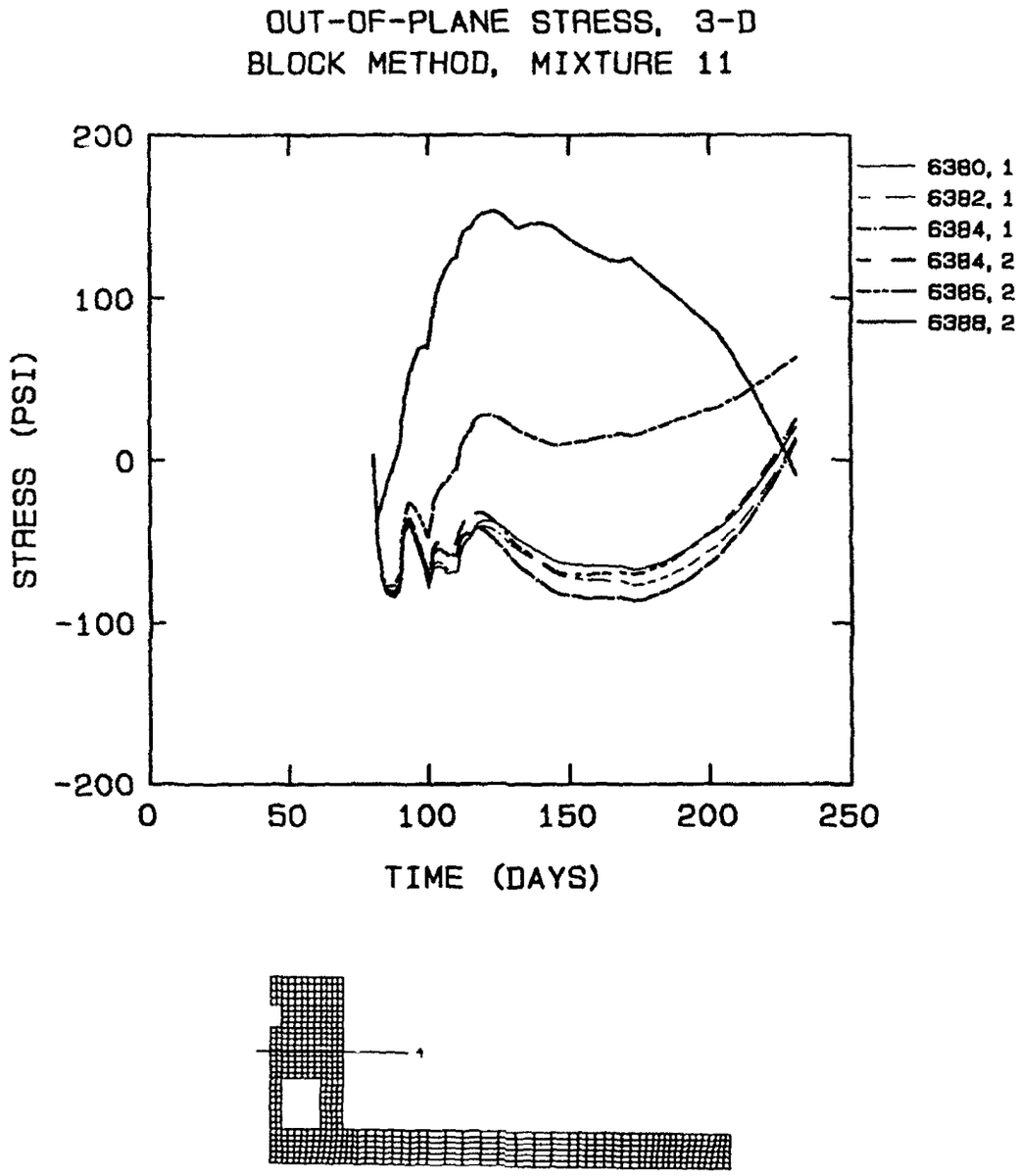

Figure 112. Z-directional stress at section 4, 3-D analysis

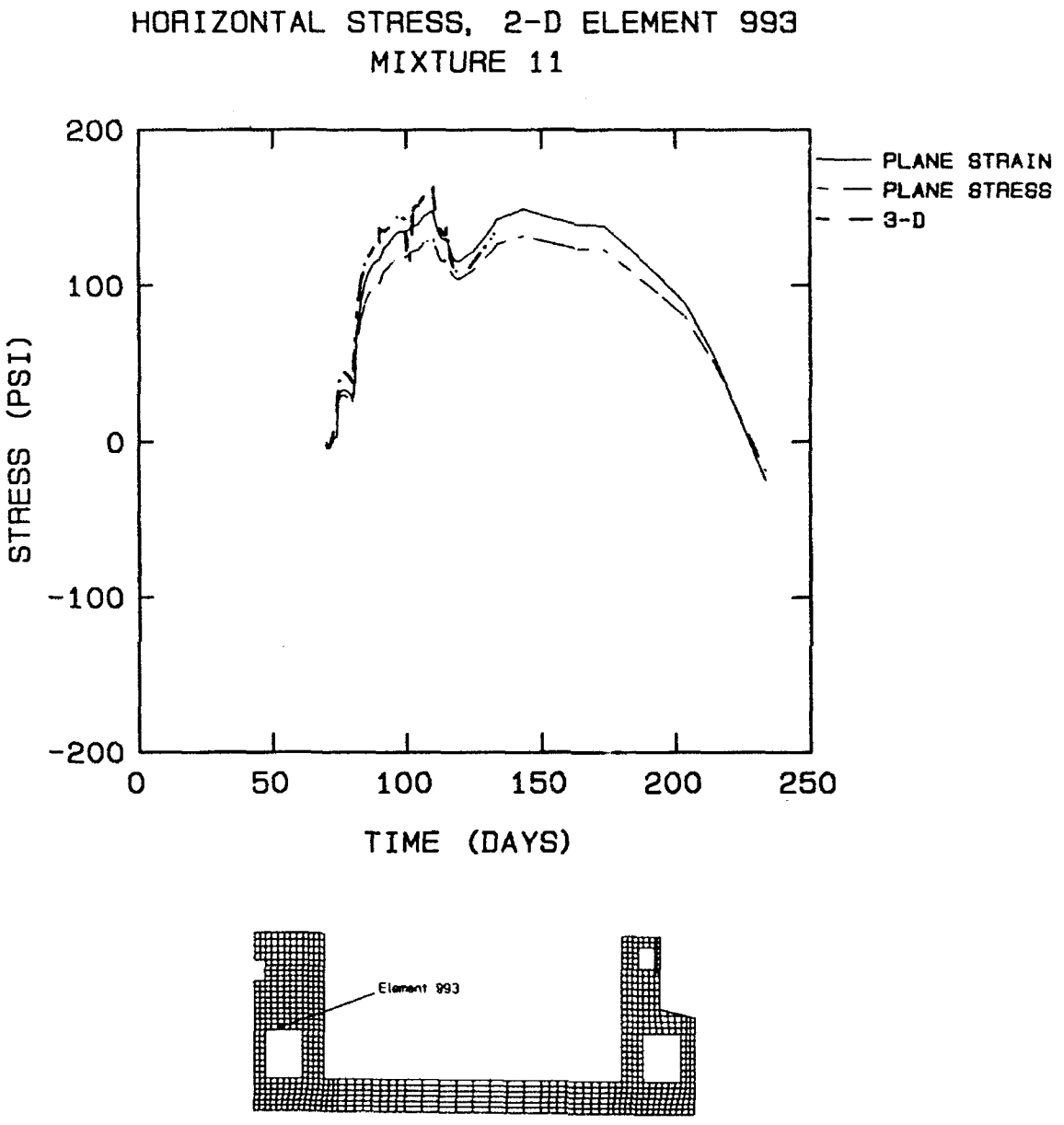

Figure 113. Horizontal stress at top of center wall culvert, mixture 11 analysis

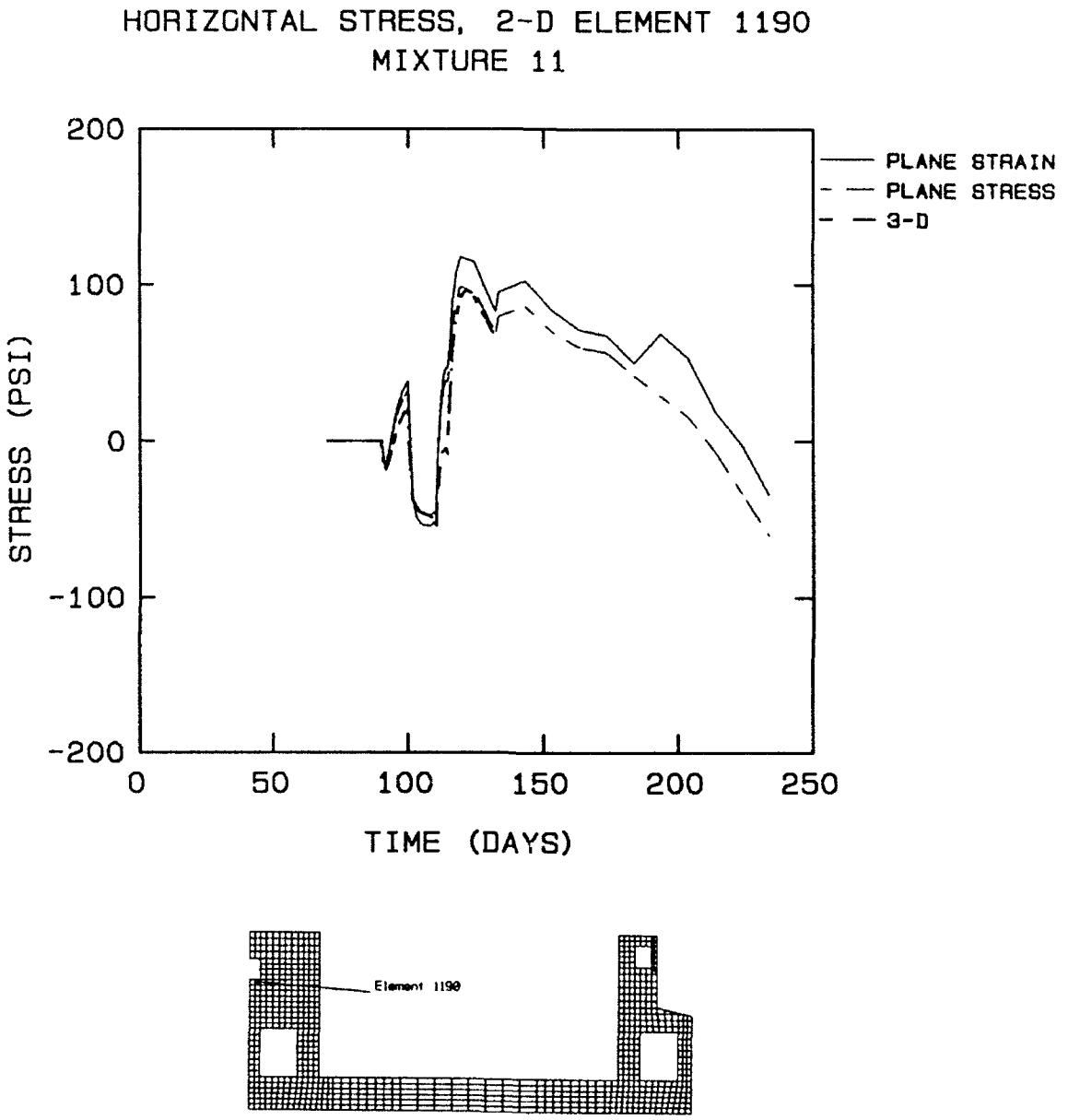

Figure 114. Horizontal stress at corner of center wall top opening, mixture 11 analyses

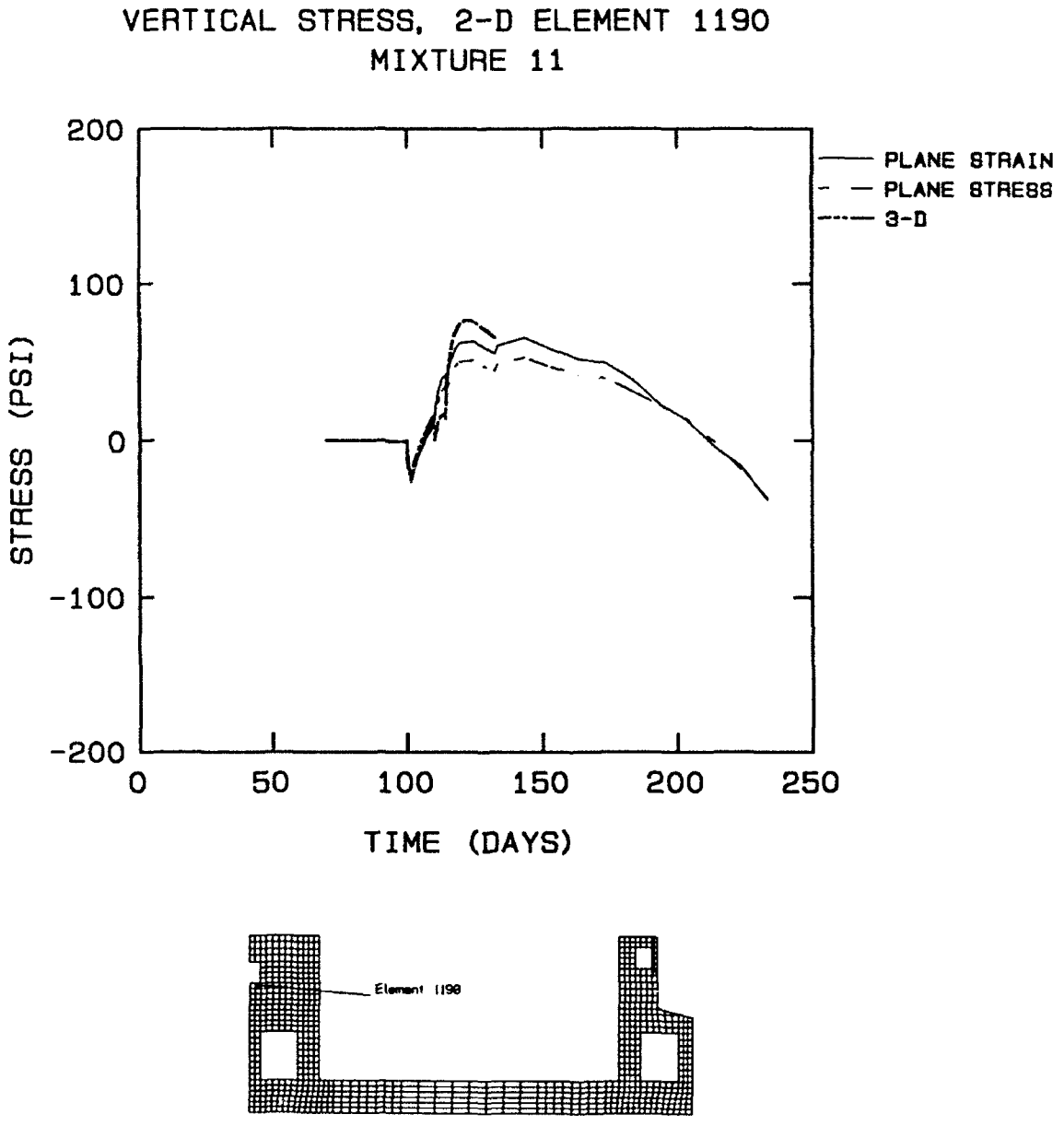

Figure 115. Vertical stress at corner of top opening, mixture 11 analyses

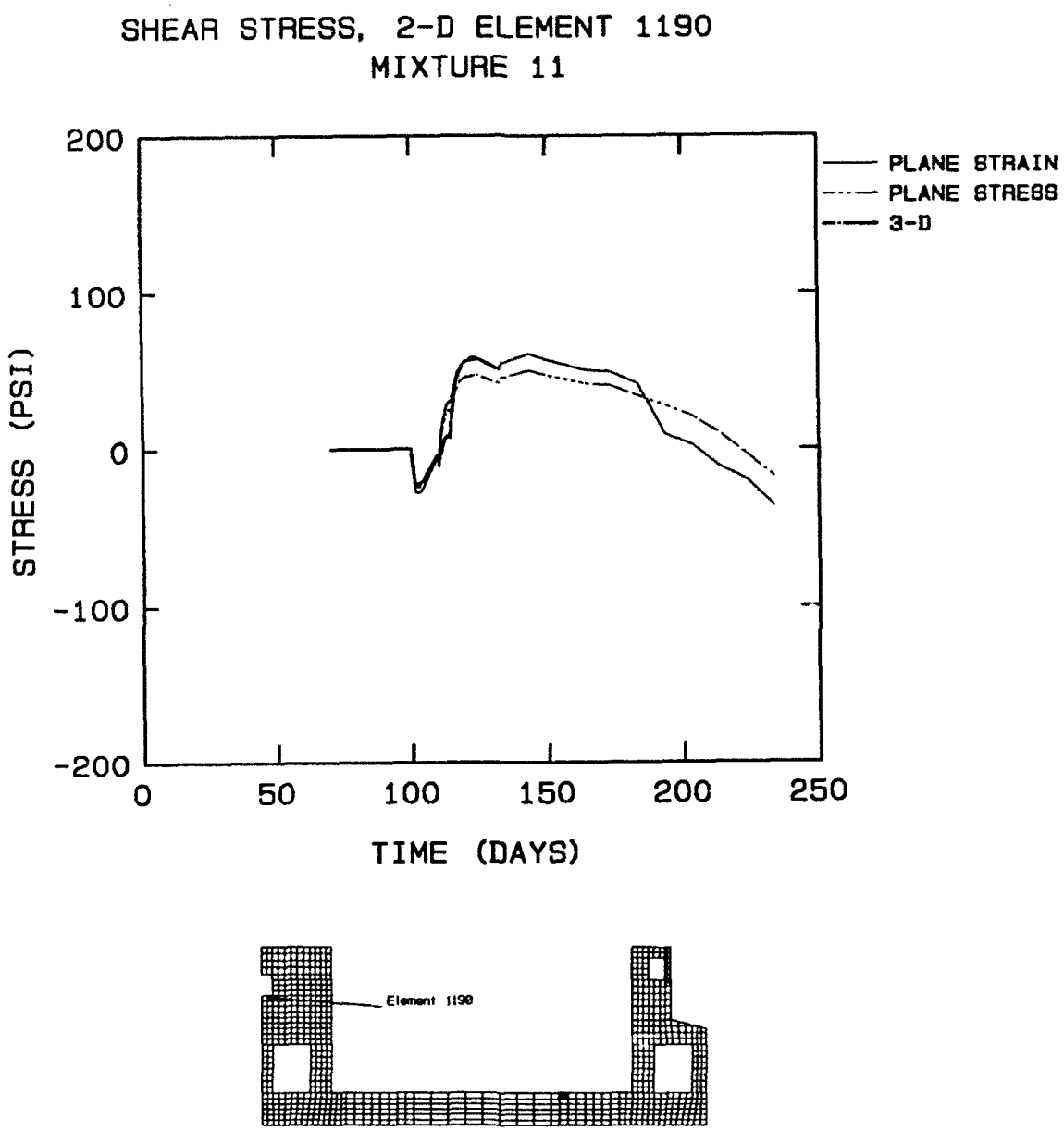

Figure 116. Shear stress at corner of top opening, mixture 11 analyses

30 days in all analyses. For a structure under compressive stress throughout this period, high early-time creep may act to reduce early compressive stresses, shifting the entire stress-time curve upward into a higher tension at late times.

118. Since early-time stresses in the floor were primarily compressive, maximum tensile stresses were due to seasonal fluctuations in ambient temperature rather than to initial heat rise in the concrete.

119. As expected, plane strain analyses generally produced higher in-plane stresses than corresponding plane stress analyses. The appropriate type of analysis depends on the geometry of the structure. A plane strain analysis is considered to be valid when the out-of-plane length is greater than three times the in-plane dimensions. This is not the case in the W-frame structure, and the plane stress results should be more realistic. Plane strain results should provide an upper bound for tensile stresses.

120. In areas of 1-D heat flow, tensile stresses tended to be perpendicular to the direction of heat flow. Stresses in the direction of heat flow and shear stresses were negligible. Areas of 1-D heat flow included the floor, culvert walls, and the top section of the outer wall.

121. Stress concentrations at wall openings in the massive center wall were due to differential displacements around the openings. These differences are a result of the variations in the amount of restraint to thermal volumetric changes provided by the concrete and the different rates of cooling for the two sides of the openings. High tensile stresses at wall openings occur relatively early after placement of the concrete (within 20 days) and may indicate problem areas for early-time cracking.

122. All analyses were made using the assumption that the structure would act monolithically. For the block placement method to produce a monolithic structure, the joint between the floor sections must be capable of sustaining the maximum level of tension in the floor to prevent the joint from opening. If the joint opens due to tensile stresses at the top, the resulting crack could propagate downward with time. Although the joint would probably not open through the entire depth of the floor, the ability of the monolith to carry stresses across the joint could be seriously affected.

123. In the strip placement method, the top floor joint is also in tension, and joints at lower elevations experience low tensile stresses at early times. If these joints do not remain closed, cracking is likely to occur in lifts above the joints. While this cracking will not prevent the

structure from acting as a monolith, it can lead to maintenance problems. Open joints in the floor could fill with silt which would not allow the joint to close if expansion occurred. Cracks in the wall over the center joint could potentially be exposed to freeze-thaw conditions which would tend to aggravate cracking.

124. All analyses were based on average ambient daily temperatures. No attempt was made to simulate short-term perturbations such as a strong cold front or longer-term variations, such as an unusually cold winter or hot summer.

125. All results and conclusions apply only for the mixtures and geometries used in the analyses. Additional analyses may be required to determine the effects of significant changes in mixture proportions or monolith geometry.

3-D analysis conclusions

126. Stresses predicted in this analysis were slightly lower than those predicted in the 2-D analyses in the floor and were generally within the bounds of plane stress and plane strain predictions in the walls. These results indicate that the 2-D block placement model was a valid approximation of a 3-D problem. Since tensile stresses in the direction of flow are much smaller than those transverse to the direction of flow, as shown in both the 2-D and 3-D block placement analyses, tensile stresses normal to the joints will be lower for the strip placement method. These lower construction joint tensile stresses coupled with the less critical layout of the construction joints, transverse rather than parallel to the flow orientation, indicate the strip method is the preferable method of placement.

Recommendations

127. The assumption of monolithic behavior upon which the analysis is based is valid for the strip placement scheme but may not be valid for the block placement scheme. For this reason and the reasons outlined in the conclusion section, only the strip placement method need be considered for Phase II.

128. Due to the difficulty of preparing vertical construction joints in a manner that will ensure the expected levels of tensile stress across the joints to be maintained, consideration should be given to reducing the monolith spacing in order to eliminate vertical joints within a monolith.

129. Based on potential cracking due to plane strain modeling effects, the complexity of 3-D analyses, and similarity of results from the 2-D plane stress, 2-D plane strain, and 3-D results, only the 2-D plane stress model need be considered for Phase II. However, due to unknown effects caused by banding material parameters, both concrete mixtures should be considered for Phase II.

130. Final results of Phase II should be compared to Phase I to prove the validity of using this approach to reduce the number of parameters to consider in the Phase II study.

PART IV: PHASE II

General

131. Upon completion of the Phase I analyses, a decision was made by the U.S. Army Engineer District, Louisville, to decrease the monolith lengths to 54 ft based on the results from Phase I which indicated tension acting across the vertical construction joints. Based on this decision, the final set of analyses were performed on a model without vertical lift joints and included the banding of material properties as required in ETL 1110-2-324 (Headquarters, Department of the Army, 1990). Banding of the material properties is intended to address uncertainties in mechanical properties due to variation in testing procedures and any small differences of the mixtures used in the lab compared to those used in the field.

132. In Phase II, six additional analyses were performed using mixture 6 properties and four additional analyses using mixture 11 properties. Table 14 lists the load cases considered during the Phase II study. Load cases 1 through 4 for mixture 6 correspond to the required load cases specified in ETL 1110-2-324. Load cases 1 and 2 were run only for mixture 6 to minimize the computational effort and because load cases 1 and 2 are used primarily for purposes of comparison and evaluation of the effects of gravity and creep and shrinkage. Load cases 5 and 6 were not required by ETL 1110-2-324. Load case 5 was added because it was felt that this combination of creep and shrinkage would produce the highest stresses in many instances. Although load case 6 was not expected to produce the maximum stresses, it was added for completeness.

133. The maximum and minimum designations for creep and shrinkage shown in Table 14 indicate adjustments either up (maximum) or down (minimum) to the curves obtained from testing. The average designation in Table 14 indicates the curve obtained from test results. For Phase II analyses adjustments of $\pm$10 percent were applied to both the creep compliance and shrinkage curves obtained in the testing of mixtures 6 and 11. The creep compliance and shrinkage curves as well as the factored curves are shown in Figures 117 through 119. Decisions on these bandwidths were reached among representatives of the U.S. Army Engineer Division, Ohio River, the Louisville District, and WES as reasonably expected variations to the creep and shrinkage curves.

Table 14

Load Cases for Phase II Analyses

Load Case	Aging Modulus	Creep	Shrinkage	Adiabatic Temp. Rise	Mechanical Loads
			Mixture 6		
1	Average	None	None	None	Gravity
2	Average	None	None	Average	Gravity + Service
3	Average	Max.	Max.	Average	Gravity + Service
4	Average	Min.	Min.	Average	Gravity + Service
5	Average	Min.	Max.	Average	Gravity + Service
6	Average	Max.	Min.	Average	Gravity + Service
			Mixture 11		
3	Average	Max.	Max.	Average	Gravity + Service
4	Average	Min.	Min.	Average	Gravity + Service
5	Average	Min.	Max.	Average	Gravity + Service
6	Average	Max.	Min.	Average	Gravity + Service

134. Since the average curve is specified in ETL 1110-2-324 load cases for the adiabatic temperature rise curve, additional heat transfer analyses were not required. *Heat transfer results from the Phase I strip* placement analyses were used in the Phase II analyses.

135. Analyses in Phase II used the strip method placing scheme, as described in Table 9, and a plane stress formulation. In addition, it was determined that the shrinkage curve obtained in the testing of mixture 11 was highly unlikely to occur in the field; therefore, for the analyses performed for mixture 11, the shrinkage curve from mixture 6 was used, which is conservative from an analysis standpoint.

136. The service loading to be applied as specified in Table 14 for load cases 2 through 6 was included in the analyses at 250 days after the start of concrete placement. This service load is a normal loading condition with water and soil elevations as shown in Figure 120. The hydrostatic loads and soil loads from this condition are shown in Figure 121, as well as the uplift loading. It should be noted that the uplift load is somewhat higher than that due to the river at the elevation shown. This difference is attributed to artisan effects that occur in the area of the Olmsted project.

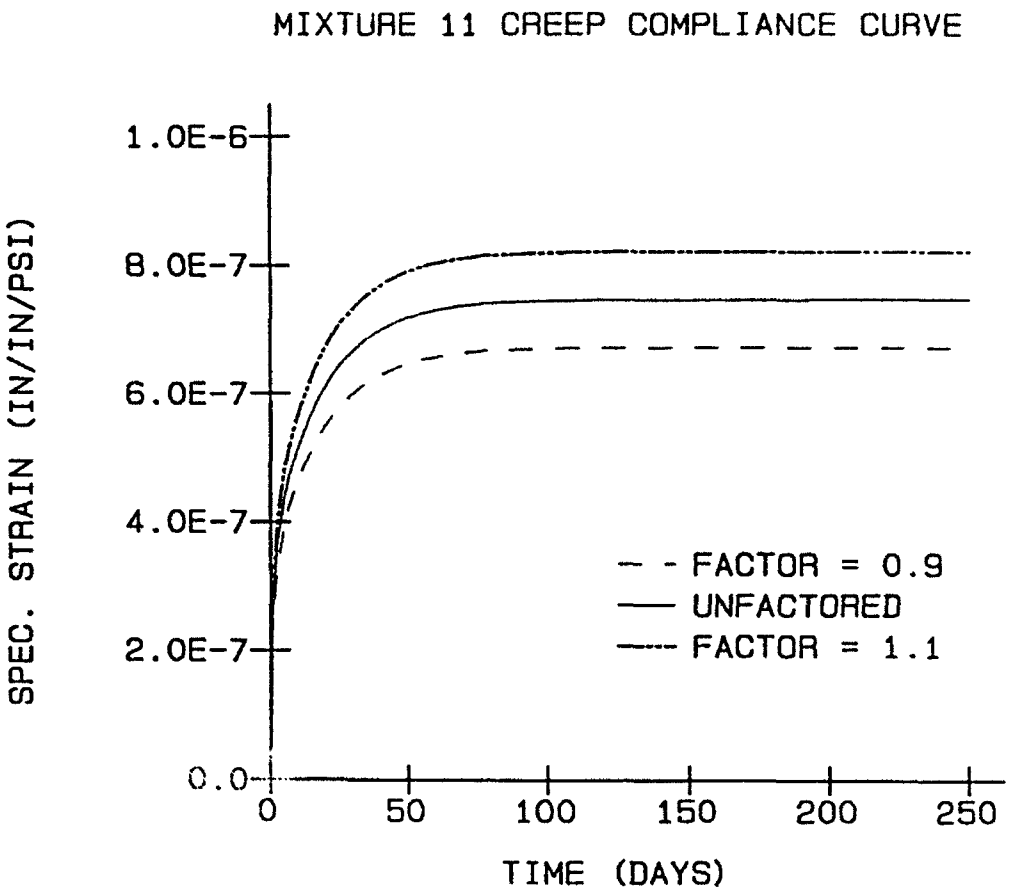

Figure 117. Factored creep compliance curve for mixture 11

137. Time-history plots of the horizontal stress at various integration points within the structure are used to compare the various analyses. Many of these points are the same as points that were evaluated in the first phase of the study. One extra time-history plot is included at the point in the base slab which exhibited the maximum stress. Integration points at elements located 5 ft from the land wall in the base slab (elements 503, 665, and 773) were also added. Stresses at these points will be added to stresses calculated in seismic analyses. Finally, points in elements 973 and 1125 were added to provide additional insight into the behavior of the walls of the monolith. In addition, stress distributions are presented at a section near the lock chamber center line and at a section 5 ft from the land wall.

138. It should also be noted that one of the requirements of ETL 1110-2-324 for presenting the results of a NISA is the inclusion of strain time histories. However, strain time histories will not be included in this report because the strains which ABAQUS outputs directly are total strains and are

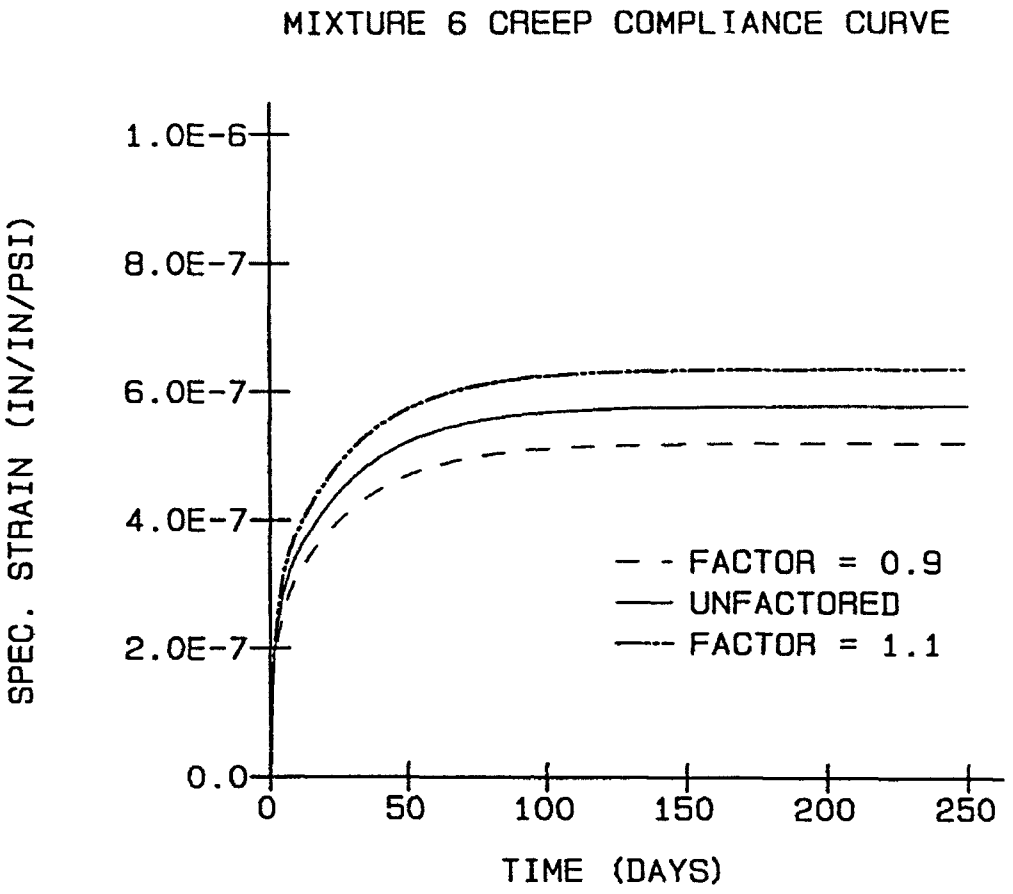

Figure 118. factored creep compliance curves for mixture 6

not strains which are related to real stresses in the structure. The strain output by ABAQUS is a measure of the displacement occurring within the structure. The strain used within the UMAT subroutine in its calculations would be appropriate in evaluating the structure but is not currently available as an output option.

139. As in Phase I, the results from the mixture 11 analyses are presented first, followed by presentation of the results from mixture 6 analyses. While the major points from the two sets of analyses are the same, the presentation of results will differ to provide an opportunity for presenting various aspects of the results and to avoid repetition from one section to the next.

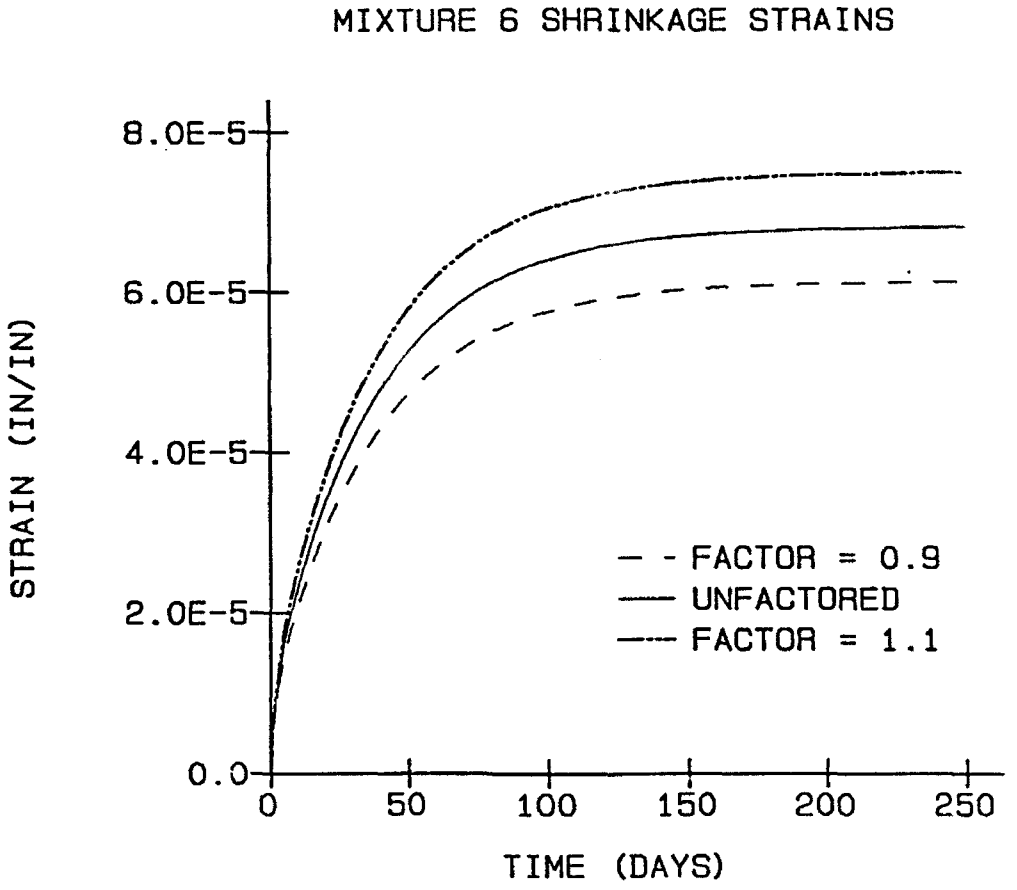

Figure 119. Factored shrinkage curves for mixture 6

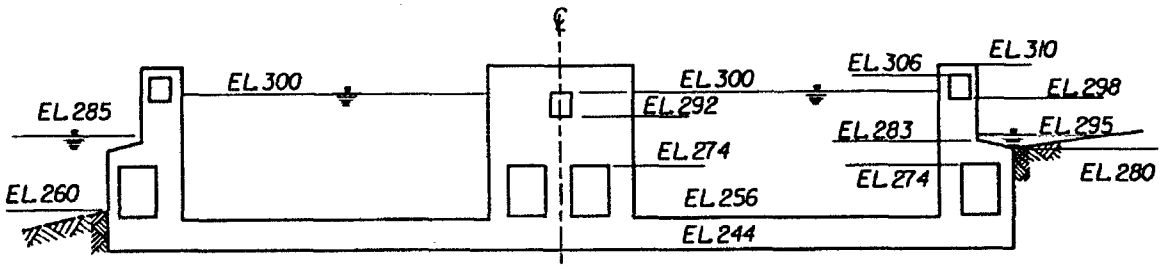

Figure 120. Normal service load condition

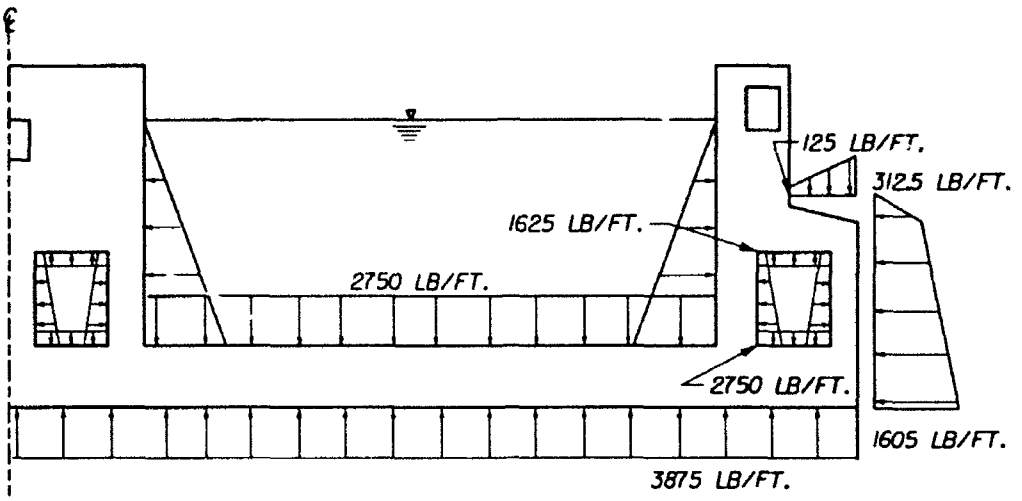

Figure 121. Applied loads for normal service load condition

Mixture 11 Analyses

140. Results from the four analyses are shown in Figures 122 through 159. In general, tensile stresses for load cases 4 and 5 were higher than those for the load case 3 and 6 analyses, with maximum tensile stresses occurring in load case 5 at the top of the lock floor. The minimum creep curve was used in both the load case 4 and load case 5 analyses. In both cases, decreasing the magnitude of the creep compliance curve by a uniform factor resulted in increased tensile stresses. However, mixture 11 tensile stresses were slightly higher than corresponding mixture 6 stresses. This may have been due to the combination of lower early modulus and higher early creep in mixture 11. This combination would tend to result in lower stresses at early times when stresses were compressive near the top of the lock floor, possibly shifting the stress toward tension at later times.

141. Horizontal stress histories at section 3 from Figure 46 are compared with the ETL 1110-2-324 allowable stress in Figures 122 through 124. The three elements selected are at the base of the floor (element 493), the center of the floor (element 655), and the top of the floor (element 763). Maximum floor stresses in the Phase I analyses were produced by the OMSTDS3 analyses. Stresses in element 763 for the Phase II cases are compared with stresses from the Phase I OMSTDS3 analysis in Figure 125. Stresses from the Phase I analysis fall within the bounds of the Phase II analyses. Tabulated values of tensile stress and percentage of ETL 1110-2-324 allowable stress are presented in Table 15. Stresses in elements 493 and 655 were either

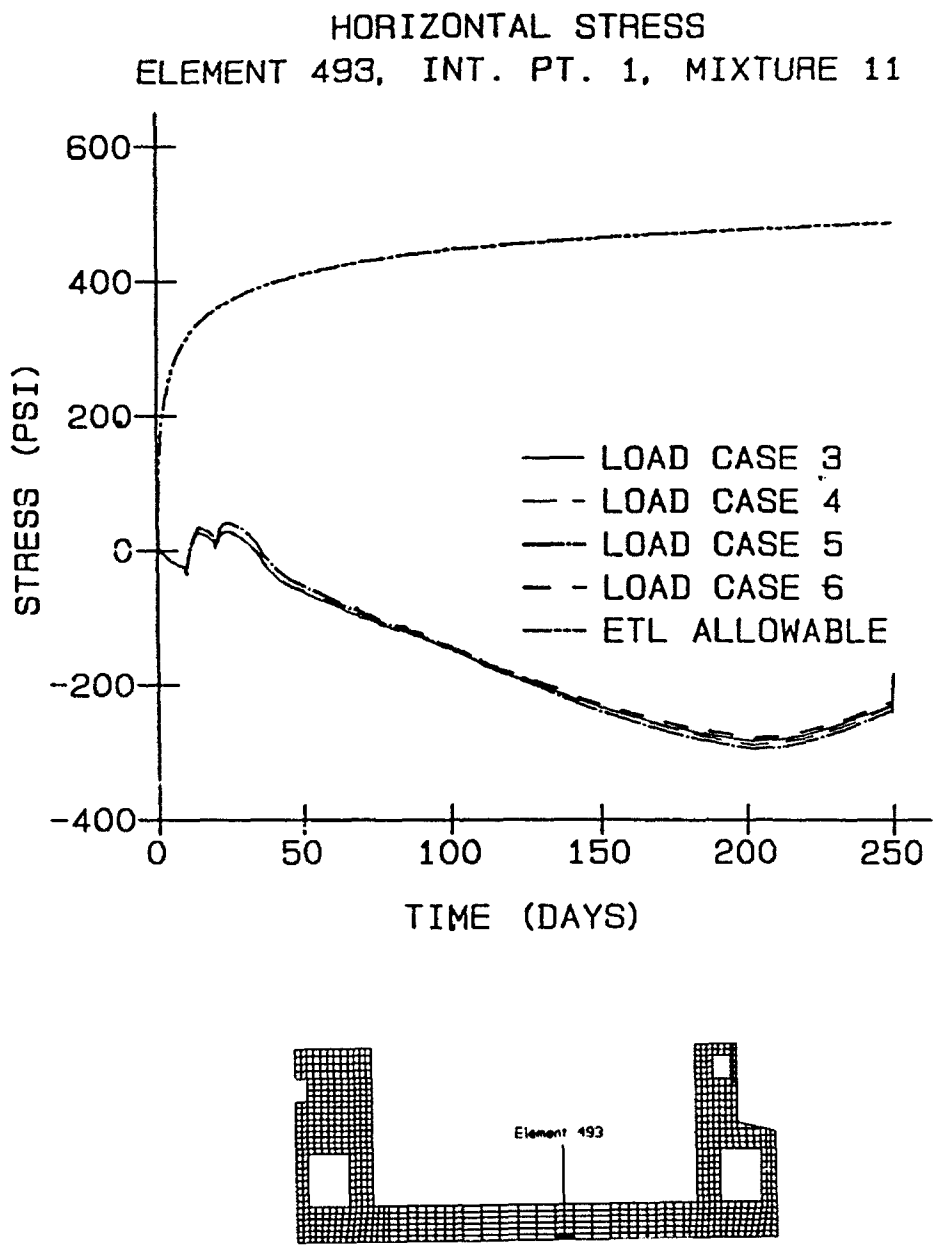

Figure 122. Horizontal stresses, element 493, point 1

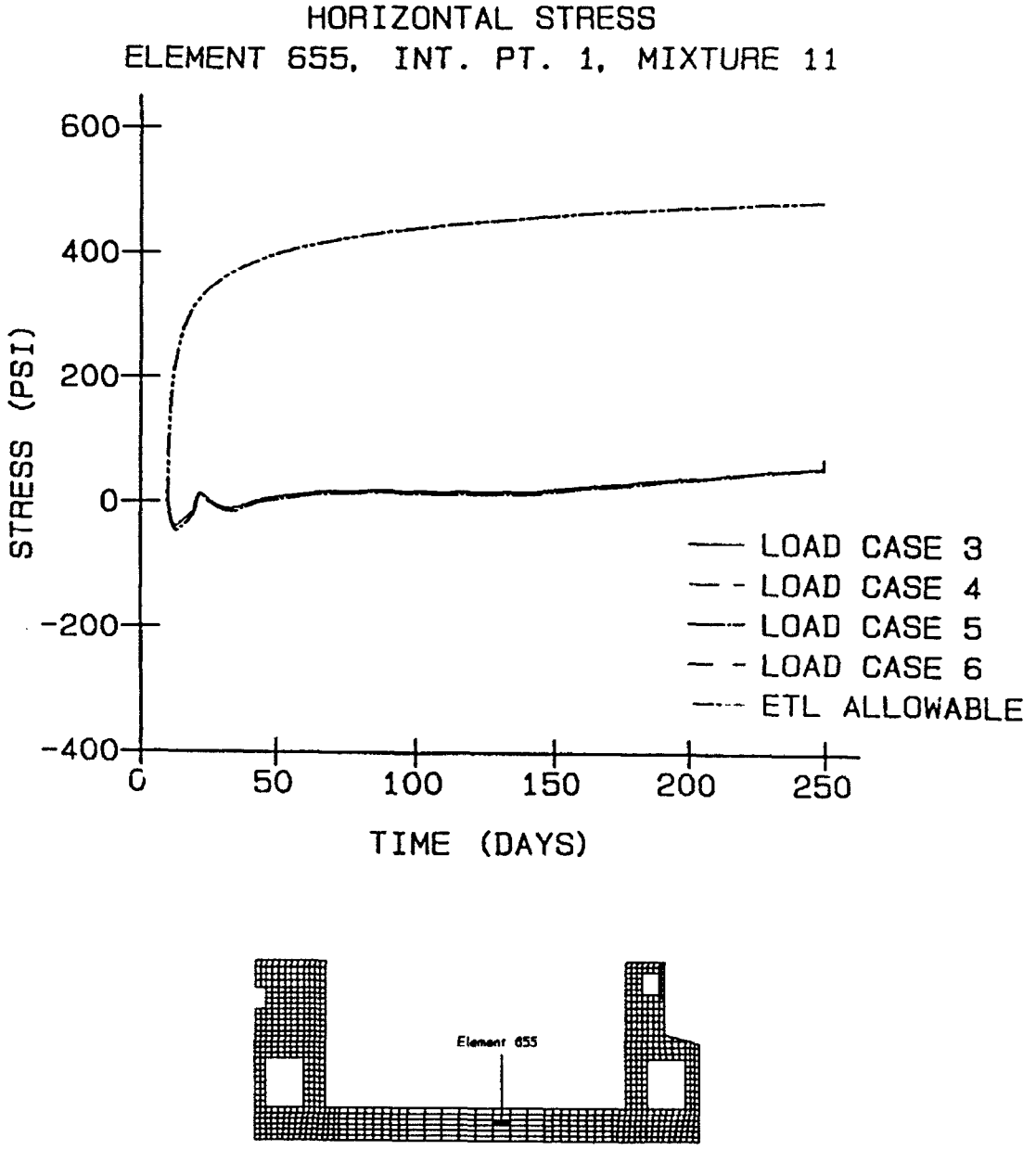

Figure 123. Horizontal stresses, element 655, point 1

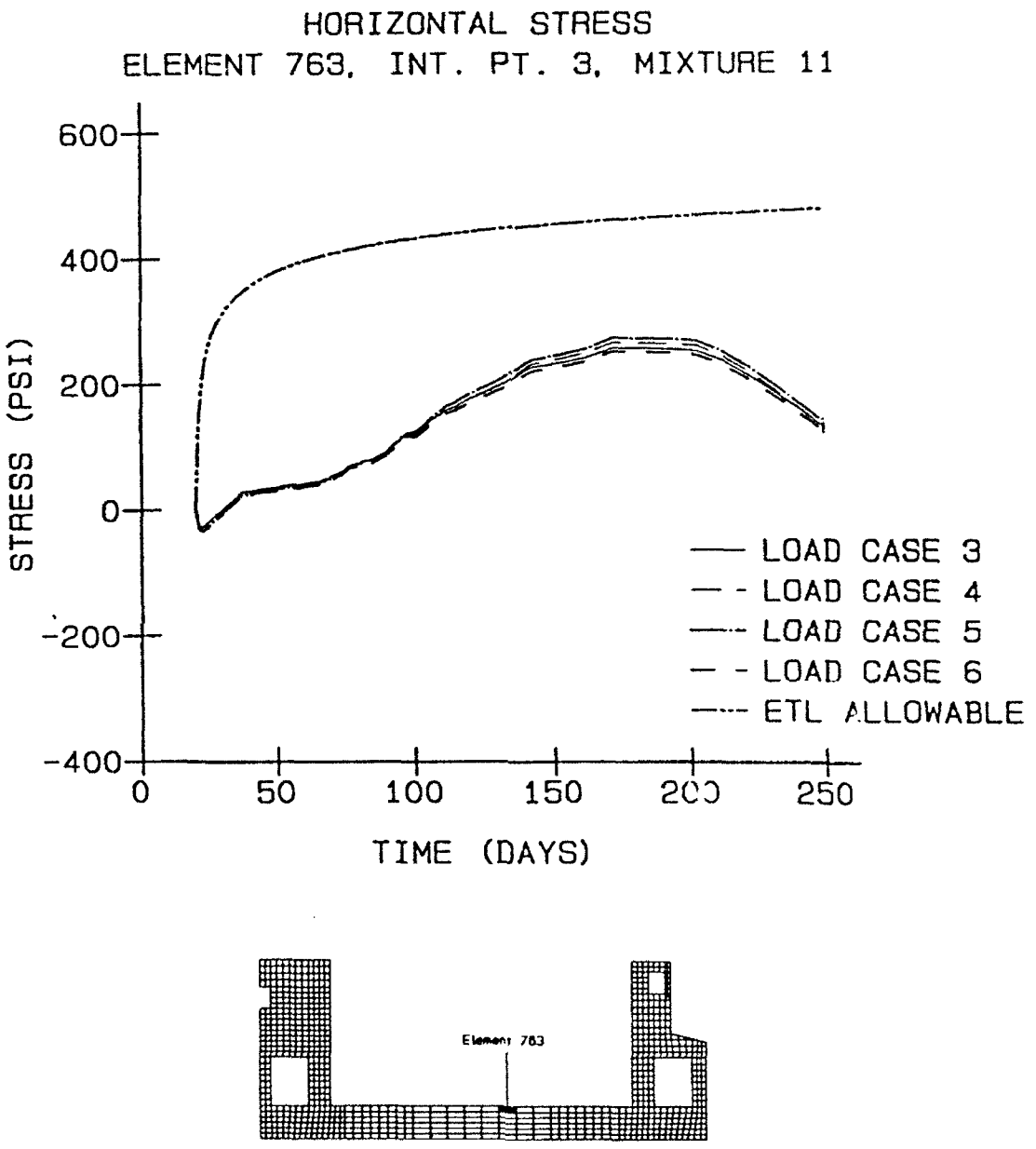

Figure 124. Horizontal stresses, element 763, point 3

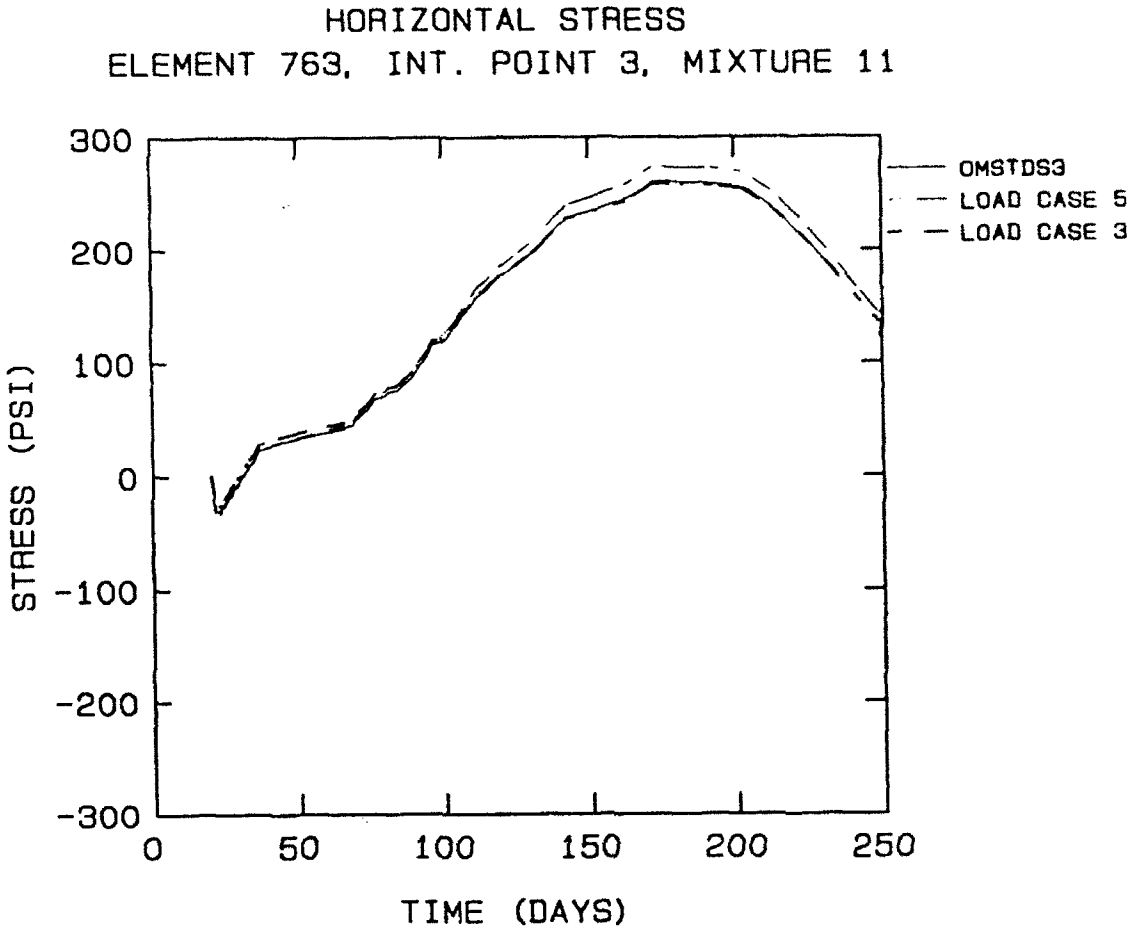

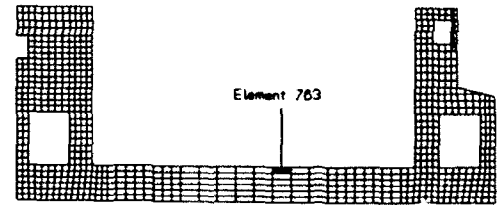

Figure 125. Part I & II horizontal stresses, element 763, point 1

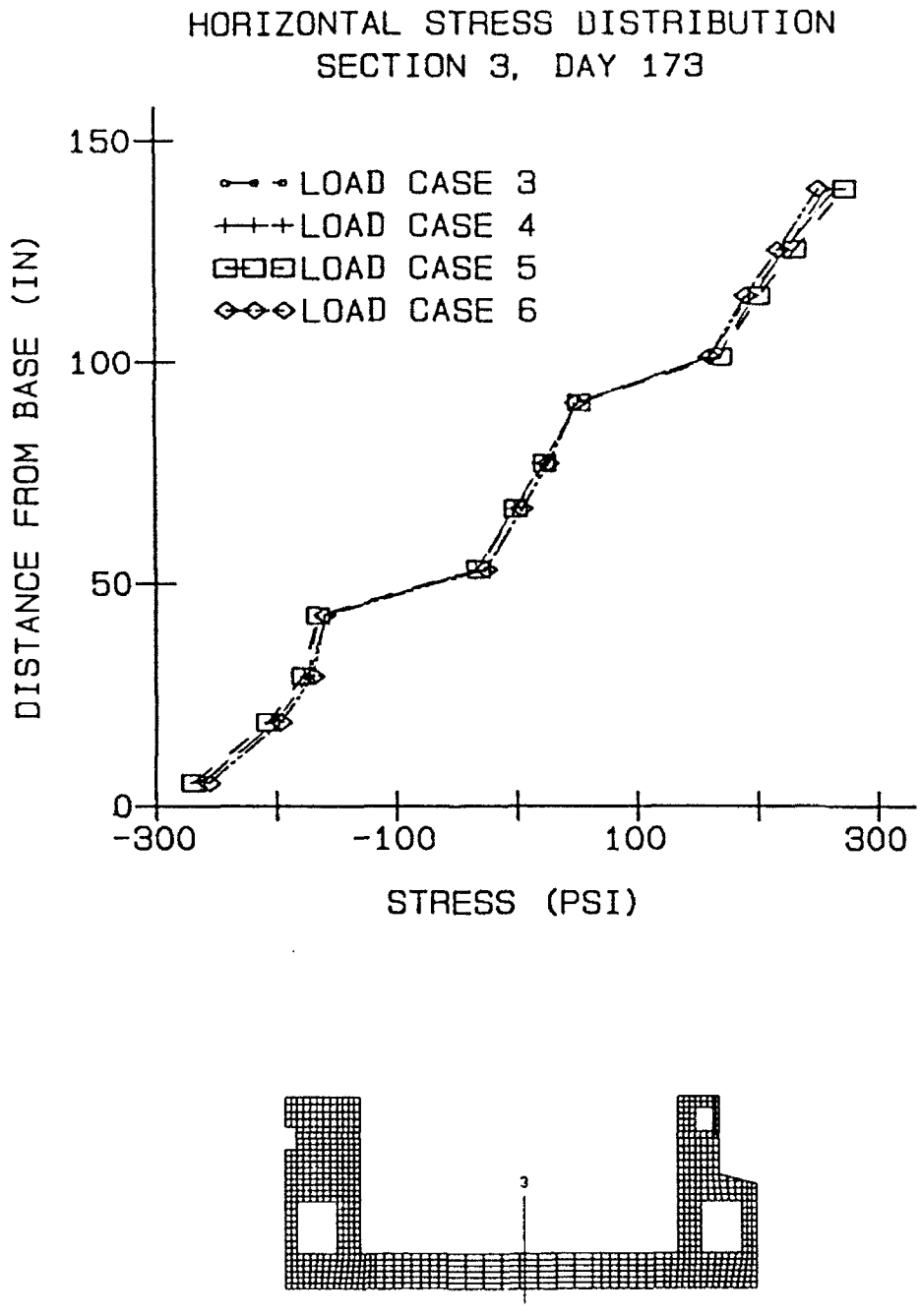

Figure 126. Stress distributions at floor section 3, day 173

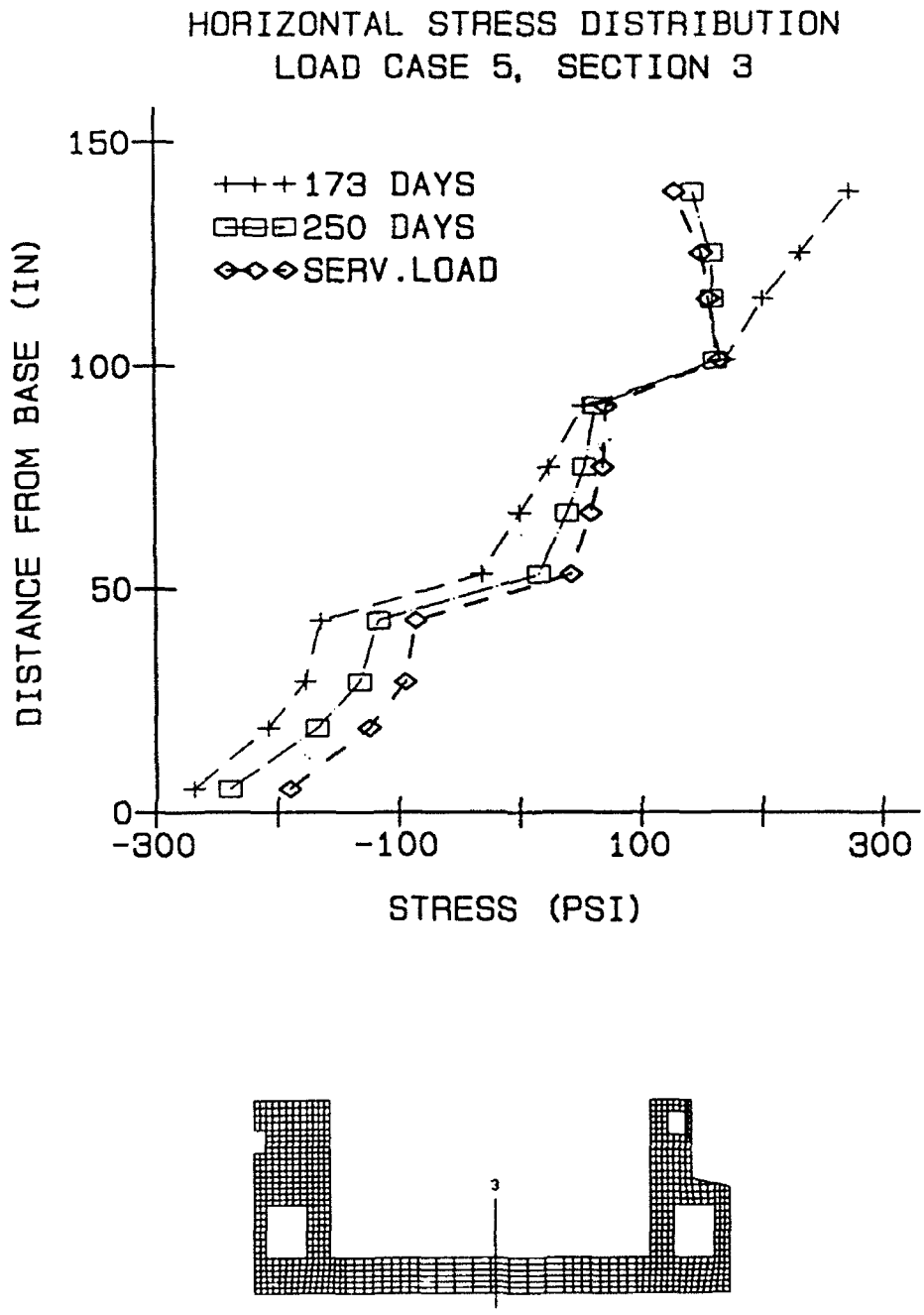

Figure 127. Stress distributions at floor section 3, day 173 and day 250, before and after service load application for load case 5

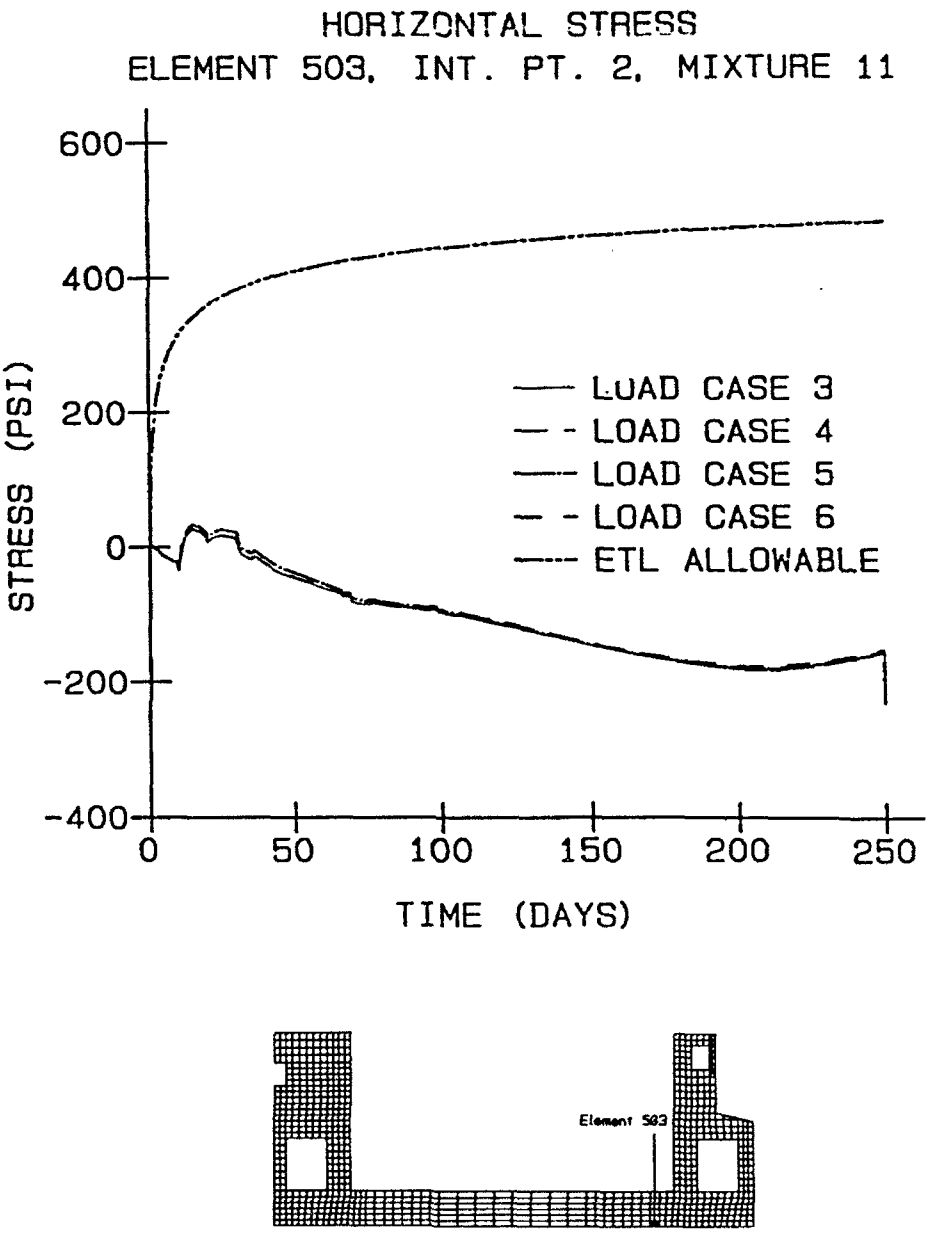

Figure 128. Horizontal stresses, element 503, point 2

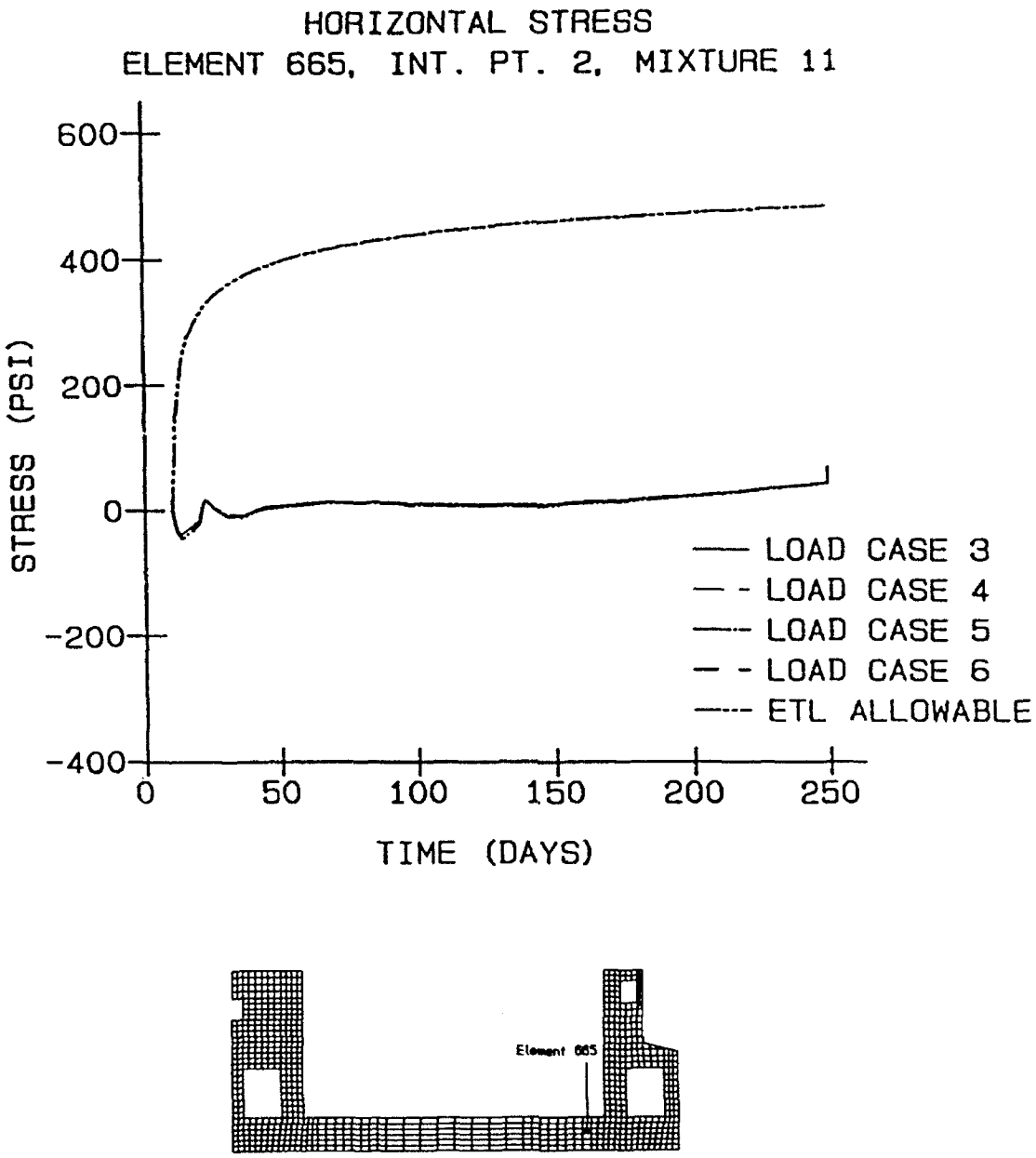

Figure 129. Horizontal stresses, element 65, point 2

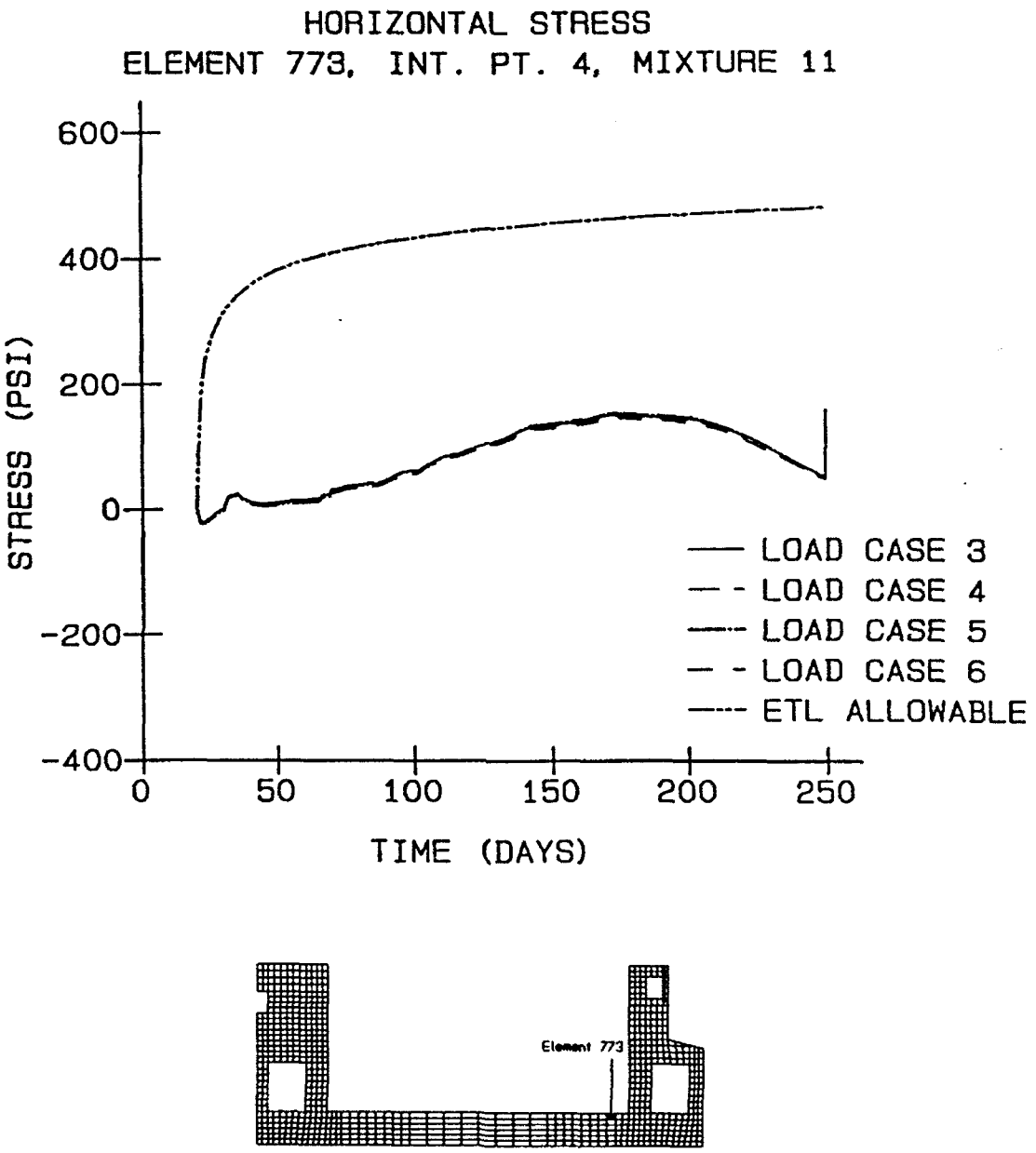

Figure 130. Horizontal stresses, element 773, point 4

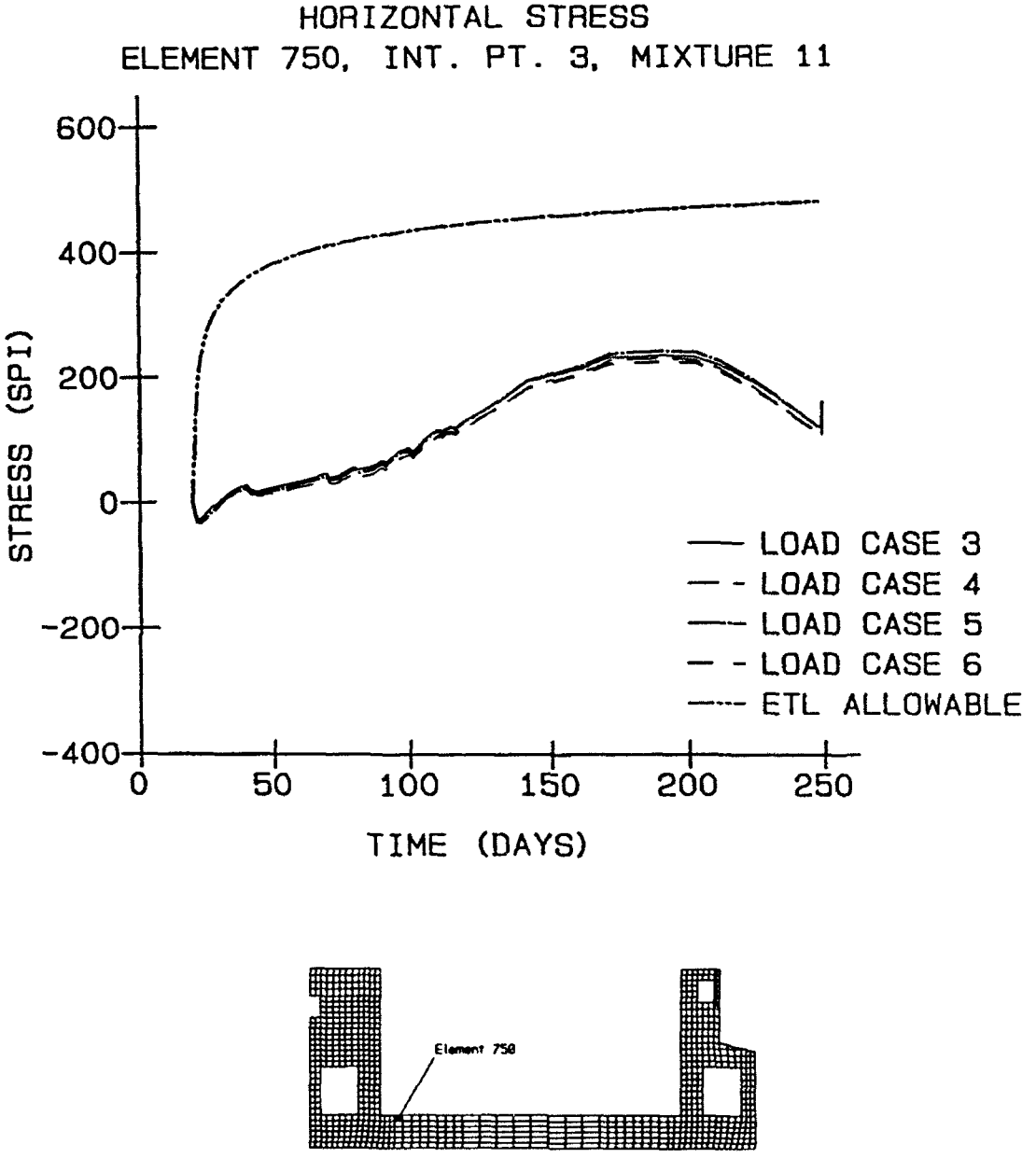

Figure 131. Horizontal stresses, element 750, point 3

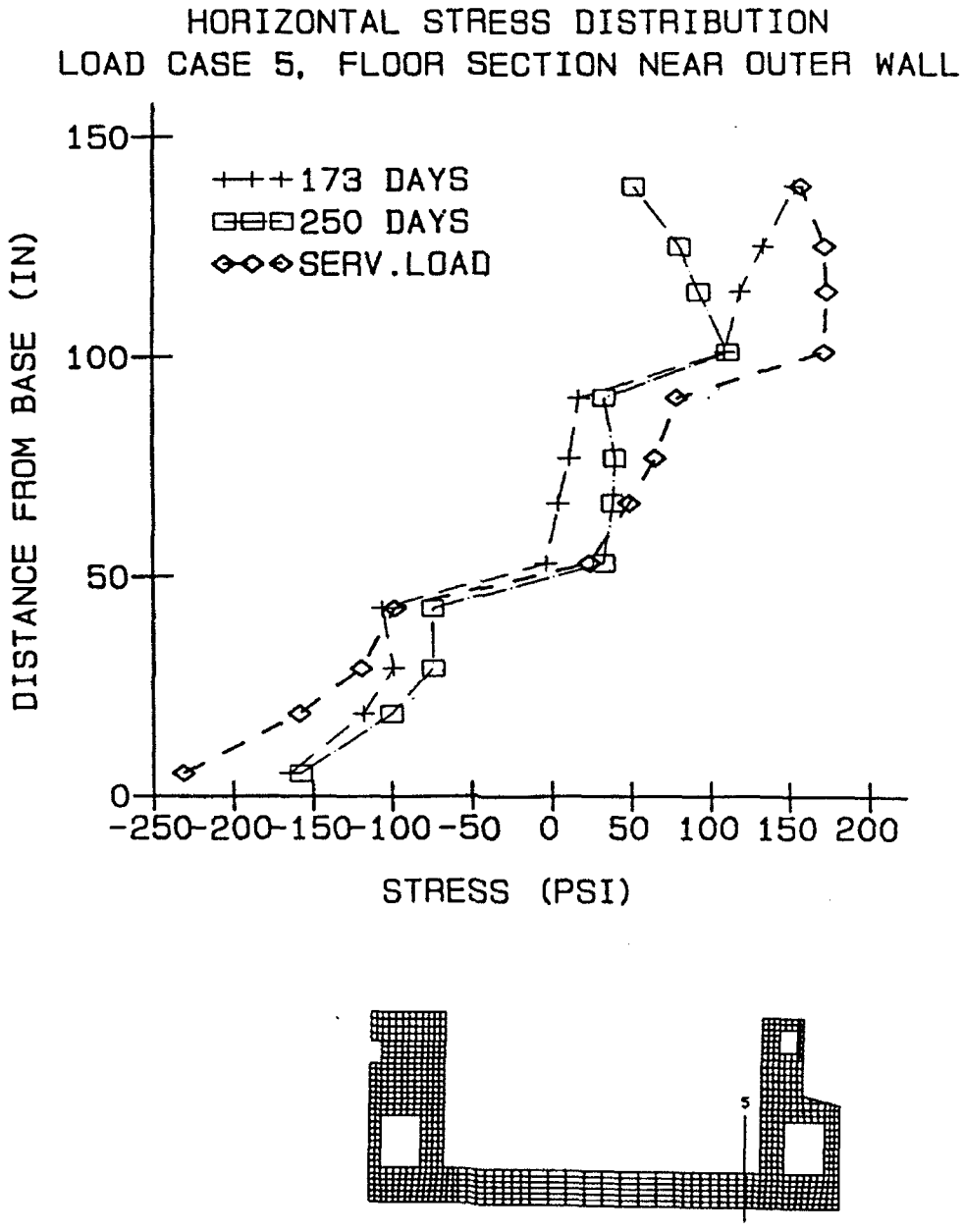

Figure 132. Horizontal stress distribution at section 5

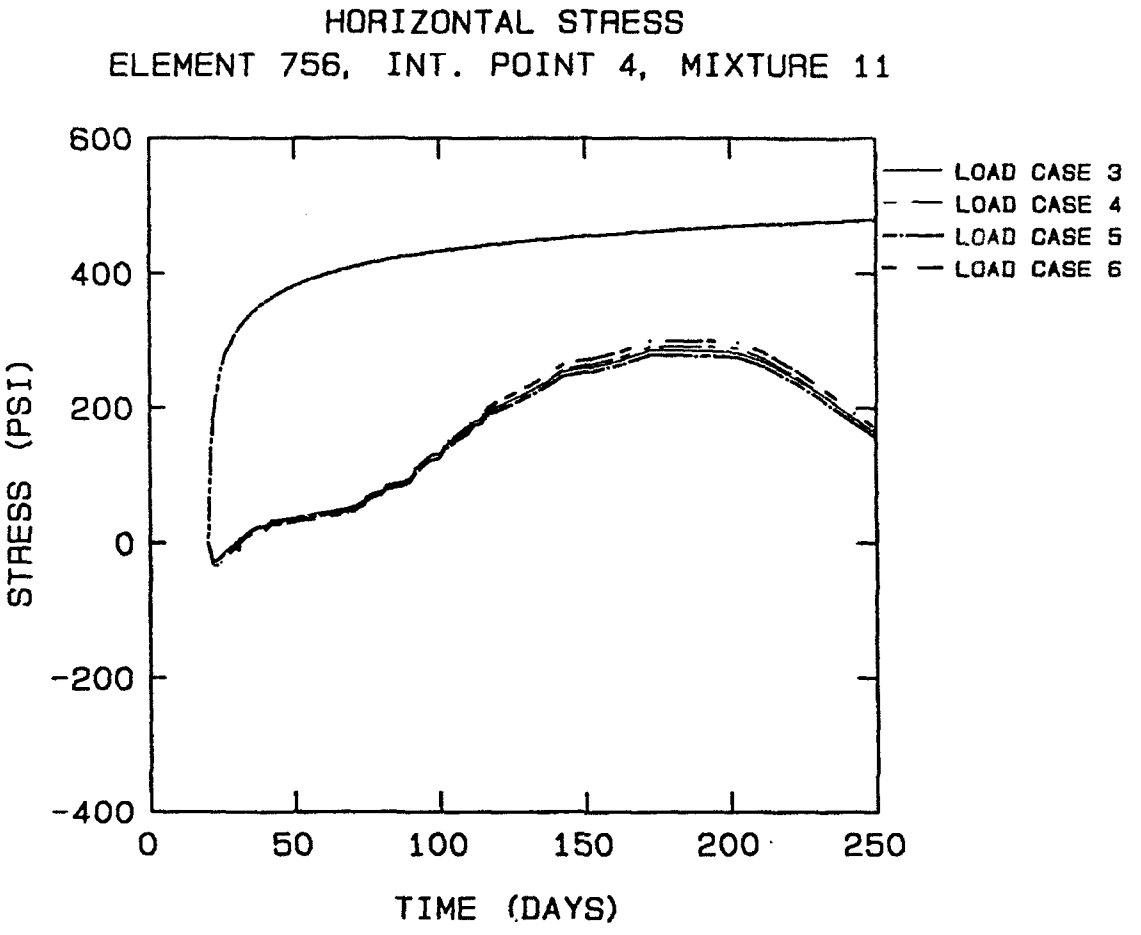

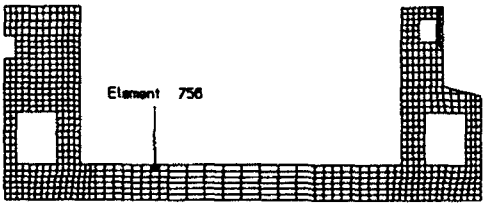

Figure 133. Horizontal stresses, element 756, point 4

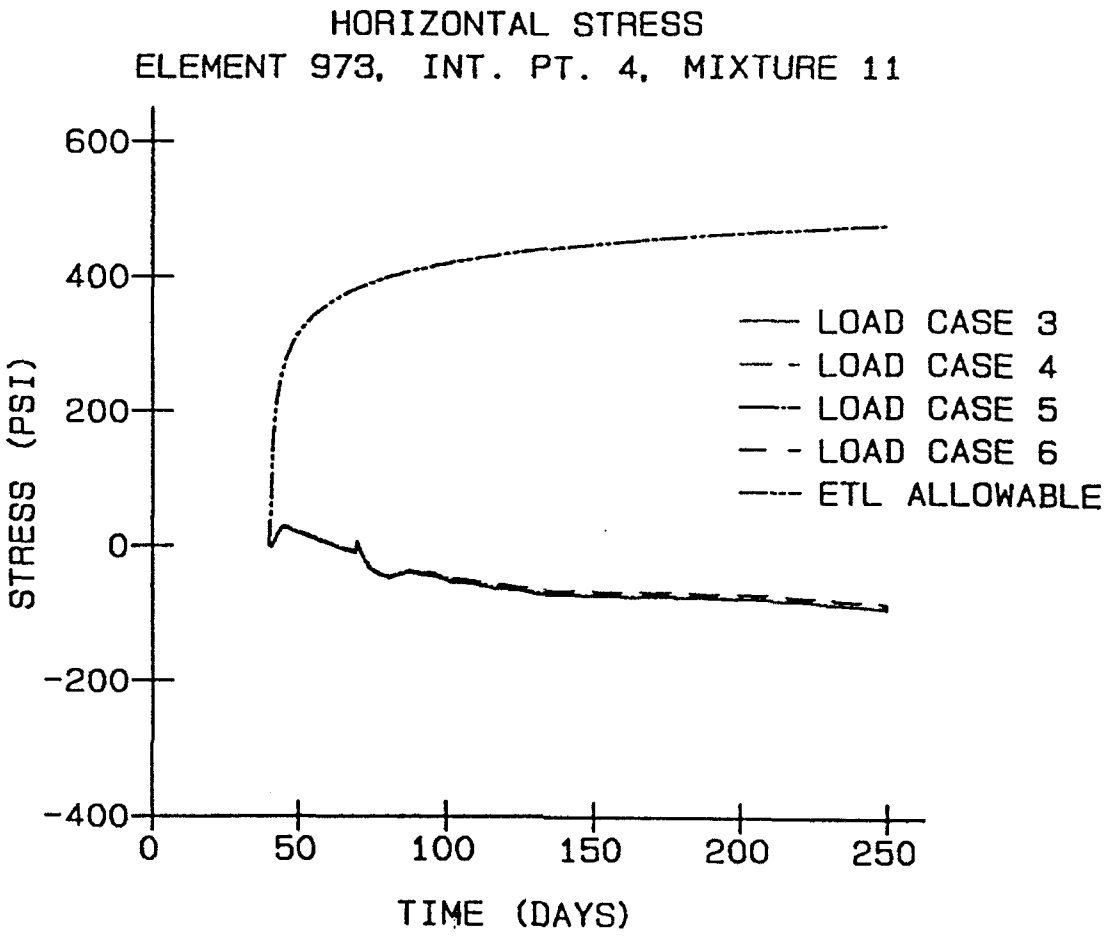

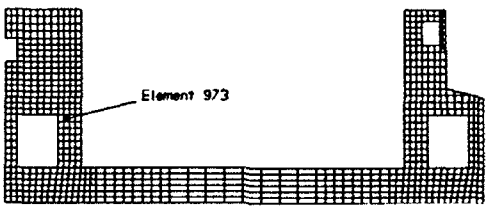

Figure 134. Horizontal stresses, element 973, point 4

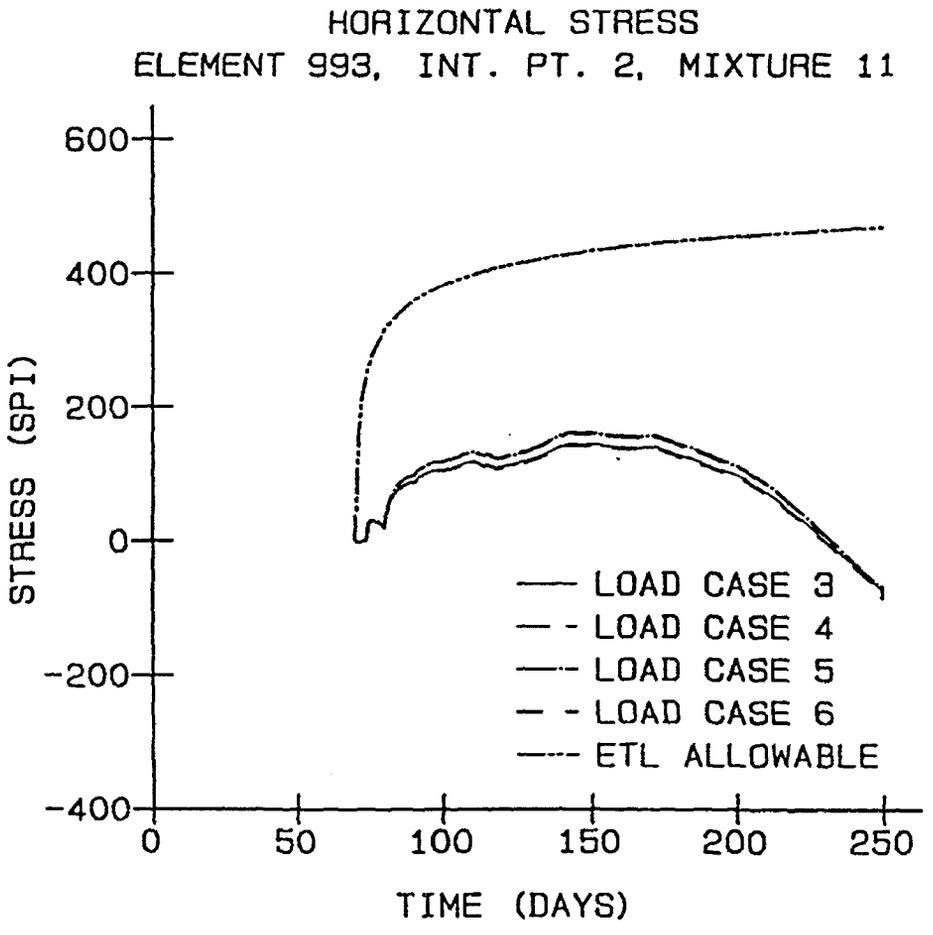

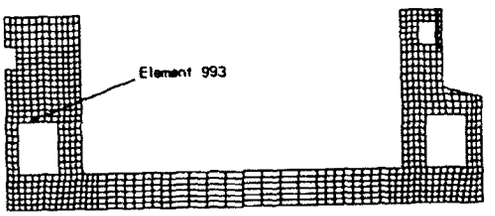

Figure 135. Horizontal stresses, element 993, point 2

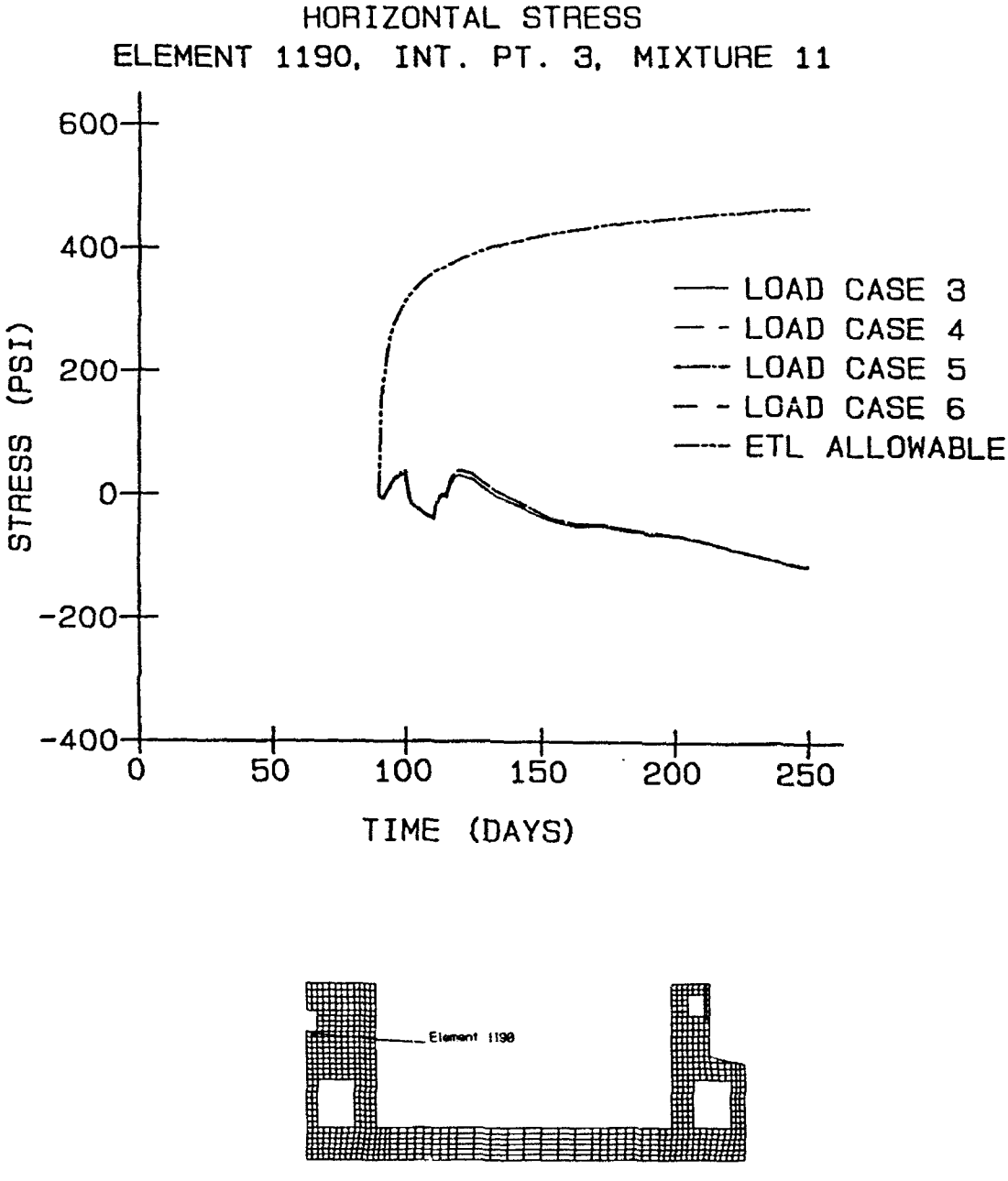

Figure 136. Horizontal stresses, element 1190, point 3

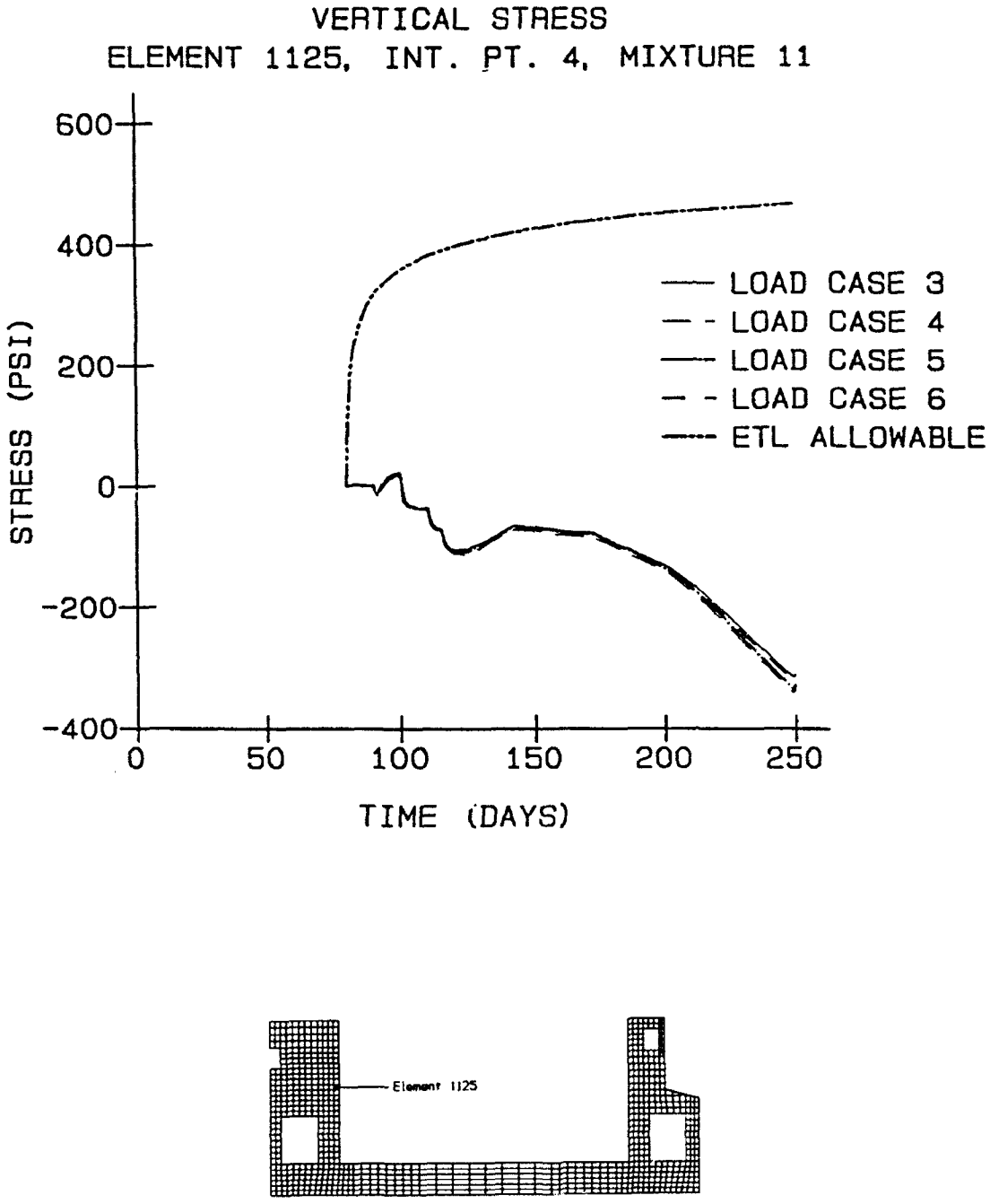

Figure 137. Vertical stresses, element 1125, point 4

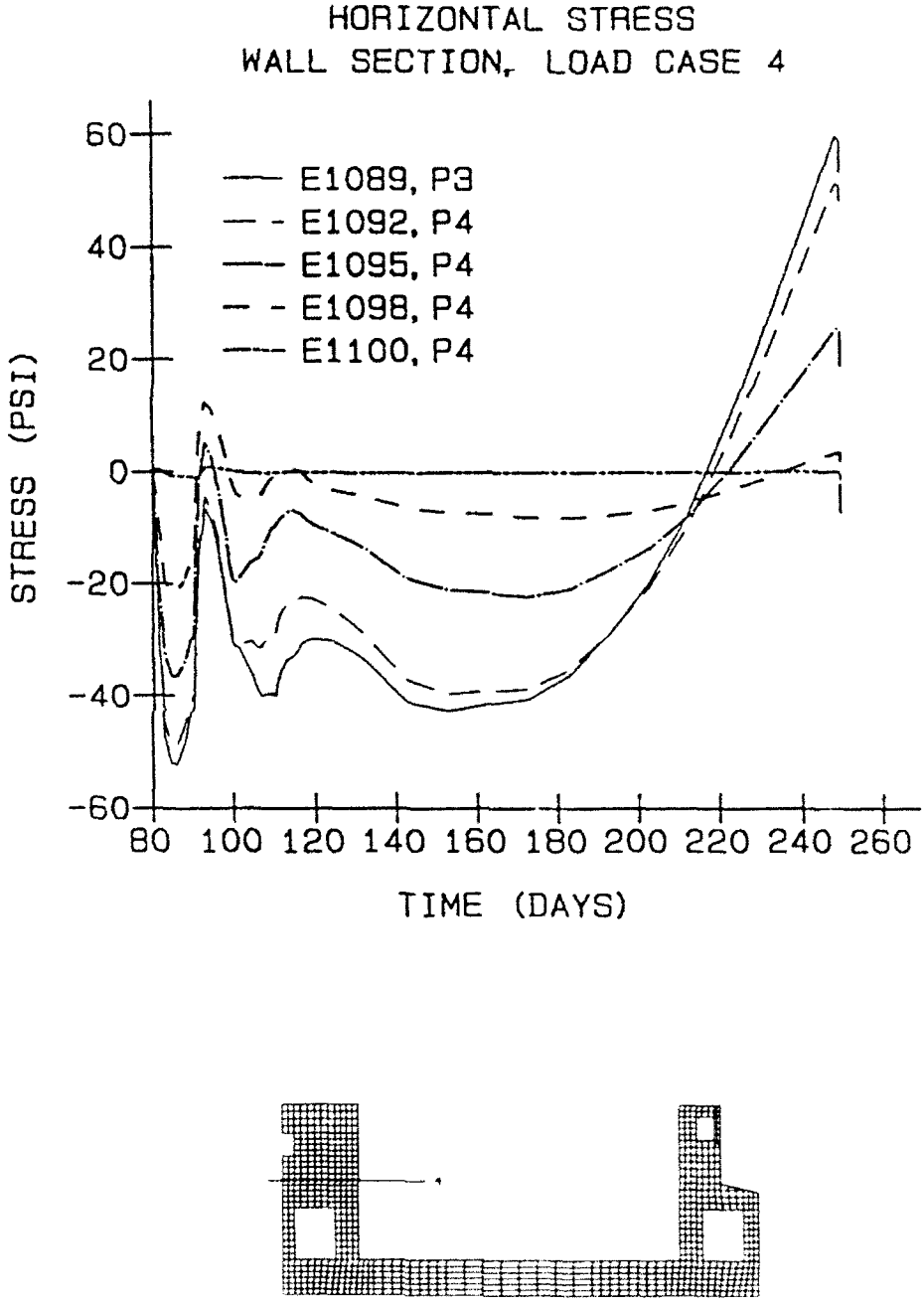

Figure 138. Horizontal stresses at wall section, load case 4

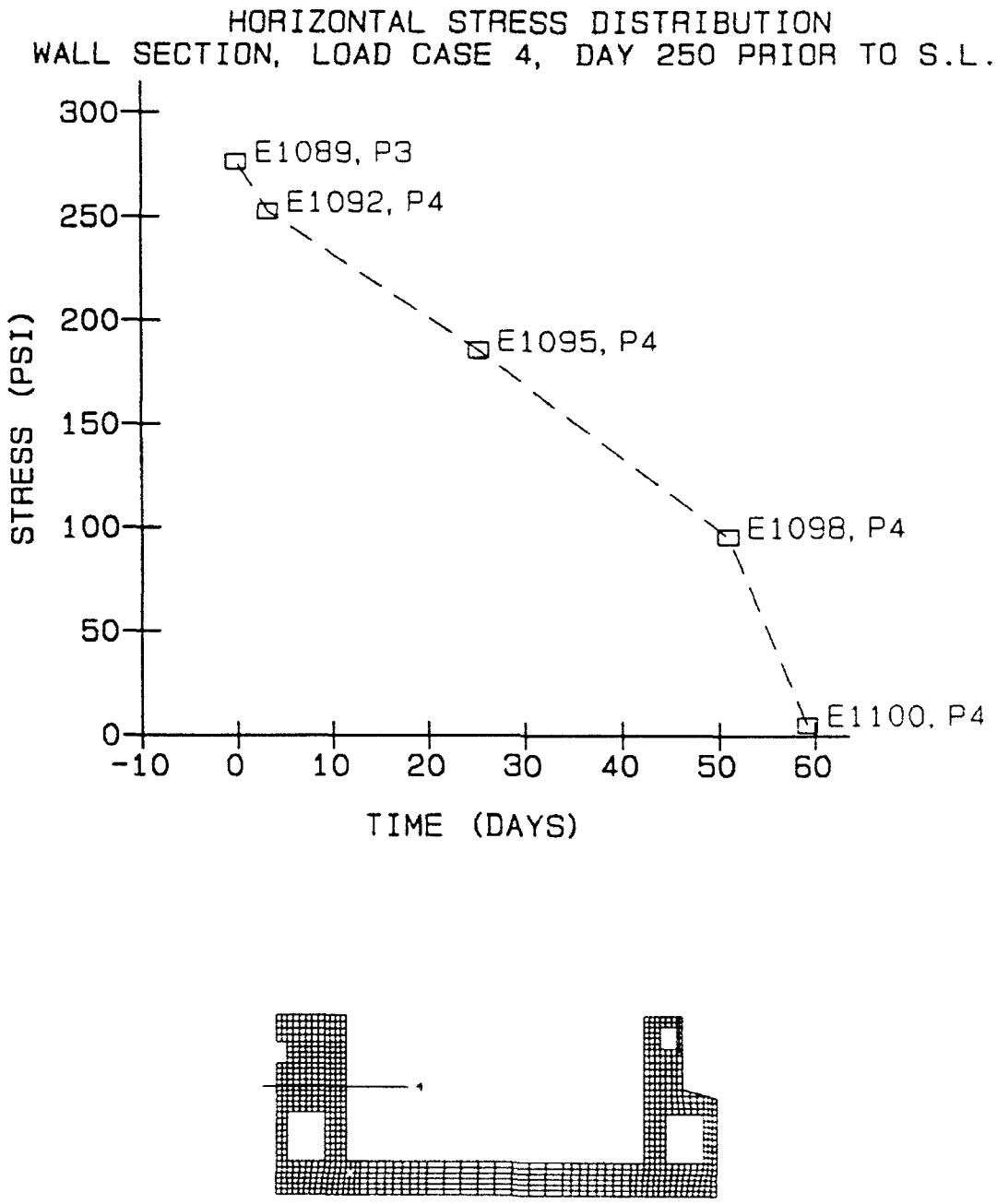

Figure 139. Horizontal stress distribution at wall section, load case 4

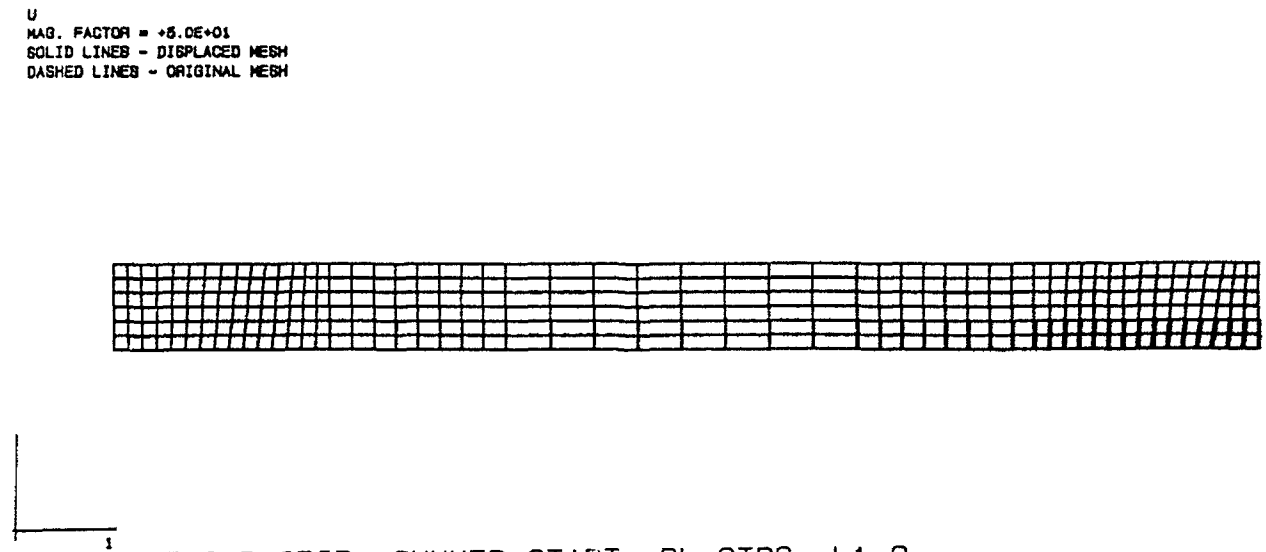

Figure 140. Displaced shape at 30 days, load case 5

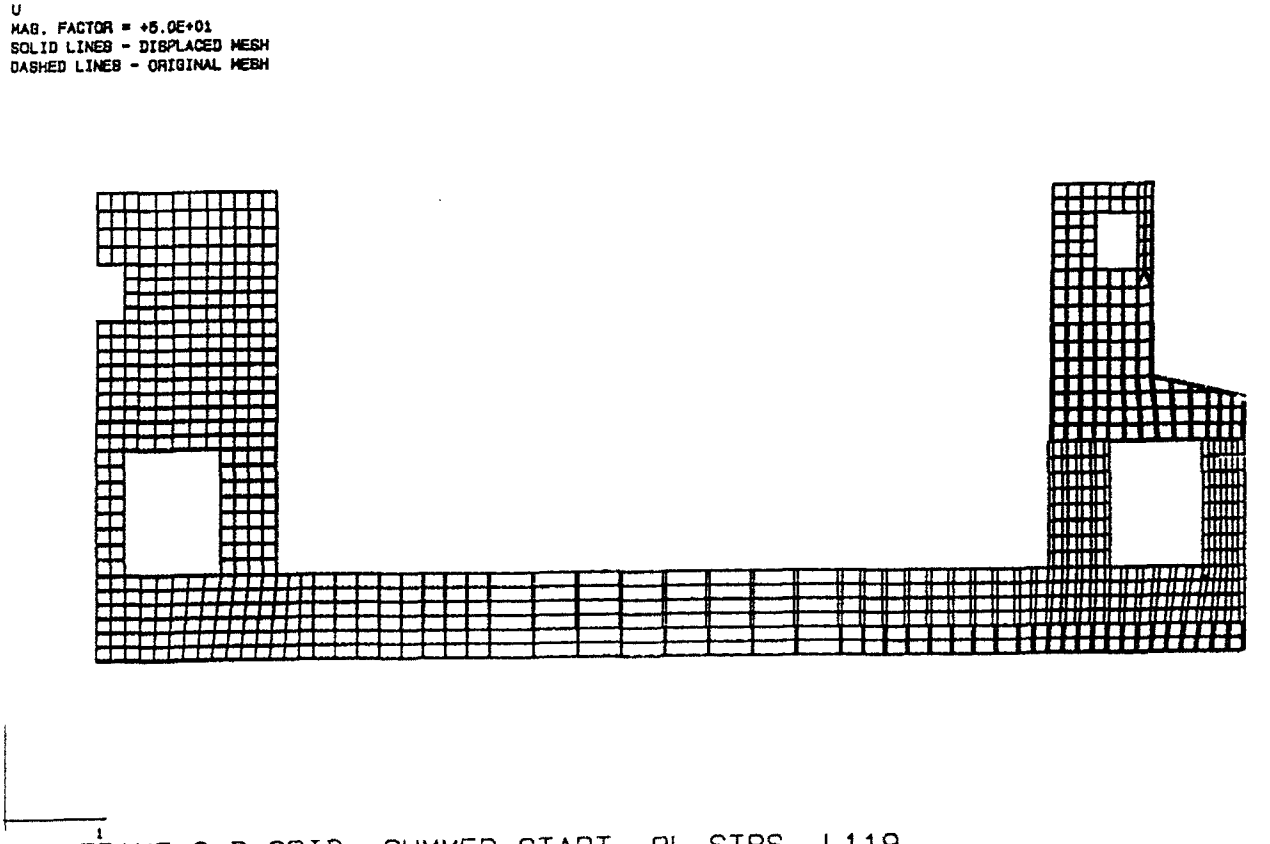

Figure 141. Displaced shape at 120 days, load case 5

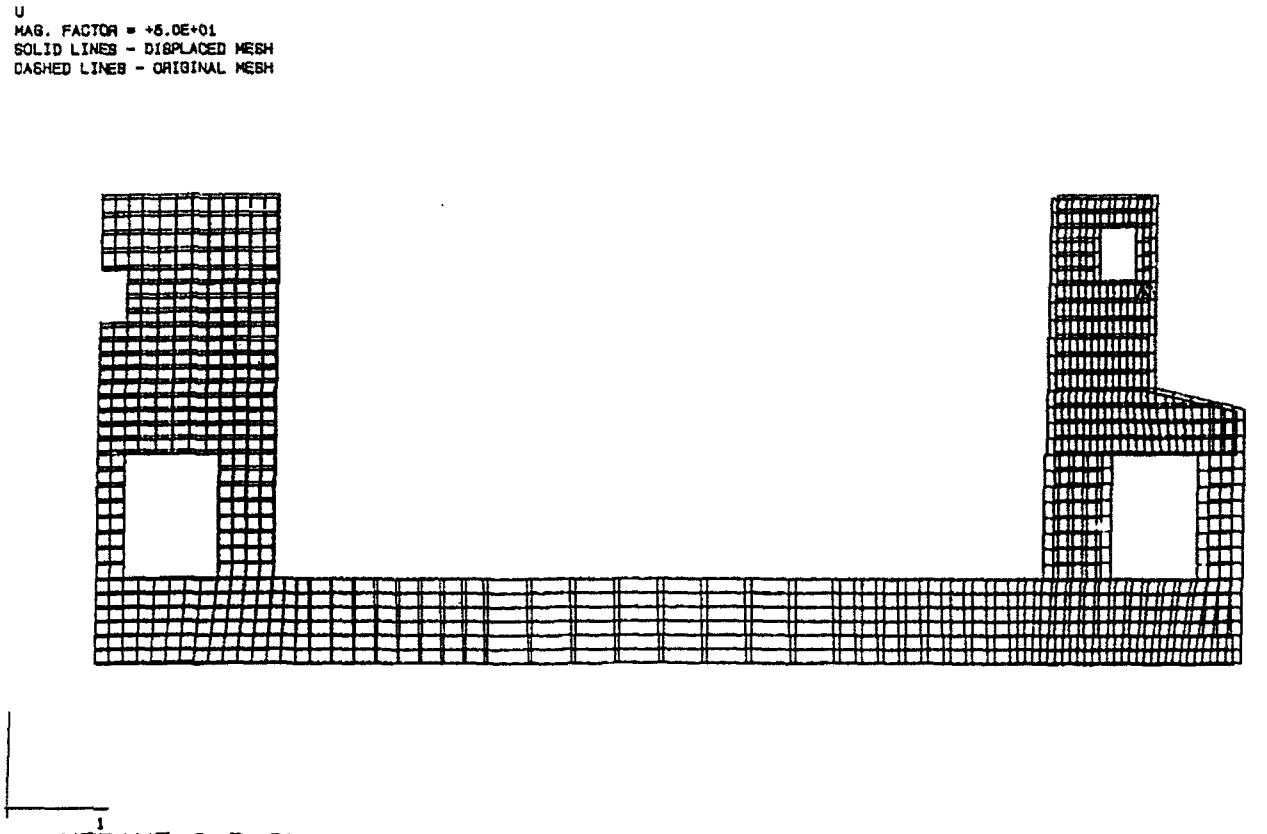

Figure 142. Displaced shape at 250 days, load case 5

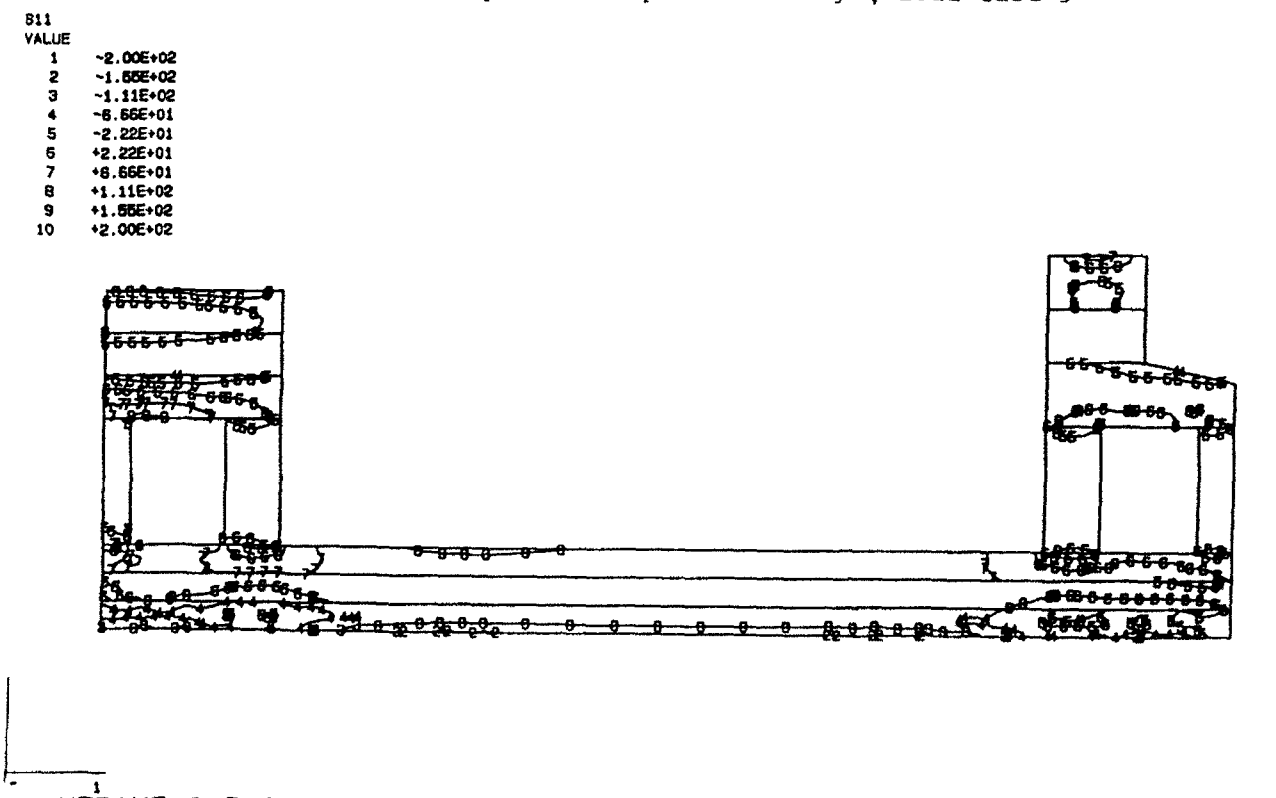

Figure 143. Horizontal stress contours, day 95, load case 5

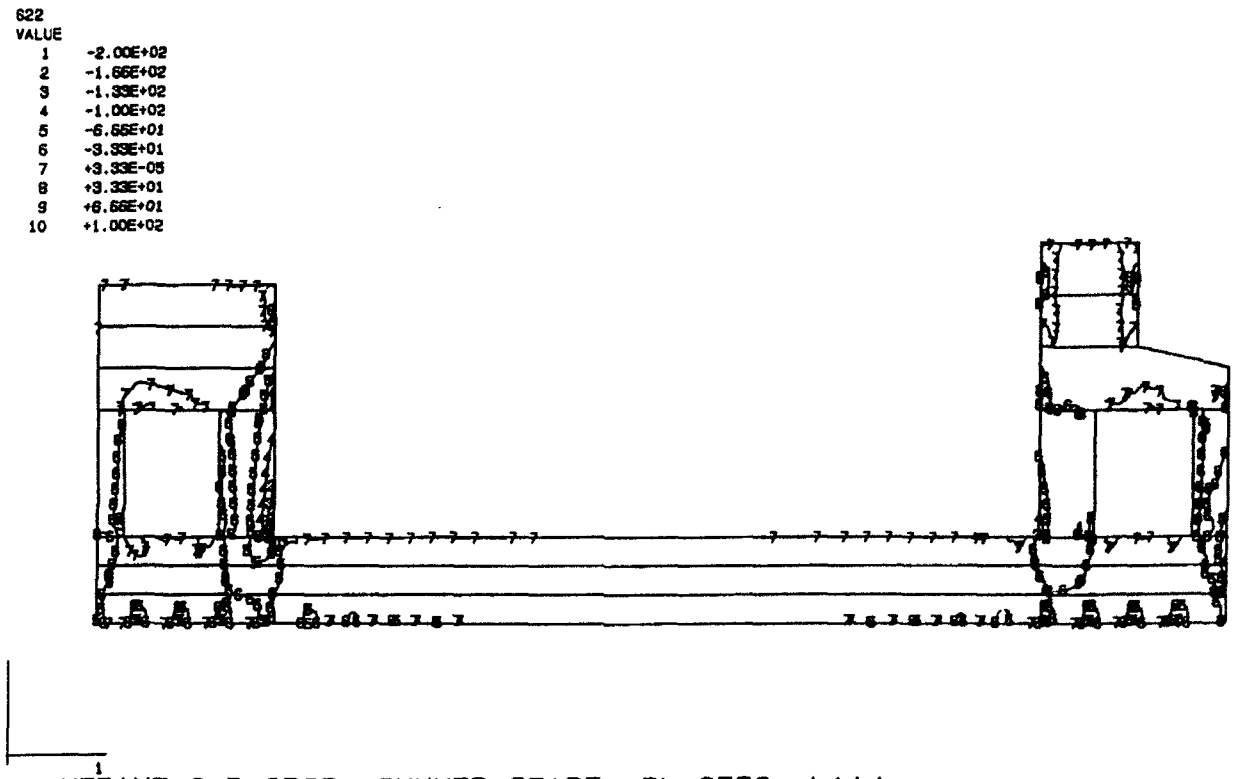

Figure 144. Vertical stress contours, day 95, load case 5

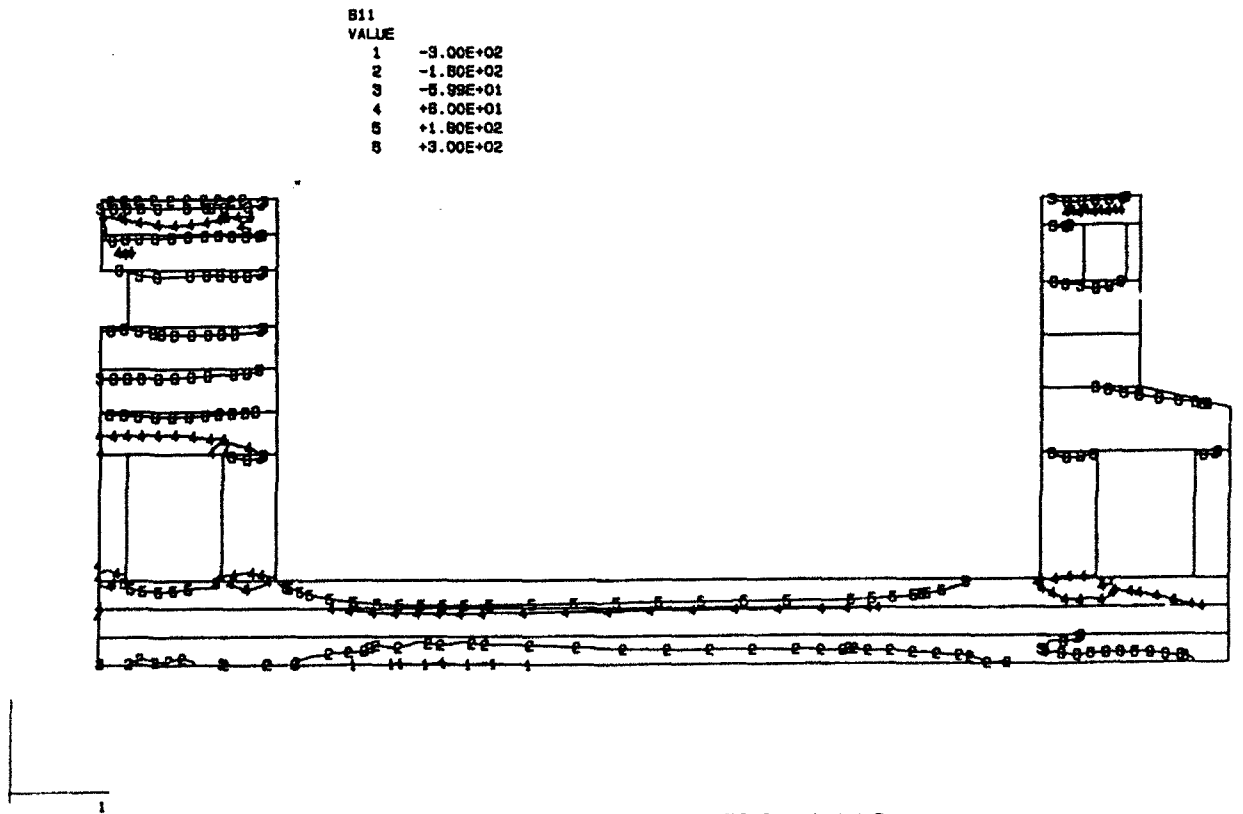

Figure 145. Horizontal stress contours, day 183, load case 5

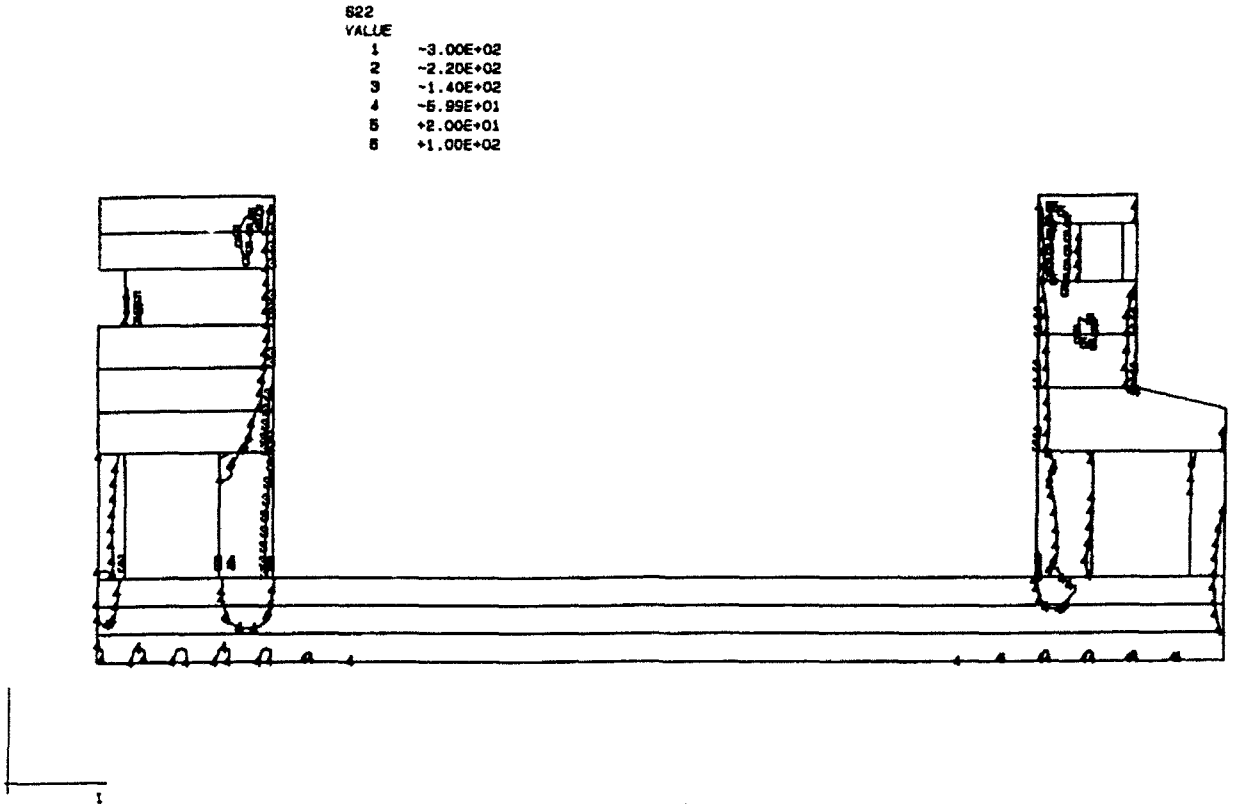

Figure 146. Vertical stress contours, day 183, load case 5

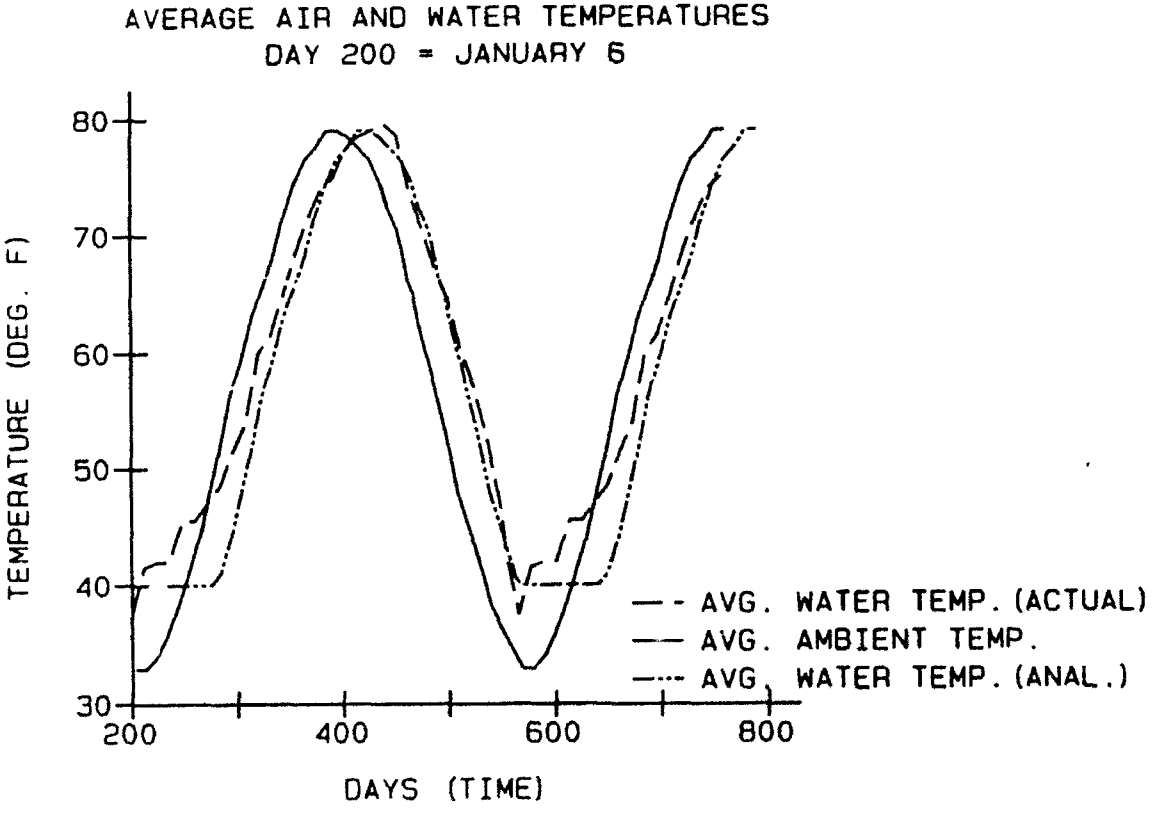

Figure 147. Air and water temperatures for 500-day analysis

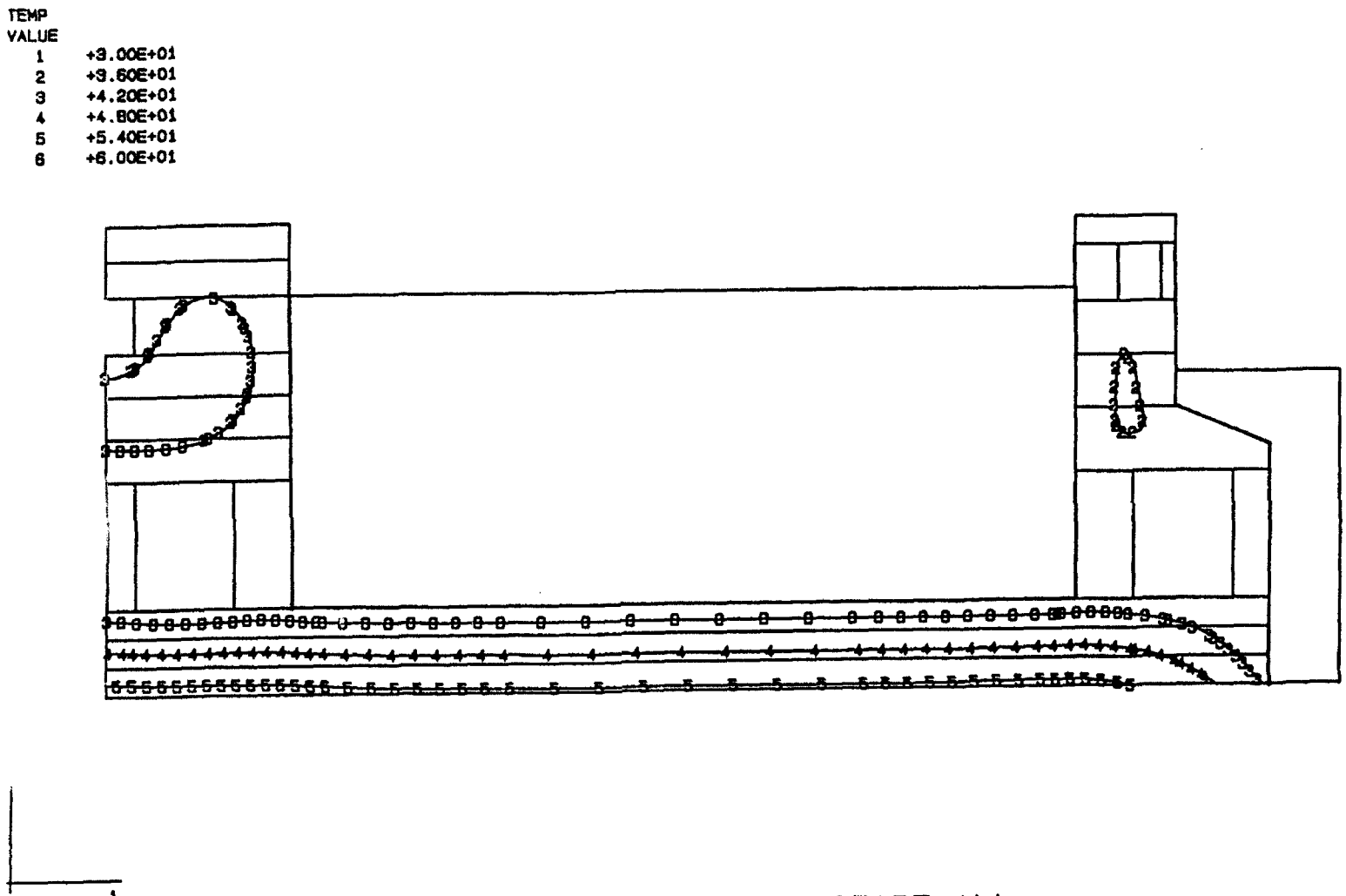

Figure 148. Temperature contours, day 250

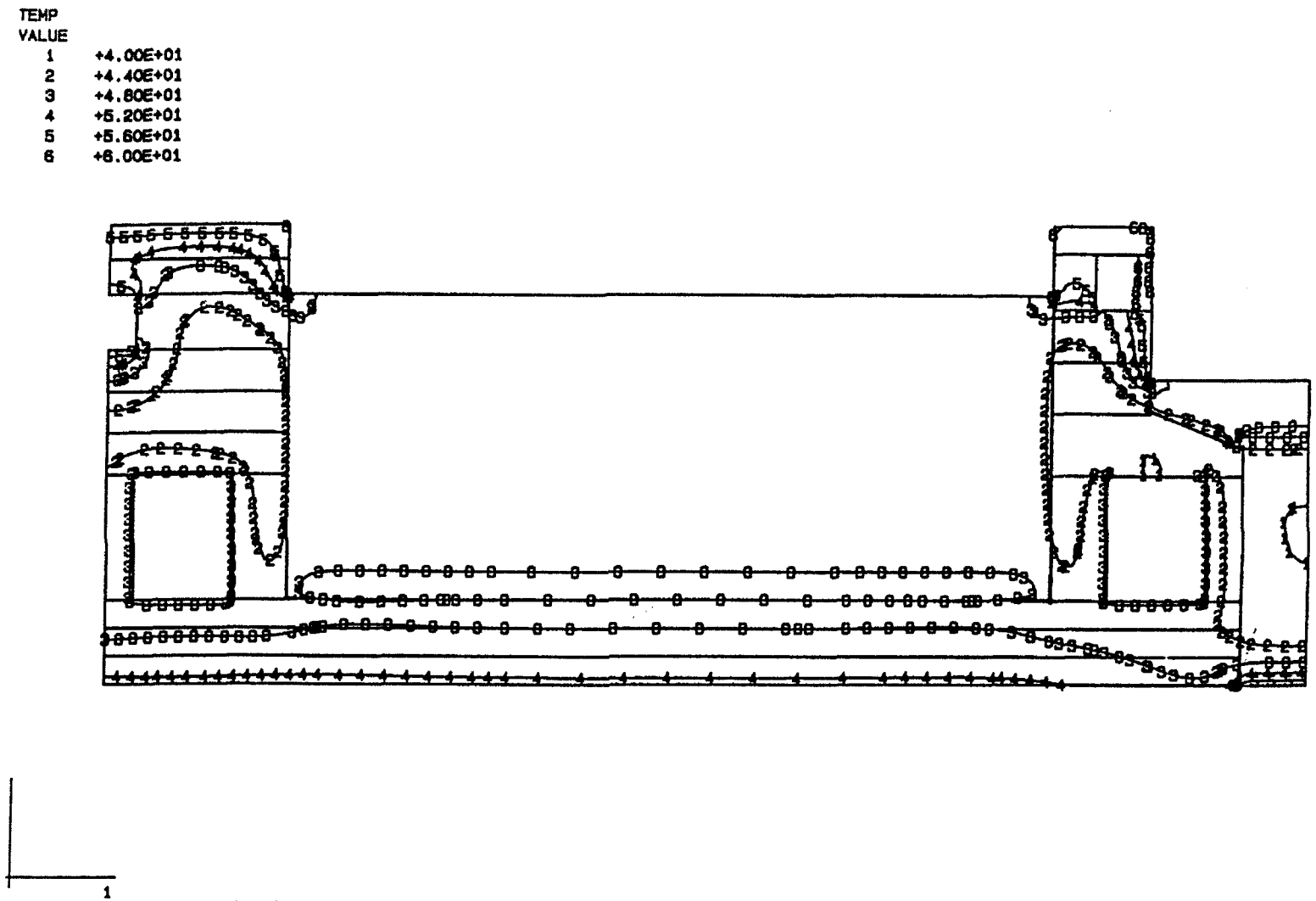

Figure 149. Temperature contours, day 306

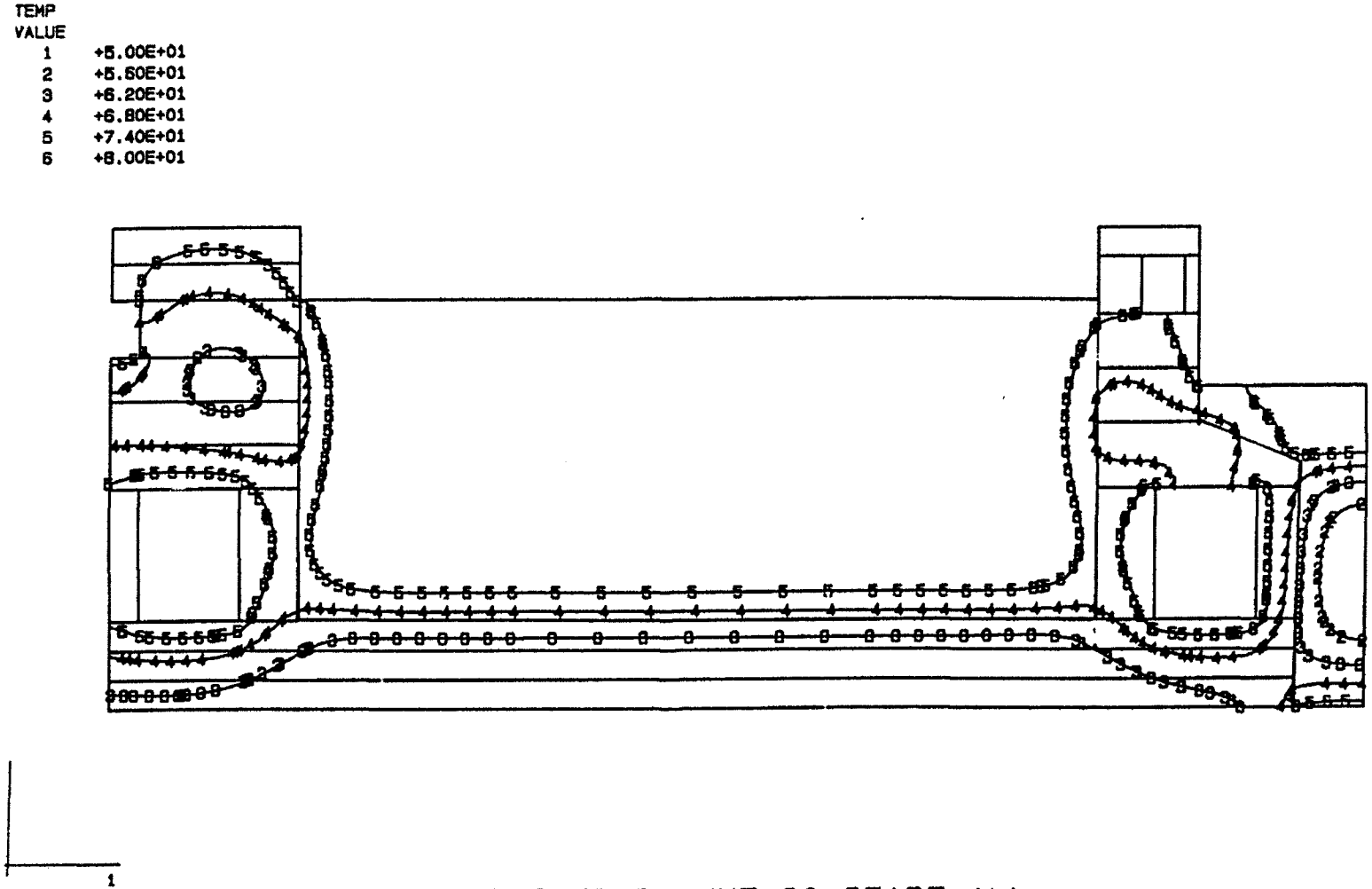

Figure 150. Temperature contours, day 424

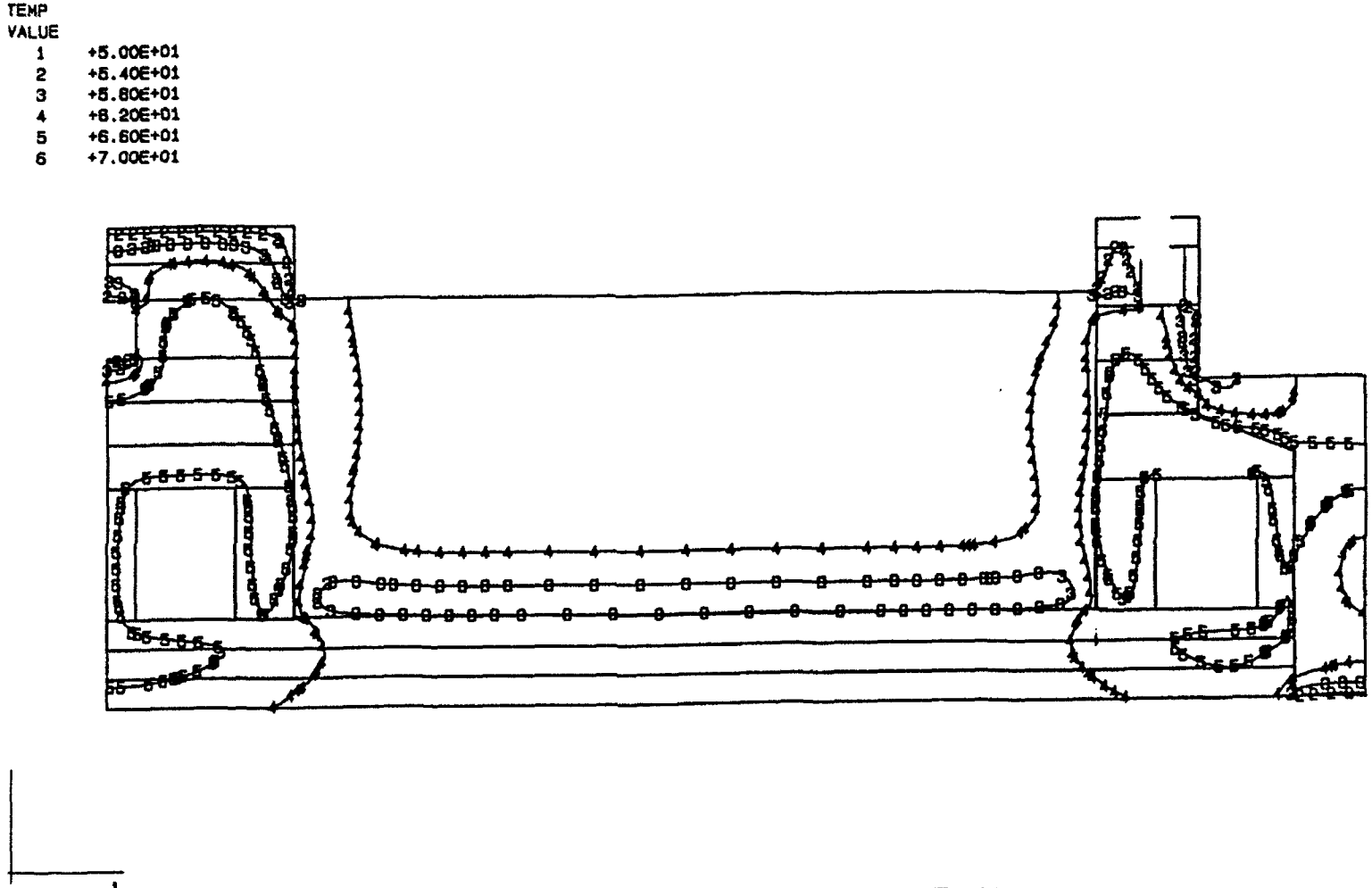

Figure 151. Temperature contours, day 501

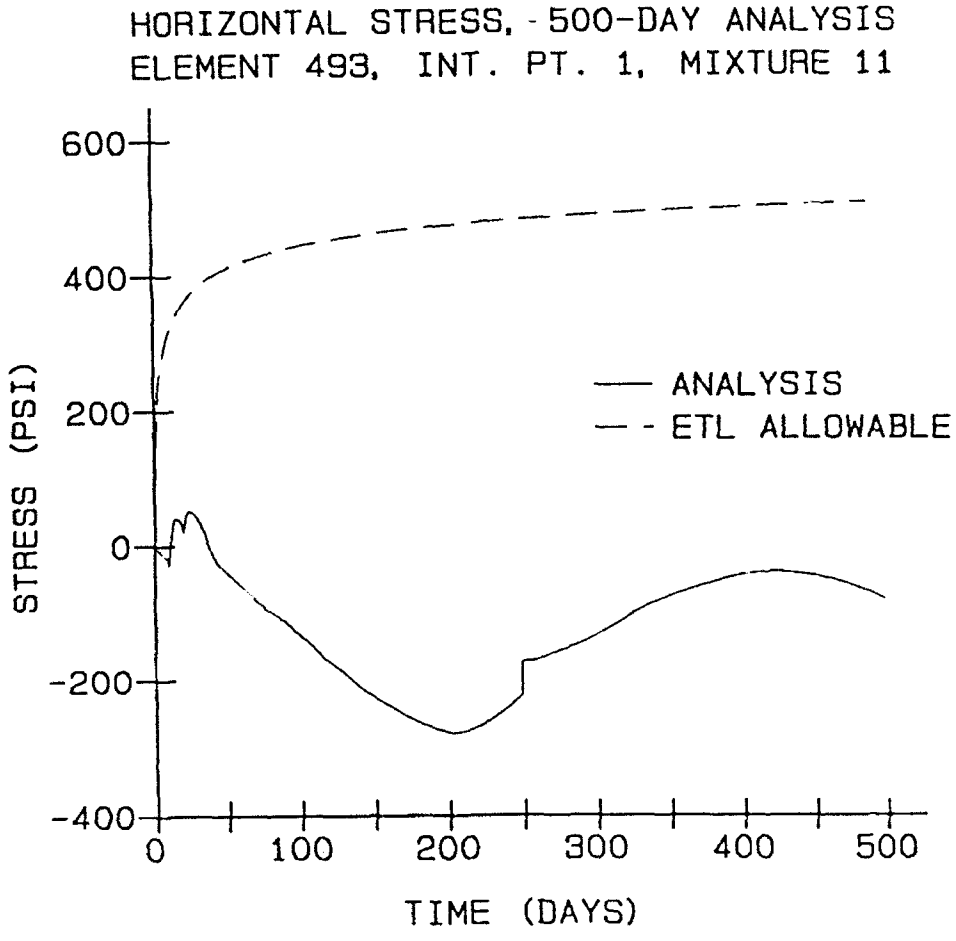

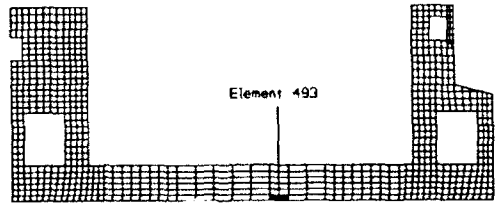

Figure 152. Horizontal stresses in element 493, point 1, 500-day analysis

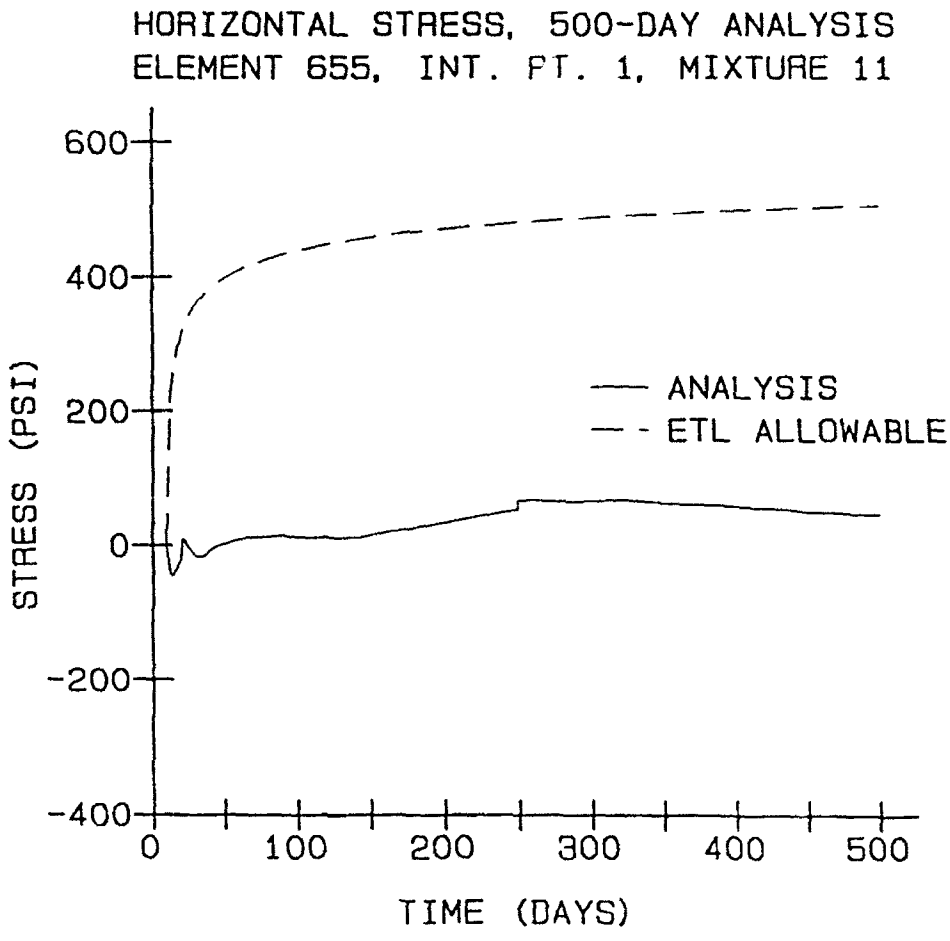

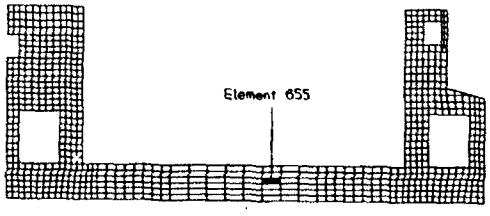

Figure 153. Horizontal stresses in element 655, point 1, 500-day analysis

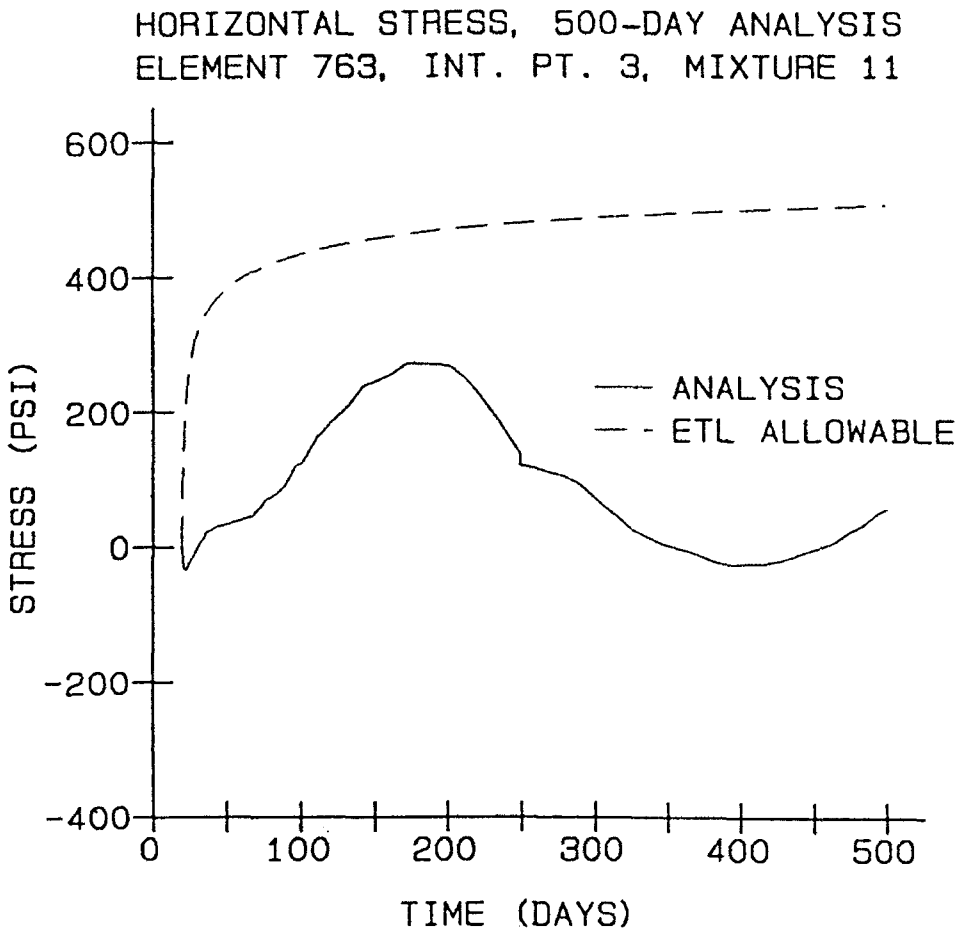

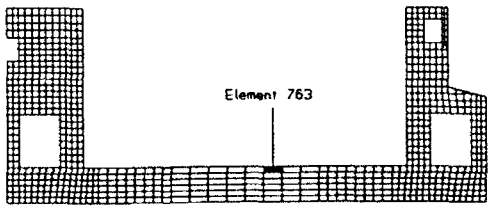

Figure 154. Horizontal stresses in element 763, point 3, 500-day analysis

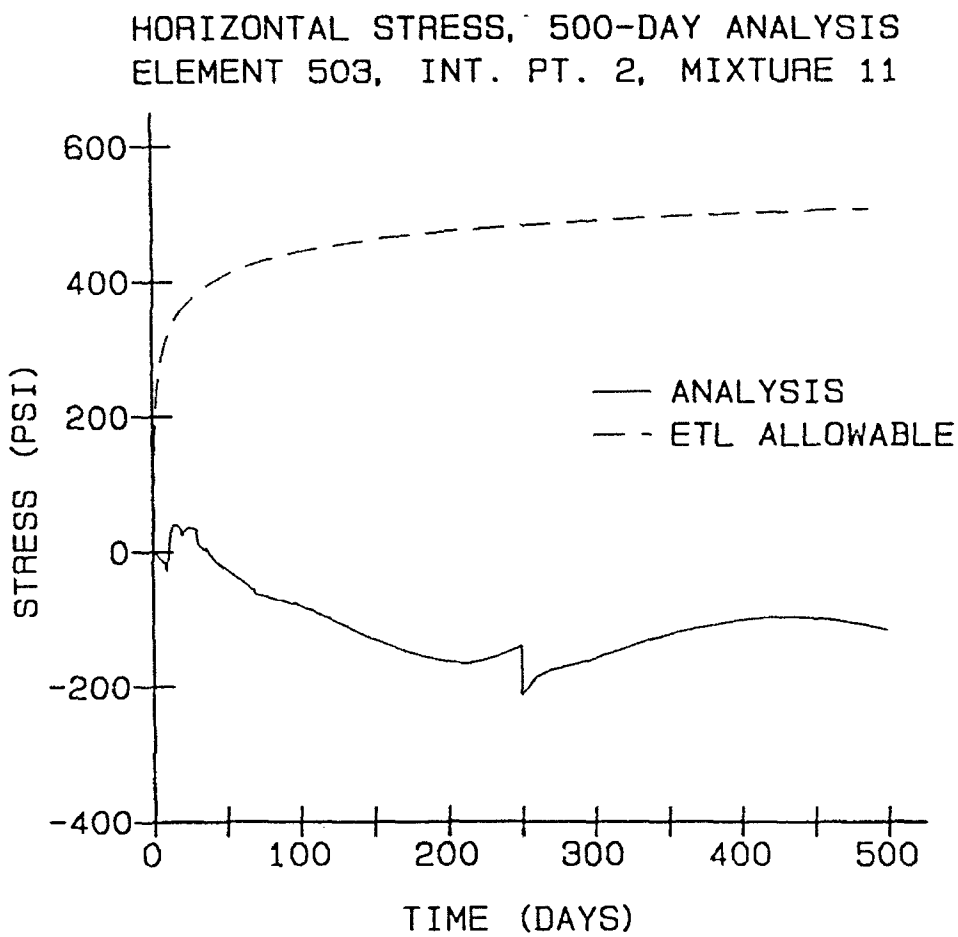

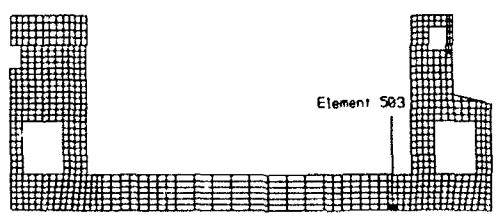

Figure 155. Horizontal stresses in element 503, point 2, 500-day analysis

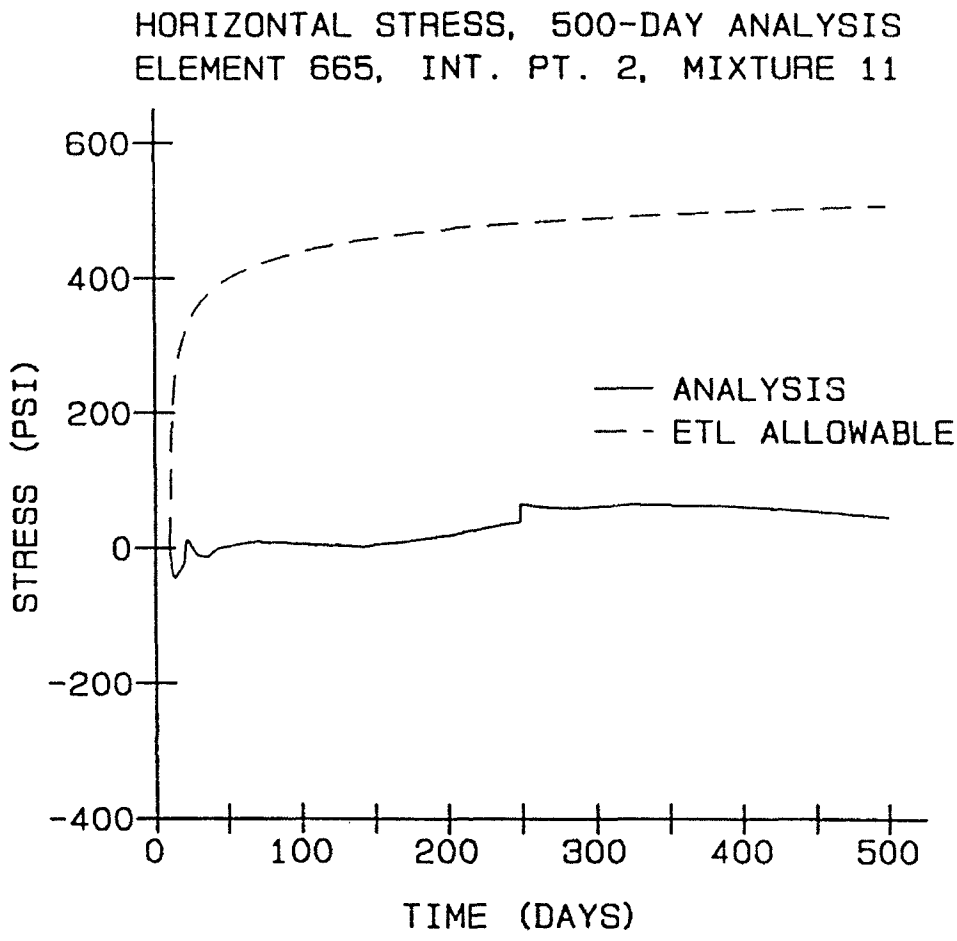

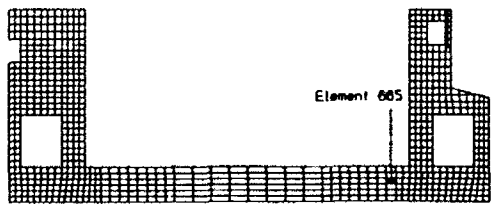

Figure 156. Horizontal stresses in element 665, point 2, 500-day analysis

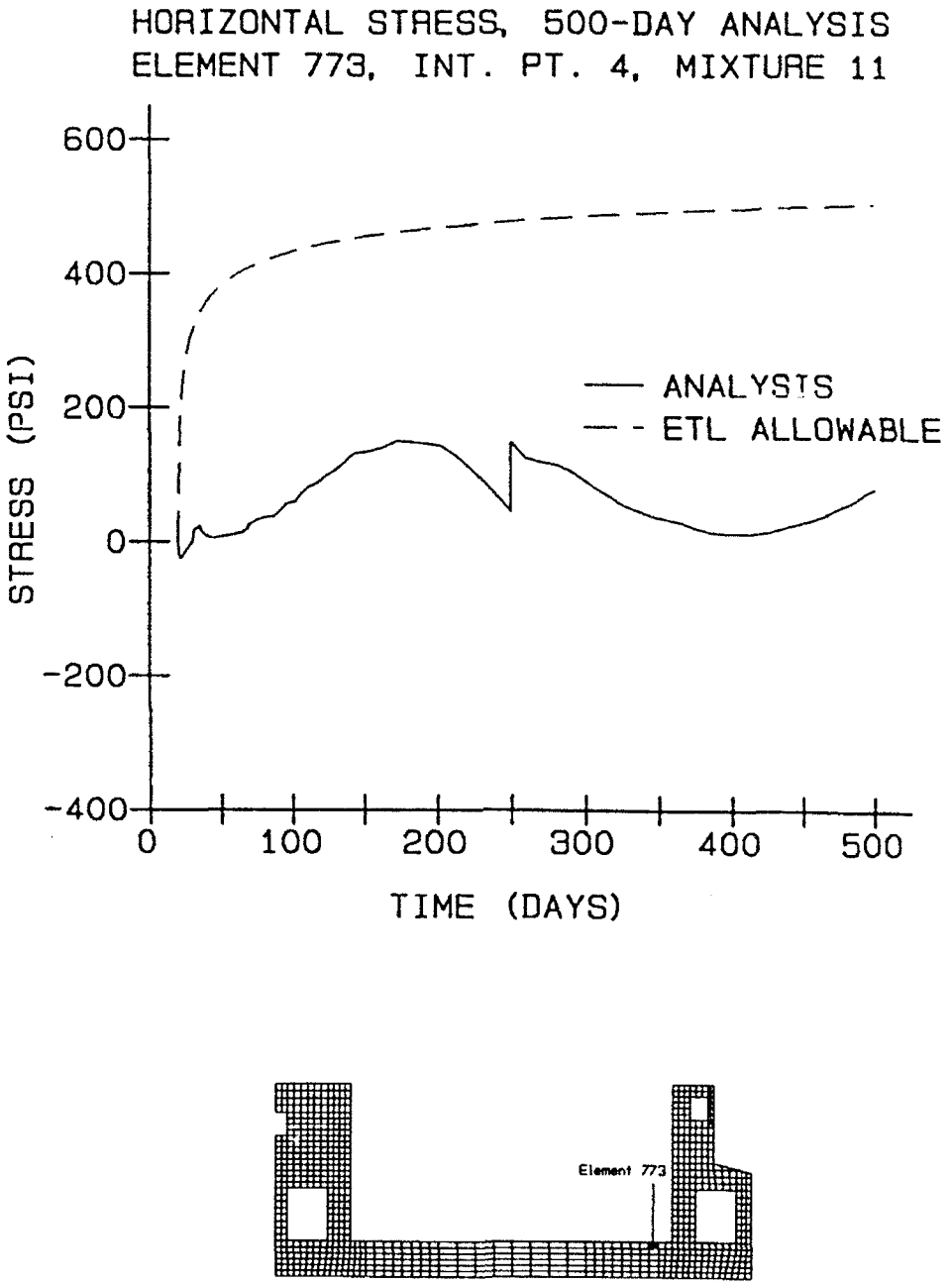

Figure 157. Horizontal stresses in element 773, point 4, 500-day analysis

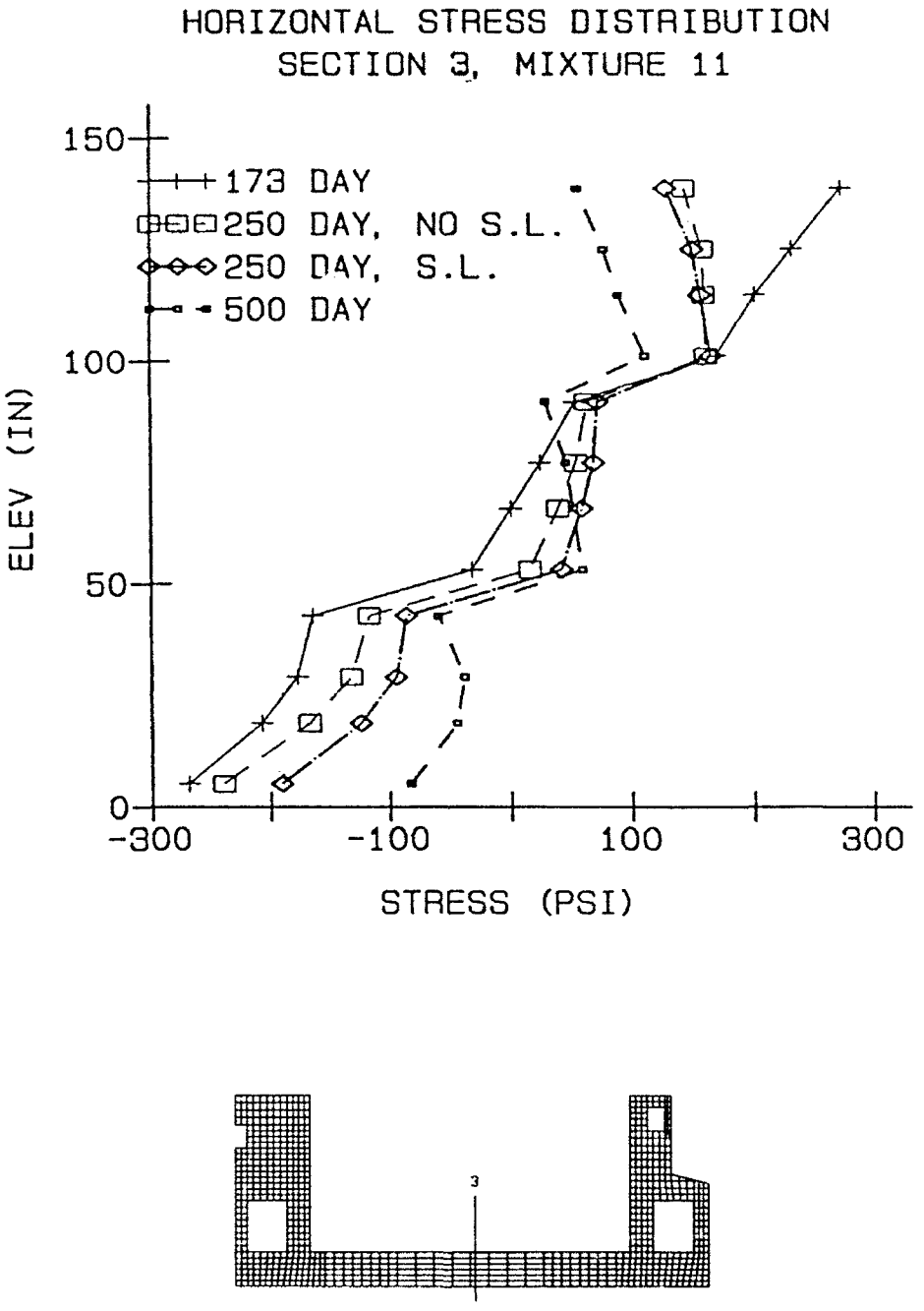

Figure 158. Horizontal stress distributions at section 3

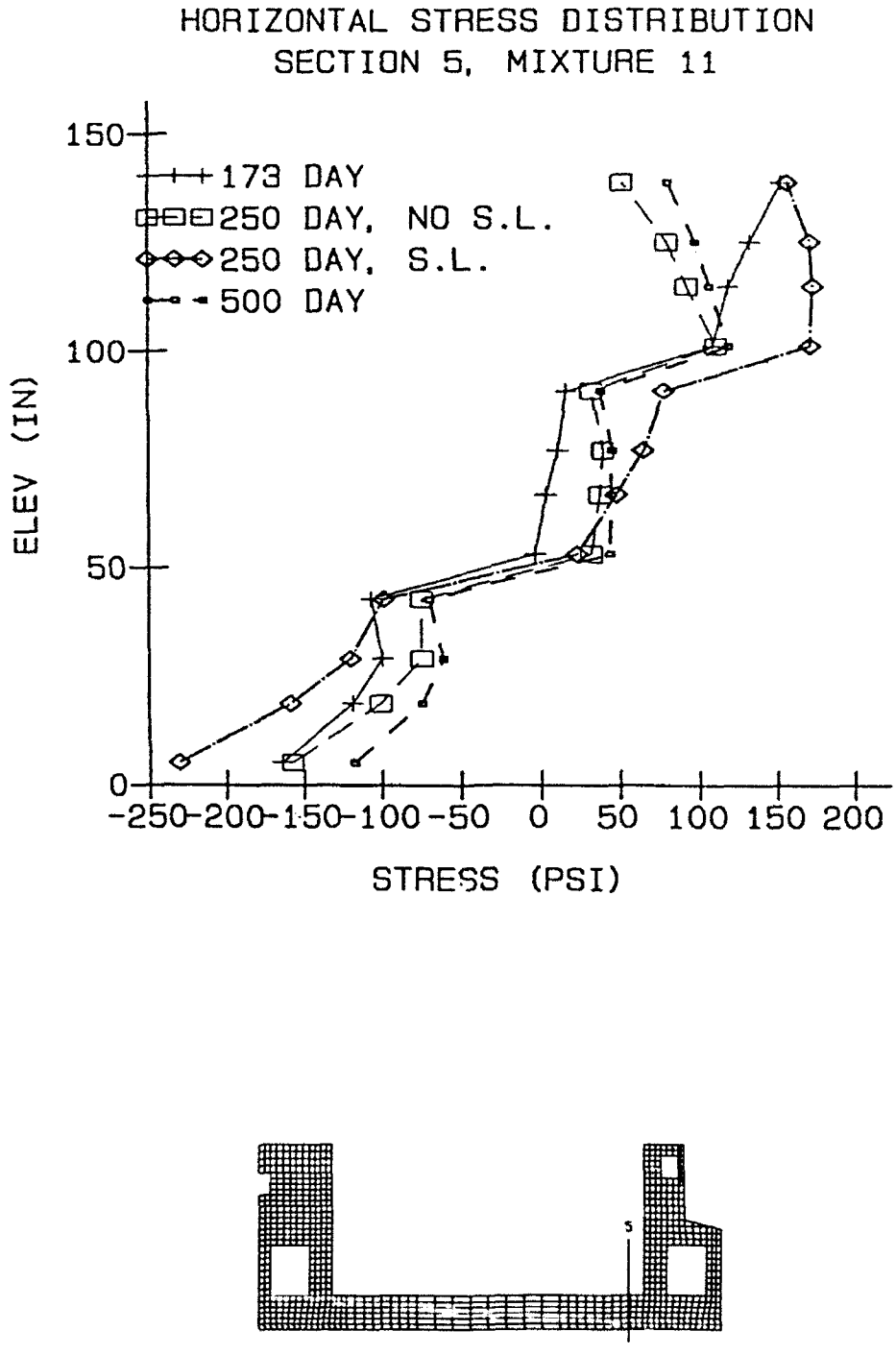

Figure 159. Horizontal stress distributions at section 5

Table 15

Horizontal Stresses at Elements 763, Point 3 for Mixture 11

Time	Allowable Stress	Load Case 3		Load Case 4		Load Case 5		Load Case 6	
		Stress	% Of Allowable	Stress	% Of Allowable	Stress	% Of Allowable	Stress	% Of Allowable
20.8	101.0	-16.2	-----	-18.7	-----	-16.2	-----	-16.7	-----
30.0	313.4	3.4	1.1	-5.7	-----	-3.4	-----	1.4	0.5
36.5	345.9	28.2	8.2	20.0	5.8	22.9	6.6	25.8	7.5
40.0	357.8	30.7	8.6	22.7	6.3	25.8	7.2	28.1	7.8
65.8	405.0	47.7	11.8	39.8	9.8	44.7	11.0	43.6	10.8
68.0	407.6	50.5	12.4	42.6	10.5	47.6	11.7	46.2	11.3
70.0	409.7	55.3	13.5	47.7	11.6	52.8	12.9	51.0	12.4
80.0	419.1	75.0	17.9	68.6	16.4	74.2	17.7	70.3	16.8
90.0	426.9	92.8	21.7	87.5	20.5	93.4	21.9	87.7	20.5
100.0	433.4	121.2	28.0	117.8	27.2	124.2	28.7	115.7	26.7
110.0	439.0	153.9	35.1	152.8	34.8	159.6	36.3	148.1	33.7
119.5	443.7	176.5	39.8	177.5	40.0	184.6	41.6	170.4	38.4
129.5	448.1	194.8	43.5	197.4	44.0	204.5	45.6	188.6	42.1
142.5	453.1	227.7	50.2	232.7	51.4	239.9	53.0	221.5	48.9
152.5	456.6	234.7	51.4	240.8	52.7	248.1	54.3	228.4	50.0
162.5	459.7	243.4	53.0	250.3	54.4	257.7	56.0	237.1	51.6
172.5	462.6	258.9	56.0	266.7	57.7	274.2	59.3	252.5	54.6
182.5	465.3	258.0	55.4	266.1	57.2	273.7	58.8	251.5	54.0
192.5	467.8	256.9	54.9	265.1	56.7	272.6	58.3	250.3	53.5
202.5	470.1	253.8	54.0	261.9	55.7	269.5	57.3	247.3	52.6
212.5	472.3	237.3	50.2	244.5	51.8	252.1	53.4	230.7	48.9
222.5	474.3	213.1	44.9	218.7	46.1	226.4	47.7	206.5	43.5
232.5	476.2	184.4	38.7	188.1	39.5	195.7	41.1	177.8	37.3
242.5	478.0	153.6	32.1	155.1	32.4	162.7	34.0	147.1	30.8
249.5	479.2	136.6	28.5	136.4	28.5	144.1	30.1	130.0	27.1
249.5	479.2	121.9	25.4	121.8	25.4	129.4	27.0	115.3	24.1

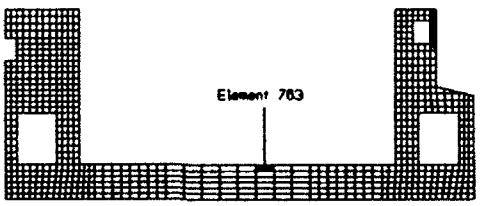

compressive or much lower than the allowable tensile stress, and differences in stresses between the four analyses were negligible for these elements. Therefore, only stresses at the top of the floor in element 763 have been included.

142. Maximum tensile stress in element 763, integration point 3 occurred at 173 days after the start of construction. The minimum tensile stress predicted at this time was 252.5 psi in load case 6. The maximum, 274.2 psi, occurred in load case 5. The difference of 21.7 psi was approximately 8 percent of the average of the four analyses. Since the difference in the maximum and minimum material properties is 20 percent of the average, it is obvious that simply factoring the curves will result in differences in late-time tensile stresses that are small when compared with the differences in the factors.

143. A comparison of stress distributions at this section at 173 days for all mixture 11 analyses is presented in Figure 126. Since differences between the analyses are hard to determine at the scale used in this figure, no further comparisons of stress distributions between analyses were shown for mixture 11. Figure 127 is a plot of stress distributions at this section at day 173, day 250 prior to service loading, and day 250 after service loading for load case 5. Stresses at this section decreased with time and service loading.

144. Tensile stresses in the floor at approximately 5 ft from the inner and outer walls were also plotted, since these locations are where the largest stresses occurred in the seismic analysis (Bevins, Garner, and Hall in preparation). Elements 503, 665, and 763 are from the section near the outer wall, which will be called section 5. Stress histories from theses elements are compared with the ETL 1110-2-324 allowable stress in Figures 128 through 130. Tensile stresses in element 750, located approximately 5 ft from the inner wall, are presented in Figure 131.

145. The stresses in these areas show trends similar to those in corresponding elements in section 3. Stress distributions from the load case 5 analysis at section 5 are shown in Figure 132. Distributions are plotted at 173 days and before and after adding service loads at 250 days. Tables 16 and 17 contain tabulated values of stress and percentage of ETL 1110-2-324 allowable tensile stress for elements 750 and 773.

146. The maximum tensile stress in all analyses occurred in element 756 at approximately 173 days. Stress histories for the four analyses at this

point are compared with the ETL 1110-2-324 allowable stress in Figure 133 and Table 18. Maximum stresses in all analyses are less than 65 percent of the ETL 1110-2-324 allowable stress.

147. Horizontal stress histories in the center wall are compared with the ETL 1110-2-324 allowable stress in Figures 134 through 136. Differences between the four analyses are almost negligible at element 973 (Figure 134) and element 1190 (Figure 135), and stresses at both locations are primarily compressive. The largest stress differences occurred in element 993 (Figure 136). Stresses in this element from the four analyses are presented in Table 19. The maximum stress difference occurred at approximately 153 days, with load case 6 producing the minimum predicted stress of 140.6 psi and load case 5 producing the maximum predicted stress of 160 psi. This difference of 19.5 psi was approximately 13 percent of the average value. As in the floor, high tensile stresses occurred at relatively late times, and factoring the creep compliance and shrinkage curves had little effect on predicted results.

148. Vertical stresses at the outer face of the thick center wall section were compressive throughout the analyses. Vertical stresses for the four analyses at element 1125 at the face of the center wall are presented in Figure 137. High vertical tensile stresses can occur in a thin wall, where the direction of heat flow is horizontal. However, the center wall, which was 52 ft thick, was placed in 4- to 6-ft lifts at 10-day intervals. Even though heat flow occurred in two directions, the primary direction of heat flow was vertical, resulting in horizontal stresses that increased toward the center of the wall, where horizontal displacement was restrained by the boundary conditions. For this type of heat flow, vertical tensile stresses at the wall face should be low or nonexistent.

149. This behavior is illustrated in Figure 138, a plot of horizontal stresses throughout a wall section for load case 4. The highest stresses occur near the center of the wall in element 1089. Horizontal stresses decrease as the outer face of the wall is approached at element 1100. The horizontal stress distribution at 250 days is shown in Figure 139.

150. Plots of the displaced structure at 30, 119.5, and 248.5 days from the load case 5 analysis are presented in Figures 140 through 142. All plots use a magnification factor of 50 for displacements. These plots show the contraction with time of the structure as cooling occurs. As is expected, vertical displacements are small when compared with horizontal displacements.

Table 16

Horizontal Stresses at Element 750, Point 3

for Mixture 11

Time	Allowable Stress	Load Case 3		Load Case 4		Load Case 5		Load Case 6	
		Stress	% Of Allowable	Stress	% Of Allowable	Stress	% Of Allowable	Stress	% Of Allowable
20.8	101.0	-16.0	----	-18.5	----	-17.9	----	-16.5	----
24.5	256.9	-18.5	----	-27.7	----	-25.9	----	-20.0	----
30.0	313.4	3.5	1.1	-5.3	----	-2.9	----	1.5	0.5
35.0	339.9	20.3	6.0	12.0	3.5	14.8	4.4	17.9	5.3
40.0	357.8	29.1	8.1	21.0	5.9	24.3	6.8	26.4	7.4
40.8	360.0	25.6	7.1	17.3	4.8	20.6	5.7	22.8	6.3
45.0	371.1	19.8	5.3	10.6	2.8	14.3	3.9	16.6	4.5
65.8	405.0	40.8	10.1	30.7	7.6	36.0	8.9	36.3	9.0
68.0	407.6	44.0	10.8	33.9	8.3	39.3	9.7	39.3	9.6
70.0	409.7	46.7	11.4	36.6	8.9	42.2	10.3	41.8	10.2
70.8	410.5	42.9	10.5	32.4	7.9	38.2	9.3	37.9	9.2
80.0	419.1	56.9	13.6	45.4	10.8	52.2	12.5	51.0	12.2
90.0	426.9	67.9	15.9	55.1	12.9	62.9	14.7	61.1	14.3
100.0	433.4	88.6	20.4	75.7	17.5	84.4	19.5	81.0	18.7
110.0	439.0	116.3	26.5	104.2	23.7	113.7	25.9	106.1	24.6
115.0	441.6	122.3	27.7	110.2	25.0	120.1	27.2	113.7	25.8
129.5	448.1	153.5	34.3	143.0	31.9	153.5	34.3	144.4	32.2
152.5	456.6	203.1	44.5	196.2	43.0	207.2	45.4	193.5	42.4
172.5	462.6	231.7	50.1	226.7	49.0	238.0	51.4	221.9	48.0
182.5	465.3	233.3	50.1	228.7	49.1	240.1	51.6	223.3	48.0
192.5	467.8	234.2	50.1	229.8	49.1	241.3	51.6	224.2	47.9
202.5	470.1	232.9	49.5	228.4	48.6	240.0	51.1	222.8	47.4
212.5	472.3	218.4	46.2	213.1	45.1	224.7	47.6	208.2	44.1
232.5	476.2	168.1	35.3	159.5	33.5	171.1	35.9	157.9	33.2
249.5	479.2	120.6	25.2	108.2	22.6	119.9	25.0	110.4	23.0
249.5	479.2	160.7	33.5	148.3	31.0	160.0	33.4	150.6	31.4

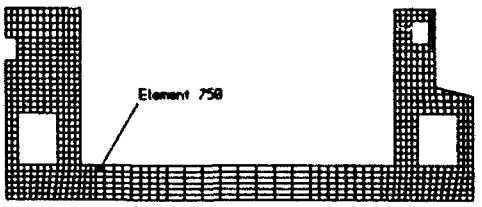

Table 17

Horizontal Stresses at Element 773, Point 4,

for Mixture 11

Time	Allowable Stress	Load Case 3		Load Case 4		Load Case 5		Load Case 6	
		Stress	% Of Allowable	Stress	% Of Allowable	Stress	% Of Allowable	Stress	% Of Allowable
20.8	101.0	-14.4	-----	-16.5	-----	-16.0	-----	-14.8	-----
30.0	313.4	3.0	0.9	-2.6	-----	-0.7	-----	1.4	0.4
36.5	345.9	18.5	5.3	13.3	3.9	15.6	4.5	16.5	4.8
40.0	357.8	12.5	3.5	6.6	1.8	9.1	2.5	10.4	2.9
45.0	371.1	9.3	2.5	2.7	0.7	5.5	1.5	6.9	1.9
65.8	405.0	19.0	4.7	11.1	2.7	14.8	3.6	15.8	3.9
70.0	409.7	31.7	7.7	24.0	5.8	27.8	6.8	28.4	6.9
80.0	419.1	40.5	9.7	33.1	7.9	37.3	8.9	36.8	8.8
90.0	426.9	48.2	11.3	41.0	9.6	45.5	10.7	44.3	10.4
100.0	433.4	62.7	14.5	56.3	13.0	61.1	14.1	58.6	13.5
110.0	439.0	82.1	18.7	76.6	17.4	81.6	18.6	77.7	17.7
119.5	443.7	93.8	21.1	88.9	20.0	94.2	21.2	89.2	20.1
129.5	448.1	107.2	23.9	103.3	23.0	108.5	24.2	102.6	22.9
142.5	453.1	130.8	28.9	128.2	28.3	133.5	29.5	126.1	27.8
152.5	456.6	134.1	29.4	131.9	28.9	137.3	30.1	129.3	28.3
162.5	459.7	139.3	30.3	137.4	29.9	142.8	31.1	134.5	29.3
172.5	462.6	149.7	32.4	148.3	32.1	153.8	33.2	144.9	31.3
182.5	465.3	147.1	31.6	145.7	31.3	151.2	32.5	142.3	30.6
192.5	467.8	145.2	31.0	143.7	30.7	149.2	31.9	140.3	30.0
202.5	470.1	142.1	30.2	140.3	29.9	145.9	31.0	137.2	29.2
212.5	472.3	128.9	27.3	126.5	26.8	132.1	28.0	124.0	26.3
222.5	474.3	110.5	23.3	107.1	22.6	112.7	23.8	105.6	22.3
232.5	476.2	89.1	18.7	84.4	17.7	90.0	18.9	84.2	17.7
242.5	478.0	66.4	13.9	60.2	12.6	65.8	13.8	61.5	12.9
249.5	479.2	53.7	11.2	46.6	9.7	52.2	10.9	48.8	10.2
249.5	479.2	159.2	33.2	152.1	31.8	157.7	32.9	154.3	32.2

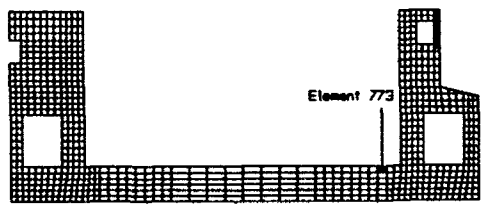

Table 18

Horizontal Stresses at Element 756, Point 4

For Mixture 11

Time	Allowable Stress	Load Case 3		Load Case 4		Load Case 5		Load Case 6	
		Stress	% Of Allowable	Stress	% Of Allowable	Stress	% Of Allowable	Stress	% Of Allowable
20.8	101.0	-16.0	-----	-18.5	-----	-17.9	-----	-16.5	-----
30.0	313.4	3.6	1.2	-5.2	-----	-2.8	-----	1.7	0.5
36.5	345.9	23.8	6.9	15.7	4.5	18.6	5.4	21.3	6.2
40.0	357.8	27.3	7.6	19.3	5.4	22.5	6.3	24.6	6.9
65.8	405.0	50.0	12.3	41.7	10.3	46.7	11.5	45.7	11.3
68.0	407.6	52.2	12.8	43.9	10.8	49.1	12.0	47.8	11.7
70.0	409.7	54.1	13.2	45.8	11.2	51.1	12.5	49.5	12.1
80.0	419.1	76.8	18.3	69.1	16.5	75.0	17.9	71.8	17.1
90.0	426.9	98.1	23.0	91.0	21.3	97.4	22.8	92.6	21.7
100.0	433.4	130.8	30.2	125.4	28.9	132.2	30.5	124.8	28.8
110.0	439.0	169.3	38.6	166.0	37.8	173.3	39.5	163.0	37.1
119.5	443.7	202.6	45.7	201.2	45.3	208.9	47.1	196.0	44.2
129.5	448.1	221.1	49.3	221.4	49.4	229.2	51.1	214.3	47.8
142.5	453.1	254.2	56.1	257.0	56.7	265.0	58.5	247.4	54.6
152.5	456.6	261.6	57.3	265.6	58.2	273.6	59.9	254.7	55.8
162.5	459.7	270.6	58.9	275.4	59.9	283.5	61.7	263.6	57.3
172.5	462.6	286.2	61.9	292.0	63.1	300.2	64.9	279.1	60.3
182.5	465.3	285.7	61.4	291.9	62.7	300.2	64.5	278.5	59.9
192.5	467.8	285.0	60.9	291.3	62.3	299.6	64.1	277.8	59.4
202.5	470.1	282.5	60.1	288.6	61.4	297.0	63.2	275.3	58.6
212.5	472.3	266.7	56.5	272.0	57.6	280.4	59.4	259.4	54.9
222.5	474.3	243.2	51.3	246.9	52.1	255.4	53.8	235.9	49.7
232.5	476.2	215.2	45.2	217.0	45.6	225.4	47.3	207.9	43.7
242.5	478.0	185.0	38.7	184.5	38.6	193.0	40.4	177.8	37.2
249.5	479.2	168.3	35.1	166.2	34.7	174.7	36.5	161.0	33.6
249.5	479.2	159.9	33.4	157.9	32.9	166.3	34.7	152.6	31.8

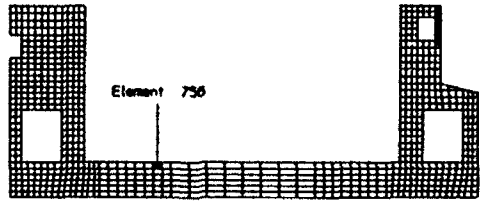

Table 19

Horizontal Stresses at Element 993, Point 2

for Mixture 11

Time	Allowable Stress	Load Case 3		Load Case 4		Load Case 5		Load Case 6	
		Stress	% Of Allowable	Stress	% Of Allowable	Stress	% Of Allowable	Stress	% Of Allowable
70.8	101.0	-3.0	-----	-3.3	-----	-3.2	-----	-3.1	-----
74.0	248.1	0.0	0.0	0.0	-----	0.3	0.1	-0.2	-----
75.0	264.7	27.3	10.3	28.3	10.7	28.6	10.8	27.0	10.2
75.8	274.9	28.3	10.3	29.7	10.8	30.1	10.9	28.0	10.2
80.0	313.4	19.9	6.3	21.5	6.9	22.0	7.0	19.5	6.2
80.8	318.2	34.8	10.9	37.3	11.7	37.7	11.8	34.5	10.8
85.0	339.9	77.2	22.7	85.3	25.1	85.3	25.1	77.2	22.7
90.0	357.8	87.1	24.4	97.4	27.2	97.5	27.3	86.9	24.3
95.0	371.1	101.3	27.3	112.8	30.4	113.2	30.5	100.9	27.2
100.0	381.7	105.1	27.	117.8	30.9	118.4	31.0	104.5	27.4
100.8	383.1	106.0	27.7	118.5	30.9	119.2	31.1	105.3	27.5
105.0	390.4	111.6	28.6	124.4	31.9	125.3	32.1	110.7	28.3
110.0	397.8	119.2	30.0	133.1	33.5	134.3	33.8	118.1	29.7
110.8	398.8	117.2	29.4	130.9	32.8	132.2	33.2	116.0	29.1
115.0	404.1	114.3	28.3	127.1	31.5	128.9	31.9	112.7	27.9
118.0	407.6	109.4	26.8	121.2	29.7	123.2	30.2	107.5	26.4
124.5	414.2	114.6	27.7	126.6	30.6	129.0	31.1	112.4	27.1
132.5	421.2	127.0	30.2	139.6	33.1	142.2	33.8	124.7	29.6
142.5	428.6	145.8	34.0	159.5	37.2	162.3	37.9	143.3	33.4
152.5	434.9	143.2	32.9	157.1	36.1	160.1	36.8	140.6	32.3
172.5	445.1	139.7	31.4	153.3	34.5	156.6	35.2	136.8	30.7
192.5	453.3	110.0	24.3	121.8	26.9	125.2	27.6	106.9	23.6
212.5	459.7	65.6	14.3	74.4	16.2	77.9	16.9	62.5	13.6
232.5	465.3	-7.3	-----	-3.8	-----	-0.3	-----	-10.5	-----
249.5	469.4	-67.5	-----	-68.9	-----	-65.3	-----	-70.7	-----
249.5	469.4	-82.0	-----	-83.4	-----	-79.9	-----	-85.2	-----

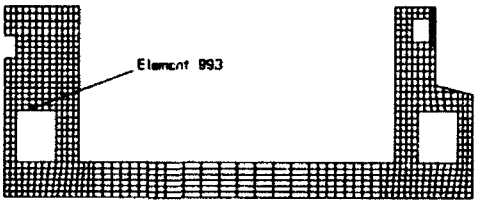

Vertical displacements occur for three reasons: (a) the structure is contracting in the vertical direction as it cools, (b) differences in horizontal displacement and restraint across the floor section result in differences in vertical pile displacement across the base of the structure, and (c) small differences in pile displacement occur due to the nonuniform gravity load distribution. For our analyses, bending and stresses due to the dead load of the structure were small when compared to stresses due to the restraint of thermally induced strains.

151. Contour plots of stresses in the x and y directions at 94.5 and 182.5 days are presented in Figures 143 through 146. In Figure 144, maximum vertical tensile stresses are in lifts 13 and 14, the most recently placed lifts, and are less than 100 psi. This indicates that maximum vertical tensile stresses at the face of the concrete occur approximately 10 to 15 days after placement of a lift and are relatively low. Figures 145 and 146 show stress contours at approximately the time of maximum stress in the floor. Horizontal stresses are compressive at the base of the floor and tensile at the top due to the temperature gradient, the restraint to thermally induced strains in each lift provided by adjoining concrete lifts, and moments induced by the dead load of the structure. The temperature differential across the floor at these late times occurred as the base was maintained at a relatively high temperature while the surface was at roughly ambient temperature.

152. An additional analysis was performed to determine the effects of including the thermal properties of water in the analysis. The heat transfer analysis was modified at 250 days by the addition of elements to represent still water inside the chamber to elevation (el) 300* and outside the land-side wall to el 285. Soil was also included at the land-side wall to el 280. Water in the culverts under 15 ft of head has a velocity of 8.6 ft/sec and was simulated by changing the culvert wall film coefficients to 85.4 Btu/day-in^2°F. This film coefficient was calculated using the Nusselt equation, an empirical equation for turbulent flow in a duct. A record of water temperature versus time for the Ohio River at a location slightly upstream of the Olmsted site was provided by the USAED, Louisville. The water temperature curve roughly paralleled the ambient air temperature curve, with an approximate 30-day offset. Except for a short period, the minimum water temperature

---

* All elevations (el) cited herein are in feet referred to the National Geodetic Vertical Datum (NGVD).

was near 40 °F. Since the curves were so similar, the ambient water temperature for the analysis was obtained by shifting the ambient air temperature curve by 30 days and using a minimum 40 °F temperature. A plot of ambient air and water temperature curves used in the analysis and river water temperature obtained from the Louisville District is shown in Figure 147. Thermal properties for water used in the analysis are given in Table 20.

Table 20

Thermal Properties for Water

Property	Value
Density, lb/in^3	0.0361
Specific heat, Btu/lb-°F	1.001
Thermal conductivity, Btu/day-$in.^2$-°F	0.700

153. After the addition of the water elements at 250 days, the heat transfer analysis was continued for an additional 250 days. Temperature contours from this analysis at 250, 306, 424, and 501 days are shown in Figures 148, 149, 150, and 151. These figures show the gradual dissipation of the thermal gradient in the floor.

154. A stress analysis was performed using the temperatures at nodes from the heat transfer analysis as the thermal loading. As in previous analyses, the service loads were applied at 250 days, and the analysis was continued for an additional 250 days. Stress histories at sections 3 and 5 are shown in Figures 152 through 157, and stress distributions at 173, 250, and 500 days are shown in Figure 158 and 159.

Mixture 6 Analyses

155. In the evaluation of the time-history plots shown in Figures 160 through 172, it is easily seen that for the load cases which include creep and shrinkage (load cases 3 through 6) there is very little difference in behavior from one load case to the next. To quantify the difference created by changing the bounds of the creep and shrinkage, the difference at the maximum tensile point in the slab can be used to illustrate the change by comparing the case providing the highest tensile value to the case providing the lowest

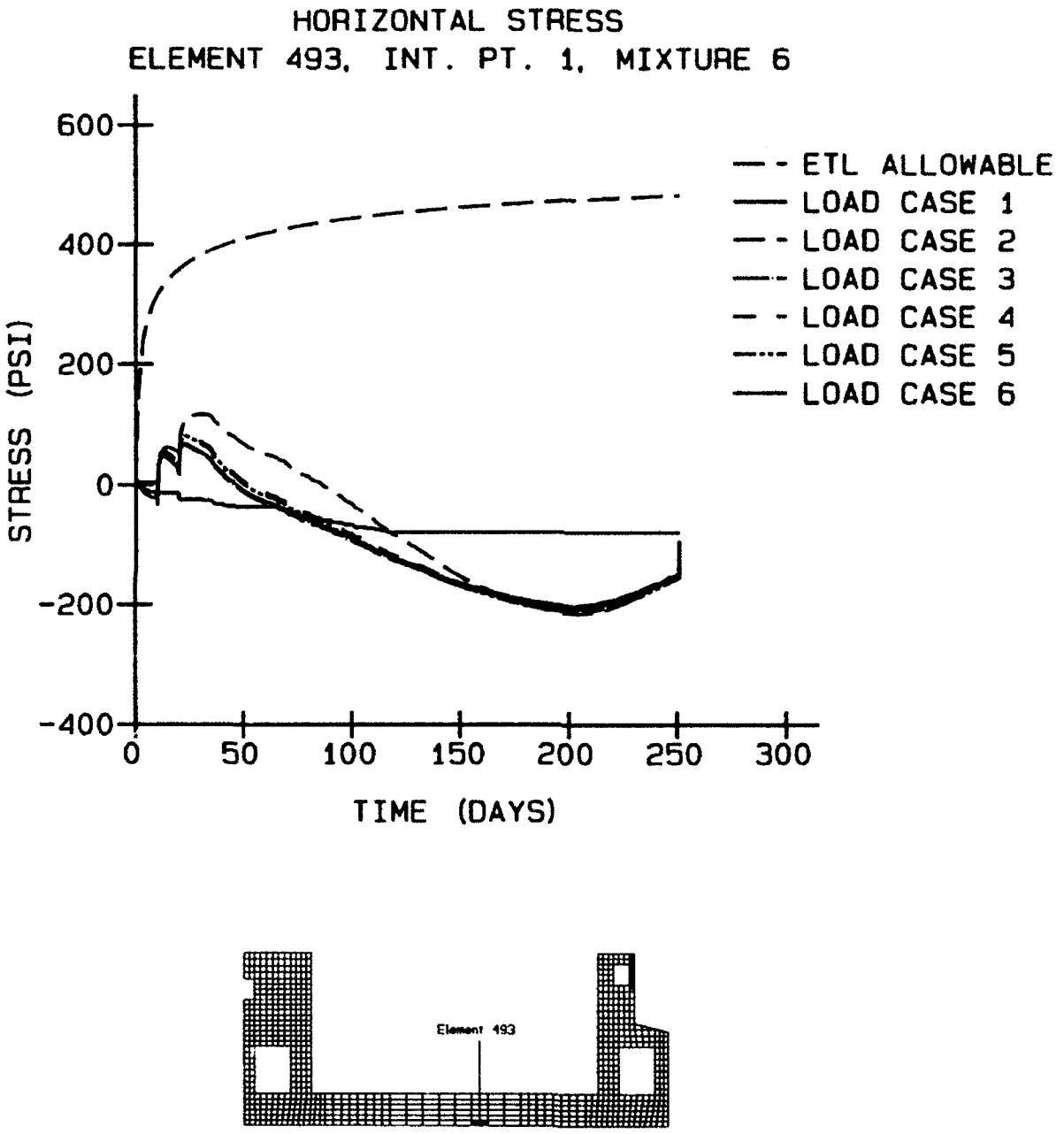

Figure 160. Horizontal stresses, element 493, point 1

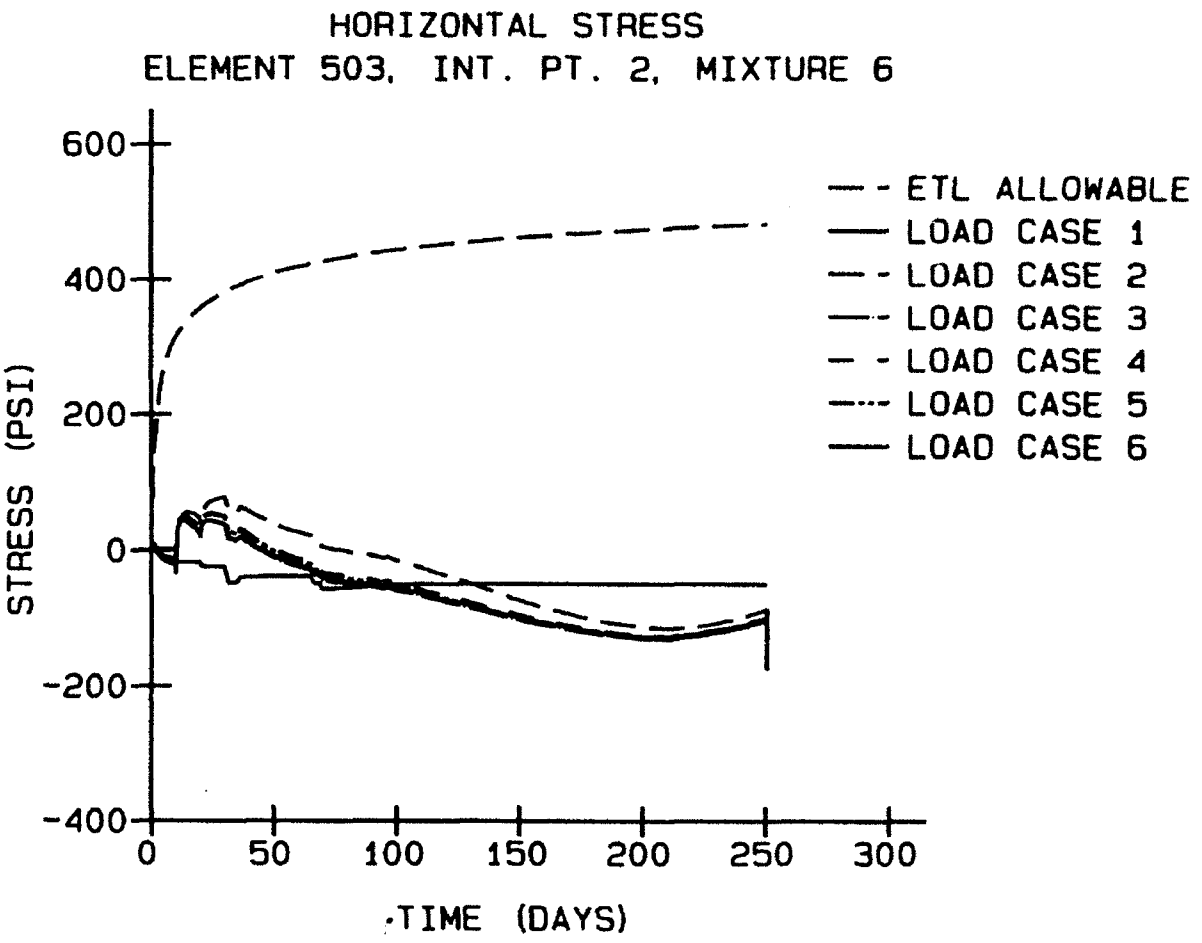

Figure 161. Horizontal stresses, element 503, point 2

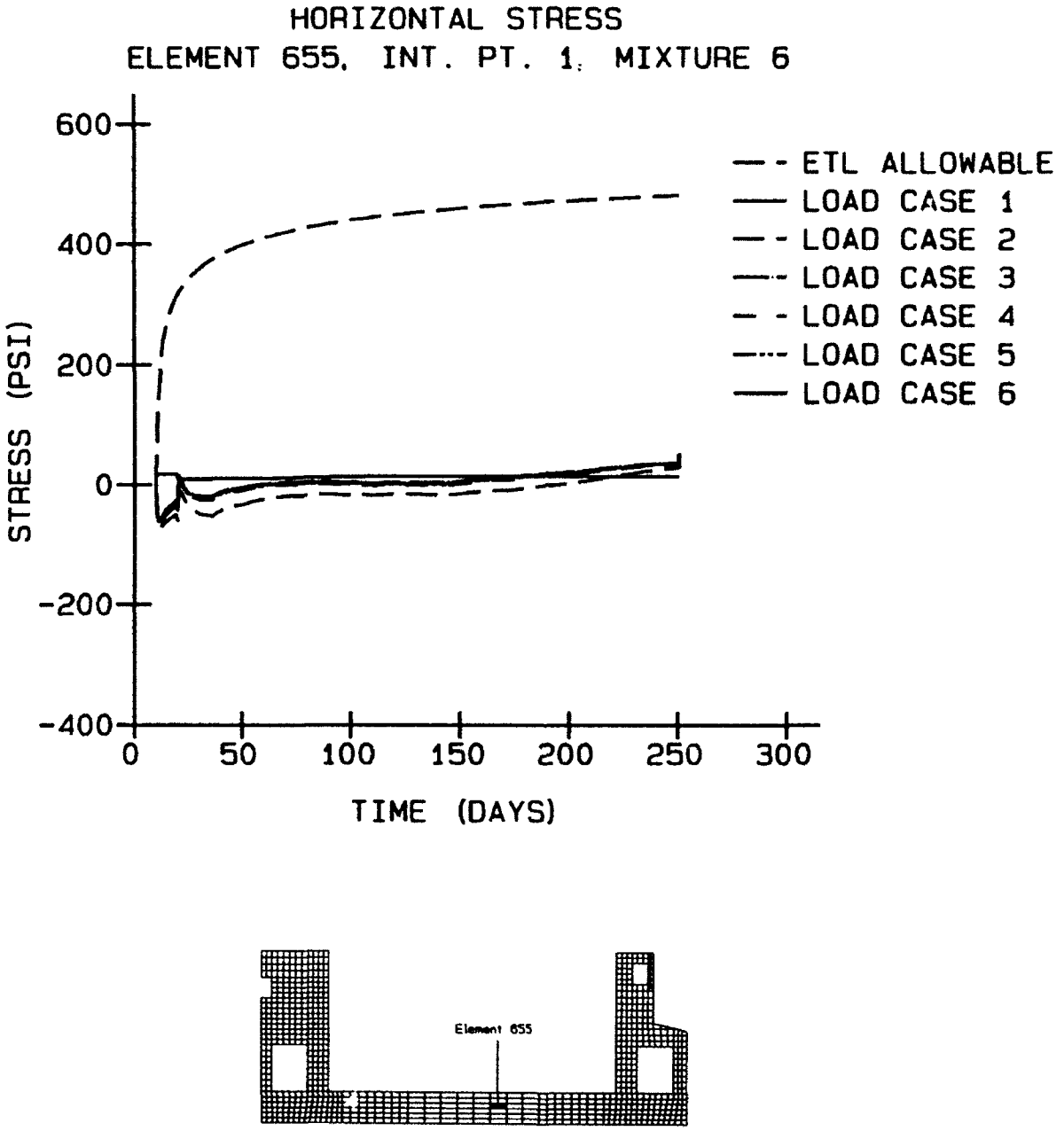

Figure 162. Horizontal stresses, element 655, point 1

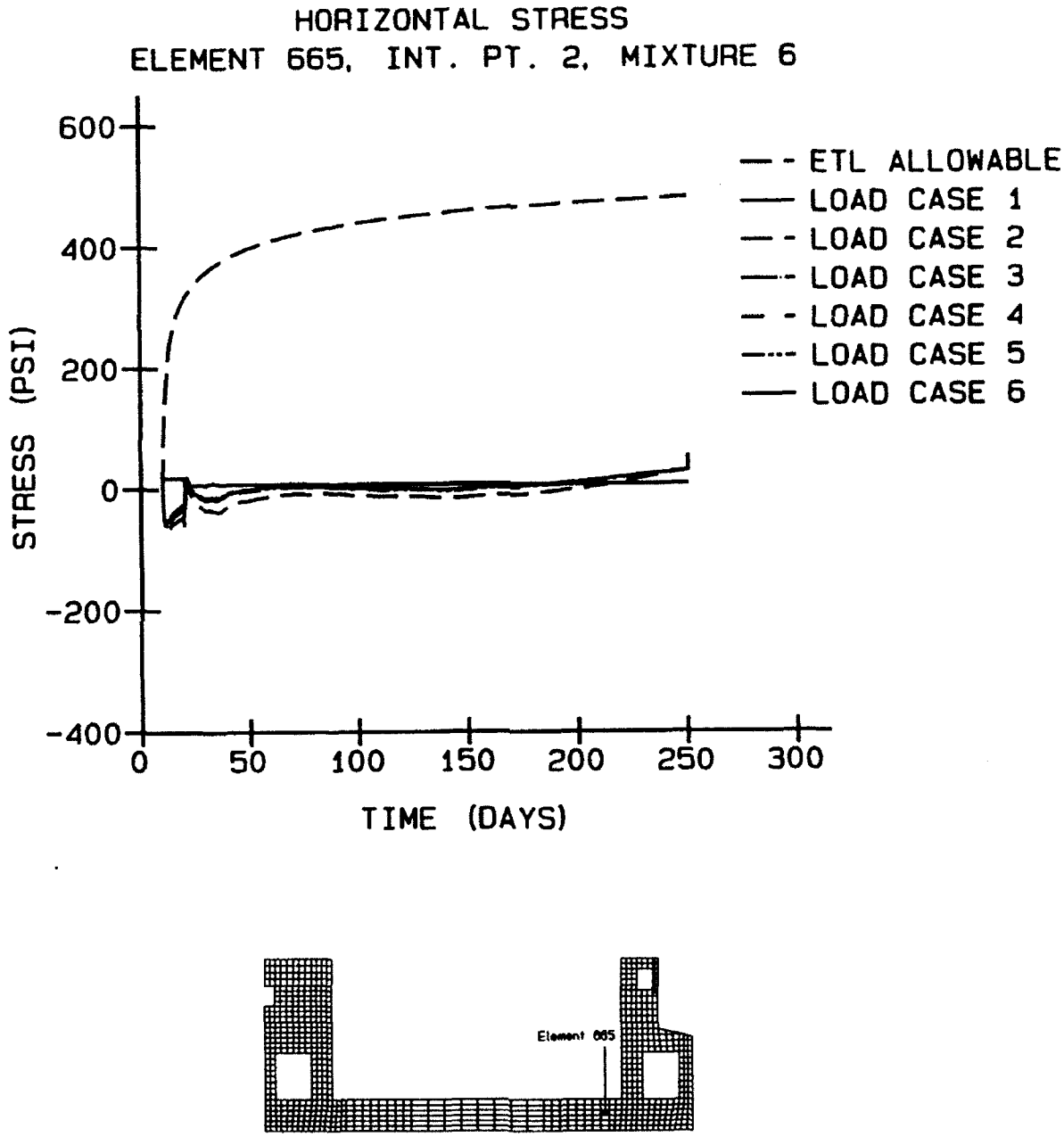

Figure 163. Horizontal stresses, element 665, point 2

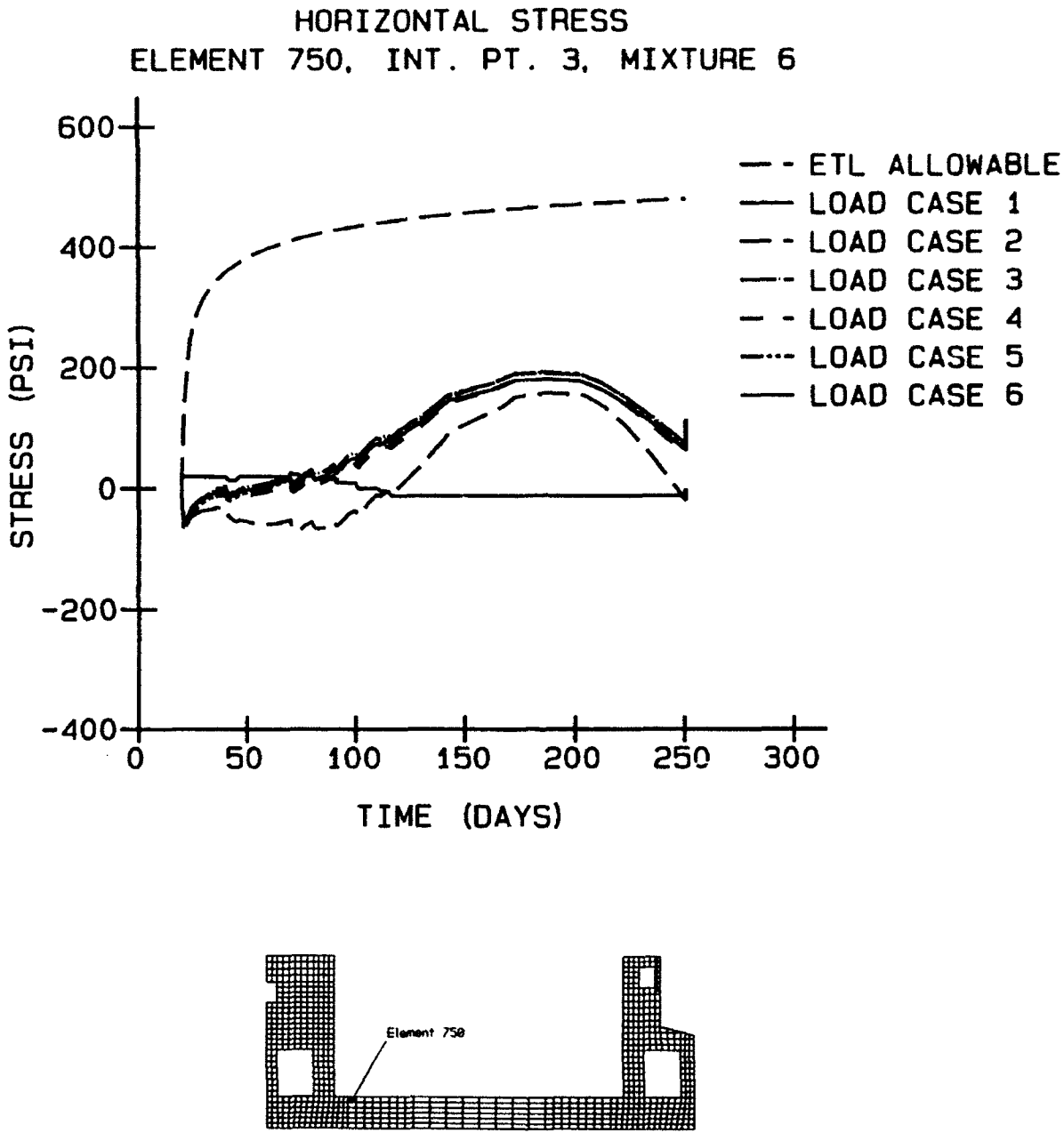

Figure 164. Horizontal stresses, element 750, point 3

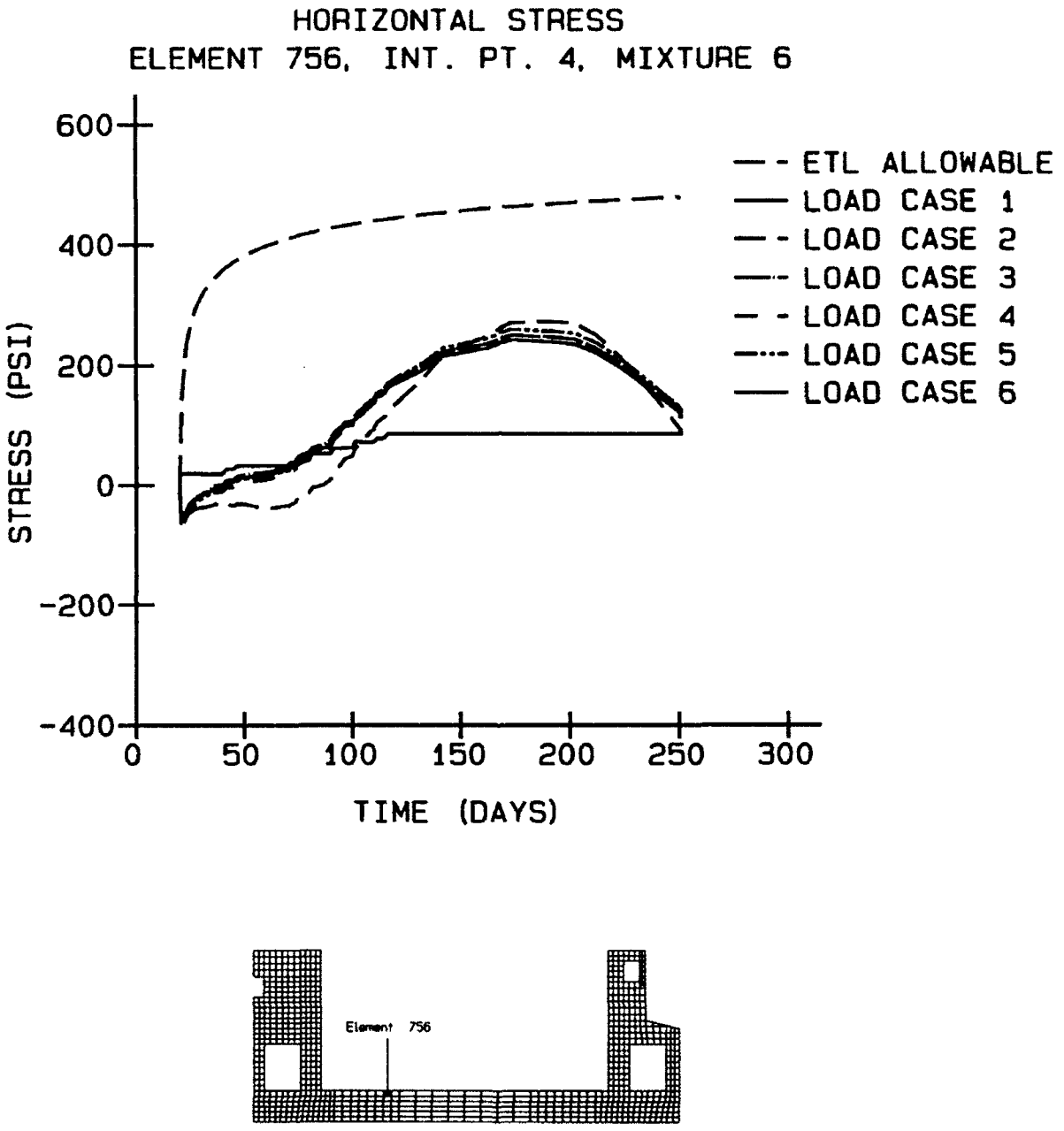

Figure 165. Horizontal stresses, element 756, point 4

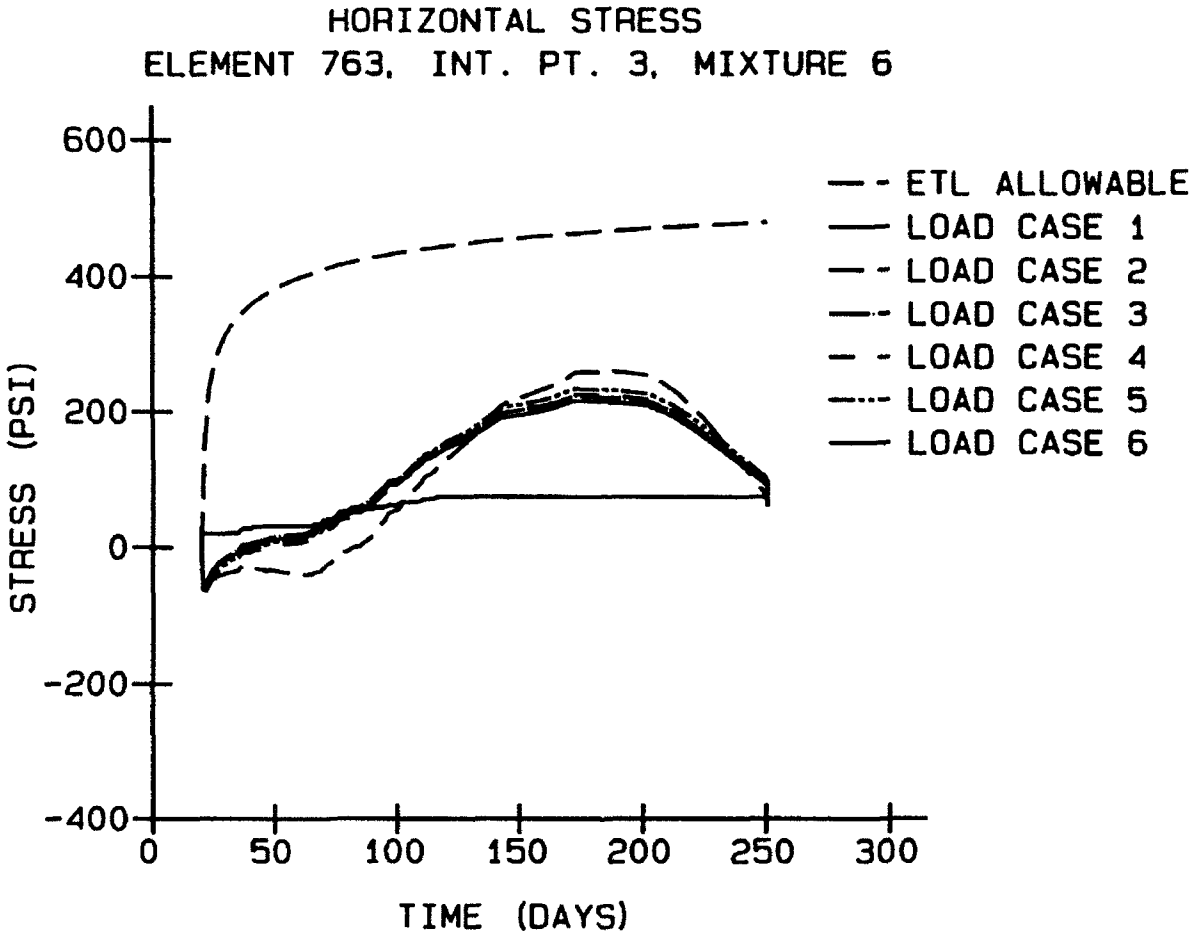

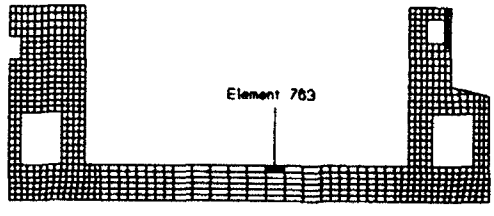

Figure 166. Horizontal stresses, element 763, point 3

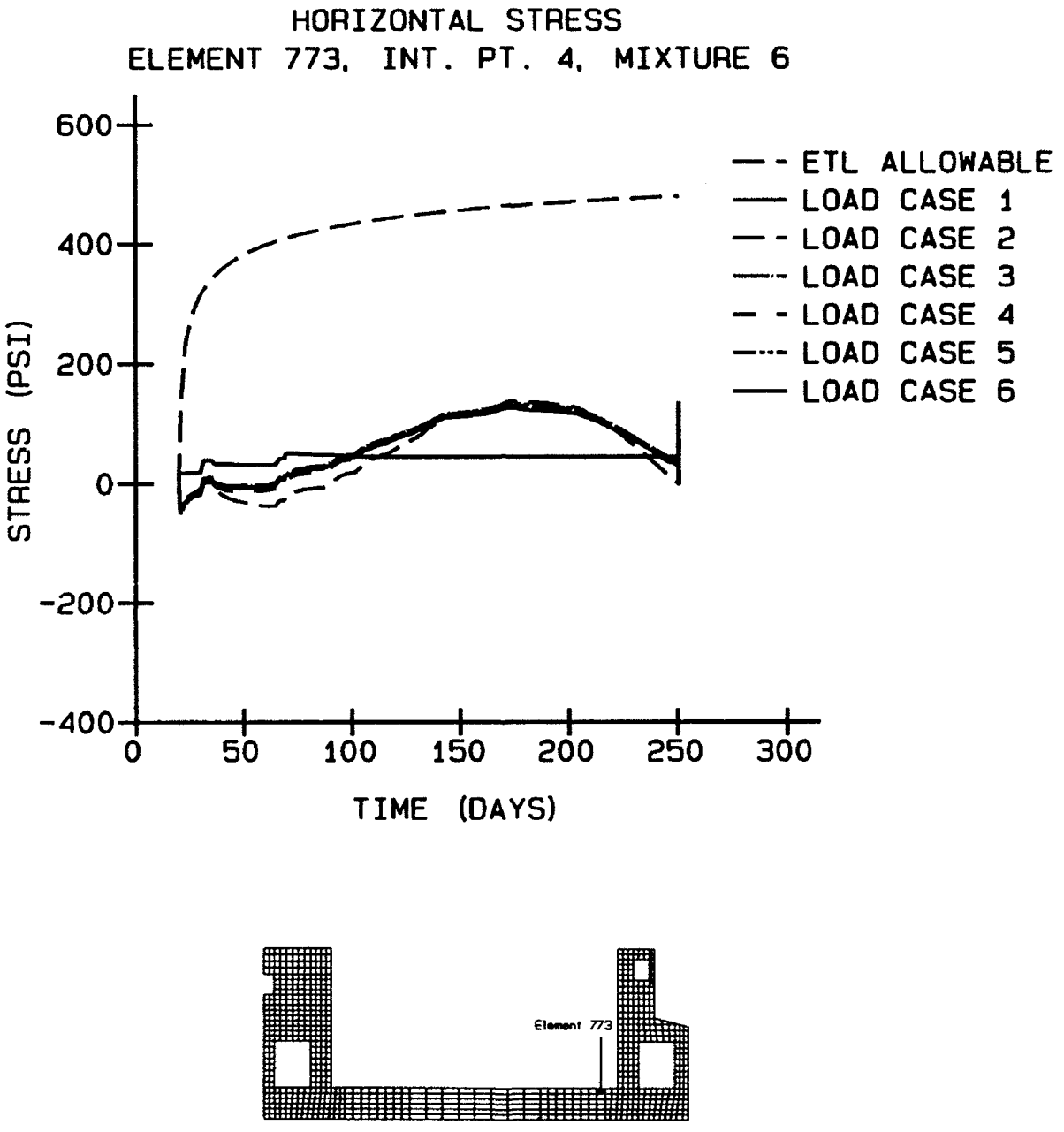

Figure 167. Horizontal stresses, element 73, point 4

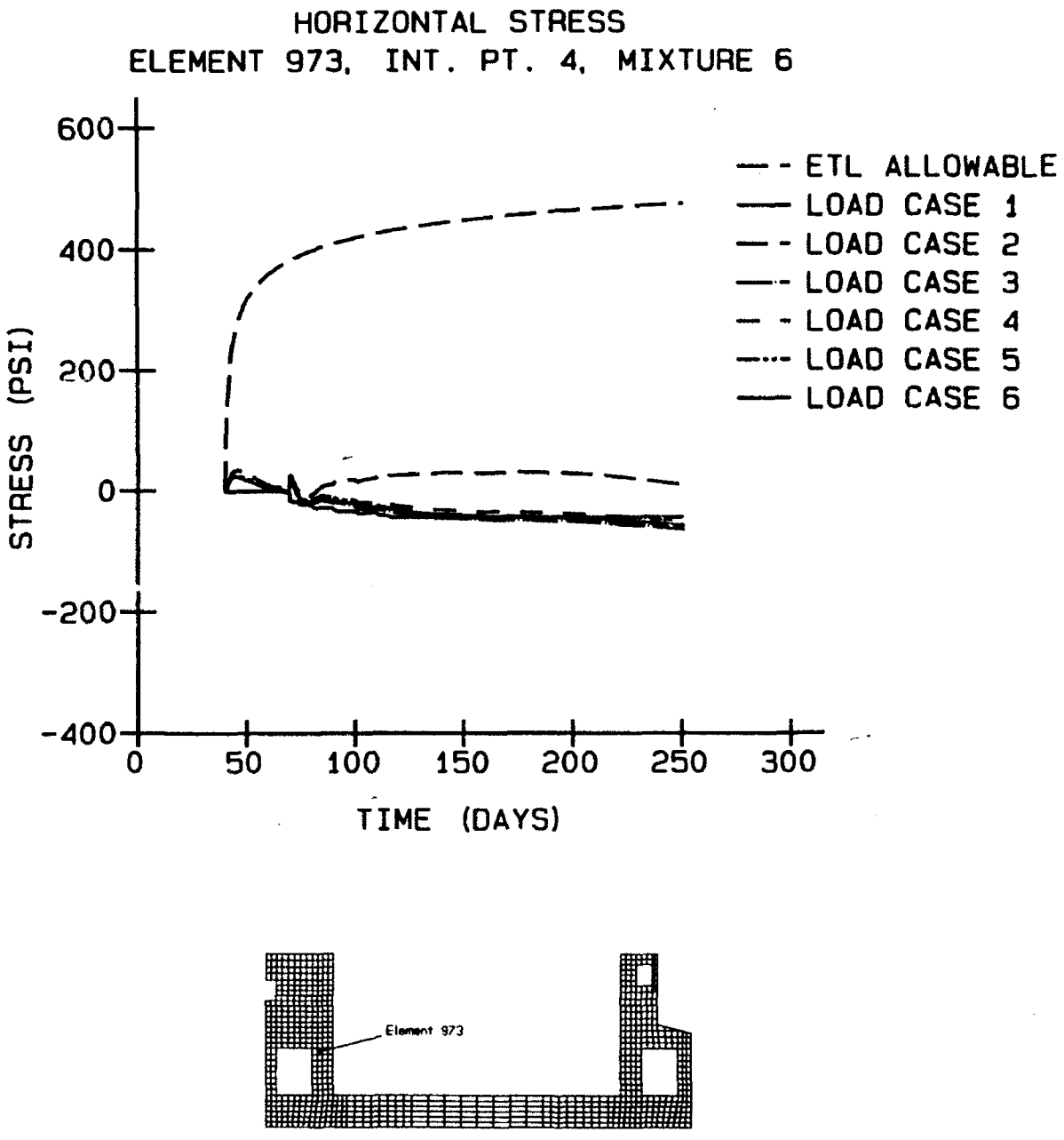

Figure 168. Horizontal stresses, element 973, point 4

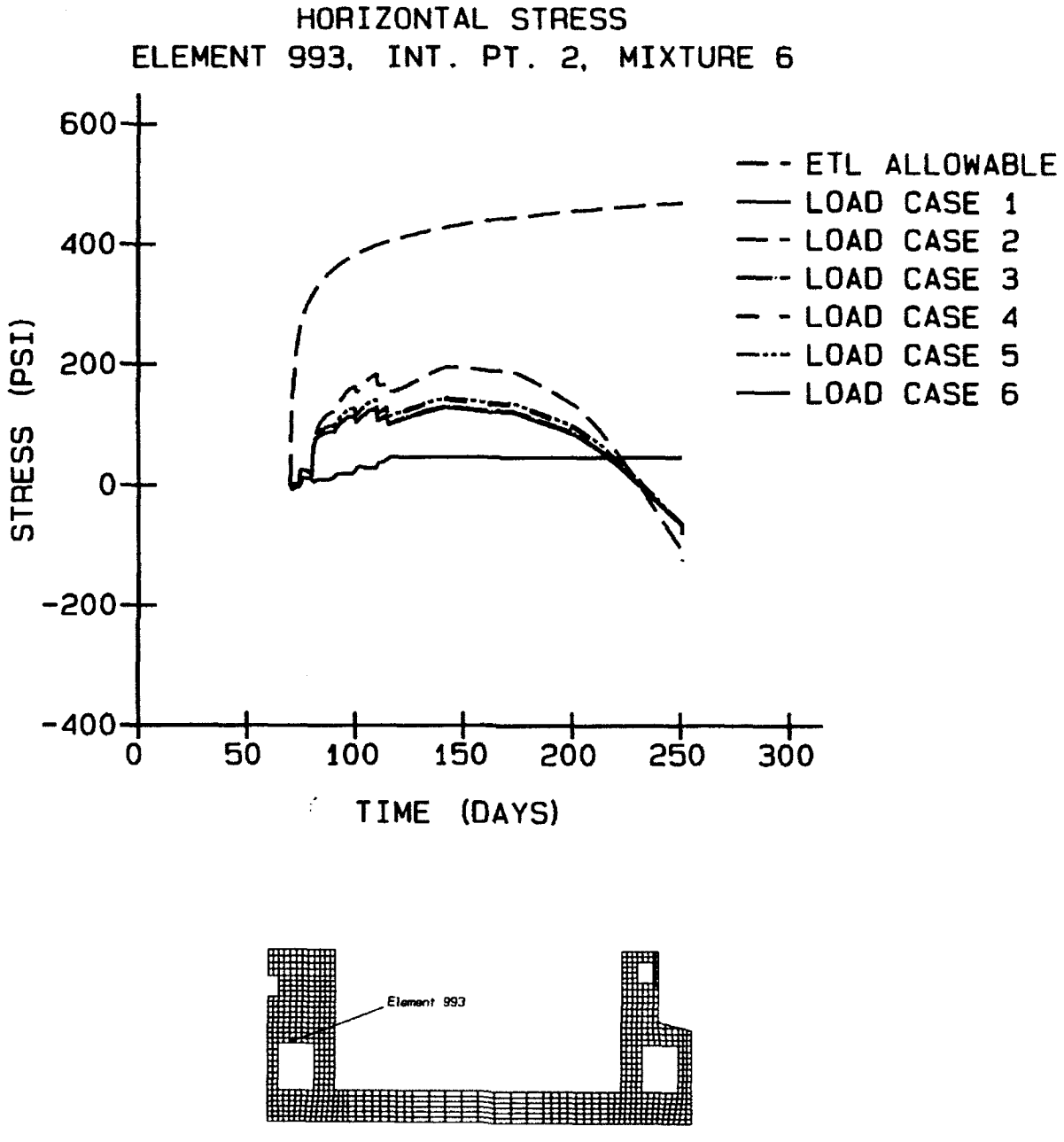

Figure 169. Horizontal stresses, element 993, point 2

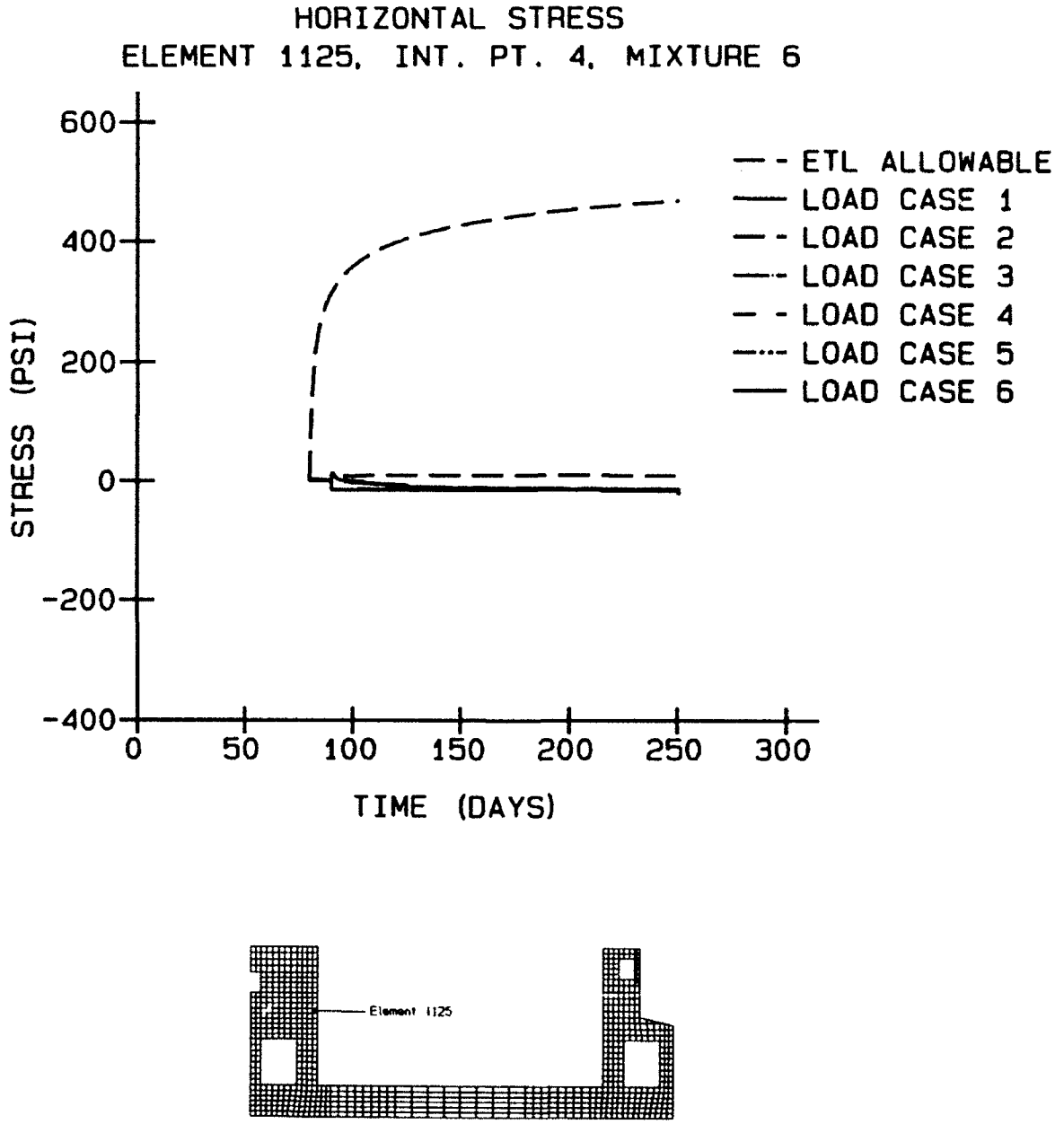

Figure 170. Horizontal stresses, element 1125, point 4

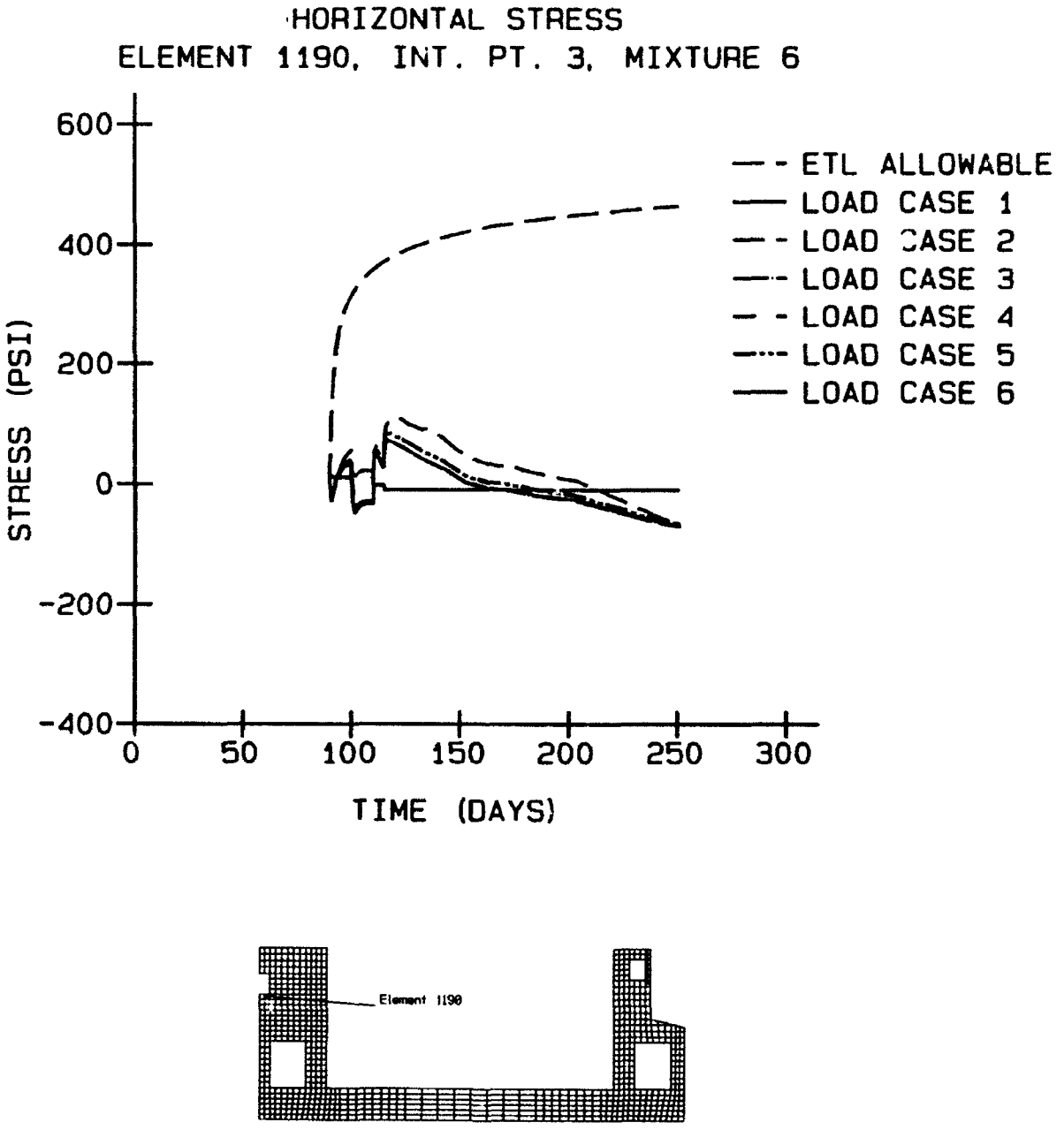

Figure 171. Horizontal stresses, element 1190, point 3

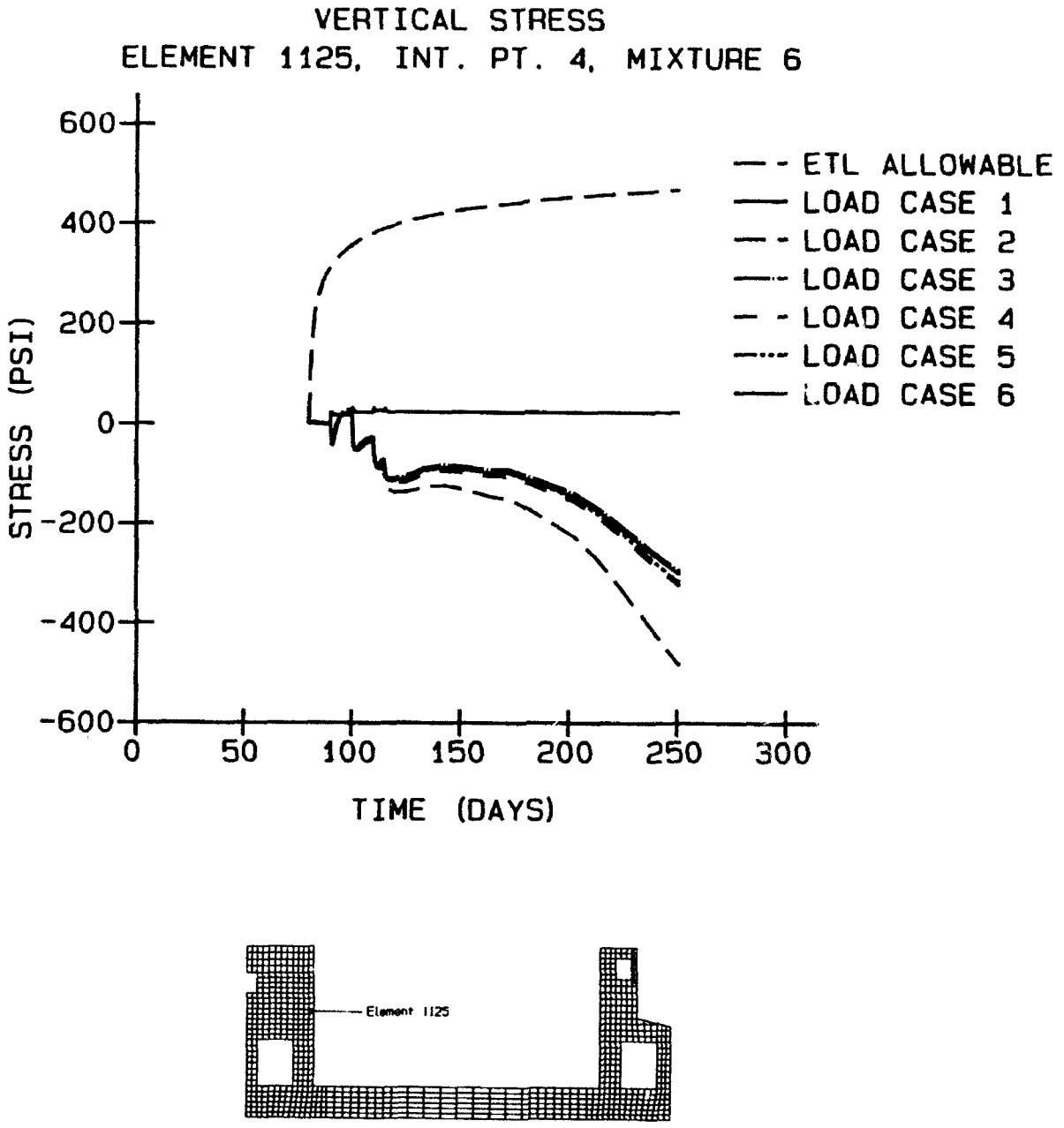

Figure 172. Vertical stresses, element 1125, point 4

tensile value. As seen in Figure 165, the maximum tensile stress for element 756 from load case 5 is 259.0 psi, while the minimum tensile stress from load case 6 is 242.0 psi. This difference in stress is a total change of 6.8 percent. Likewise at element 493, which shows the maximum compressive stress of the points presented, the stress is -213.5 psi from load case 5 and -202.4 psi from load case 6 which provides a change of 5.3 percent. These differences indicate that the 20 percent change in the creep and shrinkage of the mixture do not provide a similar change in the stress.

156. Sudden jumps in stress at 250 days can be seen in Figures 160 through 167 and are a result of the application of service loads. Service loads were applied in an effort to determine results of combining the service loads with temperature loads. As was discussed previously, load case 5 for mixture 11 provided the highest tensile stresses, and therefore the application of service loads was continued to day 500, and results are included under the discussions for mixture 11.

157. While differences tended to be small from load case to load case, for the load cases containing creep and shrinkage, load case 5 (minimum creep and maximum shrinkage) provided the highest stresses in areas experiencing tensile stresses. This can be seen clearly in Figures 165 and 166. A case with the minimum amount of creep and the maximum amount of shrinkage such as load case 5 should be expected to be the controlling case in most instances. The fact that lower levels of creep will produce higher tensile stresses in a NISA can be seen in Figures 165 and 166 by the fact that load case 2, which has no creep and shrinkage, produces the highest tensile stresses.

158. The effects of creep can be seen in Figures 173 and 174 where Figure 173 is an enlarged portion of Figure 164 and Figure 174 is an enlarged portion of Figure 165. In Figure 173 the relaxation of compressive stresses is illustrated by the large gap between the curve for load case 2 which contains no creep and the curves for load cases 3 through 6. The effect of creep is further seen by the fact that load cases 4 and 5, which are cases of minimum creep, are beneath load cases 3 and 6, which are cases of maximum creep. The differences between load cases 4 and 5 and load cases 3 and 6 can be attributed to creep. In Figure 174 the relaxation of tensile stresses can be seen by the higher rate of change of stress with respect to time for load case 2 as compared to the load cases which contain creep. A close look at the plot will also reveal that stresses associated with load cases 4 and 5 are changing at faster rate than those associated with load cases 3 and 6, which once again

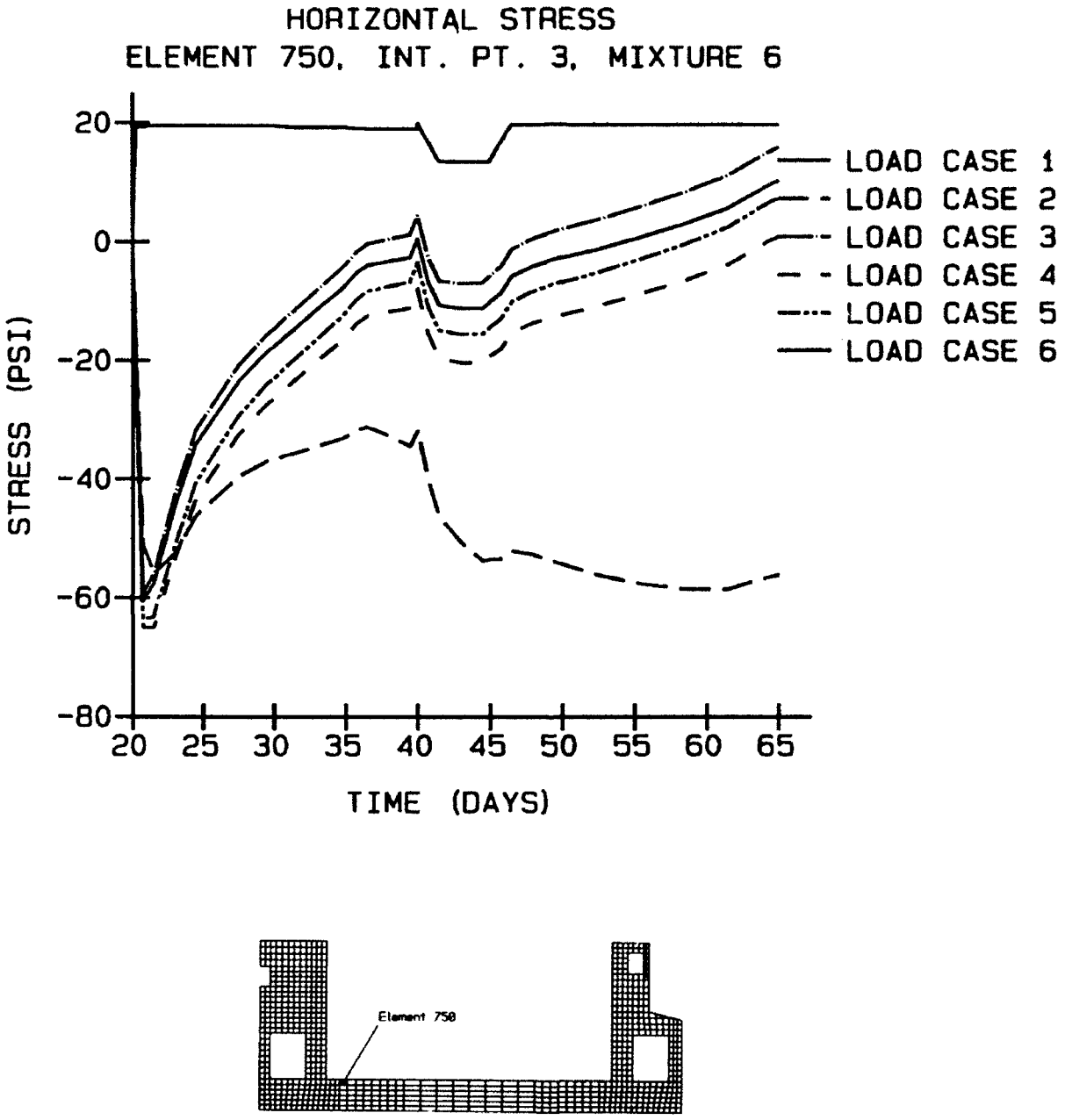

Figure 173. Window of horizontal stresses, element 750, point 3

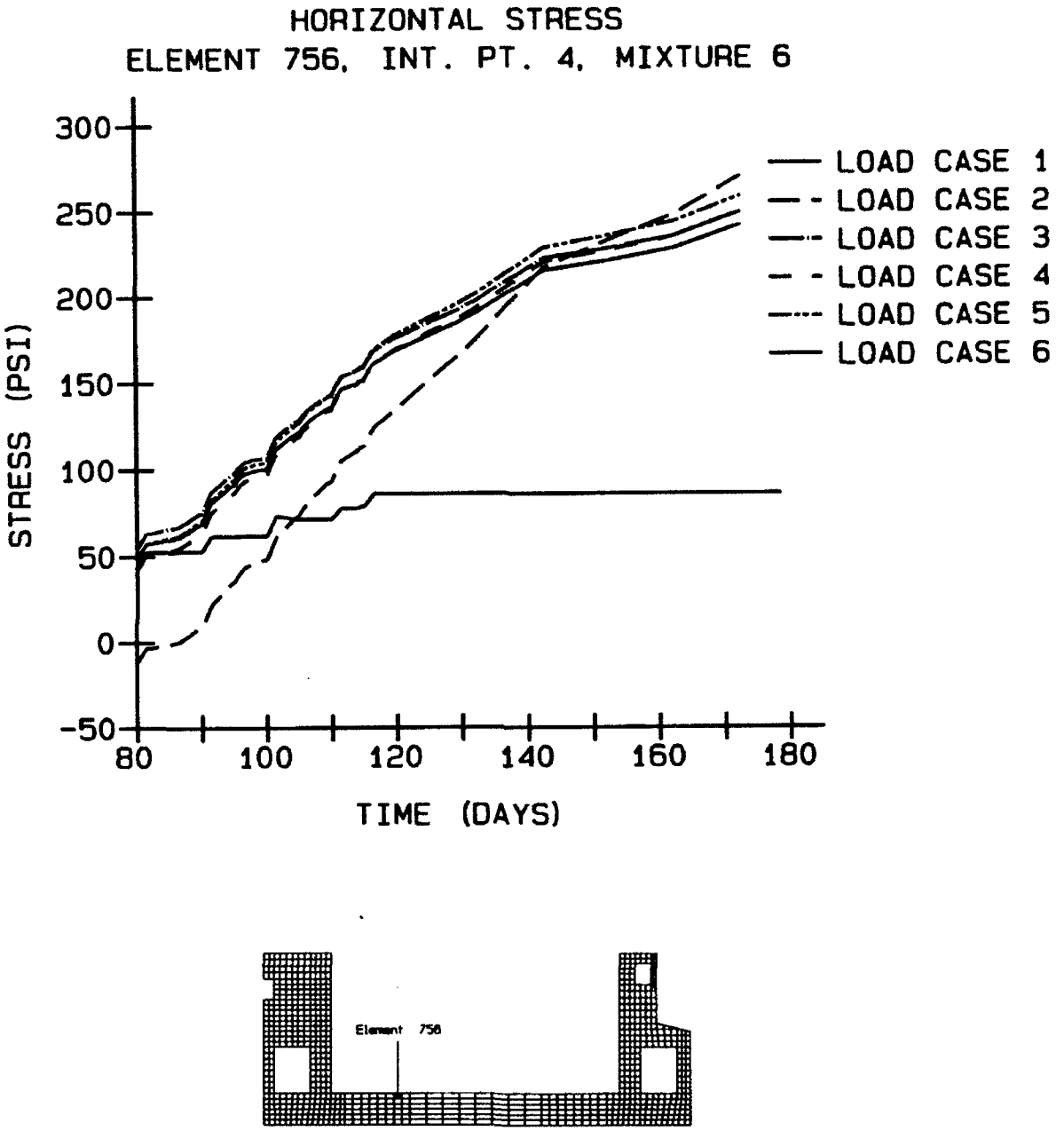

Figure 174. Window of horizontal stresses, element 756, point 4

can be attributed to the difference in creep between these two sets of load cases.

159. Another item which becomes evident through the review of the plots in Figures 160, 161, 164, 165, 166, and 167 is that the contribution of gravity, as shown by load case 1, to the overall stress in the base slab is not very large. The effects of temperature, particularly the ambient temperature, are the dominant factor in the structural behavior. This is best illustrated in Figure 164 where at approximately 75 days the effect on the stress due to gravity load (load case 1) is to cause a decrease in stress at the top of the base slab, yet the curves which include thermal loading continue to rise. In addition, looking at Figure 165 and comparing the maximum stress for the controlling case (load case 5) to the stress due to gravity loading shows that the stress due to gravity is only 33 percent of the total stress.

160. Figures 164, 165, 166, and 167 support the statements made in the first phase of the report with regard to the ambient temperature driving the behavior of the stresses in the slab. As previously stated, the final lift is placed at 115 days at which time the curve for load case 1 remains at a constant stress, yet the curves for load cases 2 through 6 continue to rise and after 200 days begin to fall. The point where the stresses reach their peak corresponds closely with the coldest period of the ambient temperature curve.

161. As was seen in Phase I of the study, stresses in the wall are low. Horizontal stresses in the wall are shown in Figures 168, 169, 170, and 171, and a plot of vertical stress at the chamber face is shown in Figure 172. Figures 169 and 171, plots at elements 993 and 1190, respectively, do have some tensile stresses of significance. At element 993 the tension is a result of bending and restraint between the two side walls, and the tension at element 1190 can be attributed primarily to its close proximity to the corner of the gallery. In general, the plots of the stresses in the wall remain low compared to the stresses in slab.

162. Another item which is easily identified when reviewing the time-history plots in Figures 160 through 172 is that at no time in the analysis do the stresses approach the allowable stress outlined in ETL 1110-2-324 (Headquarters, Department of the Army, 1990). This is given in tabular form for elements in the top of the slab and element 993 above the culvert in Tables 21 through 25. As was mentioned previously, the maximum point of stress in the monolith was element 756, and the load case providing the highest tensile stresses was load case 5. Looking at element 756 of load case 5 in Table 22,

Table 21

Horizontal Stresses at Element 750, Point 3

for Mixture 6

		Load Case 1		Load Case 2		Load Case 3		Load Case 4		Load Case 5		Load Case 6	
Time	Allowable Stress	Stress	% Of Allowable	Stress	% Of Allowable	Stress	% Of Allowable	Stress	% Of Allowable	Stress	% Of Allowable	Stress	% Of Allowable
20.8	101.0	19.4	19.2	-51.1	-----	-59.3	-----	-65.0	-----	-63.7	-----	-60.5	-----
24.5	256.9	19.5	7.6	-46.1	-----	-31.7	-----	-43.2	-----	-40.5	-----	-34.1	-----
30.0	313.4	19.5	6.2	-36.8	-----	-14.7	-----	-26.5	-----	-23.1	-----	-17.7	-----
35.0	339.9	19.2	5.6	-32.9	-----	-3.8	-----	-15.9	-----	-11.9	-----	-7.3	-----
40.0	357.8	19.9	5.6	-31.8	-----	4.5	1.3	-7.8	-----	-3.3	-----	0.6	0.2
40.8	360.0	16.7	4.6	-40.2	-----	-2.8	-----	-15.4	-----	-10.9	-----	-6.8	-----
45.0	371.1	13.7	3.7	-53.5	-----	-5.6	-----	-19.3	-----	-14.3	-----	-10.0	-----
49.5	380.7	19.7	5.2	-53.9	-----	1.7	0.5	-12.5	-----	-7.1	-----	-3.0	-----
61.5	399.8	19.7	4.9	-58.5	-----	11.1	2.8	-3.8	-----	2.5	0.6	5.7	1.4
70.0	409.7	25.2	6.1	-52.9	-----	21.9	5.3	6.9	1.7	13.7	3.4	15.9	3.9
70.8	410.5	24.1	5.9	-66.8	-----	9.7	2.4	-5.9	-----	1.1	0.3	3.6	0.9
80.0	419.1	21.4	5.1	-55.1	-----	30.6	7.3	14.0	3.3	22.0	5.2	23.5	5.6
90.0	426.9	16.0	3.8	-54.9	-----	38.7	9.1	20.6	4.8	29.6	6.9	30.8	7.2
100.0	433.4	8.8	2.0	-37.2	-----	57.7	13.3	39.3	9.1	49.1	11.3	49.1	11.3
110.0	439.0	0.7	0.2	-11.2	-----	81.8	18.6	63.8	14.5	74.4	16.9	72.6	16.5
115.0	441.6	-5.3	-----	-6.1	-----	87.0	19.7	68.8	15.6	79.8	18.1	77.4	17.5
129.5	448.1	-11.8	-----	34.3	7.6	117.4	26.2	100.8	22.5	112.2	25.0	107.4	24.0
152.5	456.6	-11.8	-----	109.0	23.9	163.7	35.9	150.8	33.0	162.5	35.6	153.4	33.6
172.5	462.6	-11.8	-----	150.2	32.5	189.1	40.9	178.1	38.5	190.1	41.1	178.6	38.6
182.5	465.3	-11.8	-----	154.9	33.3	189.5	40.7	178.9	38.5	191.0	41.1	178.9	38.5
192.5	467.8	-11.8	-----	156.7	33.5	189.5	40.5	179.1	38.3	191.2	40.9	178.9	38.2
202.5	470.1	-11.8	-----	155.0	33.0	187.4	39.9	177.0	37.7	189.2	40.2	176.8	37.6
212.5	472.3	-11.8	-----	136.4	28.9	173.2	36.7	162.1	34.3	174.3	36.9	162.5	34.4
232.5	476.2	-11.8	-----	64.4	13.5	125.2	26.3	110.8	23.3	123.1	25.8	114.5	24.0
250.5	479.4	-11.8	-----	-19.3	-----	73.8	15.4	55.5	11.6	67.8	14.1	63.1	13.2
250.5	479.4	-----	-----	19.5	4.1	112.6	23.5	94.3	19.7	106.6	22.2	101.9	21.3

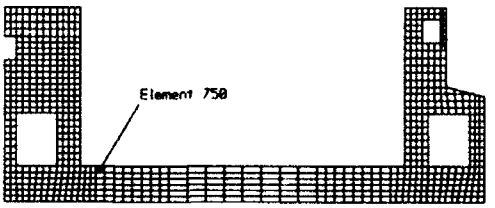

Table 22

Horizontal Stresses at Element 756, Point 4

for Mixture 6

		Load Case 1		Load Case 2		Load Case 3		Load Case 4		Load Case 5		Load Case 6	
Time	Allowable Stress	Stress	% Of Allowable	Stress	% Of Allowable	Stress	% Of Allowable	Stress	% Of Allowable	Stress	% Of Allowable	Stress	% Of Allowable
20.8	101.0	19.4	19.2	-51.2	-----	-59.5	-----	-65.1	-----	-63.9	-----	-60.7	-----
30.0	313.4	19.5	6.2	-37.0	-----	-14.6	-----	-26.5	-----	-23.0	-----	-17.6	-----
36.5	345.9	19.2	5.6	-31.4	-----	-0.1	-----	-12.3	-----	-8.2	-----	-3.7	-----
40.0	357.8	19.5	5.5	-34.1	-----	2.6	0.7	-9.8	-----	-5.4	-----	-1.3	-----
49.5	380.7	33.1	8.7	-31.4	-----	18.0	4.7	5.1	1.3	10.3	2.7	13.4	3.5
61.5	399.8	33.1	8.3	-38.3	-----	23.5	5.9	10.2	2.6	16.2	4.0	18.3	4.6
70.0	409.7	34.4	8.4	-34.1	-----	31.9	7.8	18.8	4.6	25.1	6.1	26.3	6.4
80.0	419.1	43.9	10.5	-12.5	-----	54.5	13.0	41.9	10.0	48.8	11.6	48.5	11.6
90.0	426.9	53.1	12.4	8.9	2.1	74.9	17.5	62.8	14.7	70.2	16.4	68.5	16.0
100.0	433.4	61.9	14.3	48.3	11.2	106.8	24.6	96.3	22.2	104.1	24.0	100.1	23.1
110.0	439.0	71.7	16.3	93.2	21.2	142.8	32.5	134.2	30.6	142.4	32.4	135.7	30.9
119.5	443.7	86.0	19.4	133.2	30.0	175.3	39.5	168.5	38.0	177.1	39.9	167.9	37.8
129.5	448.1	86.0	19.2	165.7	37.0	192.3	42.9	187.4	41.8	196.0	43.7	185.0	41.3
142.5	453.1	86.0	19.0	217.3	48.0	222.7	49.2	220.4	48.7	229.0	50.5	215.3	47.5
152.5	456.6	86.0	18.8	233.6	51.2	228.7	50.1	227.6	49.8	236.2	51.7	221.3	48.5
162.5	459.7	86.0	18.7	248.5	54.0	236.0	51.3	235.7	51.3	244.4	53.2	228.5	49.7
172.5	462.6	86.0	18.6	270.3	58.4	249.5	53.9	250.2	54.1	259.0	56.0	241.9	52.3
182.5	465.3	86.0	18.5	272.6	58.6	247.8	53.3	248.8	53.5	257.7	55.4	240.2	51.6
192.5	467.8	86.0	18.4	272.7	58.3	246.1	52.6	247.2	52.8	256.1	54.8	238.4	51.0
202.5	470.1	86.0	18.3	269.5	57.3	242.9	51.7	243.9	51.9	252.8	53.8	235.2	50.0
212.5	472.3	86.0	18.2	249.3	52.8	227.4	48.2	227.7	48.2	236.6	50.1	219.8	46.5
222.5	474.3	86.0	18.1	216.4	45.6	204.9	43.2	203.7	42.9	212.6	44.8	197.2	41.6
232.5	476.2	86.0	18.1	175.4	36.8	178.3	37.4	175.2	36.8	184.2	38.7	170.6	35.8
242.5	478.0	86.0	18.0	129.6	27.1	150.0	31.4	144.7	30.3	153.6	32.1	142.3	29.8
250.5	479.4	86.0	17.9	92.1	19.2	127.7	26.6	120.6	25.2	129.6	27.0	120.0	25.0
250.5	479.4	-----	-----	83.9	17.5	119.5	24.9	112.4	23.4	121.3	25.3	111.8	23.3

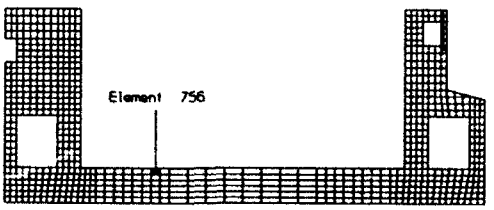

Table 23

Horizontal Stresses at Element 763, Point 3

for Mixture 6

Time	Allowable Stress	Load Case 1		Load Case 2		Load Case 3		Load Case 4		Load Case 5		Load Case 6	
		Stress	% Of Allowable	Stress	% Of Allowable	Stress	% Of Allowable	Stress	% Of Allowable	Stress	% Of Allowable	Stress	% Of Allowable
20.8	101.0	19.6	19.4	-52.3	-----	-60.9	-----	-66.7	-----	-65.4	-----	-62.1	-----
30.0	313.4	19.7	6.3	-38.9	-----	-15.3	-----	-27.6	-----	-24.2	-----	-18.3	-----
36.5	345.9	27.1	7.8	-27.7	-----	3.7	1.1	-8.8	-----	-4.6	-----	0.1	0.0
40.0	357.8	27.1	7.6	-31.4	-----	5.2	1.5	-7.4	-----	-2.9	-----	1.4	0.4
49.5	380.7	30.8	8.1	-33.8	-----	14.9	3.9	2.1	0.5	7.2	1.9	10.4	2.7
61.5	399.8	30.8	7.7	-40.9	-----	20.2	5.0	6.9	1.7	12.8	3.2	15.1	3.8
70.0	409.7	38.6	9.4	-30.5	-----	33.3	8.1	20.4	5.0	26.7	6.5	27.9	6.8
80.0	419.1	46.3	11.1	-6.5	-----	53.0	12.7	41.4	9.9	48.0	11.5	47.3	11.3
90.0	426.9	54.3	12.7	15.1	3.5	70.3	16.5	59.8	14.0	66.7	15.6	64.3	15.1
100.0	433.4	60.9	14.0	53.3	12.3	98.0	22.6	89.4	20.6	96.7	22.3	91.7	21.2
110.0	439.0	67.4	15.4	94.3	21.5	128.3	29.2	121.8	27.8	129.4	29.5	121.8	27.7
119.5	443.7	73.6	16.6	125.3	28.2	150.0	33.8	145.5	32.8	153.4	34.6	143.2	32.3
129.5	448.1	73.6	16.4	157.0	35.0	166.8	37.2	164.1	36.6	172.0	38.4	160.0	35.7
142.5	453.1	73.6	16.2	207.6	45.8	196.9	43.5	196.8	43.4	204.7	45.2	190.1	42.0
152.5	456.6	73.6	16.1	222.8	48.8	202.5	44.4	203.4	44.5	211.4	46.3	195.7	42.9
162.5	459.7	73.6	16.0	236.5	51.4	209.6	45.6	211.2	45.9	219.3	47.7	202.6	44.1
172.5	462.6	73.6	15.9	257.5	55.7	223.0	48.2	225.6	48.8	233.7	50.5	216.0	46.7
182.5	465.3	73.6	15.8	258.9	55.6	220.9	47.5	223.9	48.1	232.0	49.9	213.9	46.0
192.5	467.8	73.6	15.7	257.8	55.1	218.9	46.8	221.9	47.4	230.1	49.2	211.9	45.3
202.5	470.1	73.6	15.6	253.8	54.0	215.3	45.8	218.1	46.4	226.3	48.1	208.2	44.3
212.5	472.3	73.6	15.6	232.7	49.3	199.2	42.2	201.2	42.6	209.4	44.3	192.1	40.7
222.5	474.3	73.6	15.5	199.1	42.0	176.0	37.1	176.5	37.2	184.8	39.0	168.9	35.6
232.5	476.2	73.6	15.4	157.4	33.0	148.8	31.2	147.4	31.0	155.6	32.7	141.7	29.8
242.5	478.0	73.6	15.4	111.2	23.3	119.8	25.1	116.3	24.3	124.6	26.1	112.8	23.6
250.5	479.4	73.6	15.3	73.6	15.4	97.2	20.3	91.9	19.2	100.1	20.9	90.1	18.8
250.5	479.4	-----	-----	59.5	12.4	83.1	17.3	77.7	16.2	86.0	17.9	76.0	15.9

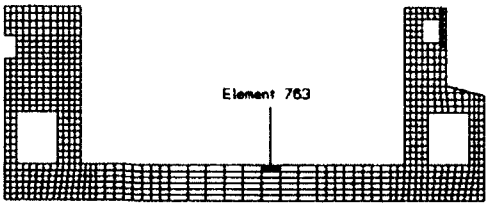

Table 24

Horizontal Stresses at Element 773, Point 4

for Mixture 6

Time	Allowable Stress	Load Case 1		Load Case 2		Load Case 3		Load Case 4		Load Case 5		Load Case 6	
		Stress	% Of Allowable	Stress	% Of Allowable	Stress	% Of Allowable	Stress	% Of Allowable	Stress	% Of Allowable	Stress	% Of Allowable
20.8	101.0	17.6	17.5	-41.3	-----	-46.2	-----	-50.2	-----	-49.2	-----	-47.2	-----
30.0	313.4	18.4	5.9	-18.3	-----	-9.0	-----	-16.0	-----	-13.3	-----	-11.3	-----
36.5	345.9	32.8	9.5	-7.9	-----	2.9	0.8	-4.1	-----	-0.9	-----	0.1	0.0
40.0	357.8	32.7	9.1	-17.8	-----	-1.1	-----	-8.8	-----	-5.4	-----	-4.1	-----
49.5	380.7	32.4	8.5	-30.0	-----	-2.5	-----	-11.3	-----	-7.4	-----	-6.0	-----
61.5	399.8	32.4	8.1	-37.8	-----	-0.9	-----	-10.6	-----	-6.2	-----	-4.9	-----
70.0	409.7	50.8	12.4	-18.9	-----	18.7	4.6	9.1	2.2	13.9	3.4	14.5	3.5
80.0	419.1	49.6	11.8	-8.6	-----	27.6	6.6	18.3	4.4	23.4	5.6	23.0	5.5
90.0	426.9	48.5	11.4	-0.6	-----	34.9	8.2	25.9	6.1	31.2	7.3	30.2	7.1
100.0	433.4	46.3	10.7	18.3	4.2	49.4	11.4	41.1	9.5	46.7	10.8	44.5	10.3
110.0	439.0	45.6	10.4	41.2	9.4	67.6	15.4	60.2	13.7	66.0	15.0	62.4	14.2
119.5	443.7	45.4	10.2	56.0	12.6	79.2	17.8	72.4	16.3	78.5	17.7	73.8	16.6
129.5	448.1	45.4	10.1	76.5	17.1	92.2	20.6	86.5	19.3	92.4	20.6	86.8	19.4
142.5	453.1	45.4	10.0	110.0	24.3	114.6	25.3	110.3	24.3	116.3	25.7	109.2	24.1
152.5	456.6	45.4	10.0	117.0	25.6	117.3	25.7	113.5	24.9	119.6	26.2	112.0	24.5
162.5	459.7	45.4	9.9	124.4	27.1	121.9	26.5	118.3	25.7	124.4	27.1	116.4	25.3
172.5	462.6	45.4	9.8	137.5	29.7	131.3	28.4	128.3	27.7	134.4	29.1	125.9	27.2
182.5	465.3	45.4	9.8	135.4	29.1	128.4	27.6	125.4	27.0	131.6	28.3	122.9	26.4
192.5	467.8	45.4	9.7	132.6	28.4	126.2	27.0	123.1	26.3	129.3	27.6	120.7	25.8
202.5	470.1	45.4	9.7	128.2	27.3	122.9	26.2	119.7	25.5	125.9	26.8	117.4	25.0
212.5	472.3	45.4	9.6	111.2	23.6	110.3	23.4	106.4	22.5	112.6	23.8	104.8	22.2
222.5	474.3	45.4	9.6	86.3	18.2	92.7	19.5	87.8	18.5	94.0	19.8	87.2	18.4
232.5	476.2	45.4	9.5	56.5	11.9	72.3	15.2	66.2	13.9	72.4	15.2	66.6	14.0
242.5	478.0	45.4	9.5	24.2	5.1	50.8	10.6	43.3	9.1	49.5	10.4	45.3	9.5
250.5	479.4	45.4	9.5	-1.6	-----	34.1	7.1	25.5	5.3	31.7	6.6	28.6	6.0
250.5	479.4	-----	-----	100.0	20.9	135.7	28.3	127.1	26.5	133.3	27.8	130.2	27.2

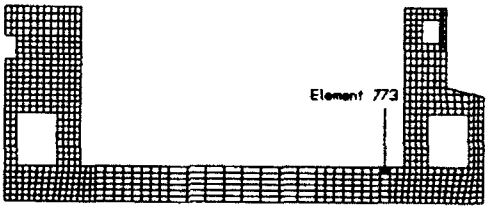

Table 25

Horizontal Stresses at Element 993, Point 2

for Mixture 6

Time	Allowable Stress	Load Case 1		Load Case 2		Load Case 3		Load Case 4		Load Case 5		Load Case 6	
		Stress	% Of Allowable	Stress	% Of Allowable	Stress	% Of Allowable	Stress	% Of Allowable	Stress	% Of Allowable	Stress	% Of Allowable
70.8	101.0	2.1	2.1	-7.0	-----	-7.0	-----	-7.6	-----	-7.5	-----	-7.2	-----
74.0	248.1	1.7	0.7	-3.0	-----	-1.7	-----	-2.3	-----	-2.0	-----	-2.0	-----
75.0	264.7	1.7	0.6	25.0	9.5	23.4	8.9	23.5	8.9	23.9	9.0	23.0	8.7
75.8	274.9	11.7	4.2	28.8	10.5	25.6	9.3	26.0	9.5	26.5	9.6	25.2	9.2
80.0	313.4	8.7	2.8	19.2	6.1	16.6	5.3	17.3	5.5	17.7	5.7	16.2	5.2
80.8	318.2	5.7	1.8	58.8	18.5	58.8	18.5	61.7	19.4	61.9	19.4	58.7	18.4
85.0	339.9	9.3	2.7	106.8	31.4	83.5	24.6	91.5	26.9	91.3	26.9	83.6	24.6
90.0	357.8	12.2	3.4	120.6	33.7	87.7	24.5	97.4	27.2	97.4	27.2	87.7	24.5
95.0	371.1	18.9	5.1	146.7	39.5	106.4	28.7	117.3	31.6	117.6	31.7	106.2	28.6
100.0	381.7	23.4	6.1	159.7	41.8	110.8	29.0	123.2	32.3	123.6	32.4	110.3	28.9
100.8	383.1	27.9	7.3	153.3	40.0	103.5	27.0	115.2	30.1	115.8	30.2	102.9	26.9
105.0	390.4	28.5	7.3	167.6	42.9	116.7	29.9	128.8	33.0	129.6	33.2	115.9	29.7
110.0	397.8	28.5	7.2	178.7	44.9	121.7	30.6	135.1	34.0	136.1	34.2	120.7	30.3
110.8	398.8	34.5	8.7	165.1	41.4	106.6	26.7	118.8	29.8	120.1	30.1	105.4	26.4
115.0	404.1	42.6	10.5	166.1	41.1	112.1	27.7	123.2	30.5	125.0	30.9	110.4	27.3
118.0	407.6	46.5	11.4	154.8	38.0	104.1	25.5	113.3	27.8	115.5	28.3	102.1	25.0
124.5	414.2	46.4	11.2	164.9	39.8	113.4	27.4	122.9	29.7	125.4	30.3	111.1	26.8
132.5	421.2	46.4	11.0	180.9	42.9	122.6	29.1	132.5	31.5	135.3	32.1	120.1	28.5
142.5	428.6	46.4	10.8	195.5	45.6	130.6	30.5	140.9	32.9	143.9	33.6	127.9	29.8
152.5	434.9	46.4	10.7	193.0	44.4	126.5	29.1	136.7	31.4	139.8	32.2	123.7	28.4
172.5	445.1	46.4	10.4	188.5	42.3	123.4	27.7	133.3	30.0	136.6	30.7	120.4	27.1
192.5	453.1	46.4	10.2	151.7	33.5	97.9	21.6	106.3	23.5	109.8	24.2	94.8	20.9
212.5	459.7	46.4	10.1	92.9	20.2	60.1	13.1	65.8	14.3	69.3	15.1	56.9	12.4
232.5	465.3	46.4	10.0	-8.0	-----	-3.2	-----	-2.1	-----	1.4	0.3	-6.4	-----
250.5	469.7	46.4	9.9	-108.8	-----	-62.8	-----	-66.6	-----	-63.0	-----	-65.9	-----
250.5	469.7	-----	-----	-123.5	-----	-77.4	-----	-81.2	-----	-77.7	-----	-80.6	-----

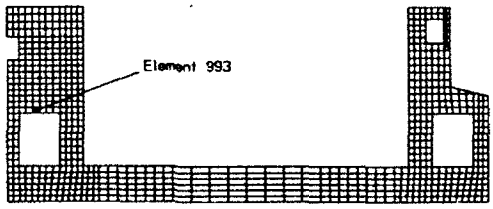

at 172.5 days after the start of construction the maximum stress is 259.0 psi and is only at 56.0 percent of the allowable stress. Even for load case 2 which contains no creep and shrinkage, the maximum stress of 272.8 psi at 182.5 days is only 58.6 percent of the allowable stress. Based on the figures and tables, the stresses are not critical and do not indicate that cracking of the structure is imminent.

163. To validate the results of the Phase I study with respect to requirements in ETL 1110-2-324, comparisons of results from Phase I were compared to results from Phase II. Comparison of the two sets of results showed that the results from Phase I fell within the bounding analyses performed in Phase II. One such comparison is shown in Figure 175. In this figure, the time history of horizontal stress from Phase I is plotted for element 763 versus load cases from Phase II. Load cases 3 and 4 were deleted so that the curve from Phase I could be clearly seen. As can be seen in Figure 175, the curve from the Phase I study falls between the upper- and lower- bound curves (load cases 5 and 6) from the Phase II study. The close proximity of the curves indicates that results from Phase I would not change dramatically.

164. Figures 176 through 181 are plots of horizontal stress distribution through the base slab of the lock at two locations. Figures 176 and 177 are plotted at 172.5 days after start of construction at which time the stresses in the slab have reached the maximum. If these stress distributions were converted into a resultant axial force and bending moment, it can be seen, particularly in Figure 176 for the section near the center of the lock, that the cases which include temperature effects would produce resultant forces and moments significantly larger than those for the gravity only case (load case 1).

165. Figures 178 and 179 are horizontal stress distribution plots at 250.5 days and just prior to the placement of service loads. For this particular time in the analysis, the magnitude of the resultant axial forces and bending moments differ only slightly from the gravity-only case to the cases containing thermal effects. The fact that the distributions are so similar can be attributed to the temperature rise which occurs and causes the temperature of the structure to approach its original condition. This, in turn, minimizes the stresses due to thermal effects. Since the temperatures in the structure at 250.5 days are beginning to approach the temperatures at which the structure was placed, the stresses due to thermal loads are getting very

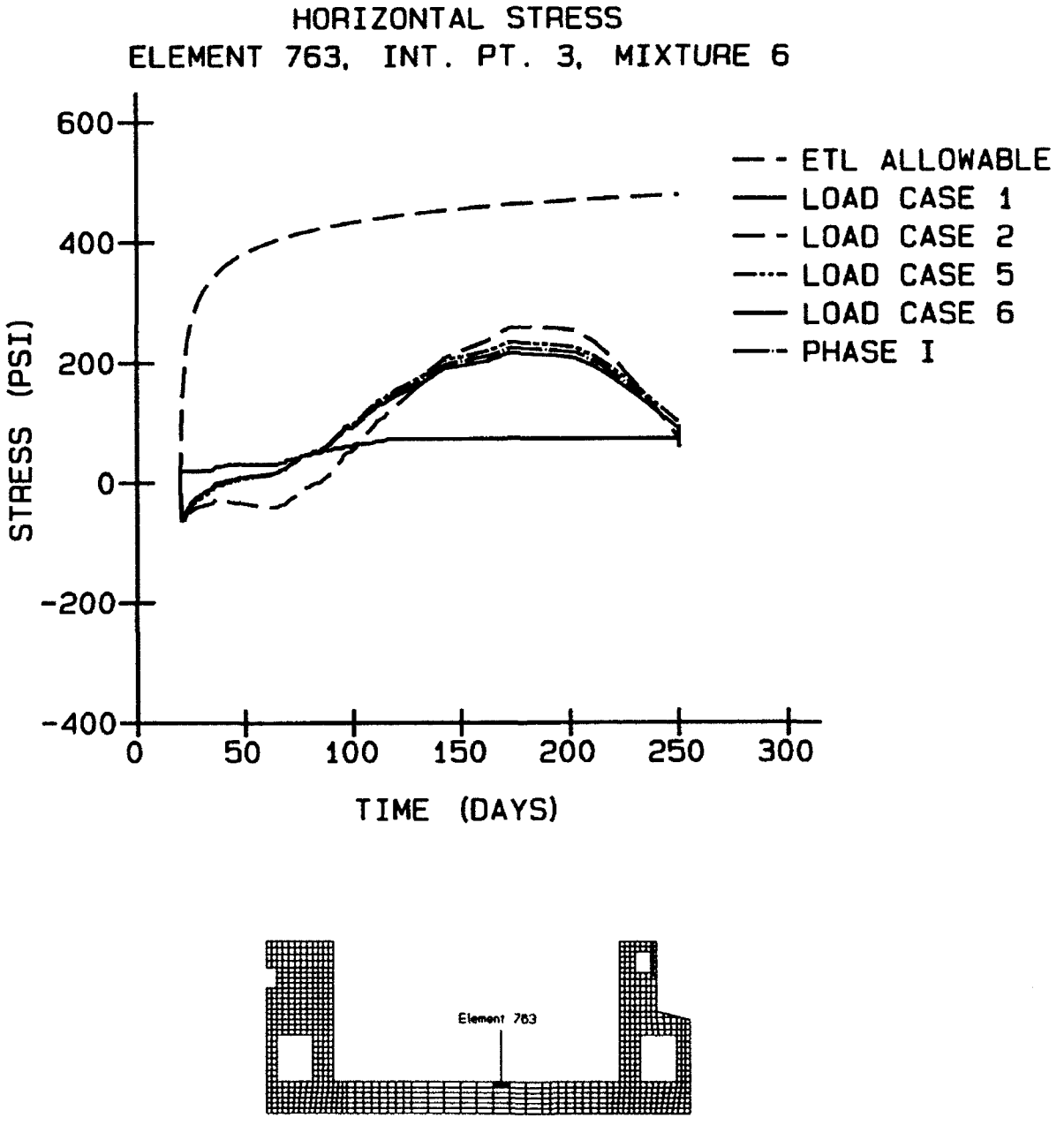

Figure 175. Phase I and II horizontal stresses, element 763, point 1

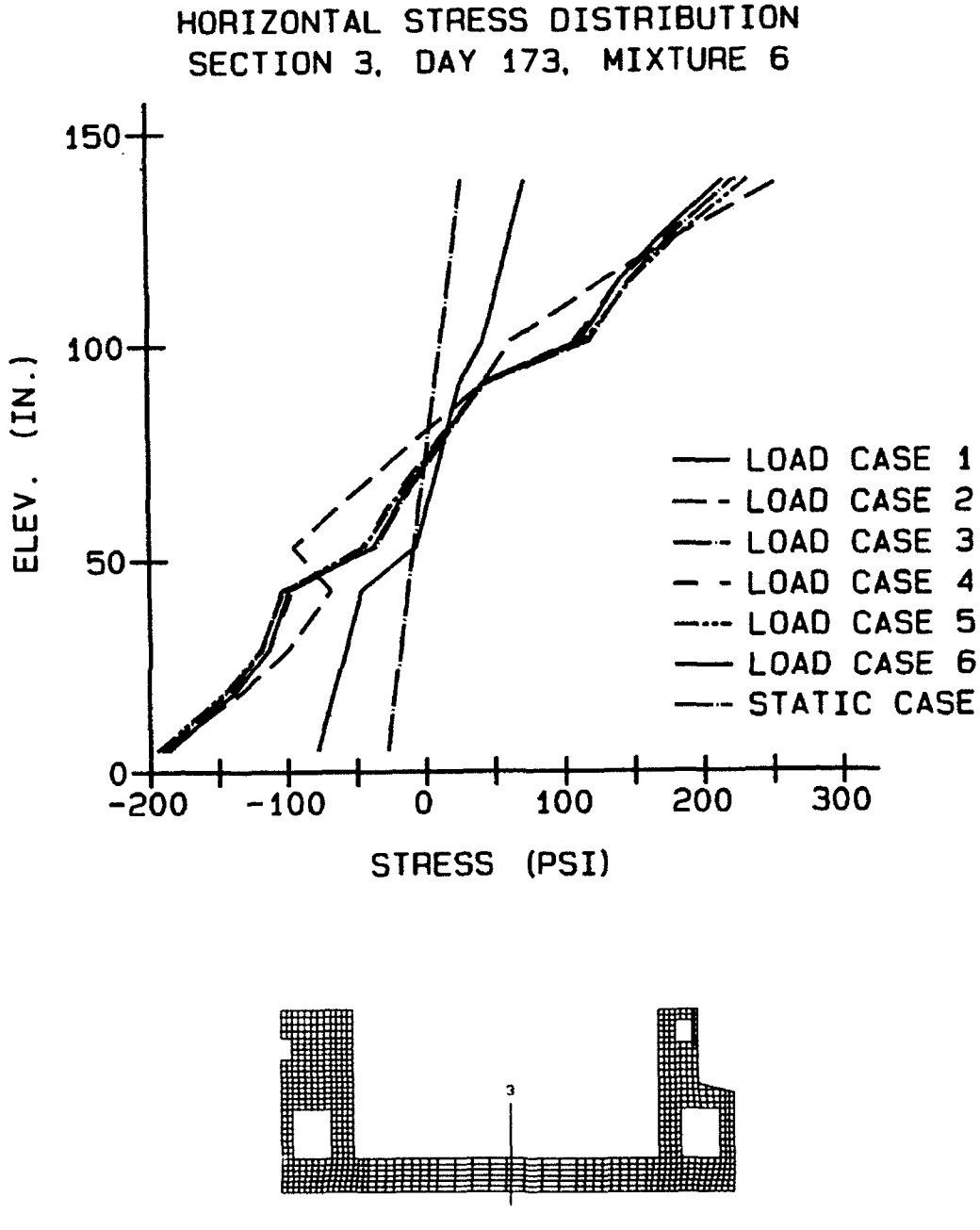

Figure 176. Stress distribution at floor section 3, day 173, no service load included

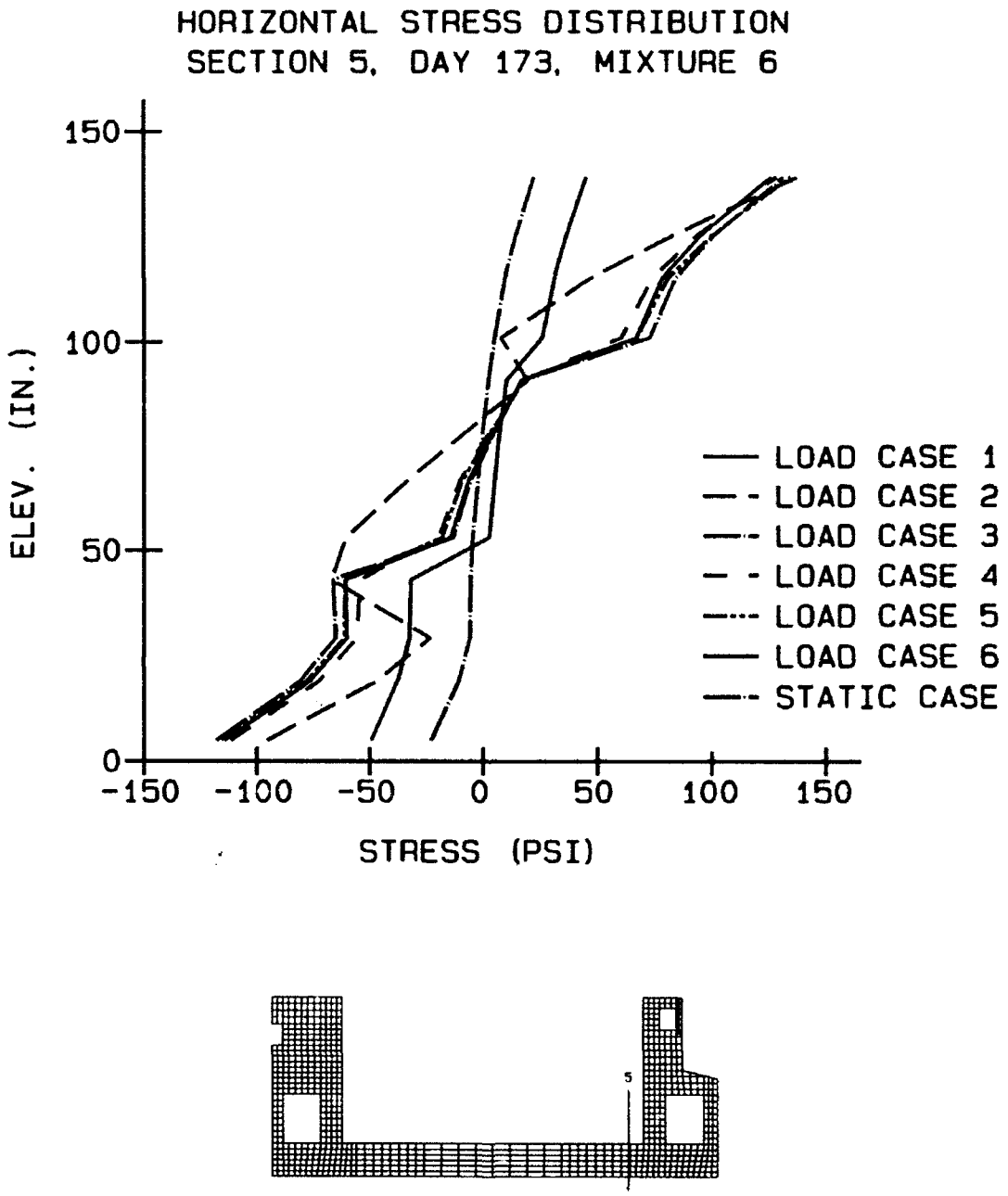

Figure 177. Stress distributions at floor section 5, day 173, no service load included

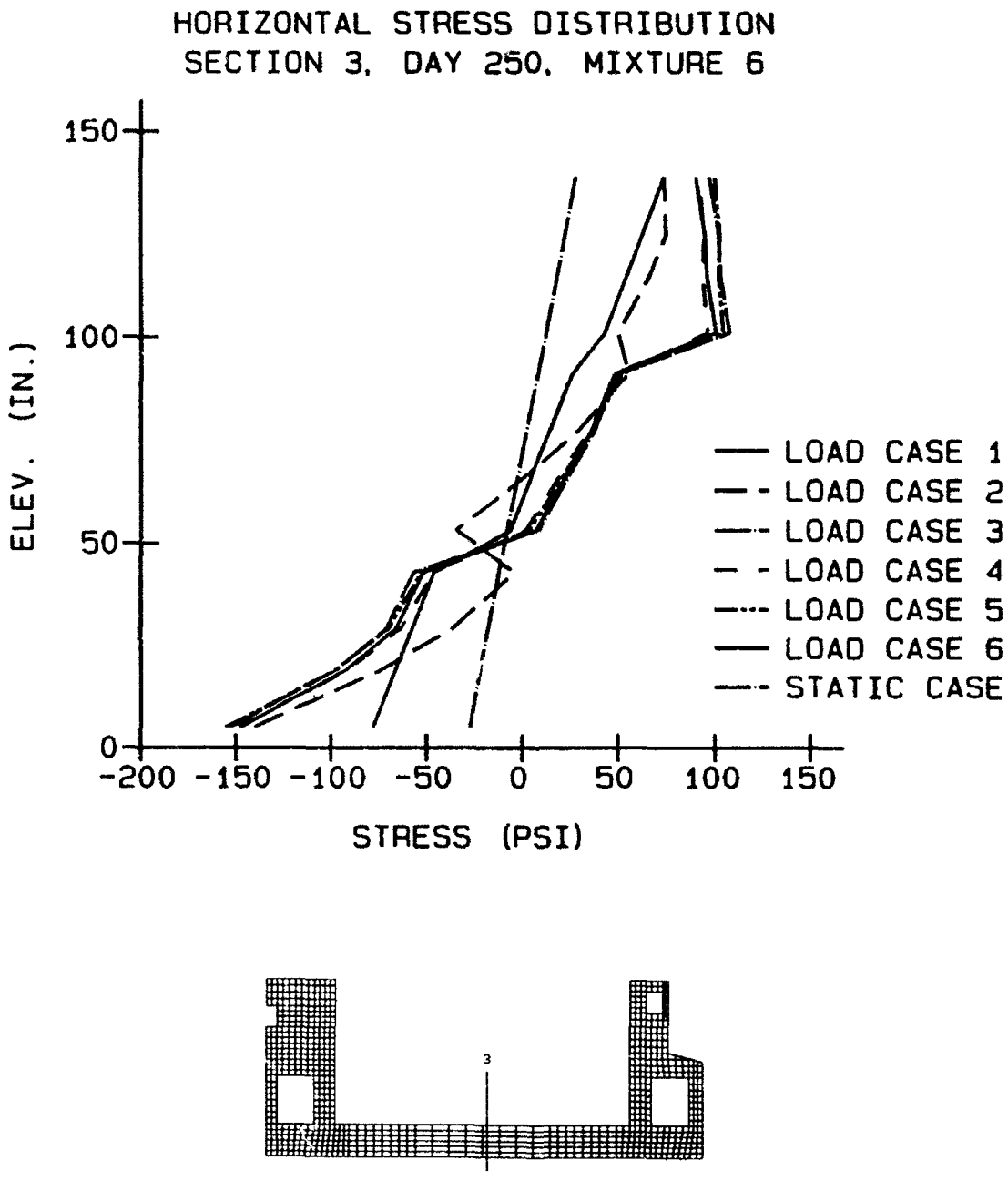

Figure 178. Stress distributions at floor section 3, day 250, no service load included

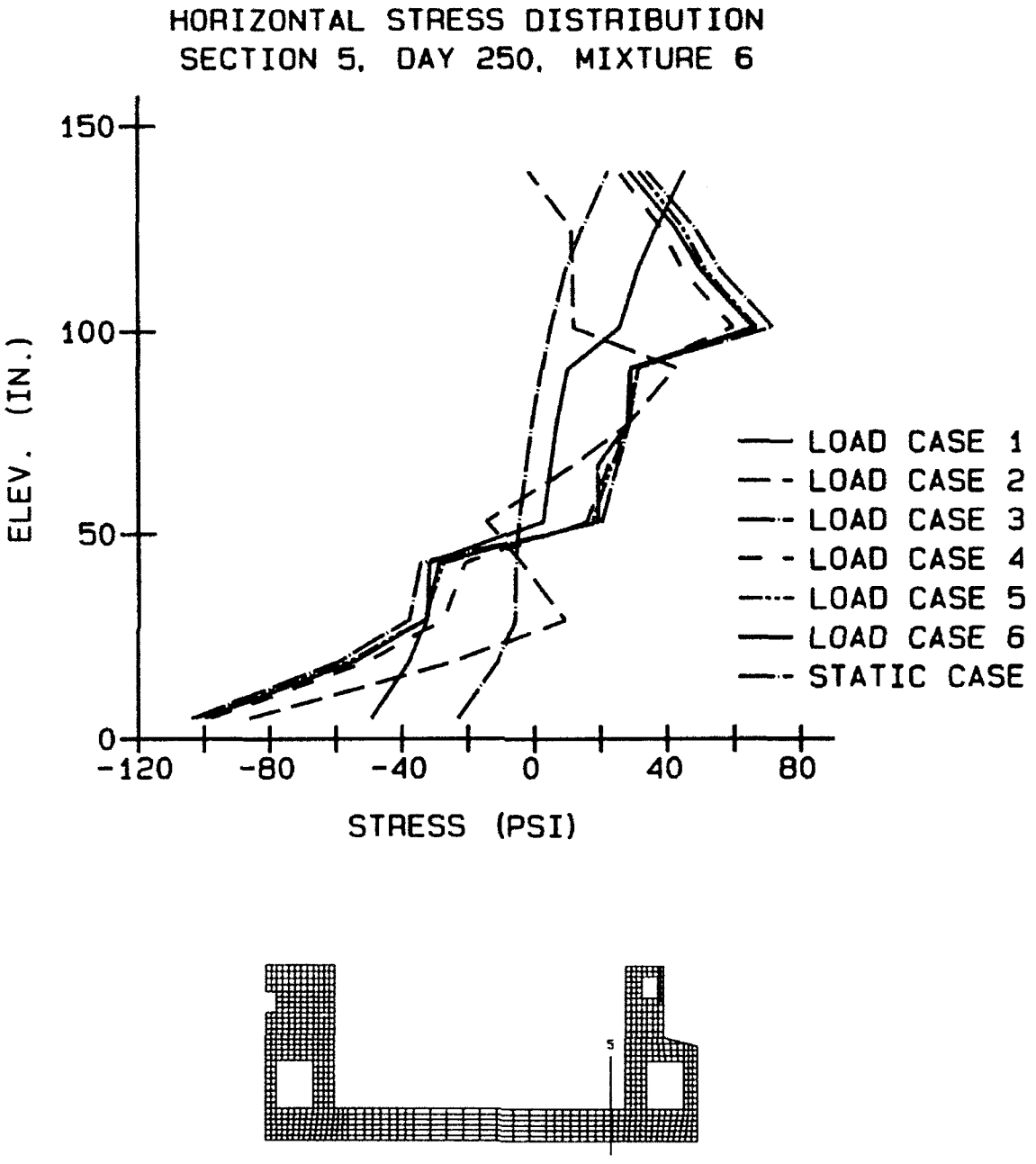

Figure 179. Stress distribution at floor section 5, day 250, no service load included

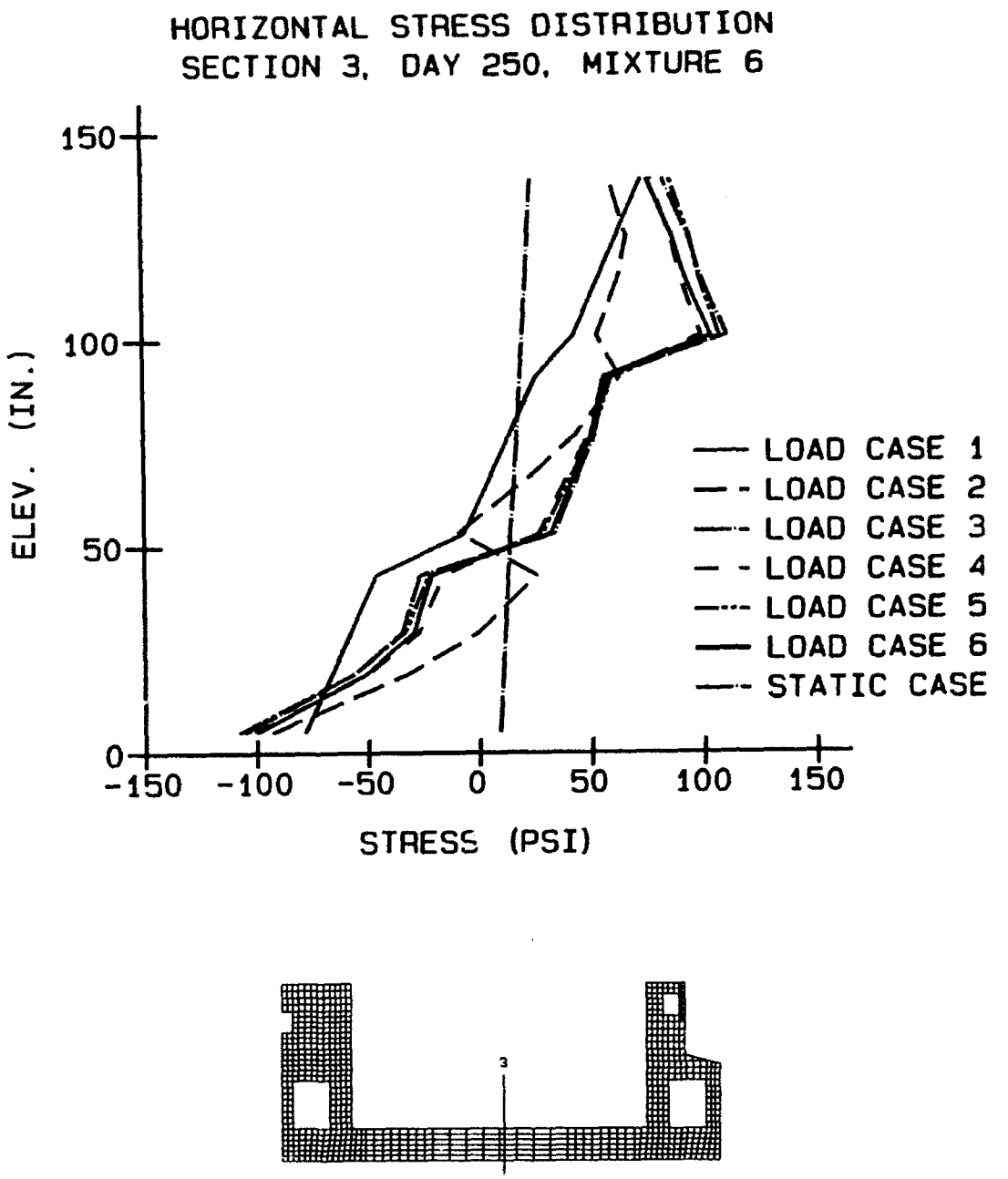

Figure 180. Stress distributions at floor section 3, day 250, service load included

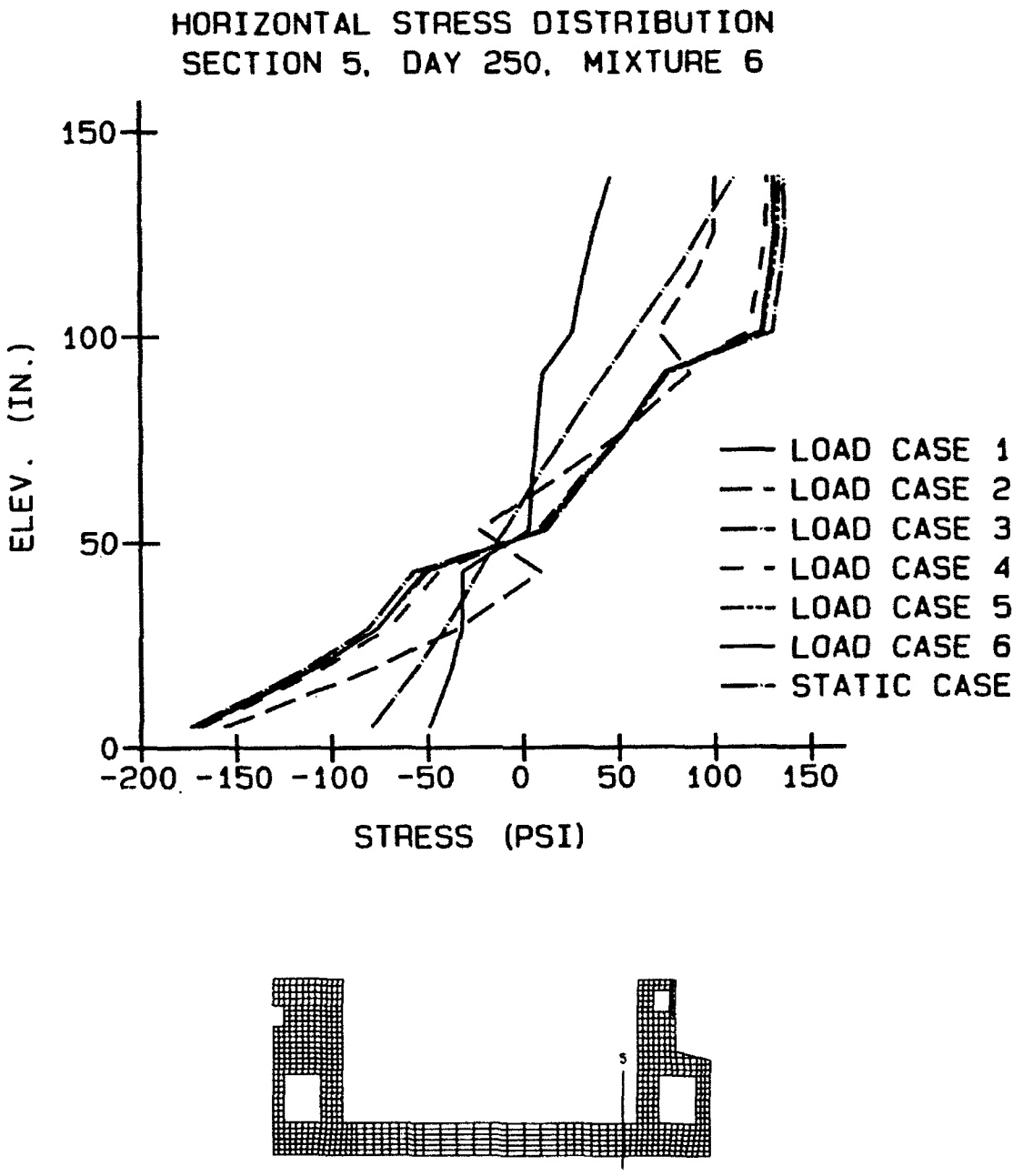

Figure 181. Stress distributions at floor section 5, day 250, service load included

low and the total stress at this point in time is due primarily to gravity loads.

166. Figures 180 and 181 are horizontal stress distribution plots in which service loads have now been applied. Comparing Figures 178 and 180, distributions at the center of the base slab before and after service loads are applied, the change in the distribution is very small despite the additional service loads. In comparing Figures 179 and 181 however, distributions near the land wall before and after service load application, there is a significant increase in the magnitude resultant axial force and bending moment upon the introduction of the service loads. This is the result of the combination of two effects. First, because the uplift is a considerably larger load than the resultant of the remainder of the service load forces, there is a reverse in the bending effect acting on the structure. Secondly, due to the stiffness of the walls, the slab between the two walls behaves very much like a fixed beam. The fixed-beam action creates a situation where the moment due to the service loads will be larger near the wall than at the center of the slab, and the direction of bending from the uplift will create tensile stresses in the top of the slab at the wall and negative stresses in the top of the slab near the center.

167. Also included in Figures 176 through 181 is a plot of the horizontal stress distribution of a gravity turn on analysis, designated as the static case. This case is similar to what is done in a design office when performing a finite element analysis. As can be seen in each of the Figures 176 through 179, the distribution for the static case, due to dead weight of the structure only, differs slightly from the distribution for load case 1 which is the incrementally constructed model which neglects creep, shrinkage, and thermal effects. The static case in Figures 180 and 181 includes service loads. Comparison of the static case and load case 1 in Figures 176 through 179 indicates that due to the incremental construction process alone, a change in the stress state occurs. It is anticipated that this difference can be attributed to the locked-in stresses, resulting from the incremental construction, causing a redistribution of stress.

168. Figures 182 through 186 are contour plots of the horizontal stresses at a point in time when the stresses are near the maximum. As can be seen in the figures, the plots are very similar from load case to load case. Each plot shows how the stress gradient through the slab is fairly constant except near the walls and that the stresses within the walls are minimal

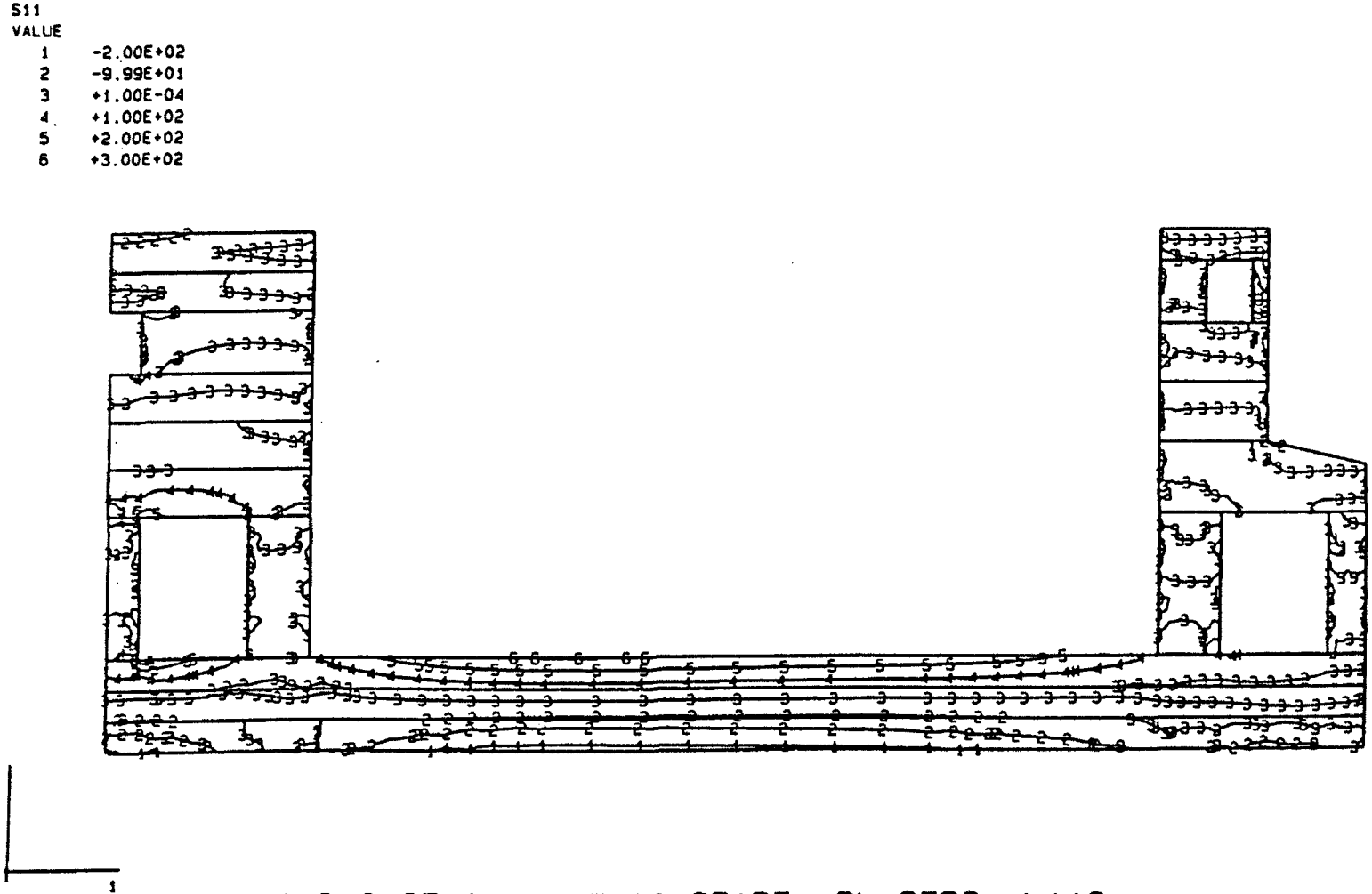

Figure 182. Horizontal stress contours, day 183, load case 2

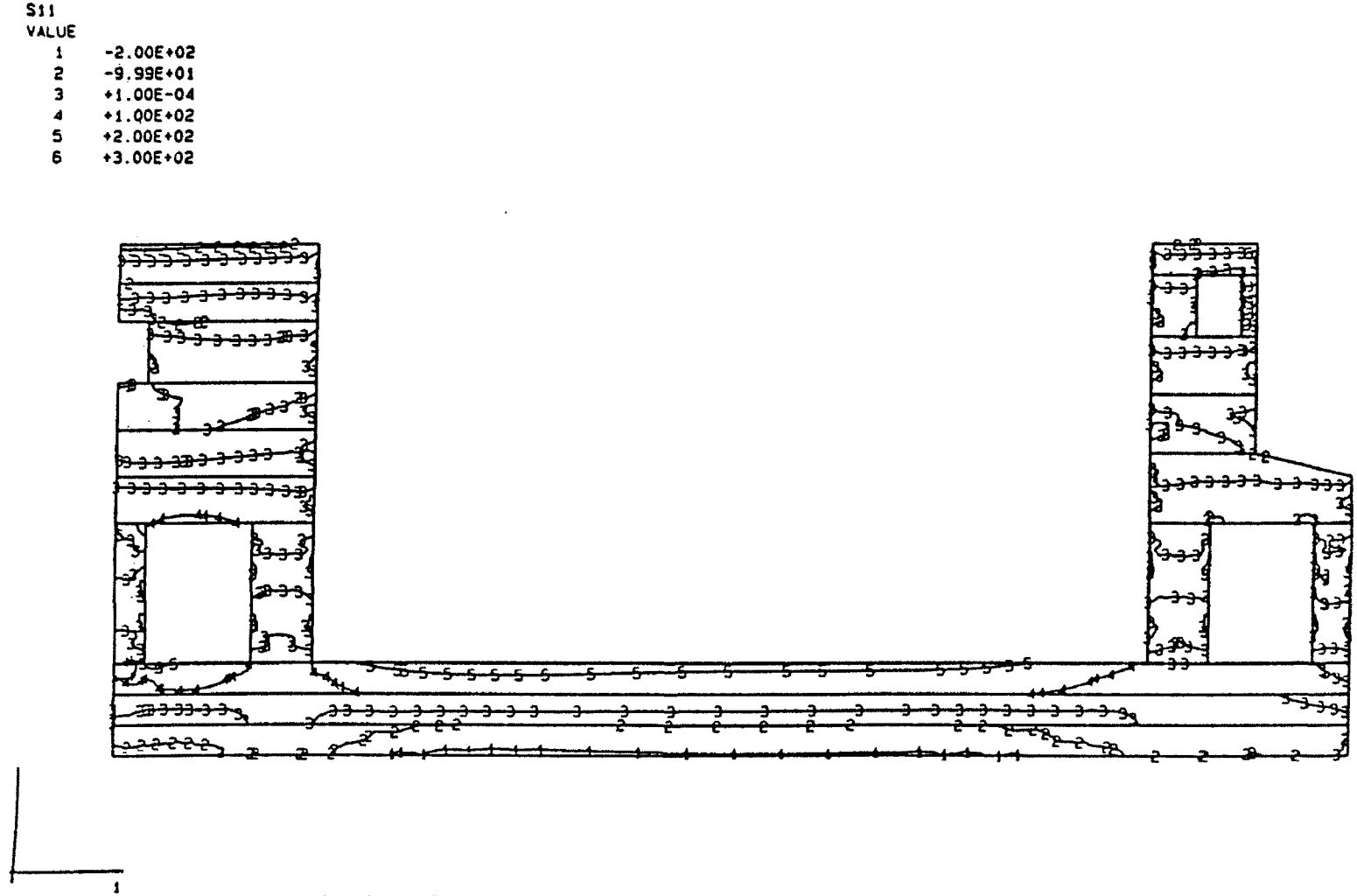

Figure 183. Horizontal stress contours, day 183, load case 3

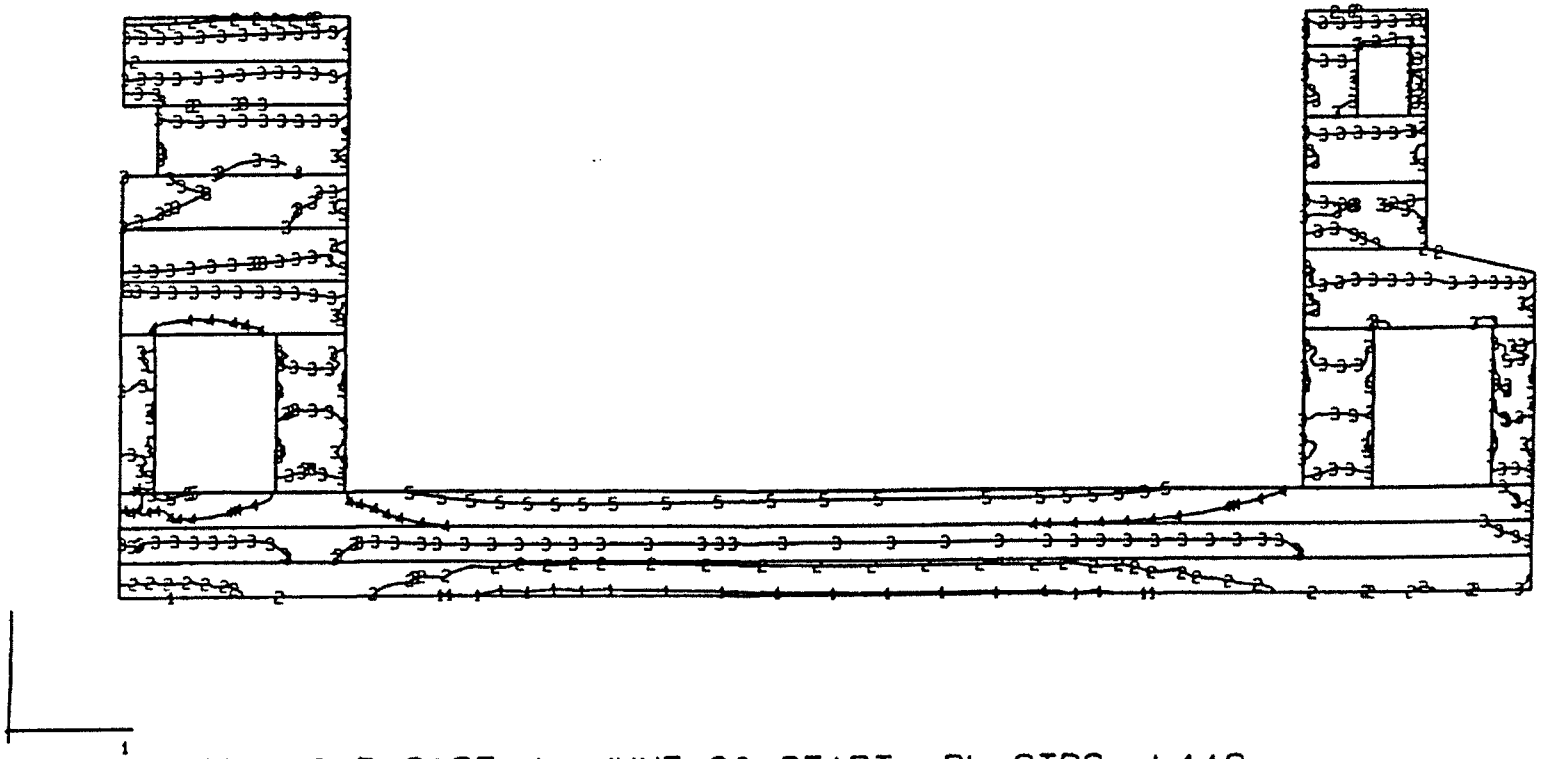

Figure 184. Horizontal stress contours, day 184, load case 4

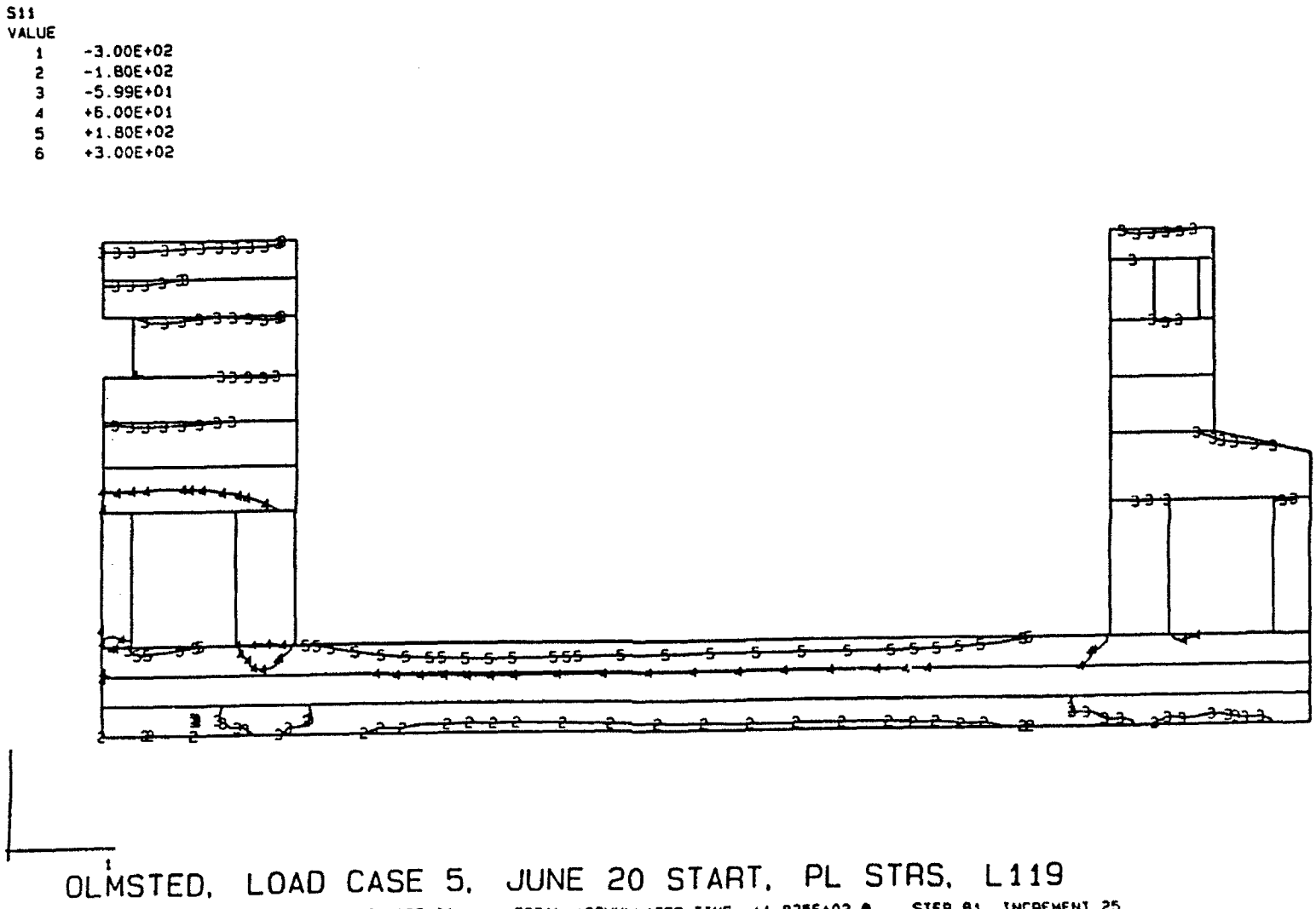

Figure 185. Horizontal stress contours, day 183, load case 5

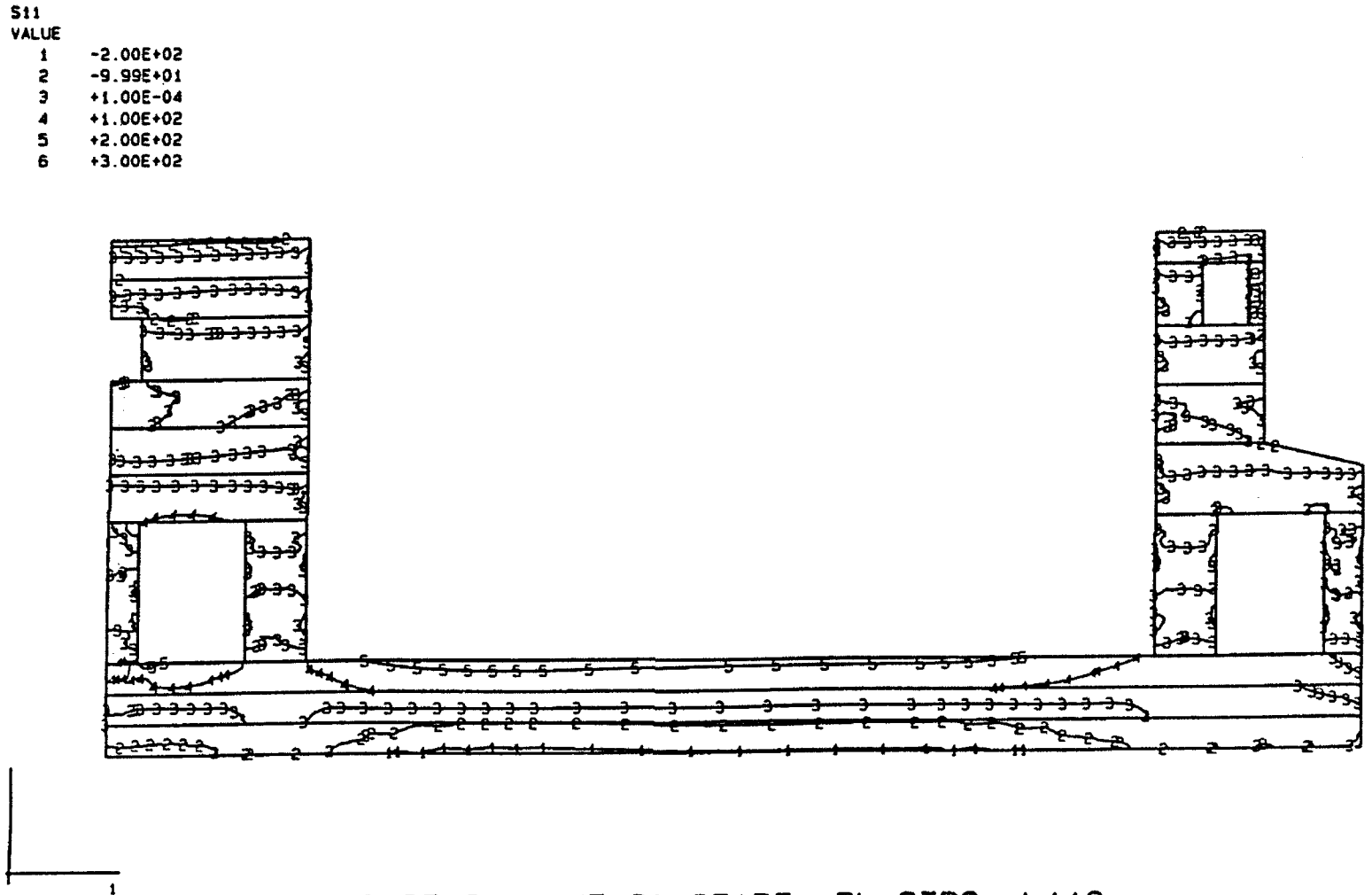

Figure 186. Horizontal stress contours, day 186, load case 6

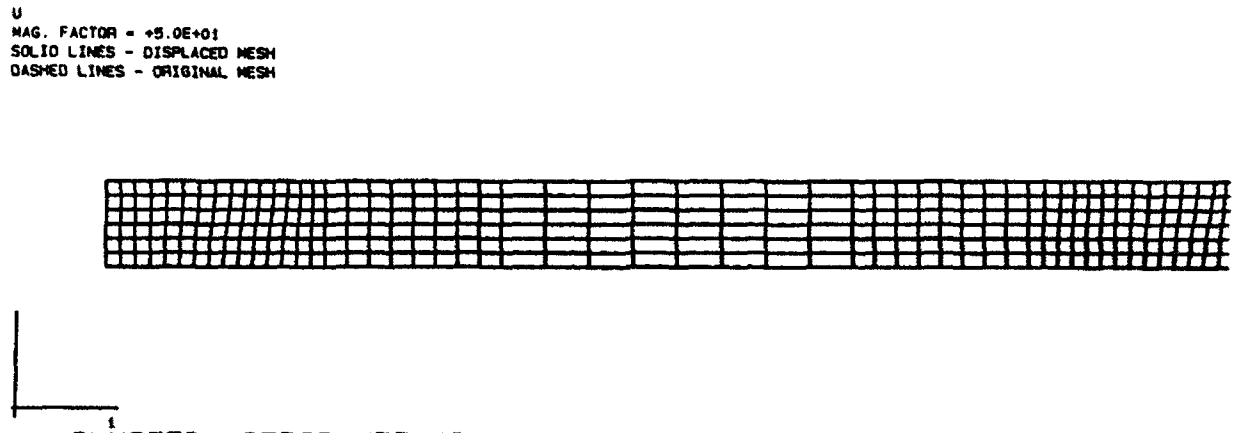

Figure 187. Displaced shape at 30 days, load case 5

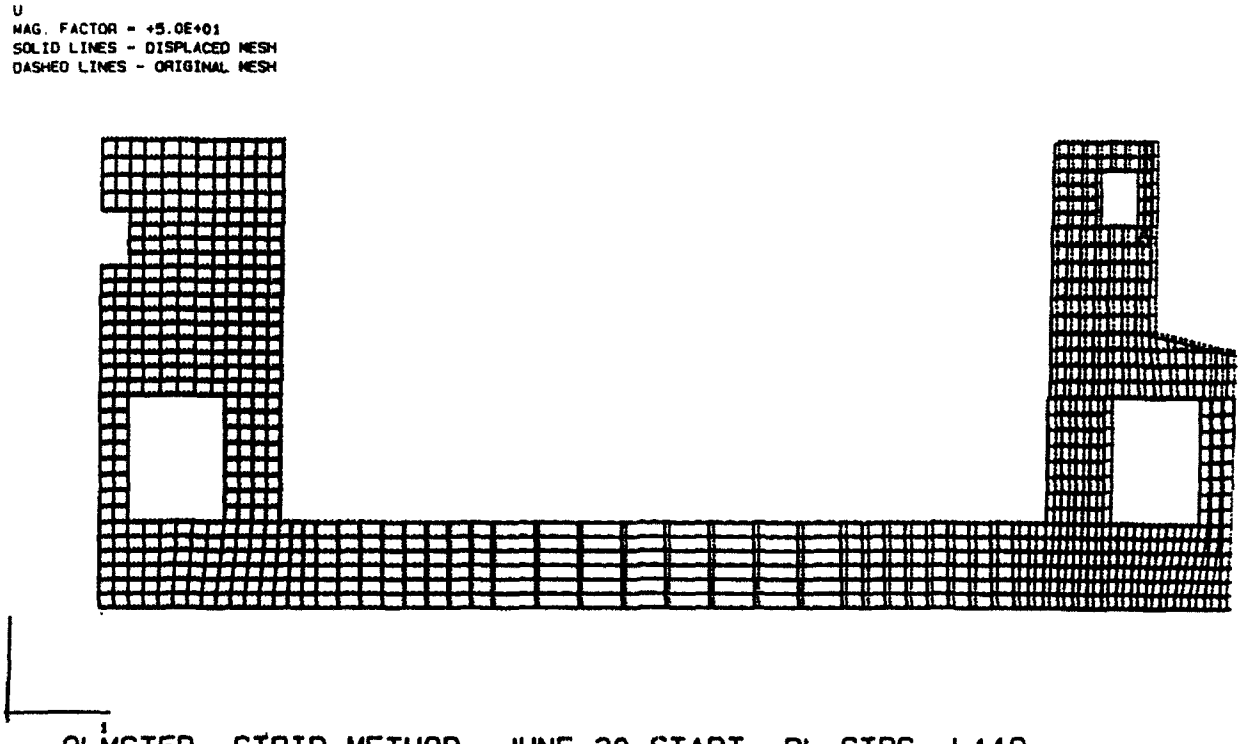

Figure 188. Displaced shape at 120 days, load case 5

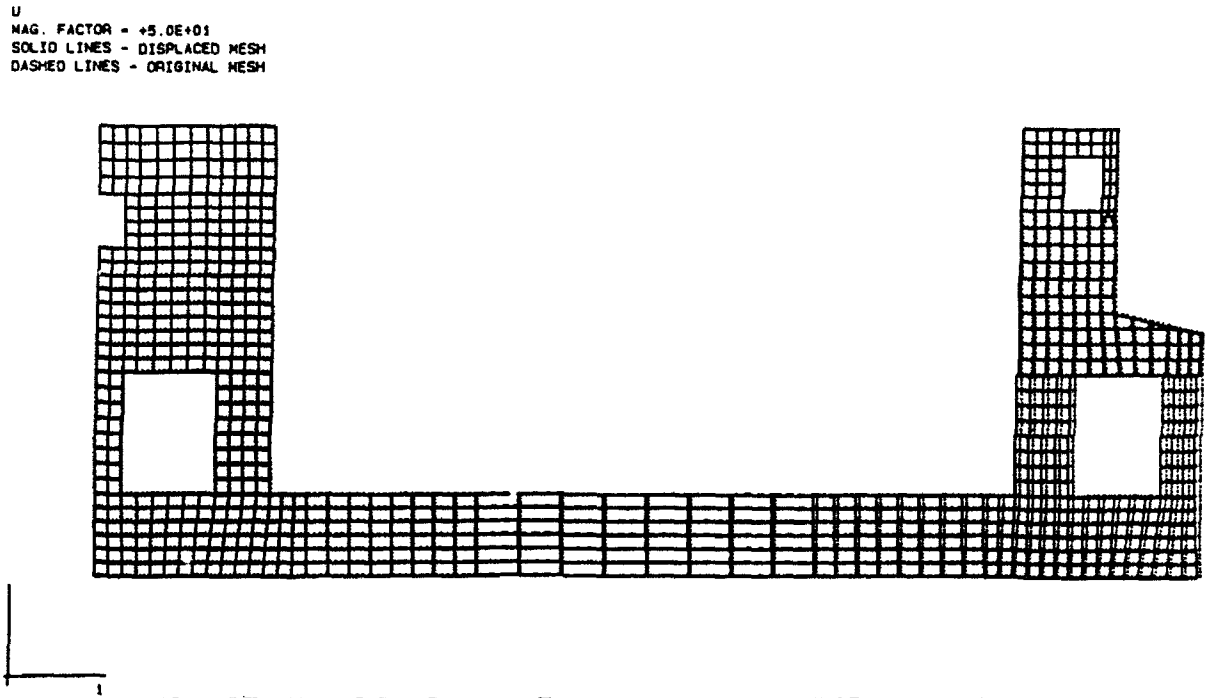

Figure 189. Displaced shape at 173 days, load case 5

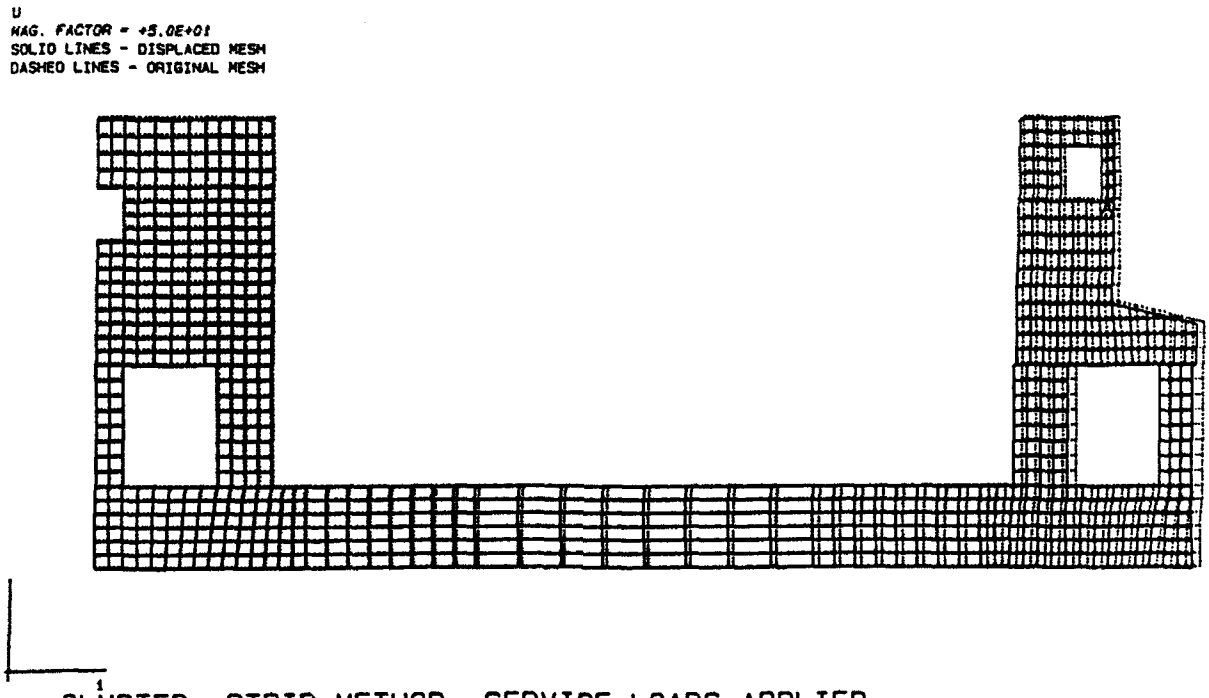

Figure 190. Displaced shape at 250 days, load case 5

except near the corners of the culvert. While the gradient within the slab is fairly constant, the effects of the model not being completely symmetrical about the lock center line can be seen by the slight dips in the contour lines which occur at about one-third of the distance within the chamber from the middle wall.

169. Finally, displaced shapes for the worst case are shown in Figures 187 through 190. These displaced shapes are for load case 5 at 30, 119.5, 172.5, and 250.5 days after the start of construction and are plotted at a magnification of 50. Through close examination of Figure 189, the bending of the slab which produces the tensile stresses in the top of the slab can be seen. Discontinuities at the lift lines is a result of the manner in which the model was constructed. New lifts are placed in a stress-free state and in their defined configuration. Since the lift below a newly placed lift has already deformed, a discontinuity exists when the new lift is placed. This discontinuity is retained throughout the analysis by specifications made in the input data.

Conclusions

170. An important conclusion to be drawn from the fact that for both mixtures 6 and 11 the results from Phase I were enveloped by the results of Phase II. Therefore, the Phase I results are validated for the variation in material properties as modeled in Phase II, and it can be concluded that the monolith is constructable under the conditions assumed for these analyses.

171. The stresses obtained in the Phase II analyses were significantly below the allowable tensile stresses specified in ETL 1110-2-324 (Headquarters, Department of the Army, 1990) . The maximum stress obtained out of the 10 analyses performed was less than 6[illegible] percent of the ETL 1110-2-324 allowable, indicating that cracking of the structure in the cross-sectional plane is not a problem.

172. The bounding analyses performed in the Phase II study also showed that the changes in the creep compliance and shrinkage curves due to factoring do not produce comparable percentage changes in the stresses. Although differences in stresses from one load case to the next were small, the controlling load case for both mixtures was load case 5, minimum creep and maximum shrinkage.

173. Even though factoring of creep and shrinkage did not produce significant changes in stresses, it should be noted that decreases in the creep compliance produced increases in the magnitude of tensile stresses. Close examination of time-history plots indicated that creep had a more significant change on resulting stresses than shrinkage.

174. The results from Phase II showed the tensile stresses within the structure are primarily temperature related and are being driven by the ambient air conditions at late times. This was particularly evident in the base slab where stresses at the top of the slab continued to rise for 2 months after the last lift was placed, eliminating the placement of concrete in the walls as a reason for these stresses. As a result of the stresses being driven by ambient temperatures, a cycling of the stresses with respect to time can be seen in the time-history plots; and, therefore, the stresses within the structure will never stabilize.

175. Comparisons of the gravity only load case to the cases containing the effects of temperature show significant differences in the structural response. These comparisons also show that, for the concrete mixtures used, gravity load is not the major contributor to the maximum tensile stresses.

176. As stated in the Phase I conclusions, the analyses performed provide valid results for an early summer construction start, the mixtures specified, and the geometries used. Changes to these parameters may require additional analyses to be performed.

177. Finally, it should be mentioned that reinforcing steel is not considered in this NISA study. Generally, reinforcement steel tends to provide strength, stability, and ductility at a section should a crack occur. Also, reinforcement steel tends to more evenly distribute cracks should they occur. However, the inclusion of reinforcing steel in the analysis will have minimal effect on the stresses as long as no cracking occurs. When interpreting and evaluating the results of the NISA study, it is important to remember the general conservatism in the assumption of no reinforcing steel.

Recommendations

178. Based on the conditions assumed for the analyses performed, the construction scheme used, with 54-ft long monoliths and no vertical construction joints, appears to be constructable.

179. Since some concrete is likely to be placed at times outside the time frame of these analyses, at least one analysis should be made using a late fall or early winter start of placement.

180. Since tensile stresses in the floor are primarily due to long-term temperature changes rather than heat rise during hydration of the cementitious materials, the requirement of a 60 °F placement temperature in the floor may not be necessary. Using a higher placement temperature would result in a cost savings for the USAED, Louisville, and should be investigated.

181. Since load case 5 (see Table 14) provided the worst case for both mixtures, it is recommended that load case 5 be used in performing any additional analyses. This would ensure that conservative results would be obtained.

REFERENCES

ACI Committee 209. 1989. "Prediction of Creep, Shrinkage and Temperature Effects in Concrete Structures," Report 209-R82, Manual of Concrete Practice, American Concrete Institute, Detroit, MI.

American Society for Testing and Materials. 1990. 1990 Annual Book of ASTM Standards, Philadelphia, PA.

Bevins, T. L., Garner, S., and Hall, R. L. "Two-Dimensional Seismic Analysis of Olmsted Locks, Chamber Monolith, Lower Miter Gate Monolith, and Bridge Pier Monolith" (Technical Report in preparation), U.S. Army Engineer Waterways Experiment Station, Vicksburg, MS.

Bombich, A. A., Norman, C. D., and Jones, H. W. 1987. "Thermal Stress Analyses of Mississippi River Lock and Dam 26 (R)," Technical Report SL-87-21, U.S. Army Engineer Waterways Experiment Station, Vicksburg, MS

CASE Task Group on Pile Foundations. 1983 (Sep). "Basic Pile Group Behavior," Technical Report K-83-1, U.S. Army Engineer Waterways Experiment Station, Vicksburg, MS.

Garner, S., and Hammons, M. 1991. "The Development and Use of a Time-Dependent Cracking Model for Concrete," Technical Report SL-91-7, U.S. Army Engineer Waterways Experiment Station, Vicksburg, MS.

Hammons, M., Neeley, B., Alexander, M., Bombich, A., and Garner, S. 1991. "Concrete Mixture Selection and Characterization Study, Olmsted Locks and Dam, Ohio River," Technical Report SL-91-9, U.S. Army Engineer Waterways Experiment Station, Vicksburg, MS.

Hammons, M., Smith, Donald M., and Neely, Billy D. 1990 (Jul). "Red River Waterway Thermal Studies," Technical Report SL-90-8, U.S. Army Engineer Waterways Experiment Station, Vicksburg, MS.

Headquarters, Department of the Army. 1990. "Engineering and Design, Special Design Provisions for Massive Concrete Structures," Engineering Technical Letter 1110-2-324, Washington, DC.

Hibbit, Karlsson, and Sorenson. 1988. ABAQUS User's Manual, Version 4.8, Providence, RI.

Hough, B. K. 1969. Basic Soils Engineering, 2nd ed., Ronald Press Co., New York, NY.

Jurges, W. 1924. "Der Warmeubergang en einer evenen Wand" (Heat Transfer to a Plane Mass), Beih. z. Ges. Ing. 1, No. 19.

Kersten, M. S. 1949. "Lab Research for the Documentation of the Thermal Properties of Soils," Final Report, U.S. Army Engineer District, St. Paul, St. Paul, MN.

Norman, C. D., Campbell, R., and Garner, S. 1988. "Analysis of Concrete Cracking in Lock Wall Resurfacing," Technical Report REMR-CS-15, U.S. Army Engineer Waterways Experiment Station, Vicksburg, MS.

Reese, L., Cooley, L., and Radhakrishnan, N. 1984. "Laterally Loaded Piles and Computer Program COM624G," Technical Report K-84-2, U.S. Army Engineer Waterways Experiment Station, Vicksburg, MS.

Truman, K. Z., Petruska, D., and Fehri, A. 1992. "Evaluation of Thermal and Incremental Construction Effects for Monoliths AL-3 and AL-5 of the Melvin Price Locks and Dams," Contract Report ITL-92-3, U.S. Army Engineer Waterways Experiment Station, Vicksburg, MS.

US Army Corps of Engineers. 1990. "Special Design Provisions for Massive Concrete Structures," Engineering Technical Letter 1110-2-324, Washington, DC.

Waterways Experiment Station Cataloging-in-Publication Data

Garner, Sharon
Nonlinear, incremental structural analysis of Olmsted locks and dams / by Sharon Garner ... [et al.] ; prepared for US Army Engineer District, Louisville.
2 v. : ill. ; 28 cm. — (Technical report ; SL-92-28)
Includes bibliographical references.
1. Locks (Hydraulic engineering) — Ohio River. 2. Thermal stresses — Computer programs. 3. Concrete — Thermal properties. Structural analysis (Engineering) I. Garner, Sharon B. II. United States. Army. Corps of Engineers. Louisville District. III. U.S. Army Engineer Waterways Experiment Station. IV. Series: Technical report (U.S. Army Engineer Waterways Experiment Station) ; SL-92-28.
TA7 W34 no.SL-92-28